New methods to study macrophage biology *in vitro* and *in vivo*.

A thesis submitted for the degree of
Doctor of Philosophy in Cardiovascular Science

University of Oxford

Trinity Term 2022

Agata Natalia Rumianek

St Edmund Hall

Sir William Dunn School of Pathology

Abstract

Macrophages are heterogeneous and plastic cells, which populate almost every organ in the body and migrate towards sites of inflammation. However, tools designed for studying macrophage biology, particularly genetic models and chemotaxis assays, are standardised to investigate a broad range of leukocyte populations. They fail to capture the unique properties of macrophages and distinguish them from other ontologically related populations. In this thesis, I set out to create novel *in vitro* and *in vivo* tools that are adjusted for studying macrophage biology. To address the *in vivo* arm of this project, I phenotyped a novel tamoxifen-inducible hCD68-CreERT2 mouse line. Having established an optimal protocol for tamoxifen dosing, I detected robust expression of Cre recombinase activity in tissue-resident macrophage populations in peritoneum, spleen and liver. Importantly, the expression was restricted to tissue-resident macrophages with marginal effects in blood leukocyte populations and splenic non-macrophage populations. When compared to other 'macrophage-specific' lines, hCD68-CreERT2 mice had fewer 'off-target' effects. Additionally, I was able to successfully use hCD68-CreERT2 mice to target macrophages present in atherosclerotic lesions. To address the *in vitro* arm of this project, I used the Freestyle Fluidics (FF) platform to design and optimise circuits that can be used to study macrophage migration. I created a passive diffusion-based system and an active pumping system that created stable controllable gradients. I showed that both chemotaxis and chemokinesis can be readily detected and quantified in both systems. Using the FF chemotaxis assay, I observed novel properties of macrophage behaviour such as population-level coordination of chemotaxis and the ability to sense the gradients both spatially and temporally. In summary, this project advanced the macrophage-specific technology platforms available to researchers.

Acknowledgements

This thesis is a product of almost 5 years of hard work, but also 5 years of being surrounded by people who made my time at Oxford unforgettable and the greatest adventure of my life so far. This work could not have come to such fruitful completion without your constant support in and out of the lab.

First and foremost, I would like to thank my supervisor, Professor David Greaves for believing in me as a scientist from the day we met, encouraging me to apply for a DPhil at Oxford and subsequently giving me the space in his laboratory to grow as a scientist and a person, and for guiding and supporting me throughout my journey. The work presented in this thesis could not have happened without Dr Gareth Purvis and Dr Cyril Deroy - working with you every day was an absolute pleasure and made me a better scientist but also gave me friends for life. Gareth, you taught me my way around the animal house but the memories I'll cherish the most are the many pints (preferably not spilled on any white trousers), dinners and dancefloors that we shared over the years and our single most hilarious boating adventure. Cyril, what was meant to be a quick rotation project turned into years of truly multidisciplinary collaboration and I couldn't be more grateful for it as with the work came many hours that we spent talking in the TC room and over coffee about our lives, DPhils, welfare and anything in-between and you always supported me with valuable advice when I needed it the most. I would also like to thank all present and past members of the Greaves Lab and Cook-Walsh Lab for being the best colleagues I could have imagined and creating an amazing, friendly and inspiring atmosphere. In particular, I would like to thank Laura Chaffey, Vincent Luscombe, Annabell Roberti and Federico Nebuloni, even though we are at different stages of our DPhils, I am thankful for sharing this experience with you - you made all the ups of it even higher and

all the lows much more bearable and I hope that my cakes spoke more than words about my appreciation of you. I wish you the best of luck for finishing up your DPhils, you've got this!

Even though I knew nothing about colleges in Oxford, Teddy Hall went beyond anything I could have imagined and I'm forever grateful for all the memories I've created, especially with the MCR community, and all the people that became my second family there. Yasemin, you made RHC a true home, not just another student flat, and living with you was the single best decision I made during my time at Oxford. You are a sister to me and I am so proud and happy of having you in my life. Carolina, Nino, Jules, Hannah, Freddie, Charlie, Marc and Tom, sharing my time at Teddy Hall and being friends with you is a privilege and even though we are already scattered around the world I am excited for all the reunions we'll have and all the new memories we'll create together.

Claudio, without you the last few months of this DPhil would be a lot darker. You found me when I needed to be found the most, brought back my faith in love, infected me with your constant enjoyment of life like I never knew before and for that I will be forever grateful. I can't wait to see what the future holds for us, pololo.

Finally, I would like to thank my parents, you thought me the value of knowledge, the joy of learning and supported my academic aspiration for my entire life. Without you I would not be where I am now or who I am now. Dziękuję wam.

Abbreviations

4-OHT	4-hydroxy tamoxifen
AAV	Adeno-associated virus vector
AM	Alveolar macrophage
ApoB-LP	Apolipoproteins B-containing lipoprotein
ATM	Adipose tissue-associated macrophage
BCG	Bacillus Calmette–Guérin vaccine
BM	Bone marrow
BMDM	Bone marrow-derived macrophage
cDC	Conventional dendritic cell
CDP	Common dendritic cell precursor
CHAK	Chemokine-activated killers
CI	Cell index
CLP	Common lymphoid precursor
cMoP	Common monocyte progenitor
CMP	Common myeloid precursor
CreERT2	Tamoxifen inducible Cre recombinase
C5a	Complement component 5a
DAMP	Danger-associated molecular pattern
DC	Dendritic cell
DMEM	Dulbecco's Modified Eagle's Medium
DMSO	Dimethyl sulfoxide
DPBS	Dulbecco's Phosphate Buffered Saline
ECM	Extracellular matrix
EDTA	Ethylenediaminetraacetic acid
EGFP	Enhanced green fluorescent protein
EIM	Erythroblastic island macrophage
EPO	Erythropoietin
ER	Endoplasmic reticulum
ESAM	Endothelial cell-selective adhesion molecule
FcγR	Immunoglobulin-like receptor Fc gamma
FF	Freestyle Fluidics
FLT3-L	Ligand for the receptor tyrosine kinase FLK-2
FMO	Fluorescence minus one
FRed	FusionRed
FRET	Fluorescence resonance energy transfer
G-CSF	Granulocyte colony stimulating factor
GM-CSF	Granulocyte macrophage colony stimulating factor
GMP	Granulocyte and macrophage progenitor
GPCR	G protein-coupled receptor
GRK3	G protein-coupled receptor kinase 3
hCD68	Transgenic human CD68
HFD	High fat diet
HSC	Haematopoietic stem cell
HSP90	Heat shock protein 90

ICAM-1	Intracellular adhesion molecule-1
IFN	Interferon
IL-1β	Interleukin-1 beta
IL-7	Interleukin-7
IL-7R	Interleukin-7 receptor
IL-10	Interleukin-10
iNOS	Inducible nitric oxide synthase
I.P.	Intraperitoneal
IP-9	Interferon gamma-induced protein 9
IP-10	Interferon gamma-induced protein 10
IVS-1	intervening sequence 1, first intron of human CD68 gene
JAM-A	Junctional adhesion molecule A
KC	Kupffer cell
KO	Knock-out
LAM	Lipid-associated macrophage
LAMP	Lysosomal/endosomal-associated membrane glycoprotein
LC	Langerhans cell
(L)CM	(Liver) Capsular macrophage
LDL	Low-density lipoprotein
LDLR	Low-density lipoprotein receptor
LFA-1	Lymphocyte function-associated antigen-1
LPM	Large peritoneal macrophae
LPS	Lipopolysaccharide
LysM	Lysozyme M
MAC	Membrane attack complex
Mac-1	Macrophage-1 antigen
MBL	Mannose-binding lectin
MCP	Mast cell precursor
M-CSF	Macrophage colony stimulating factor
MDP	Monocyte/dendritic progenitor
MDR	Macrophage disappearance reaction
MEP	Megakaryocyte and erythrocyte progenitor
MFI	Mean fluorescent intensity
MI	Myocardial infarction
MIG	Monokine induced by gamma interferon
MMP	Matrix metalloproteinase
Mono-KC	Monocyte-derived Kupffer cell
MPO	Myeloperoxidase
MPP	Multipotent precursor
MØ	Macrophage
NDGR	Net-to-gross displacement ratio
NET	Neutrophil extracellular trap
NFκB	Nuclear factor kappa B
NK cell	Natural killer cell
NLR	Nucleotide-binding oligomerization domain-like receptor
NO	Nitric oxide
oxLDL	Oxidised low density lipoprotein

PAN	Proangiogenic neutrophil
PAMP	Pathogen-associated molecular pattern
pDC	Plasmacytoid dendritic cell
PDMS	Polydimethylsiloxane
PECAM-1	Platelet/endothelial-cell adhesion molecule 1
PH	Pleckstrin homology
PI3K	Phosphoinositide 3-kinase
PIP2	PI 4, 5-bisphosphate
PIP3	Phosphatidylinositol 3, 4, 5-trisphosphate
PMN	Polymorphonuclear leukocyte
PRR	Pattern recognition receptor
P/S	Penicillin plus streptomycin
PSGL-1	P-selectin glycoprotein ligand-1
RA	Rheumatoid arthritis
RANKL	Receptor activator of nuclear factor kappa-B ligand
RANTES	Regulated upon activation normal T cell expressed and secreted
RLR	Retinoid acid-inducible gene I-like receptor
RNA	Ribonucleic acid
ROCK	Rho kinase
ROS	Reactive oxygen species
RTK	Tyrosine kinase receptor
rtTA	Reverse tetracycline-controlled transactivator
SAM	Sympathetic neuron-associated macrophage
SEM	Standard error mean
SMC	Smooth muscle cell
SPM	Small peritoneal macrophage
TCA	Tricarboxylic acid cycle
tdTom	tandem dimer Tomato
TF	Transcription factor
TGFβ	Transforming growth factor beta
TLR	Toll-like receptor
TNF	Tumour necrosis factor
TRE	Tetracycline response element
VCAM-1	Vascular cell adhesion molecule-1
VEGF	Vascular endothelial growth factor
VLA4	Very late antigen 4
VLDL	Very low-density lipoprotein
VVO	Vesiculo-vacuolar organelle
WAT	White adipose tissue
WT	Wild type

Contents

List of figures

List of tables

Chapter 1

Introduction

1.1. Acute and chronic inflammatory responses

An acute inflammatory response is rapidly mounted by the host when sentinel cells detect infection or damage to the tissue. Inflammation is a tightly-controlled, innate immunity-driven protection mechanism that isolates and removes noxious agents, repairs damage and restores tissue homeostasis (*1*). However, if any of the steps of the acute inflammatory response fails it can cause tissue damage and turn into a chronic pathology (*2*).

An acute inflammatory response is initiated when tissue-resident macrophages and mast cells sense pathogens or endogenous danger molecules, which causes them to produce a plethora of pro-inflammatory mediators (*3*, *4*). These mediators induce local accumulation of fluid (oedema) and trigger signalling cascades that lead to the extravasation of neutrophils and monocytes from the blood. Neutrophils are the first responders of the immune system that act directly to remove the noxious stimulus while monocytes differentiate into macrophages to aid that process (*3*, *5*). If the danger persists, professional antigen presenting cells, mainly dendritic cells, engage the adaptive immune system with T cell-driven responses and B cells antibody production (*6*). Once the danger is contained, tissue repair can begin.

Return to homeostasis is termed resolution of inflammation and is considered to be an active process driven by anti-inflammatory macrophages (*7*). They release pro-resolution signals, which stop further influx of neutrophils and monocytes and induce fibroblasts to start laying new extracellular matrix (ECM) (*8*). At the same time, macrophages engage in efferocytosis – controlled removal of dead and dying cells to prevent necrosis-driven tissue damage.

Ingestion of the apoptotic cells triggers macrophages to inhibit the release of pro-inflammatory signals such as tumour necrosis factor (TNF) and to secrete anti-inflammatory mediators such as transforming growth factor-β (TGFβ) and interleukin-10 (IL-10) (*9*, *10*). If any step of the resolution process fails, inflammation may become chronic and induce tissue damage rather than repairing it.

Chronic inflammation is a hallmark of many prevalent pathologies such as rheumatoid arthritis, obesity, atherosclerosis and neurodegeneration (*11*). It is defined as an unregulated, persistent inflammatory response, however each pathology has slightly different cellular and molecular characteristics of the chronic inflammation process (*3*). Commonly, chronic inflammation is characterised by accumulation of immune cells, death by necrosis instead of apoptosis, priming of macrophages to pro-inflammatory state, chronic release of pro-inflammatory mediators and defects in clearance of apoptotic cells. If untreated, it can persist and worsen over long periods of time leading to irreparable tissue damage.

Macrophages are key to all stages of resolving and non-resolving inflammation and therefore will be the primary focus of this thesis. I will discuss in-depth their ontology and heterogeneity of their homeostatic functions, as well as their migration. However, to provide a more comprehensive view of the field and place macrophage biology in a broader context, I will also briefly introduce other key concepts of innate immunity, inflammation, and cellular migration.

1.2. Cells of the innate immune system

The innate immune response is the first line of defence against any pathogens. It is a non-specific response which utilises common molecular motifs and danger signals to recognise

infectious agents and tissue damage (*12*). With the exception of tissue-resident macrophages, cells of the innate immune system are mostly produced in the bone marrow during the process of haematopoiesis (*13*). Due to their common origins and similar function, most innate immune cells share similar receptors on their surface. They commonly express receptors able to recognise cytokines, key immune mediators, as well as germline-encoded pattern recognition receptors (PRRs), which can recognise conserved motifs – pathogen-associated molecular patterns (PAMPs, found on invading pathogens) or danger-associated molecular patterns (DAMPs, endogenous damage signals) (*3*).

There are four main classes of PRRs that can be found in innate immune cells: Toll-like receptors (TLRs), retinoid acid-inducible gene I-like receptors (RLRs), nucleotide-binding oligomerization domain-like receptors (NLRs) and DNA sensors (DAI, AIM2 and PKR). While TLRs are expressed on cell surface or on endo-lysosomal membranes, RLRs, NLRs and DNA sensors are all cytoplasmic (*14*). TLRs are the biggest and the most extensively studied class of PRRs, they are expressed on all innate immune cells and can recognise PAMPs derived from wide variety of pathogens, including bacteria (TLR4 via LPS for gram-negative bacteria and TLR2 for gram-positive bacteria), viruses, fungi and protozoa as well as host DAMPs (*15*, *16*). RLRs are RNA helicases that are key to sensing of cytoplasmic RNA, both viral and host. Binding of double-stranded RNA or 5'-triphosphate RNA drives receptor oligomerisation and transcriptional induction of type I interferon (IFN) production (*17*). Cytoplasmic DNA is recognised independently from TLRs or RLRs by DNA sensors (DAI was the first one discovered). Similarly to RLRs, DNA sensors can lead to the activation of IFN response but they can also induce programmed cell death (*18*). This mechanism is mainly used to detect DNA viruses, retroviruses and intracellular bacteria. NLRs are defined by their nucleotide-binding

oligomerization domain (NOD), which drives oligomerisation upon ligand binding. Ligand binding ultimately leads to activation of caspases and inflammasome formation, activation of NF-κB pathway and pro-inflammatory responses (*19*). NLRs are capable of being activated by muramyl peptide present on both gram-negative and gram-positive bacteria as well as ATP, uric acid crystals, RNA and DNA, which makes them capable of detecting viral infections as well as host DAMPs (*20*).

Another mechanism that allows innate immune cells to swiftly detect and neutralise pathogens is 'trained immunity' – term coined by Netea *et al.*, who argued that traditionally non-specific innate immune system has the ability to remember previously encountered pathogens, similarly to adaptive immune system, and can mount a different inflammatory response upon secondary stimulation (*21*). Trained immunity is described as long-term functional reprogramming of innate immune cells, which is caused by exogenous or endogenous trigger and leads to different (depending on the context increased or decreased) functional response, if a second challenge occurs after the cells have returned to a non-activated state (*22*). Importantly, trained immunity is a phenomenon that causes long-term adaptation of innate immune cells (so far proven for up to a year) due to epigenetic and metabolic reprogramming, rather than causing induction of alternative transcriptional or functional state in the cells (*22*). During primary challenge, PRRs recognise specific ligands which triggers intracellular signalling cascades that leads to upregulation of metabolic pathways such as glycolysis, TCA cycle and fatty acid metabolism. Metabolites such as fumarate or coenzyme A, which derive from these pathways, modulate the activity of enzymes that are involved in epigenetic remodelling, such as histone demethylase lysine-specific demethylase 5 or histone acetyltransferase (*23*). This causes changes in histone

methylation and acetylation of genes involved in the innate immunity, which leads to the changes in their long-term responsiveness. In humans, trained immunity has been suggested to be the cause of non-specific cross-protection that live vaccines such as BCG, measles or smallpox cause against other infections (*24*). However, mechanisms of trained immunity have been also shown to be detrimental in reprogramming of circulating monocytes and myeloid progenitor cells when atherosclerosis-prone mice were fed high fat diet. Even after switching back to standard chow diet and cholesterol levels returning to normal, these mice showed persisted increase in inflammatory responses (*25*).

1.2.1. Haematopoietic lineage of innate immune cells

Post-embryonically, the main source of immune cells in the body is haematopoiesis in the bone marrow. It is a tightly-regulated process where common precursors of different pluripotency become progressively more restricted until they branch out and eventually give rise to distinct blood cell populations (*26*). At the top of this pyramid are the haematopoietic stem cells, which actively self-renew to provide a constant supply of the stem cells used for haematopoietic differentiation (*27*).

During haematopoiesis an oligopotent hematopoietic stem cell (HSC) precursor gives rise to multipotent precursors (MPP), which can then branch out into either a common myeloid precursor (CMP) or common lymphoid precursor (CLP). The CLP is a lineage-restricted precursor which can give rise only to lymphoid cells (i.e. T cells, B cells and natural killer cells) while the CMP is its myeloid counterpart, which can further differentiate only into cells of myeloerythroid lineage (*13*, *26*). This split is orchestrated by upregulation of the IL-7 receptor (IL-7R) on the CLPs as IL-7 is a critical cytokine for B cell and T cell development (*28*). The CMP can differentiate into either a committed megakaryocyte and erythrocyte progenitor (MEP)

or a committed granulocyte and macrophage progenitor (GMP). MEPs and GMPs can be differentiated by their surface expression of CD34 and immunoglobulin-like receptor Fcγ (FcγR) with MEPs being $FcγR^{-}CD34^{-}$ and GMPs being $FcγR^{hi}CD34^{+}$; additionally, upregulation of transcription factors (TFs) PU.1 and C/EBPα is exclusive to GMPs only (*29*).

GMPs can directly give rise to the granulocytes – mast cells and basophils, eosinophils (differentiated due to high expression of IL-5 receptor α chain) and neutrophils (differentiated under the influence of granulocyte colony stimulating factor (G-CSF), granulocyte macrophage colony stimulating factor (GM-CSF) and TFs C/EBPα, C/EBPε and GFI-1) or further differentiate into a lineage-committed monocyte/dendritic progenitor (MDP) under the control of TFs GATA2 and ZEB2 (*30*). MDPs were initially thought to be derived from GMPs and the sole source of monocytes, however Yánez *et al.* showed that MDPs arise directly from CMPs and that classical monocytes can be derived from both GMPs and MDPs (*31*). The MDP population is thought to divide into either dedicated common DC precursors (CDP) or into the unipotent common monocyte progenitors (cMoP) which gives rise to classical monocytes. Classical monocyte fate is specified by the sequential expression of transcription factors PU.1, IRF8, and Klf4 (*32*). Classical monocytes can be further differentiated into non-classical monocytes (associated with expression of TFs NR4A1, C/EBPβ and KLF2) and monocyte-derived macrophages - under the influence of macrophage colony stimulating factor (M-CSF). Dendritic cells (DCs) can be derived either from the myeloid or lymphoid lineage and are therefore thought of as the interface between the innate and adaptive immune systems. Conventional DCs are derived purely from the CDP, however plasmacytoid DCs are mainly derived from the CLP precursor with only a small fraction of them derived from the CDPs (*33*)

They can develop independently from M-CSF and their specification relies on the ligand for the receptor tyrosine kinase FLK-2 (FLT3-L).

1.2.2. Neutrophils

Polymorphonuclear leukocytes (PMNs, named after their characteristic multi-lobular nucleus), also known as neutrophils, are a part of the granulocyte family and also the first innate immune cells to respond to pro-inflammatory signals secreted at the site of infection or damage (*5*). They are the most abundant leukocytes in the blood stream and in the bone marrow. About 60% of the haematopoietic capacity of the bone marrow is used for generation of neutrophils with up to $2x10^{11}$ of them produced daily from the myeloid precursor (*34*, *35*). However, they have a short half-life in the blood (up to 18 hours) unless they detect a pro-inflammatory stimulus (*36*). Once activated, they are subjected to a complex multistep cascade of events, which ultimately leads to their extravasation and trafficking to the inflamed tissue. Being the 'foot soldiers' of the innate immune system, they are responsible for clearance of pathogens and release of secondary pro-inflammatory signals that drive influx and maturation of monocytes to the site of inflammation (*5*).

Traditionally, circulating neutrophils has been considered as terminally differentiated homogenous population, however recently their heterogeneity has become appreciated and functionally distinct neutrophil subsets has been proposed for both their terminal differentiation state as well as well as during maturation process in the bone marrow. Based on the granule content and nuclear shape, immature neutrophils in the bone marrow can be sub-divided into myoblasts, promyelocytes, myelocytes, metamyelocytes, band cells and segmented neutrophils, which sequentially mature into each other (*37–41*). Under homeostatic conditions only segmented neutrophils can exit the bone marrow, however

immature subsets have been found outside of bone marrow in pathological conditions such as cancer, cardiovascular diseases and viral infections (*42–44*). Mature blood neutrophils have been sub-divided in humans based on their cell surface markers expression to $CD177^+$ neutrophils, $OLFM4^+$ neutrophils and proangiogenic neutrophils (PANs) which express CXCR4, CD49d and VEGFR1 (*45*). Abundance of $CD177^+$ neutrophils vary between people with up to 10% of the population lacking this subset completely (*46*). Functionally, CD177 has been shown to regulate the activity of granule protein proteinase 3 and due to that association $CD177^+$ neutrophils have been linked to susceptibility to autoimmunity and inflammatory bowel diseases (*47*). 20-25% of blood neutrophils in all individuals express OLFM4 and they have been shown to have different ability to produce NETs as compared to $OLFM4^-$ cells (*48*, *49*). Functionally, higher percentage of $OLFM4^+$ neutrophils have been linked to greater risk of organ failure during septic shock (*50*). PANs represent around 3% of circulating neutrophils and express even higher levels of MMP9 than proinflammatory neutrophils, which allows them to contribute to ECM remodelling (*51*, *52*). Their deletion has been shown to result in delayed vascular sprouting in experimental model of hypoxia but they have also been shown to have important contributions in cancer and pregnancy (*45*, *52*). Finally, the blood also harbours a population of suppressor cells, which express typical neutrophilic markers Ly6G and CD11b but morphologically resemble both mature and immature neutrophils. These suppressor neutrophils are reported to inhibit T cell proliferation and activation, which leads to suppression of immune responses (*53*).

Neutrophils contains three main types of granules (classified by their contents), which contain potent antimicrobial compounds but are also highly cytotoxic. Primary (azurophilic) granules contain potent hydrolytic enzymes (e.g. elastase) and myeloperoxidases (MPO). Secondary

(specific) granules contain high levels of the iron-binding protein lactoferrin, while tertiary (gelatinase) granules contain matrix metalloproteinases (MMPs) (*35*). Recently, a fourth granule population has been described that was enriched in ficolin-1 (*54*). However, perhaps the most important mechanism of pathogen killing used by PMNs is the generation of reactive oxygen species (ROS) in the phagolysosomes (*55*). The NADPH oxidase complex is contained in secondary granules and once primed, relocates to the cell membrane to induce O^-_2 production. Although O^-_2 has bactericidal properties, it usually gets converted into hydrogen peroxide, which then becomes transformed into hypochlorous acid by MPO from the primary granules. If the complex remains on the surface, extracellular ROS production occurs but if the complex is endocytosed a phagolysosome is created (*55*).

Alternatively, neutrophils can induce pathogen killing by purposefully exuding their DNA in a form of neutrophil extracellular traps (NETs) (*56*). This specialised form of cell death, dubbed NETosis, occurs when chromatin mesh coated in anti-microbial peptides and MPO is released to physically catch and kill the pathogen, a *de facto* suicidal mission by the PMN.

1.2.3. Monocytes

Monocytes are the second innate immune cell type that is recruited to the site of inflammation, after neutrophils (not counting platelets). They are broadly divided into two sub-types: classical (inflammatory) and non-classical (patrolling) monocytes. In mice, this classification is based on the expression of surface marker Ly6C – the inflammatory monocytes have a high expression of this marker (therefore called $Ly6C^{hi}$ monocytes) while the patrolling monocytes have low or no expression of Ly6C (therefore called $Ly6C^{low}$ monocytes). A parallel system exists in humans based on their expression of CD14 and CD16, however three distinct subsets are recognised. $CD14^+CD16^-$ monocytes are the counterpart

of the classical monocytes and $CD14^{-}CD16^{+}$ monocytes are the counterpart of the non-classical monocytes (*3*, *26*, *57*). However, there are also intermediate monocytes, which are characterised by the expression of both markers ($CD14^{+}CD16^{+}$). Intermediate monocytes comprise about 2-8% of circulating monocytes in humans and several functions have been reported, including production of reactive oxygen species, antigen presentation, participating in the proliferation and stimulation of T cells, inflammatory responses, and angiogenesis (*57*). However, since there is no equivalent population reported in mice to date, I will not discuss them further.

Inflammatory ($Ly6C^{hi}$) monocytes are characterised by a high expression of chemokine receptor CCR2, which drives their mobilisation from the bone marrow and recruitment during inflammatory responses (*58*). Classical monocytes have a relatively short half-life (8 – 20 hours) and they participate in both bacterial killing and phagocytosis (*59*). However, once they migrate into a site of inflammation they can also differentiate into macrophages and acquire a 'macrophage-like' phenotype to help with pathogen clearing as well as efferocytosis and debris removal (*26*).

Patrolling ($Ly6C^{low}$) monocytes have been demonstrated to derive wholly from the $Ly6C^{hi}$ population, yet they differ significantly in their characteristics. Dubbed as 'macrophage-like' cells of the blood vessels, they have a significantly longer life span with half-life of 5-7 days (*59*). They have very low to no expression of CCR2 and therefore are not rapidly trafficked to the inflammation sites. Instead, they are the sentinel cells of the blood vessels – their primary role appears to be detection and repair of endothelial damage (*26*). To perform this function, they slowly crawl on the luminal side of the endothelium. If needed, they can be mobilised to the site of inflammation, which is orchestrated by the fractalkine receptor CX3CR1 (*60*).

However, they are usually one of the last cells to arrive at the site of inflammation, where they differentiate into macrophages and contribute to the resolution processes.

Recruitment of circulatory monocytes from blood to tissues follows a tightly controlled cascade of events, forming a general paradigm of leukocyte recruitment, which has been first described almost 200 years ago – rolling, adhesion and transmigration. However, it is now appreciated that these general steps of migration can be further specified into capture (tethering), rolling, slow rolling, arrest, firm adhesion and spreading, intravascular crawling and transmigration, which allows for more specific description of the whole process (*61*). Firstly during tethering process, inflammatory cytokines produced by tissue resident macrophages activate endothelium, which causes rapid expression of adhesion molecules, most importantly E- and P-selectins, intracellular adhesion molecule-1 (ICAM-1) and vascular cell adhesion molecule-1 (VCAM-1) and presentation of tethered chemokines on the luminal surface of the endothelium (*62*). All monocytes express P-selectin glycoprotein ligand-1 (PSGL-1), which binds to the selectins expressed on the endothelium, which allows them to overcome the high sheer stress caused by the blood flow and start rolling. Additionally, they also express L-selectin which facilitates secondary leukocyte capture; in fact, L- and P-selectins require sheer stress to support adhesion (*63*, *64*). Selectins are the key drivers of monocyte rolling, however integrins also participate in rolling and, later, in firm adhesion. Monocytes express very late antigen 4 (VLA4), which binds VCAM1 and mediates slow rolling thus facilitating the transition between rolling and adhesion (*65*).

Firm adhesion of monocytes is mainly mediated by CC and CXC chemokines expressed on the endothelial surface, CCL5, CCL2 and CXCL8 being key in this process (*66*, *67*). Chemokines activate integrin-mediated adhesion of VLA4 to VCAM1 and lymphocyte function-associated

antigen-1 (LFA-1) to ICAM-1, which also induces increase in affinity and conformational changes (*65*). These conformational changes contribute to the arrest of monocytes, which causes their spreading, polarisation and crawling to find the preferred site of transmigration (*68*). LFA-1 and macrophage-1 antigen (Mac-1) expressed on the monocytes interact with ICAM-1 and ICAM-2 on the endothelium to facilitate crawling and lamellipodia extension.

Finally, monocytes have to cooperate with the endothelium, basement membrane and pericytes to transmigrate out of the vessel, which they do by either paracellular or transcellular route. Paracellular route is the main cascade used during transmigration. During this process, monocytes are prompted to extend protrusions into endothelial cell junctions by ligation of ICAM-1 by Mac-1, which increases intracellular Ca^{2+} and activates MAPK and Rho GTPase, which cause increased contractility of endothelial cells and opening of interendothelial contacts (*69*). During this process VE-cadherin is distributed away from the junction to loosen the junctions, while platelet/endothelial-cell adhesion molecule 1 (PECAM-1) and junctional adhesion molecule A (JAM-A) are mobilised to the endothelial surface to create haptotactic gradient that guides migrating monocytes (*70*). Additionally, endothelium expressed JAM-B, JAM-C, ICAM-2, CD99 and endothelial cell-selective adhesion molecule (ESAM) on the surface of the junction to further support the migration (*61*). Transcellular migration occurs only in 'thin' parts of the endothelium, where the distance to cross is shorter. During this process, ICAM-1 ligation leads to its translocation to actin- and caveolar-rich regions, where they link to form vesiculo-vacuolar organelles (VVOs) (*71*). VVOs form an intracellular channel that the monocyte can cross through, with proteins such ezrin, radixin and moesin supporting the channel and the structural integrity of the endothelial cell that they are crossing through (*61*).

1.2.4. Dendritic cells

As mentioned earlier, dendritic cells are tissue sentinel cells that are thought of as the interface between the innate and adaptive immune system. They are professional antigen presenting cells that trigger and orchestrate adaptive immune responses (*72*). Under steady-state conditions they can be sub-divided into conventional dendritic cells (cDCs) and plasmacytoid dendritic cells (pDCs). cDCs specialise in antigen uptake and presentation to naïve T cells and can be further subdivided into cDC1 and cDC2, expressing the transcription factors IRF8 and IRF4, respectively. pDCs are phenotypically distinct and specialise in production of high amounts of type 1 interferons in response to viral infections (*33*).

Immature DCs migrate from the bone marrow and seed into most non-lymphoid tissue where they continuously sample their environment by extending multiple pseudopodia (dendrites) (*72*). They can detect invading pathogens thanks to their high expression of PRRs, which induce them to migrate out of the tissue and into draining lymph nodes. This migration is governed mainly by CCL19/CCL21-CCR7 axis and during this process the immature DCs undergo phenotypical and functional maturation (*73*, *74*). They upregulate co-stimulatory molecules such as CD80 and CD86 and secrete pro-inflammatory cytokines such as TNF and IL-12 (*74*, *75*). Once they reach the lymph node, they move to the T-cell zones where they actively participate in antigen presentation to naïve T cells.

Even though DCs are phenotypically and developmentally distinct from macrophages, they are both tissue sentinel cells and share common morphological and phenotypical characteristics and surface markers, which makes the two cell types particularly hard to distinguish. DCs are typically characterised by high levels of expression of CD11c and MHCII, both of which can be found on different sub-populations of macrophages. However, the

advent of single-cell RNA sequencing has allowed a more precise differentiation between the two as they are distinct in their developmental origins and transcriptomic profiles.

1.2.5. Eosinophils

Eosinophils belong to the granulocyte family and take their name for the fact that when stained with the acidic dye eosin they appear bright pink. Their maturation, specification and survival are orchestrated mainly by the cytokine IL-5, which binds to IL-5R receptor (*76*). Following their maturation, eosinophils migrate from the bone marrow to the blood as an intermediate step before tissue extravasation. Their half-life in blood is about 18 hours, after which they are recruited to tissues such as thymus, intestines and lung by cytokine CCL11 (also known as eotaxin), which binds to CCR3 receptor on their surface (*76*, *77*).

As granulocytes, eosinophils contain large granules enriched in eosinophil peroxidase, eosinophil-derived neurotoxin and eosinophil cationic protein. Their granules also contain various cytokines, enzymes and inflammatory mediators such as leukotrienes, thromboxanes and prostaglandins (*78*). During inflammation eosinophils are trafficked to inflammatory sites via IL-5 and CCL11, where they will subsequently induce degranulation, their main method of pathogen killing. Although eosinophils play a role in both bacterial and viral killing, their main function is protection against parasitic (mainly helminth) infections (*77*). However, thanks to advancements in medical treatments and hygiene measures there is a decreasing prevalence of parasitic infection in humans but an increased exposure to allergy-causing irritants, which led to eosinophils now being mainly considered as drivers of allergic reactions (*79*).

1.2.6. Mast cells

Mast cell are bone marrow-derived cells, which are released into the circulation in their immature state – mast cell precursors (MCPs). MCPs are seeded into tissues of adult

organisms where they mature mainly due to the locally produced modulatory stem cell factor c-kit and cytokine IL-3 (*80*). Fully differentiated mast cells contain cytoplasmic electron-dense vesicles which are filled with pre-formed inflammatory mediators such as histamines, prostaglandins and TNF (*81*). Mature mast cells are mainly sentinel cells monitoring for tissue damage and infection. Once activated, they release the contents of their vesicles to the extracellular space to initiate acute inflammatory response and start *de novo* production of more pro-inflammatory mediators to further potentiate the inflammatory response and recruit more innate immune cells.

1.3. Macrophages

Macrophages (Greek 'Big eaters') are phagocytic cells that reside in essentially all tissues of the body (to a varying degree) and are involved in tissue homeostasis, infection and damage detection, removal of apoptotic cells and repair of the tissue after acute inflammatory response. Macrophages are extremely plastic cells, not just functionally but also metabolically and structurally (*82*, *83*). That plasticity is highlighted by the fact that they are involved in all stages of inflammatory response from initiation to resolution and can change their function based on the environment to be either pro-inflammatory (M1 polarised) or anti-inflammatory (M2-polarised). They broadly fall into two main categories: tissue-resident (foetal-derived) and monocyte-derived cells that infiltrate tissues during inflammation. Tissue-resident macrophages are unique among all innate immune cells not only due to their foetal origin but also because of their exceptionally long half-life. Intestinal and dermal resident macrophages have been reported to have a half-life of 4-6 weeks, while cardiac and peritoneal resident macrophages were suggested to have a half-life of 8-14 weeks (*84*, *85*).

1.3.1. Developmental origins of different macrophage populations

Historically, all macrophages were thought of as the final differentiation stage of monocytes and therefore classified as a part of the 'mononuclear phagocyte system' (*86*). Initially, given that there was no evidence for dividing tissue-resident macrophages, it was assumed that they were replenished by monocytes entering the tissues (*87*). However, van Furth *et al.* also noted that in the spleen there are two macrophage populations: a self-renewing one and a continuously-recruited monocyte-derived one, which led them to create the dual origin hypothesis where half of tissue resident macrophages were renewed from circulating monocytes and the other half from local proliferation (*88*). In the early 2000s, a population of macrophages was found in the yolk sac of developing embryos as early as E7.5 during mouse development, which went on to exclusively become microglia in the brain (*89*). This finding questioned the assumptions of the dual origin hypothesis and led to further investigation into the origins of tissue-resident macrophages. Kupffer cells in the liver, epidermal Langerhans cells, microglia and pleural macrophages were shown to be unaffected by disruptions to the bone marrow-derived monocytes, suggesting no reliance on recruitment from the circulation (*90–93*). Using novel transgenic mice and fate mapping approaches, Hashimoto *et al.*, Schultz *et al.* and Yona *et al.* were able to trace the lineage of tissue-resident macrophage populations to show that they were all yolk-sac derived and unaffected by hematopoietic stem cells deletions (*59*, *94*, *95*). Further supporting this hypothesis, the relative abundance of tissue-resident macrophages in various organs has been shown to peak in the first week of postnatal life and remain stable thereafter (*96*). The only exception seemed to be intestinal tissue-resident macrophages which were shown to be initially seeded during development and proliferate locally in neonatal mice, however in adult mice they were continuously

replenished by circulating monocytes, which entered the tissue and matured into anti-inflammatory macrophages (*97*).

However, within most tissues macrophages are a heterogeneous population and several subsets can be distinguished based on their expression of markers such as F4/80 and CD11b, therefore suggesting that they may also have different origins. One current view of the field is that embryonic macrophage development takes place in several waves. Firstly, during primitive haematopoiesis, myeloid progenitors arise in the yolk sac around E7, which then give rise to early erythromyeloid precursors (*98*). According to Sheng *et al.*, only microglia and a subset of Langerhans cells are truly yolk sac derived and originate from this very first wave of primitive haematopoiesis (*99*). As development progresses, erythromyeloid precursors migrate to the foetal liver where they can differentiate into other cell types, including other tissue-resident macrophage populations. The erythromyeloid precursors also give rise to a population of premacrophages, which colonise the entire embryo by E9.5 (*100*). At the same time, the first haematopoietic progenitors arise independently in the aorta, gonads, and mesonephros, and seed into the foetal liver around E10. From E11 onwards the foetal liver becomes the main site of the 'definitive' embryonic haematopoiesis, involving myeloid precursors of different origins (*101*). Simultaneously, these haematopoietic progenitors also colonise the foetal bone marrow, where they will eventually mature into adult HSCs.

While the foetal origin of tissue-resident macrophages is widely accepted, the exact development trajectories of each of the populations are still heavily debated and multiple models of macrophage embryonic ontogeny have been proposed (*98*). However, regardless of the exact origins of the tissue-resident macrophages, it is commonly believed that in adult organisms the bone marrow haematopoietic stem cells give rise to circulatory monocytes,

which eventually can migrate into the tissues and become monocyte-derived (recruited) macrophages (*102*). In inflammatory conditions or experimental deletions, these recruited macrophages are always able to migrate into the tissues and support or replace tissue-resident macrophages (*96*).

1.3.2. Plasticity of macrophage phenotypes and functions

Macrophages are classified as professional phagocytes, however perhaps their most important function is as sentinel cells, which constantly patrol their environment in search of damage and invading pathogens (*103*). Once macrophages detect danger, usually when PRRs bind a ligand or one of their many GPCRs or TRKs detects a pro-inflammatory signal such as TNFα or IFNγ, they initiate inflammatory response by secreting pro-inflammatory mediators that mobilise neutrophil and monocyte influx into the tissue (*3*). Tissue-resident macrophages that initially send out these signals undergo so called 'macrophage disappearance reaction' (MDR) where over 90% of them disappear from the initial site after this first step of the acute inflammatory response and are subsequently replaced by monocyte-derived macrophages (*103*). MDR during peritonitis models is the best documented example and was initially proposed to involve a mixture of adherence to the tissue, cell death and emigration (*104*). However, inflammation in the peritoneum triggers the expression of chemokines by mesothelial cells and fibroblastic stromal cells in the milky spots of the omentum (*105*). The latest models of MDR have shown that these 'missing' resident macrophages are in fact trafficked to draining lymph nodes and the omentum, rather than undergoing cell death (*106*, *107*). Additionally, during bacterial infection, large peritoneal macrophages were shown to adhere to the mesothelium and form cellular aggregates that cleared the bacteria (*108*).

Pro-inflammatory cytokines such as CCL2, CCL4 and CXCL12 as well as complement cascade components such as C5a act as macrophage chemoattractants, directing them to the site of inflammation (*109*). Newly recruited macrophages that enter the site of inflammation after MDR polarise towards a pro-inflammatory (M1) phenotype – they become primed for fighting the infection. This phenotypic switch is characterised by a complete change in their metabolism, which directly translates into their functionality. Non-polarised (M0) macrophages rely mainly on oxidative phosphorylation, however when they become polarised to M1 state they switch to glycolysis as their main source of energy, a phenomenon known as the Warburg effect (*110*, *111*). Polarisation to the pro-inflammatory phenotype allows them to enhance their phagocytic potential, which improves their ability to fight the infection. However, macrophage migratory capacity is diminished when they are polarised to M1 state (*112*). M1 polarised macrophages generate nitric oxide (NO), using inducible nitric oxide synthase (iNOS), which can directly kill bacteria. Therefore, iNOS is considered one of the key markers of M1 polarisation (*83*, *113*).

Once the acute inflammation has fought off the invading pathogens, the inflammatory response has to be contained to prevent unnecessary tissue damage and facilitate a return to tissue homeostasis (*7*). Macrophages are the key cell type that modulates this process; anti-inflammatory/pro-resolving mediators such as IL-4, IL-10, IL13 and TGFβ, which are released at the site of resolving inflammation, skew macrophage phenotype towards an anti-inflammatory (M2) state (*83*, *109*). M2 macrophages utilise oxidative phosphorylation as their main source of energy and express markers such as CD206. Their ability to undergo migration is also enhanced compared to non-polarised or M1-polarised macrophages (*112*). These 'alternatively activated macrophages' are responsible for phagocytosis of dead and dying

leukocytes and cellular debris to prevent necrosis that can damage the tissue. They are also involved in angiogenesis to ensure sufficient blood supply to the healing tissue. Their relevance has been demonstrated *in vivo* in skin inflammation models where macrophage deletion prevented wound healing (*114*). M2 macrophages have been further sub-divided into M2a, M2b and M2c macrophages (*115*). All of them secrete high levels of IL-10, however they differ in the stimulus needed to drive the polarisation and their surface markers. M2a macrophages are polarised by IL-4 or IL-13, highly express CD200R and CD86 and have a low expression of CD14 and TLR4 (*115*). M2b macrophages are stimulated by LPS or IL-1β and have high CD80 and CD14 expression. M2c macrophages are stimulated by IL-10 and have high expression of CD163 but low expression of CD86 and HLA-DR (*115*).

Even though macrophages are often described as M1-like or M2-like, this paradigm was established as a simplified model for *in vitro* studies where M1 polarisation meant stimulation with LPS and INFγ, while the M2 polarisation was achieved by IL-4 stimulation and over time fused with the concept of classically and alternatively activated macrophages as proposed by Siamon Gordon in 1992 (*116*, *117*). Even though this model is extremely useful for *in vitro* investigations, it does not capture the diversity of macrophage polarisation states *in vivo*, especially in humans. Human infectious diseases are characterised by a mixed profile of pro- and anti-inflammatory signals coexisting at the same time and therefore macrophages *in vivo* being exposed to both types of polarisation at the same time (*109*). Additionally, macrophages have been shown to be able to switch between the pro- and anti-inflammatory states *in vitro* but this switch is less defined *in vivo* (*118*, *119*). However, despite these obvious limitations, macrophages in most studies are arbitrarily put into an M1 or M2 category, which inevitably influences the interpretation of results. Moreover, it introduces a duality in thinking

about macrophage populations, with most tissue-resident macrophages being classified as M2-like and monocyte-derived macrophages as M1-like despite their actual function or transcription profile. Murray *et al* and Nahrendorf & Swirski tried to overcome this nomenclature limitation by introducing alternative approaches (*120*, *121*). Murray *et al.* proposed to indicate the stimulus used for the polarization, such that M2 macrophages would become M(IL-4) macrophages while Naherndorf & Swirski proposed to use descriptive names such as 'pruning macrophages' or 'iron-recycling macrophages'. Neither of these proposed nomenclatures have been fully embraced by the macrophage community as they come with their own caveats. Naming macrophages after their activating stimuli is extremely hard, if not impossible, in *in vivo* settings and does not indicate the functional consequences of their stimulation. Similarly, naming macrophages after their functions is a slippery slope as their function is often context dependent and can change.

Plasticity and complexity of macrophage phenotypes and functions is further exemplified by the fact that macrophages can acquire phenotypes of other cell types, while other cells can become macrophage-like in certain disease contexts. Macrophages gain fibroblast-like phenotype after myocardial infarction and in renal fibrosis (*122–124*). These fibroblast-like cells do not express the same markers as conventional fibroblasts and they have been shown to pathologically contribute to fibrosis and scar formation. On the contrary, smooth muscle cells and preadipocytes have been shown to gain macrophage-like phenotype when exposed to the right environmental cues (*125–127*). Trans-differentiation of aortic smooth muscle cells (SMCs) has been first shown *in vitro* by Rong *et al.* where primary SMCs acquired the expression of canonical macrophage markers such as CD68, Mac-2 and ABCA1 after cholesterol loading (*125*). This was later extended by Shankman *et al.* who showed that more

than 80% of smooth muscle cells in murine atherosclerotic plaques *in vivo* undergo phenotypic switch to macrophages, mesenchymal stem cells and myofibroblasts and that this transition had detrimental effect on plaque stability (*127*). Similarly, Charriere *et al.* showed that genetically preadipocytes are actually closer to macrophages than adipocytes and therefore they postulated that preadipocytes should have the ability to trans-differentiate into macrophages in macrophage-inducing environment (*126*). Indeed, when preadipocytes were injected into mouse peritoneal cavity they underwent a phenotypic switch towards macrophages and started expressing macrophage markers such as F4/80 and Mac-1, indicating the essential role of local environment in shaping the phenotype and function of highly plastic cells.

1.3.3. Tissue-resident macrophage heterogeneity of phenotypes and functions in tissue homeostasis

Macrophages are found in almost every tissue in the body as sentinel immune cells but depending on their immediate environment they also perform specialised functions. Tissue-specific adaptions of resident macrophages occur mainly postnatally, correlating with the organs exiting proliferation phase and starting their adult specialisation (*96*, *100*). Most tissues have multiple sub-populations of tissue-resident macrophages coexisting together, which historically have been distinguished by their expression of surface markers or their location within the tissue. Interestingly, their phenotype is partially dependant on the environment there are in – the tissue itself seems to drive the identity of the macrophages it harbours (*128*). This was exemplified by Lavin *et al.* when they adoptively transferred peritoneal macrophages into the lung and saw evidence upregulation of lung-specific genes *Chi3l3*, *Sftpc*, *Car4* and the transcription factor *Pparg* and downregulation of peritoneum-specific gene *Alox15* and TF *Gata6* in the transplanted macrophages (*128*). It is therefore

important to understand the heterogeneity of tissue-resident macrophages both within and in between tissues.

Large scale single cell RNA sequencing and transcriptomics studies have been crucial in appreciation of tissue-resident macrophage heterogeneity across different organs. Projects such as Tabula Muris (Mouse Atlas) highlighted that expression of typical myeloid and macrophage-associated genes can be found in almost all organs (*129*). Summers *et al*. took this a step further and reanalysed published RNA sequencing data of myeloid cells across different tissues in developing and adult mice to investigate origins and phenotypes of monocytes, dendritic cells and tissue-resident macrophages (*130*). Such datasets are crucial for ontological studies as they can provide a much better way to distinguish between closely related cell types such as dendritic cells and macrophages as well as different subpopulations of each. For example, they were able to show shared clustering of transcription factors *Id3*, *Nr1h3* and *Smad6* among liver Kupffer cells, peritoneal macrophages and splenic macrophages revealing phenotypic similarities between those distinct tissue-resident macrophage populations. A caveat of such big scale sequencing datasets is the phagocytic function of macrophages, as the RNA of engulfed dying cells can be detected as expressed by the macrophages (*130*). Nonetheless, large scale sequencing gave us unique insights into human data as well as mouse models, given that a relatively small sample of patient/donor cells provides in-depth picture of the transcriptional profile of human tissues and the immune cell heterogeneity within it (*131*, *132*). For example, using RNA sequencing Evren *et al.* showed that in adult humans lung-tissue resident macrophage populations are renewed from recruited blood monocytes rather than local proliferation, which is in a striking contrast to the mouse models (*95*, *131*). They hypothesised that it may be due to the fact that

experimental mice are kept in tightly controlled germ-free conditions whereas humans are exposed to millions of pathogens since birth. Therefore, local proliferation of human lung macrophages might be exhausted early in life and need supplementing from the recruited monocyte-derived macrophages, a scenario that exemplifies the limitations of animal models. Nonetheless, the majority of our knowledge about heterogeneity of phenotypes and functions of tissue-resident macrophages comes from animal models.

Macrophages represent the most abundant immune cell population in the liver. Kupffer cells (KCs) have long been considered the only macrophage population there, however heterogeneity at steady state that includes liver capsular macrophages (LCMs) and monocyte-derived macrophages is now acknowledged (*133*). Kupffer cells are high F4/80-expressing macrophages located in the liver sinusoids and are in direct contact with the blood passing through the liver rather than the hepatocytes, which highlights their role in clearing blood-borne pathogens and cellular debris (*134*). They were one of the first populations of tissue-resident macrophages to be discovered (*133*). Liver capsular macrophages arise from adult circulating monocytes and lack the canonical KCs markers such as Tim4 and Clec4F. They reside in the hepatic capsule, just under the layer of mesothelial cells, where they have been shown to protect the liver from pathogens invading from peritoneal cavity (*135*). Monocyte-derived macrophages are typically a small liver population, which expands rapidly during inflammation to replace disappearing Kupffer cells. They tend to have lower expression of F4/80 but high expression of pan-myeloid marker CD11b and can be divided into hepatic lipid-associated macrophages (LAMs; mainly present in fatty livers) and monocyte-derived Kupffer cells based on their Clec4F expression (*136*).

In the spleen different macrophage sub-populations are found in discrete anatomical compartments – the red pulp, the white pulp and the marginal zone (*102*). Each population is adapted to reflect and aid the function of each of these spleen compartments. Red pulp macrophages highly express the archetypical macrophage marker F4/80 and efferocytose aging erythrocytes. In this process they recycle iron, catabolise haem and upregulate Spi-C transcription factor, which is implicated in erythrocyte turnover (*137*, *138*). In mice, the red pulp is also a site of monocyte production, which can be recruited to other organs (*139*). The splenic marginal zone contains unique CD169-expressing macrophages, which are responsible for defence against bacterial infections, mainly by interacting with dendritic cells and working as antigen-presenting cells to the splenic B cells (*140*). Lastly, white pulp macrophages are characterised by high expression of CD68 but almost no expression of F4/80 and are involved in clearance of apoptotic cells generated during the germinal centre reaction (*60*, *61*, *92*).

At steady state the lungs are populated with two distinct macrophage populations – alveolar macrophages and interstitial macrophages (*103*, *142*). Alveolar macrophages reside in the lumen of airways of the lungs, while the interstitial macrophages are found in the lung tissue itself and are not at all in contact with the airspace lumen. They can be distinguished by the expression of cell surface markers – alveolar macrophages express high levels of CD11c, while interstitial macrophages have low expression of CD11c but very high expression of CD11b (*142*). Alveolar macrophages (AMs) are involved in immune surveillance for inhaled pathogens and maintenance of lung homeostasis by clearance of pulmonary surfactant (*143*, *144*). Interestingly, even though AMs are embryonically derived there is evidence that they are extremely long-lived but not a fully self-renewing population and if needed they are repopulated in adulthood by blood monocyte-derived macrophages (*59*, *145*). On the other

hand, interstitial macrophages are involved in prevention of allergic responses by producing IL-10, which dampens dendritic cell-driven hyperactivity (*146*).

The peritoneum (serosal tissue surrounding the gastro-intestinal system) has been shown to be an important immunological barrier protecting the rest of the body from gut-dwelling bacteria (*147*). Because peritoneal macrophages are easily accessible and their number can be expanded rapidly by injection of thioglycolate or Bio-gel beads, they became one of the most popular sources of murine primary macrophages to use in biomedical research. They have been shown to regulate production of immunoglobulin A by interacting with peritoneal B cells (*148*). Even though they are typically looked at as one population, the peritoneum actually harbours two distinct populations of tissue-resident macrophages – the large and small peritoneal macrophages (LPMs and SPMs respectively) (*149*). They can be distinguished by size in flow cytometry studies as well as their expression of surface markers such as Gr-1 and MHCII, even though they have very similar expression pattern of the canonical macrophage markers such as F4/80 and CD11b. At steady state, the majority of macrophages present in the peritoneum are the LPMs, however any inflammatory recruitment and expansion are mainly of the SPM population, including thioglycolate-elicited macrophages. Moreover, they differ in their responses to inflammatory stimuli with LPMs retaining their capacity to produce nitric oxide *ex vivo*, while SPMs were only able to achieve this *in vivo* (*149*).

As mentioned previously, brain microglia are the only population of tissue-resident macrophages derived purely from the early yolk sac progenitors with no contribution from foetal liver haematopoiesis. At birth, there is a significant expansion of microglia driven by M-CSF and IL-34, which highlight their role in synaptic pruning during the postnatal period (*150*,

151). In adult mice, microglia have been shown to be crucial in supporting synapse plasticity in response to learning cues as well as immune surveillance and maintain homeostasis of neurotransmitters (*102*, *152*).

The heart also contains a small yet crucial population of tissue resident macrophages, which shapes heart function from development onwards. Yolk sac-derived macrophages have been shown to be one of the key pro-angiogenic cells in the developing heart. Leid *et al.* established that they mediate remodelling of coronary plexus during development and selectively promote expansion of perfused coronary vessels (*153*). Additionally, Cahill *et al.* showed that yolk sac and foetal liver-derived macrophages are indispensable for correct development of cardiac lymphatic vessels (*154*). Macrophages have been also shown to undergo local transient haematopoiesis in the endocardium during development of the heart and this population of macrophages was crucial in correct valve formation (*155*). In adult organisms, resident cardiac monocytes (distinguishable from recruited monocyte-derived macrophages by the lack of CCR2 expression) were shown to suppress inflammation following myocardial injury and be essential for preserving the function of chronically failing heart in a mouse model of dilated cardiomyopathy by the means of adaptive remodelling (*156*). Moreover, in steady state they were crucial for electrical conduction through atrioventricular node in the heart by accelerating repolarisation of cardiomyocytes that they are in contact with via connexin-43 junctions (*157*).

Gastrointestinal tissue-resident macrophages constitute the largest macrophage pool in the body are unique due to being the only tissue-resident macrophage population derived from recruited monocytes (*158*). However, they are crucial to healthy functioning of the gut and are involved in all key processes such as digestion and absorption of nutrient, peristalsis,

symbiotic interactions with the microbiota and mucosal immunity (*102*). One of their key functions is distinguishing between harmful pathogens and commensal bacteria, which they have been proposed to achieve by constitutively expressing pro-IL1β while simultaneously being hyporesponsive to TLR activation (*159*). Furthermore, Franchi *et al.* showed that commensal bacteria were unable to activate inflammasome and produce mature IL1β, while pathogenic bacteria such as Salmonella caused a robust inflammasome response (*159*).

In healthy, lean mice, resident adipose tissue-associated macrophages (ATMs) act as modulators of energy metabolism and mitochondrial function in adipocytes by producing soluble factors such as IL-10 and catecholamines. They are polarised towards an anti-inflammatory phenotype and also contribute to lipid buffering by controlling the release of free fatty acids into the circulation as well as preventing insulin resistance by PPARγ signalling (*160*, *161*). Additionally, exposure to cold promotes the anti-inflammatory phenotype and release of catecholamines to induce adaptive thermogenic response in brown adipose tissue and lipolysis in white adipose tissue (*162*). However, another population of macrophages has been shown to be important in adipose tissue health – sympathetic neuron-associated macrophages (SAMs) found in the nerve bundles within adipose tissue. Pirzgalska *et al.* showed that SAMs acted as a sink for excess noradrenaline produced by the sympathetic neurons (*163*). In contrast to ATMs, they are primed to be pro-inflammatory and even though historically they might have developed to protect the body from excess noradrenaline release to the blood stream, they were shown to hamper adaptive thermogenesis in brown adipose tissue and have pro-obesity effect.

The skin harbours another classical population of tissue-resident macrophages, Langerhans cells (LCs), which were named after Paul Langerhans who discovered them in 1868 (*164*).

Throughout history their physiological role and ontology has been extensively debated. LCs have been classified by different groups as either tissue-resident macrophages or dendritic cells, however large transcriptomic data sets have provided evidence that they are indeed specialised tissue-resident macrophages (*130*). They express typical macrophage markers such as CD11b and F4/80 as well as CD11c and Langerin, which is a LCs-specific marker. Langerin is an endocytic receptor involved in formation of Birbeck granules and capture and degradation of HIV-1 virus (*165*, *166*). Additionally, LCs are involved in priming T cell responses in the skin (*167*)

Bone resident macrophage-like cells (osteoclasts) are multinucleated giant cells, which modulate continuous growth and remodelling of bones by performing bone resorption and maintaining calcium homeostasis. They are derived both embryonically and postnatally from the bone marrow (*168*). They colonise foetal ossification centres and are essential for healthy foetal bone development as the disruption of CD115 or RANKL in erythromyeloid progenitors resulted in severe bone deformation and lack of tooth eruption in newborn mice (*169*). Additionally, the same ligands induced CD68 expression on osteoclasts (typical macrophage marker) and genetic deletion of CD68 resulted in osteoclast accumulation and dysregulation of their bone resorbing function (*170*). However, osteoclasts also seem to have an immune function. Even though the exact mechanism are not known yet, significant bone destruction has been observed in chronic inflammatory conditions such as rheumatoid arthritis, periodontitis and inflammatory bowel disease (*168*). The relationship between osteoclasts and T cells seem reciprocal with osteoclasts acting as antigen-presenting cells and priming CD4 T cells, while Th17 helper T cells are able to induce osteoclast differentiation (*171*, *172*).

The bone marrow (BM) is the principal site of haematopoiesis in the adult organism and the original source of monocyte-derived macrophages. However, there are also two sub-populations of bone marrow tissue-resident macrophages inside the bone marrow cavity itself – erythroblastic island macrophages (EIMs) and haematopoietic stem cell niche macrophages (HSC niche macrophages) (*173*). Bone marrow as a tissue has a complex topology with multiple niches and microenvironments. The first BM resident macrophage population discovered was the EIMs, which are essential for the survival of erythroblasts during their maturation. They perform their function by secreting tropic cytokines such as erythroprotein, iron transport and phagocytosis of extruded nuclei (*173*, *174*). Their essential function was confirmed by Jacobsen *et al.* when depletion of EIMs, both by clodronate-loaded liposomes and selective CD169-targeting DTR mice, blocked erythropoiesis in the bone marrow (*175*). HSC niche macrophages are critical for maintenance and correct functioning of haematopoietic stem cell niches. Winkler *et al.* showed that depletion of HSC niche macrophages, using Mafia transgenic mouse or clodronate-loaded liposomes, led to the collapse of HSC niches and pathological mobilisation of haematopoietic stem cells into the blood stream (*176*).

1.3.4. Macrophages in pathologies beyond infectious diseases.

Macrophages are key players in cardiovascular pathologies. A common disease which is driven by macrophages is atherosclerosis – the build-up of fatty plaques in arteries. As seen in Figure 1.1, macrophages are involved in all stages of atheroprogression, from lesion formation to rupture, and account for 50% of immune cells found in the plaques (*101*, *177*). Atherosclerosis is initiated when factors such as high plasma cholesterol, hypertension and low or disturbed shear stress drive endothelial disfunction which leads to increased permeability to circulating apolipoproteins B-containing lipoproteins such as low-density

lipoprotein (LDL) (*178*). In particular, LDL and very low-density lipoprotein (VLDL) accumulate in sub-endothelial space and undergo aggregation, oxidation and enzymatic modifications (*179*). Activated endothelial cells express cytokines, chemokines and adhesion molecules such as CXCL1, CXCL2, CXCL3, CXCL4, CXCL8, CCL5, MCP-1, ICAM-1 and VCAM-1 and E- and P-selectins, which attract circulating monocytes (*180*). This early stages of atherogenesis are characterised by fatty streaks where activated endothelium causes monocyte migration into the sub-endothelial lipid depositions and drives their phenotypic change to macrophages (*178*). Importantly, deletion of chemokine receptors was shown to decrease macrophage content in the plaques, which can be interpreted as reduced migration of monocytes into the lesions (*181*). Although historically, monocyte migration into the plaque was considered as the main source of macrophages in the advanced lesions, there is now ample evidence showing the importance of local proliferation and self-renewal in response to M-CSF present in the plaque environment that drives macrophage accumulation (*182*).

Lipoprotein uptake by monocyte-derived macrophages and their transition into foam cells is one of the earliest pathogenic events in the developing atherosclerotic plaque. Although homeostatic macrophages are capable of clearing lipoproteins through their LDL receptor (LDLR), increased cellular cholesterol drives downregulation of this receptor early in the process of foam cell formation (*183*). Instead, modified LDL is recognised by other mechanisms – most importantly oxidised LDL binds to macrophage scavenger receptors SR-A1, SR-A2 (MARCO), CD36, SR-B1 and LOX1; internalisation by pinocytosis can also contribute to macrophage LDL uptake (*184*). SR-A1 ad CD36 have been shown to be instrumental in degradation of modified LDL by macrophages as their deficiency partially inhibited foam cell formation in $Apoe^{-/-}$ mice model of atherosclerosis (*185*). After internalisation, LDL particles

are trafficked to lysosomes and there broken down to free cholesterol and fatty acids. Free cholesterol is then re-esterified in the endoplasmic reticulum (ER) by ACAT1 enzyme (*184*). However, excessive cholesterol uptake leads to its accumulation in the ER membranes and defective esterification by ACAT1, which further increases cholesterol storage and ER stress. This mechanism contributes to increased apoptosis in progressing plaques, which is accompanied by impaired clearance of dying cells and eventually leads to necrotic core formation in advanced atherosclerotic plaques (*183*).

In established lesions macrophages can be separated into five distinct subtypes based on meta-analysis of single-cell RNA sequencing and mass cytometry data (*186*). The majority of macrophages in the plaques can be classified as resident-like macrophages as they express surface markers CD206 and CD169 and genes such as Lyve1 and Mrc1. Second most abundant cluster was foamy macrophages which express TREM2 and show low expression of pro-inflammatory genes. Inflammatory macrophages, also called non-foamy macrophages, were distinct because they are thought to be derived from circulating monocytes and express high levels of pro-inflammatory genes (TNF and IL1β) as well as chemokines (CXCL1, CXCL2, CCL2, CCL3 and CCL4). IFN-inducible macrophages were shown to express genes such as IFIT3, IRF7 and ISG15 and are proposed to be pro-atherogenic. Finally, cavity macrophages were found to be the smallest cluster of macrophages found in the plaques. They display characteristics of monocyte-derived macrophages and express CD226, CD11c and MHCII on their surface. Although their function is not known, CD11c expression has been previously correlated with high-fat diet and pro-inflammatory role (*177*, *186*). Additionally, as mentioned before, smooth muscle cells can acquire macrophage-like phenotype, which has detrimental effect on the plaques (*127*).

Inflammatory activation of lesional macrophages is driven by TLR activation of NF-κB signalling, where minimally oxidised LDL is recognised by TLR4 while moderately oxidised LDL is recognised by a heterodimer of TLR4 and TLR6. Moreover, TLR2 engages in cooperative signalling with CD36 and promotes apoptosis of macrophages undergoing ER stress (*183*). Additionally, cholesterol crystals present in the atherosclerotic plaques trigger NLRP3 inflammasome signalling (*183*). Chinetti-Gbaguidi *et al.* showed that human atherosclerotic plaques can harbour anti-inflammatory macrophages as well as the pro-inflammatory ones, which improves plaque stability (*187*). It is now appreciated that in human atherosclerotic plaques M1-like and M2-like macrophages co-exist at all stages of plaque development. M1 macrophages are dominant in rupture-prone shoulder regions, while M2 macrophages are found in vascular adventitia and stable regions of the plaque; interestingly, fibrous cap has been shown to have equal numbers of M1 and M2 macrophages (*188*). In the advanced atherosclerosis fibrous cap thinning, defective efferocytosis and expansion of the necrotic core lead to plaque vulnerability and can potentially result in plaque rupture. Vulnerable plaques are characterised by increased smooth muscle cell (SMCs) death and decreased collagen synthesis in the fibrous plaques. Additionally, macrophages have been shown to directly inhibit collagen synthesis by SMCs without killing the cells and degrade ECM components of the fibrous cap by producing matrix metalloproteinases, especially MMP-2 and MMP-9 (*178*, *189*). Plaque necrosis is triggered when apoptotic macrophages are not sufficiently efferocytosed in the plaque core and even though the exact mechanism of this defect is not know yet, defective efferocytosis has been proven to be a mechanism exclusive to the advanced lesions and not present in the earlier stages of plaque development (*190*). Necrotic core consists primarily of apoptotic macrophages that are not cleared by efferocytosis and in combination with the fibrous cap thinning can lead to the plaque rupture,

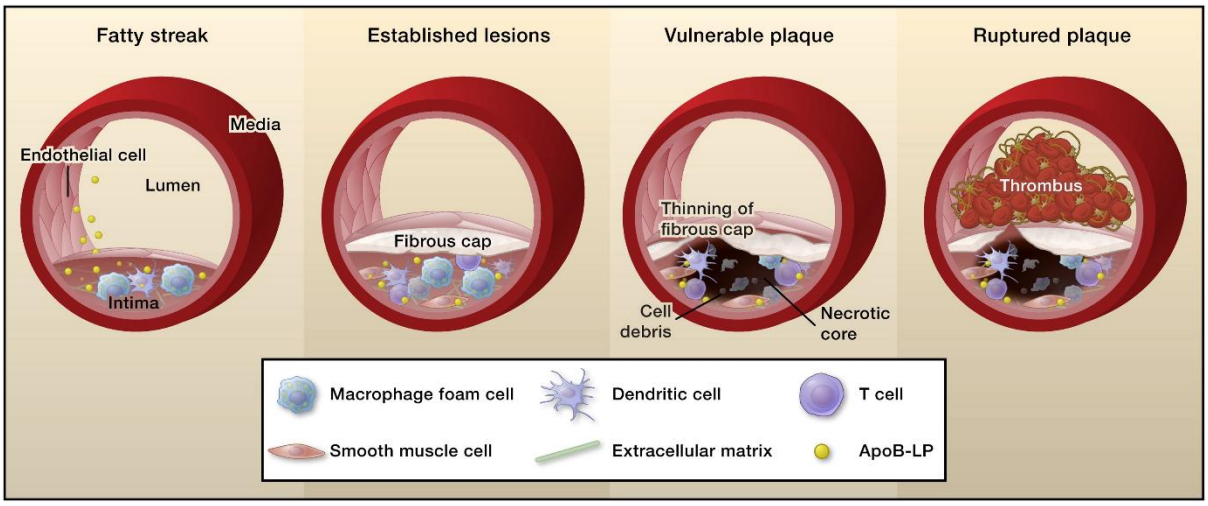

Figure 1.1. Progression of an atherosclerotic lesion. Fatty streak is the first stage of atherosclerotic lesion where endothelial damage and activation cause accumulation of circulating apolipoproteins B-containing lipoproteins (ApoB-LP) in subendothelial space and migration of dendritic cells and monocytes, which eventually engulf ApoB-LP and become macrophage foam cells. In established lesions, smooth muscle cells produce collagen that creates fibrous cap, a hallmark of a stable plaque. Additionally, T cells also migrate into the plaque. Vulnerable plaques are characterised by defective efferocytosis of dying cells, resulting in accumulation of cell debris and creation of the necrotic core, and thinning of the fibrous cap by matrix metalloproteinases produced by macrophages. Vulnerable plaques are at risk of rupture, when thrombus is created and can lead to a heart attack or stroke; figure adopted from Moore & Tabas, 2011 (189).

and subsequent thrombus formation and heart attack or stroke.

In myocardial infarction (MI) macrophages are crucial in the initial response but become detrimental over time. During the first stages of MI macrophages are actively engaged in recruitment of neutrophils and monocytes, efferocytosis and release of inflammatory mediators such as TNF, TGFβ, VEGF and matrix metalloproteinases (*101*). Whilst increased levels of TNF have been associated with increased mortality, TGFβ, VEGF and MMPs contribute to tissue remodelling and stimulation of angiogenesis (*191*, *192*). Overall, depletion of macrophages was shown to impair healing and cause worse outcomes for MI recovery (*193*, *194*). However, macrophages are also a double-edged sword as they were shown to keep expanding post-MI, leading to excessive scarring and eventual heart failure (*101*, *195*).

Macrophages are one of the key drivers of rheumatoid arthritis (RA) as they infiltrate the synovium and gain pro-inflammatory phenotype that contributes to the destruction of bone and cartilage. They have been shown to be the main producers of TNF in the diseased synovium, which is particularly important given the high efficacy of anti-TNF therapies (*196*). Additionally, a positive feedback loop is created where TNF-stimulated fibroblasts produce RANKL and M-CSF, which stimulates chronic osteoclast activity that erodes the bone (*197*). Macrophages also contribute to disease progression by constitutive secretion of CXCL8 and CCL2, which cause continuous recruitment of neutrophils and monocytes as well as by production of reactive oxygen species (*197*–*199*).

Expansion of adipose tissue due to over-nutrition leads to expansion of macrophage populations and their priming towards pro-inflammatory state, which contributes to low grade inflammation and insulin resistance. ATMs contribute to obesity and insulin resistance

by secreting pro-inflammatory cytokines such as IL-1β and TNF as well as recruitment of monocytes into WAT (*132*). Additionally, the sympathetic neuron-associated macrophages were found to accumulate noradrenaline in obesity models, which led to their pro-inflammatory activation and blunted lipolysis in WAT (*163*).

1.4. Mediators of acute inflammatory responses

1.4.1. Cytokines

Cytokines are a large class of low molecular weight proteins secreted mainly to modulate inflammation (*200*). They are broadly divided into monokines (monocyte-derived cytokines), lymphokines (lymphocyte-derived cytokines), chemokines (chemoattractant cytokines) and interleukins (ILs, cytokines made by and acting on leukocytes) with over 100 different proteins so far classified as cytokines (*200*, *201*). Most cytokines are short-lived and act locally in an autocrine and paracrine fashion, however some that are present in the blood (erythropoietin (EPO), transforming growth factor beta (TGFβ), and M-CSF), are capable of acting at a distance (*200*). These molecules orchestrate a variety of processes – their primary role is the regulation of local and systemic inflammation, but they are also involved in cellular proliferation, metabolism, chemotaxis, and tissue repair. However, the main principle behind their action is redundancy in the system – different cytokines perform similar functions and can bind the same receptors (*201*). They are produced mainly by immune cells although other cell types such as endothelial cells can also contribute (*202*). Each cytokine binds to a specific cell surface receptor (although the receptors are promiscuous for multiple cytokines) to initiate a signalling cascade that can lead to positive or negative regulation of several genes and their transcription factors. This in turn drives production of other cytokines, an increase in the

number of surface receptors for other molecules, or eventually suppression of the cytokine's own effect (*200*).

As seen in Figure 1.2, cytokines are essential for macrophage functioning – the cytokine profile in macrophage environment influences their polarisation state and therefore their function but also cytokine release is in itself a key function of macrophages (*109*). Cytokines can be either pro- or anti-inflammatory and their release is tightly linked with the phase of inflammation when they are released. Some of the most potent pro-inflammatory cytokines released by classically activated macrophages are tumour necrosis factor (TNF), IL-1, IL-6, IL-8, IL-12 and IL-23 which in turn can induce production of interferon gamma (IFNγ) (*200*). However, this is a positive feedback loop as the same cytokines, in particular TNF and IFNγ, in concert with other molecules such as LPS, can polarise macrophages towards a pro-inflammatory state. On the other hand, induction of alternatively activated macrophages can be achieved when anti-inflammatory cytokines such as IL-4 and IL-13 are present in the local environment, which can then induce the M2-like macrophages to produce further anti-inflammatory cytokines such as IL-10 and TGFβ (*200*).

1.4.2. Chemokines – chemoattractant cytokines

Chemokines are a specialised sub-family of heparin-binding cytokines, which are key mediators of leukocyte migration and tissue homing. During immune surveillance, chemokines are crucial in guiding cells of the immune system to where they are needed (sites of inflammation) (*203*). Some chemokines are also important during development by promoting angiogenesis, or by guiding cells to specific tissues (*200*). There are about 50 chemokines, which can be broadly classified into 4 classes: C, CC, CXC and CX_3C based on the location and arrangement of their conserved cysteine residues. They are named after the

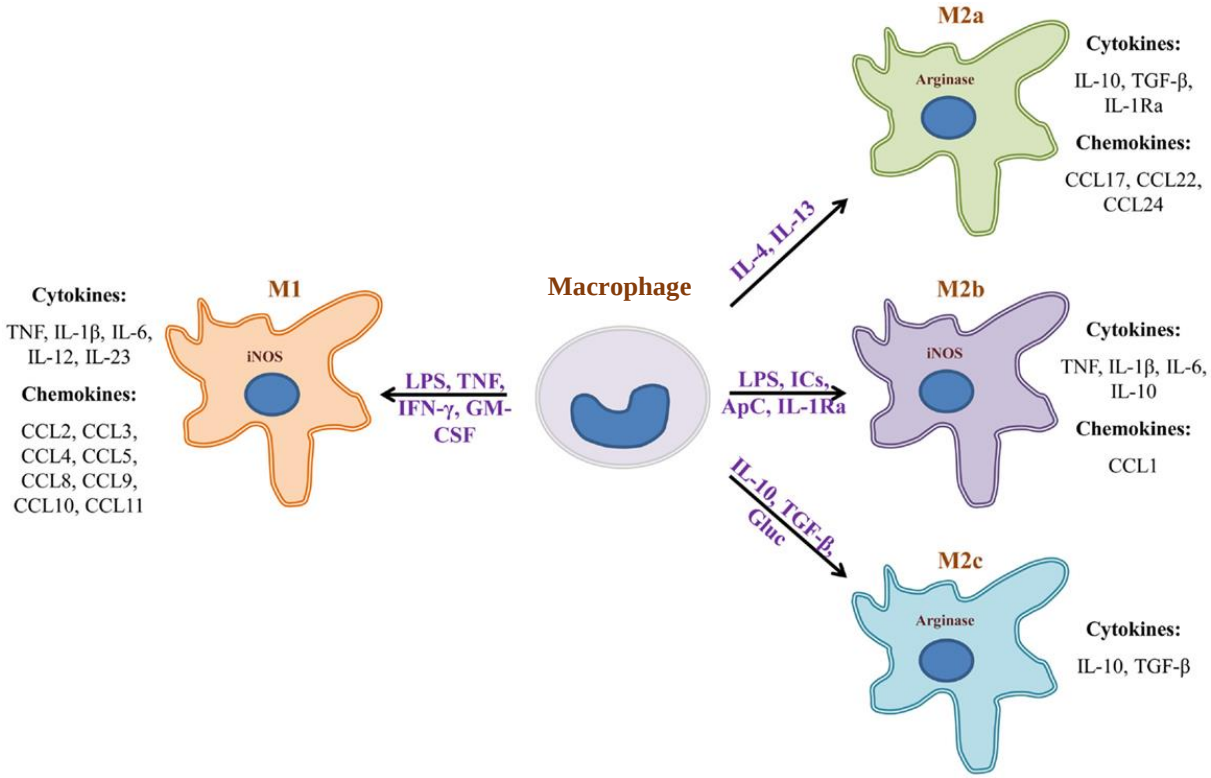

Figure 1.2. Cytokines profile of macrophage polarisation. Macrophages can be polarised to different activation states by a variety of cytokines, which determine their functions, including cytokine production. Pro-inflammatory (M1) macrophages are polarised by stimuli such as LPS or cytokines such as TNF, IFN-γ and GM-CSF. In turn, they produce cytokines such as TNF, IL-1β, IL-6, IL-12 and IL-13 and chemokines such as CCL2, CCL3. CCL4, CCL5, CCL8, CCL9, CCL10, CCL11. Anti-inflammatory macrophages (M2) have a slightly different cytokine profile depending on the stimulus that polarised them but in general they produce cytokines such as IL-10 and TGF-β; adapted from Duque & Descoteaux, 2014 (200).

class they belong to with the indication of them being a ligand, for example CCL2 or CXCL12 (*204*). Unlike other cytokines, all chemokines bind to G protein-coupled receptors (GPCRs), which are coupled to $G_{i/o}$ proteins. There are currently about 20 known promiscuous chemokine GPCRs, which are named after the chemokine classes that they bind, for example CCRs for CC chemokines and CXCRs for CXC chemokines (*205*).

Macrophages are highly migratory cells that respond to a wide range of chemokines and other molecules, which will be discussed in more details in section 1.6.1. of this chapter. However, since one of the key functions of macrophages in early stages of inflammatory response is recruitment of other immune cells, CXCL1 and CXCL2 (also known as macrophage inflammatory protein 2-α, MIP) are both secreted by monocytes and macrophages to recruit neutrophils and hematopoietic stem cells (*206*, *207*). CCL5, or the regulated upon activation normal T cell expressed and secreted (RANTES), induces migration of T cells, basophils, eosinophils, and dendritic cells to the site of inflammation but can also activate NK cells into chemokine-activated killers (CHAK) (*208*, *209*). CXCL8 (IL-8) is a potent chemoattractant for neutrophils, which also induces their degranulation. However, other cells such as keratinocytes, endothelial cells, eosinophils, and basophils can also respond to CXCL8 (*210*, *211*). CXCL9, also known as monokine induced by gamma interferon (MIG), is a strong T cell chemoattractant but it also mediates cell recruitment necessary for tissue repair (*203*). CXCL10, or interferon gamma-induced protein 10 (IP-10), is secreted not only by macrophages, but also by fibroblasts and endothelial cells and serves to attract T cells, NK cells, dendritic cells (*212*, *213*). Similarly to CXCL9 and CXCL10, CXCL11 (interferon gamma-induced protein 9, IP-9) is interferon-inducible and also mediates T cell recruitment, although more potently than CXCL9 and CXCL10 (*214*).

1.4.3. The complement cascade

The complement cascade is one of the oldest, evolutionary conserved pathways involved in defence against pathogens. It comprises of a series of over 30 plasma proteins circulating in blood and tissue fluids (*215*). The proteins are inactive at steady state but they become sequentially activated in an enzyme cascade (where the activation of one protein enzymatically cleaves and activates the next protein in the cascade) when a pathogen is detected. The main goal of this process is to opsonise noxious agents for easier detection and killing and direct lysing of the invading bacteria.

A seen in Figure 1.3, the complement cascade can be activated via three different pathways, which all converge on the activation of C3 protein, cleaving it into C3b, a large fragment that acts as an opsonin, and C3a (anaphylatoxin), a small fragment that acts as pro-inflammatory mediator. Classical pathway becomes activated by antibody-antigen complexes binding to C1 protein (*215*, *216*). Alternative pathway involves various factors, B, D, H & I, which interact with each other to create an amplification loop for C3. Alternative pathway is activated in the presence of bacterial and fungal cell walls, but is inhibited by molecules on the surface of normal mammalian cells (*215*). Finally, the lectin pathway is activated by the binding of mannose-binding lectin (MBL) to mannose residues on the pathogen surface. In all three cases, activated C3 triggers the lytic pathway, which can damage the plasma membranes of cells and some bacteria (*215*). In the lytic pathway C5 convertase cleaves C5 protein into C5a and C5b. C5a, which is an anaphylatoxin like C3a, is a potent chemoattractant for macrophages and neutrophils and also activates mast cells. C5b drives the formation of membrane attack complex (MAC) which is a multi-protein pore forming structure that can cause cell lysis (*166*, *167*).

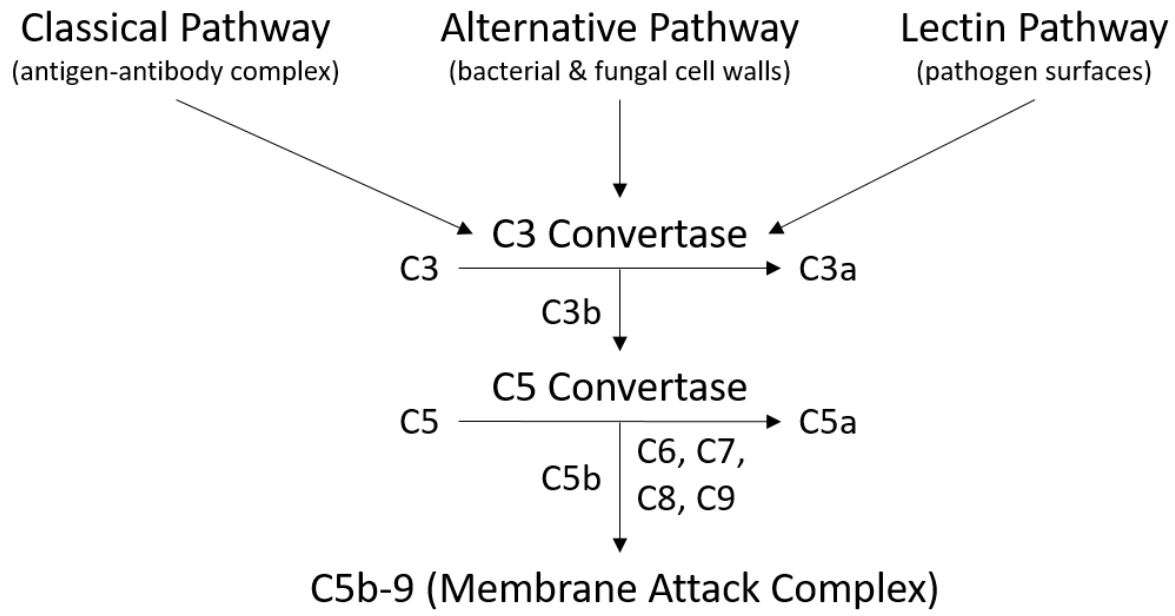

Figure 1.3. The complement cascade. There are three ways to activate the complement cascade depending on the stimulus, all of which converge on the cleavage of C3, which through the lytic pathway leads to formation of C5a and membrane attack complex.

1.4.4. Complement component C5a

Anaphylatoxin C5a is one of the main effectors of the complement cascade which acts as a potent macrophage chemoattractant, but its functions extend beyond its chemotactic ability. C5a is a 74-amino acids long glycoprotein which acts as a ligand to on two specific G protein-coupled receptors – C5aR1 (CD88) and C5aR2 (GPR77) (*217*). Once inactivated by carboxypeptidase, C5a loses the C-terminal arginine and becomes $C5a_{desArg}$, which is a low affinity ligand for CD88 and GPR77 (*218*). The main C5a receptor, C5aR1, is a canonical GPCR coupled to $G_{\alpha i2}$ and $G_{\alpha 16}$, where binding of the ligand triggers the downregulation of cAMP/protein kinase A signalling and activation of the kinase signalling cascade Raf-MEK1-ERK1/2 and subsequent intracellular calcium mobilization and β-arrestin recruitment. By contrast, C5aR2, although also a seven- transmembrane GPCR, is commonly recognized as incapable of G-protein coupling and therefore historically used to be considered as a decoy receptor. However, the current view of the field is that C5aR2 acts via β-arrestin signalling and has distinct physiological functions (*217*, *218*).

Lipopolysaccharide (LPS) is one of the most commonly used *in vitro* pro-inflammatory stimulants; it is derived from the bacterial cell wall of Gram negative bacteria and induces activation of PRR TLR4, which mediates induction of nuclear factor kappa B (NFκB). Seow *et al.* investigated the crosstalk between TLR4/C5aR signalling and found that C5a exposure of primary human monocytes and monocyte-derived macrophages from matched donors decreases LPS-induced secretion of pro-inflammatory mediators in macrophages but increased the production of the same mediators in monocytes (*219*). Haggadone *et al.* investigated this phenomenon further to show that C5a inhibits the NLRP3 inflammasome induction in LPS-stimulated macrophages, however it had the opposite effect in

monocytes (*220*). They also showed that while the monocytic response to C5a is solely dependent on C5aR1, macrophages do not require the expression of C5aR1 in this signalling pathway.

In disease context C5a signalling has been implicated in inflammatory conditions such as sepsis, obesity and asthma (*221*, *222*). Septic shock is a highly important unmet clinical need, given high mortality and lack of effective new pharmacological treatments for many years. Blocking C5a signalling by genetic ablation of both C5aR1 and C5aR2 has been shown to suppress G-MCF production in an *in vivo* model of sepsis, which is essential for neutrophil mobilisation (*218*). Additionally, blocking both C5a receptors have been shown to be protective in 'high-grade' sepsis and improve survival (*223*). As further evidence of the detrimental effects of C5a signalling during sepsis, C5aR2 has been shown to be downregulated on neutrophils during sepsis which was correlated with poor outcome for patients (*224*). Blocking C5a signalling with anti-C5a antibody preserved the loss of C5aR2 expression and improved outcomes in *in vivo* models therefore providing further evidence for important physiological functions of this receptor. C5a has been also shown to act on macrophages to drive obesity-associated inflammation and insulin resistance (*225*, *226*). C5a was found to stimulate uptake of glucose and fatty acids in adipocytes, while reducing lipolysis and blocking its action with anti-C5a antibodies ameliorated classic symptoms of obesity as well as reduced the number of pro-inflammatory macrophages in the adipose tissue and promoted the expression of anti-inflammatory IL-10.

1.5. Directional cell migration

1.5.1. General principles of chemotaxis

Directional cell migration can be observed in all living organisms, from bacteria to mammals. In unicellular organisms directional migration (called chemotaxis) serves as a simple mechanism to move the organism towards regions with high concentrations of beneficial substances (such as nutrients) or away from high concentrations of dangerous chemicals (such as toxins or antibiotics) (*227*). Specialisation of different cell types in a multicellular organism leads to specialisation of cell migration, where different cell types migrate via different mechanisms depending on the purpose of migration. Directional migration in mammals is fundamental during embryonic development, where it is involved in processes ranging from large-scale migration of cells during gastrulation to migration of single cells in the developing nervous system (*228*, *229*). In an adult organism chemotaxis is involved in maintenance of homeostasis but can also lead to pathological states such as tumour metastasis, angiogenesis and atherosclerotic plaque development (*230*–*232*). Migration of specialised eukaryotic cells can be sub-divided based on the signal the cells respond to, the physical movement and shape changes that the cells undergo or whether they migrate in single-cell or collective manner.

Single cell migration is mostly prominent in the adult organism (e.g. keratinocytes, fibroblasts and leukocytes migration) (*229*). The characteristic feature of single cell migration is that every cell polarises and moves individually in response to an attractant and therefore requires expression of the whole migratory machinery as well as receptors able to respond to the signal. On the other hand, collective migration occurs when cells interact with each other, both mechanically and chemically, to move as a coherent collective. This requires additional

mechanisms to maintain cohesiveness during movement and distributing polarisation across the whole collective (specialisation within the cluster to create front-rear asymmetry) (*171*, *172*). Collective migration is the predominant form of cell movement during development but has also been shown to contribute to cancer metastasis and wound repair (during reepithelialisation) (*233*). To date it has not been reported for any leukocyte populations and therefore will not be discussed further.

1.5.2. Types of signal-dependent migration

Directional cell migration is often broadly called chemotaxis. However, this term is technically only applicable to the directional migratory movement of cells up a concentration gradient of soluble signals (collectively known as chemoattractants) diffused in solution (*235*). In inflammation chemoattractants are usually cytokines released at the site of inflammation to orchestrate the inflammatory response (known as chemokines), however members of the complement cascade (such as complement C5a) and certain bacterial-derived molecules (e.g. fMLF and LPS) can also induce directional migration (*236*).

However, chemotaxis is not the only type of directional migration and a distinction can be made based on the signals that the cells are exposed to and the directionality of their movement:

1. Haptotaxis occurs when the chemoattractant gradient is surface-bound, for example to extracellular matrix or endothelium (*235*). Some argue that haptotaxis is the most physiologically-relevant form of leukocyte migration *in vivo*, since during extravasation cells need to adhere to endothelium and then migrate through the ECM, suggesting the need for surface-bound cues. However, there is an increasing appreciation that leukocyte

migration is most likely directed by the mixture of diffused and surface-bound chemoattractants (*235*, *237*).

2. Chemokinesis or haptokinesis happens when detection of a chemoattractant by cells causes morphological changes that lead to increased overall motility but lack of directionality of the movement. Chemokinesis can be induced either in the presence of a concentration gradient or in uniform concentration of a chemoattractant and therefore chemokinesis is an important control for chemotaxis studies (*238*, *239*).

3. Fugetaxis (also known as chemorepulsion) is defined as active migration of cells away from the source of the chemokinetic agents, which are in this case called chemorepulsants. It is thought that the interplay between chemotaxis and fugetaxis may be important in spacio-temporal regulation of leukocyte trafficking in organs such as bone marrow and thymus both in health and disease (*240*).

4. Necrotaxis occurs when necrotic and apoptotic cells release chemoattractive signals that regulate their removal. They can therefore be simultaneously chemoattractive and chemorepulsive to different cell types (*241*, *242*).

These definitions of cell migration can be applied regardless of any other conditions as they only describe the relationship between the chemokinetic agent and directionality of cell movement. It is however important to note that the same molecular mechanisms can be utilised for both positive migration (chemotaxis and haptotaxis) and negative migration (fugetaxis) or non-directional movement (chemokinesis).

1.5.3. Types of shape-dependent migration

A single migrating cell can be best described as a highly polarised entity where a rapid turnover of migratory machinery causes spatial segregation of cellular components within the cell, which in turn drives shape change and motion. However, this segregation and shape change are not ubiquitous among all migratory cell types and we can distinguish three discreet types of motion: amoeboid, mesenchymal and gliding (*243*). Amoeboid and mesenchymal migration are illustrated in Figure 1.4.

Gliding motion, also called processive migration, is unique to keratinocytes and maintains almost constant shape of cells during motion due to high level of coordination between the leading edge and the rear of the cell. Keratinocytes movement is highly directionally persistent. Cells polarise to a 'fan-like' structure where the leading edge encompasses up to a half of the cell perimeter and no distinct uropod is formed. This shape is maintained throughout the entire migration without any significant protrusions being extended (*244*).

Amoeboid migration, also called α-motility, is mainly utilised by leukocytes such as PMNs (*245*). Its characteristic features include the lack of firm adhesion points and extension of pseudopodia (actin-rich 3D structures). These features result in amoeboid movement enabling rapid cell migration up to 30 μm/min (*246*). Moreover, the migrating cells preserve the integrity of the extracellular matrix that they crawl over (*247*). Amoeboid movement is characterised by the 'hand mirror shape' where polarisation of the cell causes defined actin-rich leading edge that is responsible for sensing the environment and mitochondria-rich uropod that anchors the cell and propels it (*246*). The leading edge has a high turnover of actin filaments scaffolding that builds the pseudopodia and high density of receptors, which bind chemokinetic ligands with highly sensitivity. Those receptors are mainly G-protein

coupled receptors coupled to $G\alpha_i$ protein (pertussis-toxin sensitive). Activation of these receptors leads to engagement of PI3K and subsequent activation of Akt kinase and its downstream GTPases Cdc42 and Rac (*248*). Ultimately this signalling cascade is responsible for actin polymerisation at the leading edge by engaging Arp2/3, which is activated by WAVE(SCAR) and WASP proteins. It has been shown that WASP and SCAR are essential for amoeboid migration and their inhibition causes profound defects in migration. Co-expression of WASP and SCAR is therefore a hallmark of amoeboid movement (*249*). The uropod has a mainly anchoring function and is characterised by the enrichment of myosin II.

Mesenchymal migration is characteristic of fibroblasts and smooth muscle cells and exclusive to animal cells. It is much slower than amoeboid migration, with cells travelling less than 1 µm/min (*246*). During mesenchymal movement the leading edge and uropod are much less defined with multiple lamellipodia (2D sheets-like membrane extensions) being extended in all directions. Hallmarks of mesenchymal movement are creation of strong adhesion points and degradation of ECM that accompanies the movement (*246*). Fibroblast migratory cycle is probably the best described mechanism of migration to date. The initial steps in the signalling cascade are shared with amoeboid movement: GPCR activation signals via PI3K/PIP3 pathway to activate small GTPases Cdc43, RhoA and Rac that in turn activate Arp2/3. Arp2/3 activation leads to actin polymerisation and protrusion of lamellipodia (*250*). However, unlike in amoeboid movement, during mesenchymal migration RhoA and Cdc42 are responsible for activation of formins mDia1 and mDia2 respectively. Formins are actin nucleators that help to create nascent adhesions at the leading edge of the cells and then connect them to the mature adhesions in the mid-region of the cells (*251*). Actomyosin contractility then causes

the strengthening of the nascent adhesion points at the leading edge while myosin II disassembles the adhesion points at the rear of the cell enabling movement forward.

1.6. Macrophage chemotaxis

Even though the unique plasticity of macrophages has been recognised in many of their functions, including chemotaxis, their motility is still often discussed alongside other leukocytes assuming that they share common migratory mechanism (*246*, *252–254*). This may partially be due to the limitations of current chemotaxis assays, which do not provide easy ways to compare different leukocytes and highlight the differences between them. Regardless of their origin, macrophages are a part of the immune system and therefore historically were expected to use the same mechanisms as other leukocytes. Given that monocytes are direct precursors to tissue infiltrating macrophages the two cell types have often been grouped and discussed together assuming that the migratory machinery is preserved between them. However, recent evidence shows that macrophage migration is much more varied than monocytic chemotaxis and does not follow the exact same pathways.

1.6.1. Molecular mechanism of macrophage chemotaxis and common macrophage chemoattractants

Macrophage migration is complex because it integrates pathways involved in both amoeboid and mesenchymal movement and has been summarised in Figure 1.5 (*255*). Macrophages can induce migration in response to a wide range of different chemoattractants, thanks to the variety of receptors that they express (summarised in Table 1.1). Activation of all those receptors culminates in a common signalling pathway: phosphoinositide 3-kinase (PI3K) activation leads to conversion of PI 4, 5-bisphosphate (PIP2) to phosphatidylinositol 3, 4, 5-trisphosphate (PIP3) at the cell membrane of the leading edge (*257*) . Accumulation of PIP3

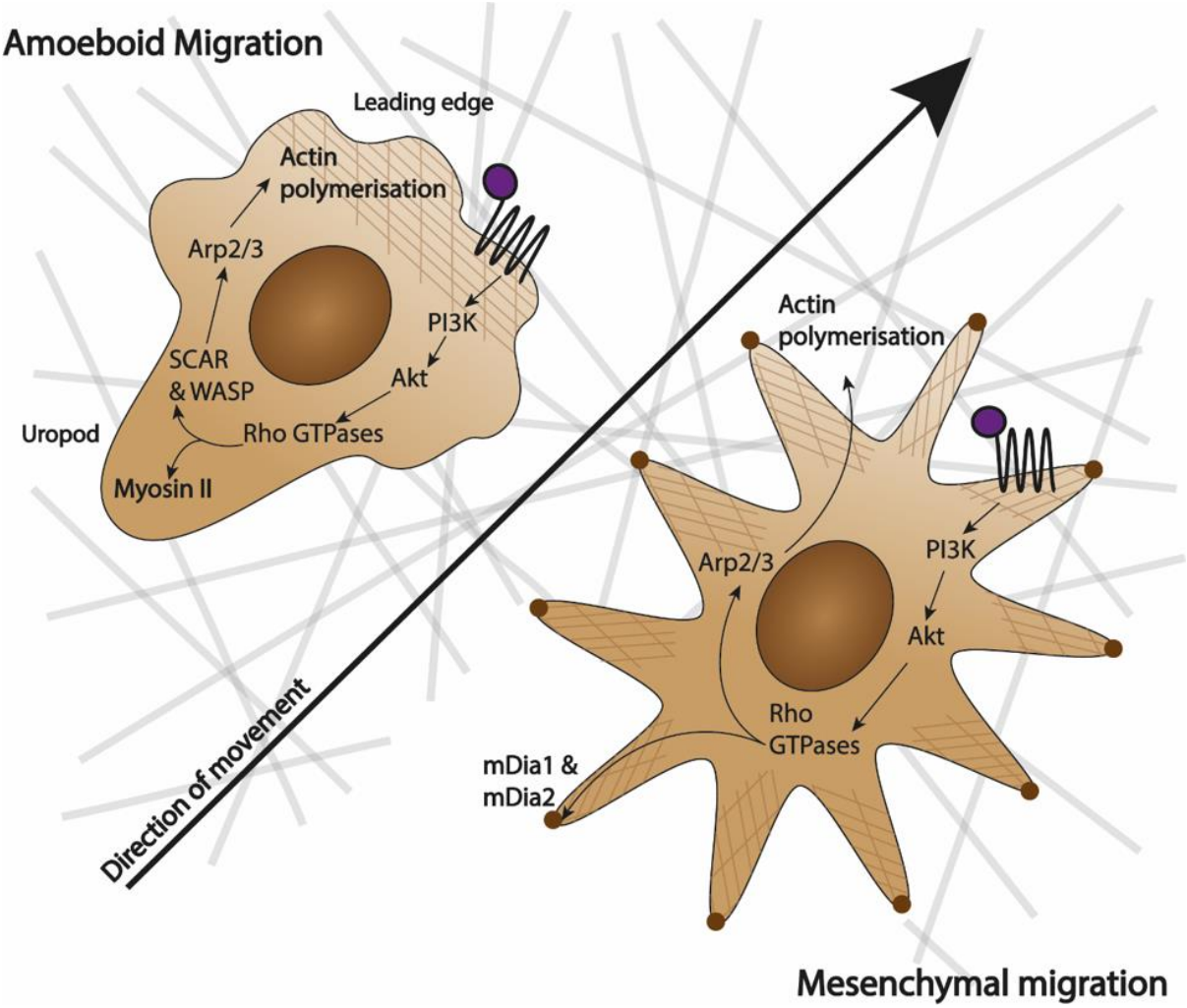

Figure 1.4. Similarities and differences between amoeboid and mesenchymal movement. Amoeboid migration is characterised by a 'hand-mirror' cell shape with a clear leading edge and a uropod whilst mesenchymal migration does not have a defined shape and is characterised by multiple lamellipodia being extended. Amoeboid cells do not degrade extracellular matrix (ECM) that they move on (represented by the grey lines) while mesenchymal cells do. When a chemoattractant attaches to a receptor (purple dot attaching to 7 transmembrane domains) in both cases it activates PI3K/Akt cascade that leads to Rho GTPases. In amoeboid cells Rho GTPases either directly activate Myosin II in the uropod or cause actin (represented by brown grid) polymerisation at the leading edge by activating SCAR and WASP proteins and subsequently Arp2/3. In mesenchymal cells Rho GTPases either activate formins mDia1 and mDia2 to create adhesion points (brown dots) to the ECM or acting via Arp2/3 cause actin polymerisation that leads to extending of lamellipodia. (published in (*256*)).

at the leading edge stimulates activation of kinases and GTPases which contain pleckstrin homology (PH) domain such as PDK1, Akt and Vav (leukocyte-specific nucleotide-specific factor). Vav is thought to activate Rho family of GTPases (*258*). Fluorescence resonance energy transfer (FRET) has been used to show that the members of the Rho family expressed in migrating macrophages are RhoA, Rac and Cdc42, and all are constitutively active at the leading edge of macrophages (*259*). They are responsible for actin polymerisation with each playing a specific role in the migratory process. Rac is thought to be involved in membrane ruffling and protruding lamellipodia while Cdc42 is responsible for filopodia formation (*260*, *261*). Both Rac and Cdc42 are involved in creation of focal complexes, while Cdc42 is also specifically involved in podosome formation (*260*). Both Rac and Cdc42 act by activating of Arp2/3 but Rac activates SCAR, while Cdc42 acts on WASP to induce cell movement (*261*, *262*). Rho does not act via Arp2/3 activation but instead is responsible for actomyosin contractility by activating Rho kinases (ROCKs), which acts via PTEN (*263*). It has been suggested that Rac and Rho mediate macrophage motility, while Cdc42 is responsible for chemoattractant sensing and cell polarisation (*260*).

When a chemokinetic signal is sensed by a macrophage (and follows the above pathway), migration is initiated by Rac-mediated membrane ruffling and lamellipodium extension. The lamellipodia then progress into filopodia once the cell has gained directionality (*260*). This reorganisation of the cell membrane requires constant formation of new attachments between the cell and the ECM. These come in a form of focal complexes in lamellipodia and podosomes in filopodia, which are driven by two main groups of proteins: formins (Dia1, Dia2 and FMLN1) and focal adhesion kinases (FAK and Pyk2) (*251*, *264–266*). Podosomes are rosette-like structures that contain over 200 proteins and are formed on the surface of

Chemoattractant	Reported concentrations	Macrophage receptor	Receptor type	Type of cells used
C5a	10 nM	C5aR1	GPCR	BMDMs, RAW264.7 (*267*)
CXCL12	50 ng/mL, 100 nM	CXCR4/CXCR7	GPCR	BMDMs (*265*, *268*)
CSF-1	1.32 nM, 120 ng/mL	CSF-1R	RTK	BAC1.2F5, BMDMs (*265*, *269*)
LPS	100 ng/mL	TLR4	PRR	BMDM (*270*)
CCL2	10 ng/mL, 10 nM	CCR2/CCR4	GPCR	Thioglycolate-elicited MØs, Biogel-elicited MØs (*271*, *272*)
CCL5	20 nM	CCR1/CCR3/ CCR5	GPCR	Thioglycolate-elicited MØs, Biogel-elicited MØs (*272*)
Leptin	1 ng/mL	LepR (ObR)	Class I cytokine receptor	Thioglycolate-elicited MØs (*271*)
CCL3	1-100 nM	CCR1/CCR5	GPCR	Biogel-elicited MØs, Thioglycolate-elicited MØs, BMDMs (*265*, *272*)
Chemerin	5 nM	ChemR23	GPCR	Bio-gel elicited MØs (*272*)

Table 1.1. List of reported macrophage chemoattractants and their respective receptors.

monocytic migratory cells to create integrin-mediated adhesion to the ECM (*266*). They are called 'macrophage feet' and have been shown crucial in promoting the movement through the ECM by directing matrix degradation and remodelling. Formins are actin nucleators, and they are the key components of podosomes. They stabilise podosome assembly and regulate WASP to induce actin polymerisation towards the podosome (*266*). Focal complexes are smaller and shorter-lived than podosomes and found mainly at the leading edge of a migrating cell. All extended lamellipodia create multiple focal complexes, which never fully mature and are dispersed as the lamellipodium retracts (*265*). In response to integrin activation upon contact with the ECM, FAK and Pyk2 are incorporated into a complex with the integrin molecules and engage their effectors: Src, paxillin and PLC-γ. This assembly then creates a feedback loop where PLC-γ signals to PI3K and that in turn activates Rac/Cdc42 signalling that promotes actin remodelling and migration (*264*, *265*).

1.6.2. Amoeboid versus mesenchymal movement of macrophages

Macrophages possess migratory machinery characteristic to both amoeboid and mesenchymal movement. They are WASP/SCAR-dependant which has been previously described as an essential feature of amoeboid but not mesenchymal migration (*249*, *262*). They also the create adhesion structures called podosomes, which provide transient yet stable adhesion and are capable of ECM degradation, a feature supposedly exclusive to mesenchymal migration (*261*, *266*). This has lead researchers to hypothesise that macrophages are capable of switching between amoeboid and mesenchymal migration modes, depending on the biophysical structure of the ECM that they have to migrate through (*273*). Such a phenotypic switch is beneficial in tumour cells, where it has been termed 'migration plasticity' (*274*). Even though migration plasticity has been observed in tumour cells all other leukocytes have been reported to use exclusively amoeboid movement

(*211*, *212*). The exceptional migration mode of macrophages might be a result of their diverse origins or an adaptation to their diverse functions.

The speed of macrophage migration varies greatly from the speed of typical amoeboid or mesenchymal migrators such as neutrophils and fibroblasts respectively. Leukocytes move on average about 20-30 µm/min while fibroblasts are traditionally thought to move <1 µm/min (*246*, *257*). Macrophages *in vitro* have been shown to move around 1 µm/min, however *in vivo* in response to injury in zebrafish they have been shown to exceed 10 µm/min (*257*, *276*). That intermediate speed of migration suggest an interplay between each of the migratory mechanism, where adhesions to the ECM slow down the macrophages, in comparison to other leukocytes, however macrophage adhesions are not as strong as those seen in typical fibroblast-like mesenchymal migration (*112*). Such intermediate migratory potential seems to reflect the unique function of macrophages. Tissue-resident macrophages do not require rapid migration as they are sentiel cells. When they encounter tissue damage resident macrophages mainly release pro-inflammatory cytokines that attract neutrophils and monocytes to the side of inflammation (*103*). Therefore, it is more crucial for other leukocytes to be fast migrators than for macrophages. The other main function of macrophages, both resident and monocyte-derived, is tissue repair during resolution of inflammation (*103*). Again, macrophages must be able to efficiently migrate towards apoptotic cells but do not need to slowly lay down the new ECM like fibroblasts, hence their intermediate migration speed might be the most optimal for their function.

Macrophage polarisation greatly influences their functional responses, skewing them either towards acute production of pro-inflammatory cytokines and phagocytosis in M1 state or

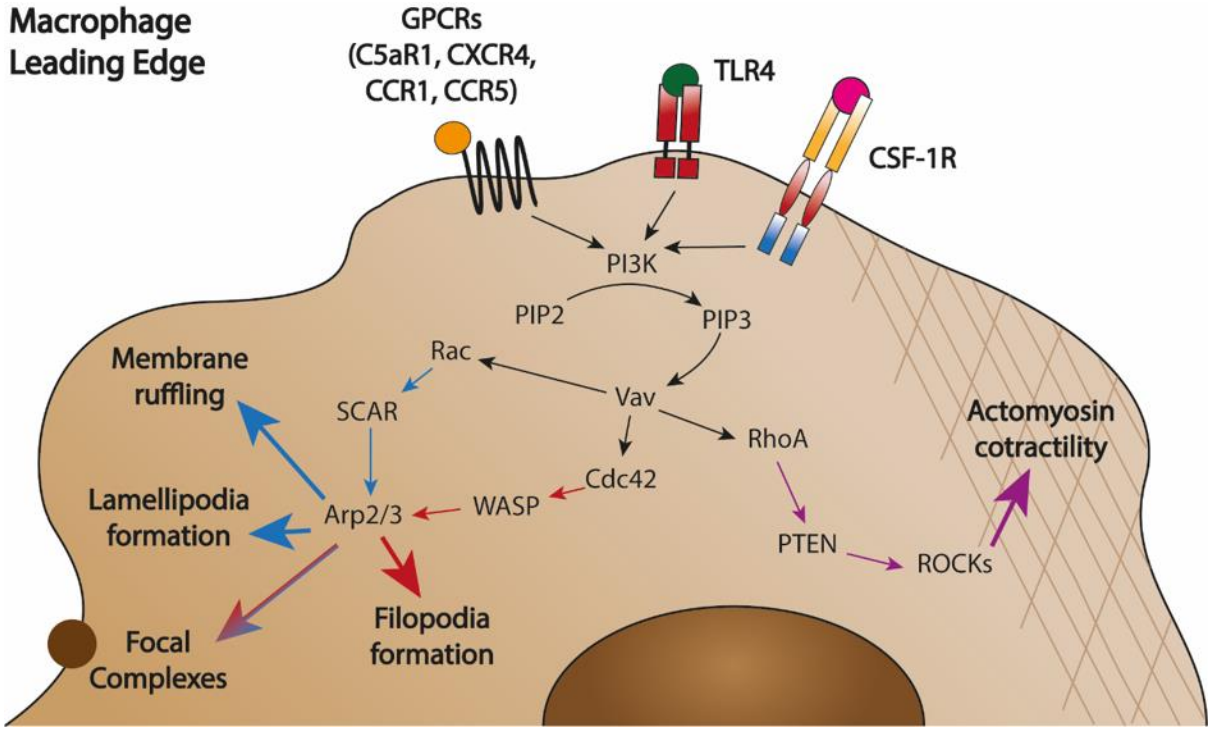

Figure 1.5. Simplified diagram of the molecular pathway inducing macrophage migration at the leading edge. Different chemoattractants (represented by coloured circles) bind to different receptors (exemplified on the diagram) which converge on a common pathway. PI3K converts PIP2 to PIP3, which in turn activates the Vav GTPase. Vav then activates the Rho GTPases Rac, Cdc42 and RhoA. Rac acts via SCAR to activate Arp2/3 while Cdc42 acts via WASP to activate Arp2/3. Rac is ultimately responsible for membrane ruffling and lamellipodia formation while Cdc42 drives filopodia formation; both Rac and Cdc42 are needed for the formation of focal complexes (represented by brown dot). RhoA acts via PTEN to activate ROCKs and ultimately cause actomyosin (represented by brown grid) contractility at the leading edge.

production of anti-inflammatory cytokines and initiation of wound repair processes in M2 (*112*). Cui *et al.* showed that this plasticity also translates into changes in chemotactic potential (*112*). They showed that due to intermediate levels of expression of CD11b and CD11d thioglycolate-elicited peritoneal M2-polarised macrophages had a higher migration capacity towards CCL2 than naïve resident or M1-polarised macrophages. This was attributed to resident macrophages having a high expression of integrin CD11b and M1-polarised macrophages upregulating their CD11d expression, both resulting in increased adhesion to ECM components that hindered the movement (*112*). A similar phenomenon was observed in human monocyte-derived macrophages by Vogel *et al.* to a wider array of chemoattractants, however the authors saw no difference in adhesion (*277*). Instead, they attributed the observed increase in chemotaxis of M2 macrophages to differences in actin rearrangement. According to their study M1-polarised macrophages were unable to form filopodia and instead adopted more spherical (amoeboid-like) shape, which prevented effective migration.

1.7. Unanswered questions in macrophage biology

Macrophages are one of the most morphologically, ontogenically and functionally diverse mammalian cell types. Even though their existence has been known since the 1800s there are still many unanswered questions about their biology and role in pathology. Whilst it is generally agreed that tissue-resident macrophages are of embryonic origin, there are conflicting accounts of the exact origin of those macrophages and how tissue-resident populations are renewed during adulthood. While single cell sequencing data sets can provide insights into the transcriptional differences and the general heterogeneity of these populations they rarely pinpoint the reasons that lie behind this variety. Since local

environment is known to shape the phenotype of different macrophage populations, the question arises as to what keeps these different sub-populations residing in the same organ separate. Another layer of complexity comes from the inter-species variability and hugely different environments that experimental mice and rats and general human population are exposed to. One might question the relevance of the specific germ-free conditions that we keep the mice in when our own bodies are exposed to millions of pathogens since the minute we are born.

Migration is one of the defining features of macrophages, often used as a functional readout in *in vitro* studies and yet there are surprising gaps in our understanding of this complex process. The ability to switch between the amoeboid and mesenchymal migration is unique to macrophages, however we do not know what governs that process other than the 3D structure that the macrophages find themselves in. In addition, it is reasonable to assume that tissue-resident macrophages are simultaneously exposed to multiple surface-bound and soluble chemoattractants, all of which constantly changing gradients. Therefore, macrophages have to constantly make decisions as to their route of travel and which chemoattractant gradient to follow. Very little is known about this process of cellular decision making during migration, with one of few studies on mammalian immune cells indicating that dendritic cells tend to follow the path of the least resistance in porous environments (*278*). Whether the same is true for macrophages or whether changes in gradients alone influence their movement remains to be elucidated.

One of the key limitations in advancing the understanding of macrophage biology and how they differ from other innate immune cells is the lack of *in vivo* and *in vitro* tools which can capture their uniqueness. Current 'macrophage-targeting' mouse models often target with

equal, if not better, efficiency other populations such as neutrophils, monocytes and dendritic cells. Similarly, migration assays are generally designed to look at all migratory cell types and lack the ability to study the complexity of macrophage chemotaxis, for example their transition between the amoeboid and mesenchymal movement or their responses to shifting gradients. Therefore, at the start of my graduate studies in 2017 there was a clear need to develop novel *in vivo* and *in vitro* techniques, which are crucial for addressing any of the aforementioned unanswered questions in macrophage biology.

1.8. Original hypothesis

At the start of my studies I wanted to expand the current toolkit of methods available to study macrophage biology. As such, this is a technology development-driven thesis and does not have *per se* an original biological hypothesis. However, I hypothesised that with my studies I could improve upon the already available techniques to study macrophages *in vivo* and *in vitro* and that, using my novel tools, I would be able to observe previously unknown features of macrophage biology.

1.9. Experimental aims

The importance and extent of technology development in my project has greatly expanded since the beginning of my graduate studies. Initially I was planning to only focus on the *in vitro* assay development, however the project evolved to incorporate phenotyping of a novel *in vivo* model. As such, I set out the following experimental aims for this thesis:

- To thoroughly phenotype a novel tamoxifen-inducible hCD68-CreERT2 mouse lines, which was created for the Greaves laboratory as a possible improvement in macrophage targeting compared to the constitutively expressed hCD68-GFP mouse line.

- To validate this mouse in a model of macrophage-driven disease (atherosclerosis) and to compare it to existing lines that are commonly used to target macrophages.

- To create and validate an *in vitro* chemotaxis assay using Freestyle Fluidics, which will improve the flexibility of design, control of the gradients and imaging of cell migration.

- To use this novel *in vitro* assay to study macrophage responses to changes in chemoattractant gradients.

Chapter 2

Materials and Methods

2.1. Reagents

All reagents were bought from Sigma-Aldrich unless otherwise specified. Recombinant mouse complement component 5a (C5a) was bought from R&D Systems. Recombinant mouse chemokine CXCL12 was bought from Peprotech. 60 mm and 35 mm Petri dishes as well as microplates were bought from Corning. Molecular grade agarose was bought from Bioline. BioMix Red was purchased from Meridian. Penicillin plus streptomycin (P/S) and ACK lysing buffer were bought from Gibco. Tamoxifen was bought from MP Biomedicals. DNas2. e I was bought from ThermoFisher Scientific. Fluorophore-conjugated flow cytometry antibodies and the unconjugated CD16/32 antibody were all bought from BioLegend apart from FITC-CD8a, which was bought from BD Biosciences. eBioscience FOXP3/Transcription Factor Staining Buffer Set, the UltraComp eBeads™ Compensation Beads, SYBR Safe DNA gel stain and ProLong Gold antifade reagent were bought from InVitrogen. OCT matrix for embedding frozen sections was bought from CellPath. Sucrose 'AnalaR' was bought from BDH Reagents & Chemicals. Fluorocarbon FC40 was made in-house by iotaSciences.

2.2. Animal experimentation

2.2.1. Ethical statement

All animal experiments were conducted in accordance to the Animal (Scientific Procedures) Act 1986, with procedures reviewed by the Sir William Dunn School of Pathology (SWDSOP) ethical review body (AWERB) and conducted under project license P144E44F2 at the University of Oxford. I hold a personal licence IC72AF226 and have been authorised to

perform Schedule 1 procedures. All animal experiments were performed according to the guidelines from the National Centre for the Replacement Refinement & Reduction of Animal Research (NC3Rs). I addressed reduction by obtaining the greatest possible number of tissues to process from each animal per experiment, which resulted in fewer mice being used. Additionally, tissues that were not used in my experiment were offered to my collaborators. I addressed refinement by optimising the tamoxifen dosing protocol to avoid any unnecessary side-effects to the mice. In regard to replacement, the benefit of using primary mice cells over cell lines in the chemotaxis experiments meant that I chose not to replace primary mouse cells in my project.

2.2.2. Mouse strains and husbandry

C57BL/6 mice were bred locally (used to extract bone marrow for experiments in Chapter 4) in the Pathology Support Building at the University of Oxford or bought from Charles River (used for breeding). The Balb/c mice were bought from Charles River. C.129S4(B6)-C5ar1tm1Cge/J (C5aR1$^{-/-}$) mice were bought from the Jackson Laboratory. B6.129P2-Lyz2tm1(cre)Ifo/J (LysM-Cre) and Gt(ROSA)26Sortm27.1(CAG-COP4*H134R/tdTomato) (tdTomato$^{fl/fl}$) mice were originally bought from the Jackson Laboratory, however studs for my colonies were kindly donated by the Sibson Lab at the Department of Oncology and the Channon Lab at the Wellcome Trust Centre for Human Genetics at the University of Oxford. The C57BL/6-Tg(CD68-EGFP)1Drg/J (hCD68-GFP) mouse was originally developed in the Greaves lab and maintained in-house ever since (*279*). All colonies were maintained in-house after the initial purchase or donation and genotype of the offspring was confirmed using PCR. Animals were housed in individually ventilated cages (between 2 and 6 mice per cage) in specific pathogen free conditions. All animals were provided with standard chow and water

ad libitum and, maintained on a 12 h light: 12 h dark cycle at controlled temperature (20–22°C) and humidity.

2.2.3. Generation of hCD68-CreERT2 mouse line[1]

A tamoxifen inducible Cre recombinase cDNA (CreERT2) was cloned downstream of a CD68 promoter, consisting of 2.9 kb of CD68 5' flanking sequence with the 83-bp first intron (IVS-1) of the CD68 gene (*280*), together with a rabbit beta-globin polyadenylation sequence. This transgenic cassette was subcloned into the pExchange4-CB9 vector suitable for PhiC31 integrase mediated cassette exchange at the Gt(ROSA)26Sor locus (*281*). The resulting vector, CB9-CD68-CreERT2 contained a promoterless neomycin phosphotransferase cassette, upstream of CD68-CreERT2-pA, and the whole array was flanked by PhiC31 attP sites.

CB9-CB68-CreERT2 DNA (5 μg) was electroporated into 1 × 106 RS-PhiC embryonic stem cells, a C57BL/6N JM8F6 derived line (*282*), using the Neon transfection system (Life Technologies) (3 × 1400 V, 10 ms), and selected in 210 μg/ml G418 for 7 days. Resistant colonies were isolated, expanded and screened for correct cassette exchange at the Gt(ROSA)26Sor locus using primers CAG-F (5'-CAGCCATTGCCTTTTATGGT-3) and ExNeo2 (5'-GTTGTGCCCAGTCATAGCCGAATAG-3') to verify the 5' integration event and att-F1 (5'-GCACTAGTTCTAGAGCGATCCCC-3') and 3HR-R1 (5'-CGGGAGAAATGGATATGAAGTACTGGGC-3') to verify the 3' integration event. Recombinant ES cells were injected into albino C57BL/6J blastocysts, and the resulting chimeras were bred with albino C57BL/6J mice to confirm germline transmission.

[1] Generation of hCD68-CreERT2 mouse was done in the Wellcome Trust Centre of Human Genetics by Dr Ben Davies before I joined the project.

2.2.4. Breeding strategies

Breeding strategies were optimised to reduce numbers of animals used. All founder colonies (hCD68-CreERT2, tdTomato$^{fl/fl}$ and hCD68-GFP) were bred by crossing heterozygous males from those colonies with wild type (WT) C57BL/6 females. C5aR1$^{-/-}$ colony was bred exclusively by crossing homozygous males and females. In Chapter 3, tdTomato$^{fl/fl}$ heterozygous females were crossed with either hCD68-CreERT2 heterozygous males or LysM-Cre heterozygous males. Offspring in all colonies were genotyped to confirm presence of transgenes. Mice which were heterozygous for both hCD68-CreERT2 and tdTomato transgenes (hCD68-tdTom mice) or LysM-Cre and tdTomato (LysM-tdTom mice) were used to assess Cre-recombinase efficacy. In both cases littermates were used as negative controls.

2.3. Genotyping by PCR

All mice bred from heterozygous parents were ear notched for identification and the notches kept for genotyping. C5a$^{-/-}$ mice were genotyped when initially bought to confirm the lack of C5aR1 but given the hom x hom breeding strategy the offspring of the founders were not routinely genotyped. DNA was extracted from the ear notches by boiling them for 30 min in 95^{o}C in DNA extraction buffer (25 mM NaOH, 0.2 mM EDTA; pH = 12). Reaction was stopped by first putting samples on ice and then adding an equal volume of neutralising buffer (40 nM Tris-HCl; pH = 5). Extracted DNA was amplified by PCR using BioMix Red and primers listed in Table 2.1 in the SimpliAmp thermal cycler (Applied Biosciences). Presence of the transgenes was confirmed by gel electrophoresis. 1% agarose gels with SYBR Safe DNA gel stain were run for 45 min at 120 volts and were subsequently imaged using iBright FL1000 imaging system (InVitrogen).

2.4. Bone marrow-derived macrophage culture

Bone marrow was extracted from femurs and tibias of male mice by flushing it out with Dulbecco's Phosphate Buffered Saline (DPBS) and a gauge 25 needle and frozen for up to 6 months in -80^{o}C prior to use in Foetal Bovine Serum (FBS) + 10% dimethyl sulfoxide (DMSO). Upon defrosting the bone marrow was cultured in triple-vented TC non-treated 9 cm Petri dishes for 7 days (37°C, 5% CO_2) in high-glucose Dulbecco's Modified Eagle's Medium (DMEM) enriched with 10% L929-conditioned media (in-house derived, containing macrophage colony-stimulating factor), 10% FBS and 1% P/S. 8 ml of media was used for the first 4 days; then, on day 5 of differentiation 3 ml of media was removed and replaced with 5 ml fresh media. Cells were gently lifted off the Petri dishes using a cell scraper and plated in well plates, 35 mm or 60 mm Petri dishes on day 6, and experiments were performed on day 7. Quality of BMDM culture was assessed with flow cytometry (as seen in Figure 2.1) with over 95% of cultured cells expressing CD45, F4/80 and CD11b and therefore being classified as BMDMs.

2.5. Tamoxifen preparation and dosing

Tamoxifen or 4-hydroxy tamoxifen were dissolved in 100 % ethanol followed by dilution in peanut oil to a final concentration of 10 mg/ml. 8 to 13-week-old male and female mice were given tamoxifen (2 mg per day for 5 days via oral gavage) or pure peanut oil as vehicle control. Mice were killed humanely and tissues harvested as indicated in Chapter 3 timelines.

Mouse strain	Primer	Sequence
C5aR1$^{-/-}$	WT Forward	5’ - GGT CTC TCC CCA GCA TCA TA
	Mutant Forward	5’ - GCC AGA GGC CAC TTG TGT AG
	Common Reverse	5’ - GGC AAC GTA GCC AAG AAA AA
hCD68-CreERT2	Tie2cre Forward	5' - GCATAACCAGTGAAACAGCATTGCTG
	Tie2cre Reverse	5' - GGACATGTTCAGGGATCGCCAGGCG
hCD68-GFP	CD68 Forward	5’ - GGGAAAGGAGTGGAACCG
	IVS Reverse	5’ - TGGCAGAGAGGAGATGGTT
LysM-Cre	Tie2cre Forward	5' - GCATAACCAGTGAAACAGCATTGCTG
	Tie2cre Reverse	5' - GGACATGTTCAGGGATCGCCAGGCG
tdTomato$^{fl/fl}$	WT Forward	5’ - AAG GGA GCT GCA GTG GAG TA
	WT Reverse	5’ - CCG AAA ATC TGT GGG AAG TC
	Mutant Forward	5’ - CTG TTC CTG TAC GGC ATG G
	Mutant Reverse	5’ - GGC ATT AAA GCA GCG TAT CC

Table 2.1. List of primers used for genotyping transgenic animals used in this study.

2.6. Flow Cytometry

2.6.1. Tissue collection and preparation for flow cytometry

Peritoneal lavage was obtained by injecting 7 mL of ice cold PEC buffer containing 5 mM ethylenediaminetraacetic acid (EDTA) in DPBS into the peritoneal cavity of sacrificed mice. Fluid was then retrieved and 1 mL of each sample used for staining if no blood was present in the samle. Blood was collected from the vena cava into anticoagulant tubes containing EDTA powder (Teklab). Blood (50 µL) was lysed in 950 µL of ACK lysing buffer for 10 minutes as per manufacturer's instructions to remove red blood cells before the flow cytometry staining. Half of the left lobe of the liver and half a spleen were collected from each mouse into ice cold DPBS and kept on ice until processing. Livers and spleens were mechanically disrupted into single cell suspensions in 10 mL DPBS by using a 70 µm cell strainer (Greiner Bio-One). Additionally, livers were centrifuged at low speed (50g) to pellet out hepatocytes and enrich the remaining supernatant with the immune cells; 200 µL of each sample was used for flow cytometry staining.

2.6.2. Aortic digestion

Tissues were prepared using the protocol reported by Park *et al.* (*283*). Tissues were isolated in RPMI-1640 Medium enriched with 5% FBS. Tissues were cut into small pieces and digested in the enzyme cocktail (450 U/ml collagenase I, 125 U/ml collagenase XI 60 U/ml hyaluronidase and 60 U/ml DNase I) at 37 °C in a shaker for 50 min. The cells were retrieved by passing tissue pieces through a 70 µm cell strainer and the entire samples were processed for flow cytometry staining.

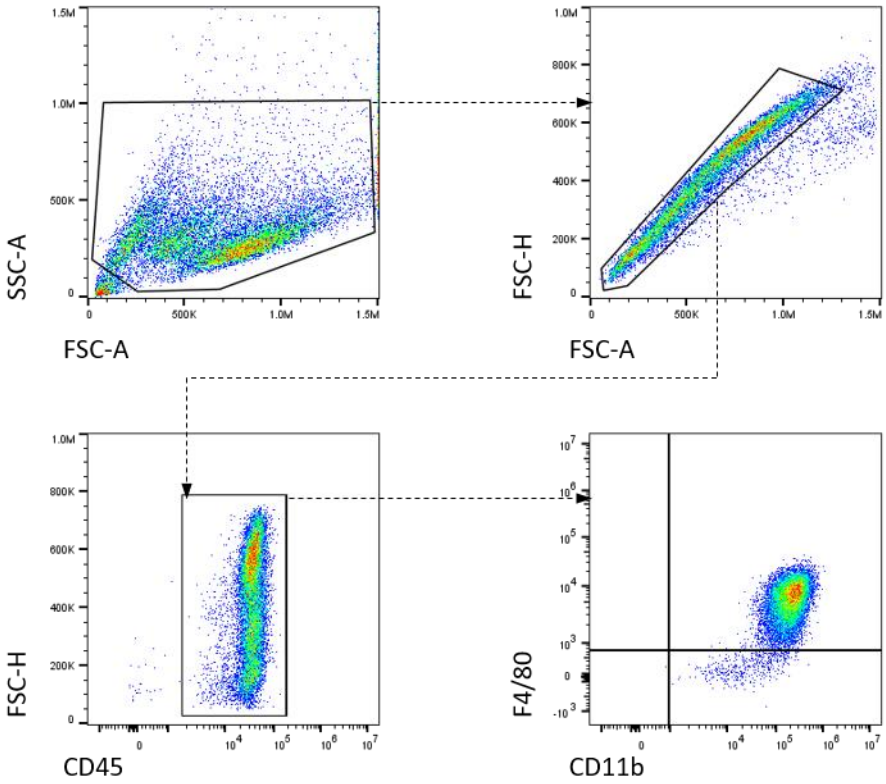

Figure 2.1. Quality of the bone marrow derived macrophage culture. Representative dot plots of flow cytometry validation performed to assess the quality of the BMDM culture using the protocol presented in this thesis. Side scatter (SSC-A) and forward scatter (FSC-A) are a measure of granularity and size, which are used to determine cells from debris at the initial stage of the analysis. FSC-H plotted against FSC-A allows for exclusion of doublets and gating for single cells only. CD45 is a pan-haematopoietic marker, while F4/80 and CD11b are markers for macrophages and myeloid cells respectively; in the plots in the second row cells positive for those markers have been gated based on fluorescence minus one controls.

2.6.3. Staining for surface markers

Cells were washed in FACS buffer containing 0.05 % Bovine Serum Albumin (BSA) and 5 mM EDTA in DPBS and blocked using anti-CD16/32 (1 µg per sample) for 15 mins at 4°C. Subsequently, cells were stained with fluorophore-conjugated antibodies for 30 min for the surface markers with isotype controls. Cells were again washed and re-suspended in 200 µL of FACS buffer without fixation. Antibodies used are listed in Table 2.2.

2.6.4. Intracellular staining

Intracellular staining was performed as per manufacturer's instructions using eBioscience FOXP3/Transcription Factor Staining Buffer Set. Briefly, after the last wash of the extracellular staining protocol, cells were fixed in Fixation/Permeabilization Buffer for 30 min at room temperature. Cells were washed and re-suspended in Permeabilization Buffer; intracellular antibodies were added for 30 min at room temperature. Cells were again washed in Permeabilization Buffer and re-suspended in FACS buffer for flow cytometry analysis.

2.6.5. Data acquisition and analysis

Data were acquired using BD Fortessa X20 cytometer and Diva software (BD Biosciences) and then analysed using FlowJo (Tree Star Inc, USA) software. Fluorescence Minus One (FMO) controls were used for gating and single stains for compensation were obtained using UltraComp eBeads™ Compensation Beads for liver, spleen, aorta and blood panels and single-stained cell samples were used for peritoneal cells and BMDMs. Myeloid cell populations of interest in the tissues studied were identified by gating on singe cells as seen in Figure 2.2.

Marker	Fluorophore	Isotype	Clone
CD3	Brilliant Violet 510	Armenian Hamster IgG	145-2C11
CD4	PE/Cyanine7	Rat IgG2b	GK1.5
CD8a	FITC	Rat IgG2a	53-6.7
CD8a	PE	Rat IgG2a	53-6.7
CD11b	Brilliant Violet 421	Rat IgG2b	M1/70
CD11c	Brilliant Violet 650	Armenian Hamster IgG	N418
CD11c	PE/Cyanine7	Armenian Hamster IgG	N418
CD19	Pacific Blue	Rat IgG2a	6D5
CD45	APC/Cyanine7	Rat IgG2b	30-F11
CD45R/B220	APC	Rat IgG2a	RA3-6B2
CD68	PE	Rat IgG2a	FA-11
CD68	APC/Cyanine7	Rat IgG2a	FA-11
CD88	PE	Rat IgG2b	20/70
CD115	PE/Cyanine7	Rat IgG2a	AFS98
CD170 (Siglec-F)	APC	Rat IgG2a	S17007L
Ly-6C	FITC	Rat IgG2c	HK1.4
Ly-6C	PerCP/Cyanine5.5	Rat IgG2c	HK1.4
Ly-6C	PE	Rat IgG2c	HK1.4
Ly-6G	Brilliant Violet 510	Rat IgG2a	1A8
F4/80	PE	Rat IgG2a	BM8
F4/80	APC	Rat IgG2a	BM8
F4/80	FITC	Rat IgG2a	BM8
F4/80	APC/Cyanine7	Rat IgG2a	BM8
I-A/I-E (MHCII)	FITC	Rat IgG2b	M5/114.15.2
I-A/I-E (MHCII)	PE	Rat IgG2b	M5/114.15.2
CLEC4F	Alexa Fluor 647	Mouse IgG1	3E3F9
Tim-4	PE/Cyanine7	Rat IgG2a	RMT4-54

Table 2.2. List of conjugated fluorescent flow cytometry antibodies used in this thesis.

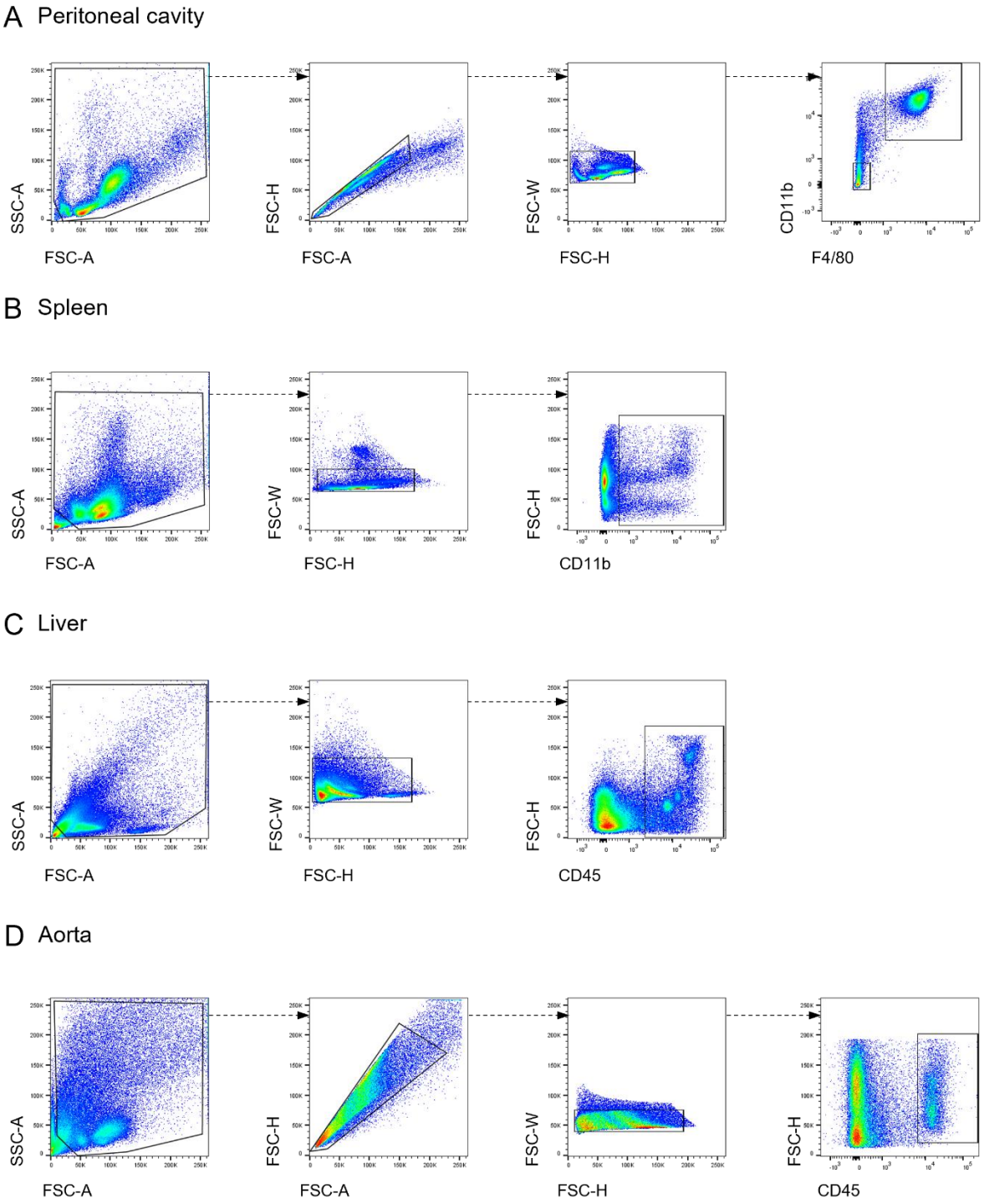

Figure 2.2. Gating on myeloid cell populations for detection of tissue resident macrophages in the tissues studied. Immune cells were gated on in (A) peritoneal cavity, (B) Spleen, (C) liver and (D) aorta to determine TdTomato expression in macrophages and other innate immune cell types. In all cases side scatter (SSC-A) and forward scatter (FSC-A) were used to determine all cells present in the sample, FSC-H vs FSC-A and FSC-W vs FSC-H were used to perform single or double discrimination of doublet cells in the samples, after which cells were gated on CD45 (marker for all immune cells), CD11b (pan-myeloid marker) or F4/80 (macrophage marker).

2.7. Fluorescent microscopy

Mice were perfused with 10-20 mL of cold DPBS and organs were harvested into 4 % paraformaldehyde and incubated at 4^{o}C for 6 hours before transferring into 30 % sucrose overnight to dehydrate. Samples were embedded in OCT matrix and sectioned at –20^{o}C at 5 µm per section. Sections were then counter-stained with DAPI and mounted using ProLong Gold antifade reagent. Images were taken using a Live Cell Olympus Confocal Microscope.

2.8. Inducible hyperlipidaemia model

hCD68-tdTom male and female mice and their control littermates were injected intravenously into the tail vein once with AAVmPCSK9 (AAV.8TBGmPCSK9D377Y, Penn Vector Core) at 5×10^{11} viral particles/mouse and placed onto a high fat and cholesterol diet (SDS 829108 Western RD diet) for 16 weeks. After 16 weeks, mice were orally gavaged with 2 mg of tamoxifen or peanut oil as a vehicle control for 5 consecutive days and tissues were collected 5 days later; refer to Figure 3.19 for timeline.

2.9. Oil Red O staining

Hearts were processed the same as other tissues for fluorescent microscopy, embedded in OCT and cut in 5 µm sections. Sections were brought to room temperature, washed with 60% isopropanol, then saturated with Oil Red O (1% w/v, 60% isopropanol) for 15 min, washed in 60% isopropanol and rinsed in distilled water. Sections were then counterstained with haematoxylin. Coverslips were applied in aqueous mounting medium.

2.10. xCELLigence chemotaxis assay

Real-time xCELLigence chemotaxis assays were performed as previously described (*272*). Briefly, CIM-16 plates were used in RTCA-DP instrument (Agilent, Santa Clara, USA). Experimental concentrations of C5a or CXCL12 were re-suspended in chemotaxis buffer (RPMI-1640 Medium+ 25 mM HEPES solution + 0.5% BSA) and 160 µL of pure chemotaxis buffer or the chemoattractant solution was placed in the bottom chamber of the CIM-16 plates. The top insert was then attached and 50 µL of pure chemotaxis buffer were added to the top chamber; the plates were left in the incubator for 30 min to allow gradient formation. BMDMs were re-suspended at $2x10^6$ cells/mL in chemotaxis buffer. After 30 min, a blank recording was taken and 50 µL BMDM suspension was added to the top chamber. Cells were left at room temperature for 10 min to attach after which recording started. Measurements of cell impedance were taken every 40 seconds for 4 hours in the RTCA-DP instrument in the incubator. Cell impedance was calculated as a cell index (CI) over time, which is a dimensionless unit that represents the background-corrected (derived from the blank recording) electrical resistance at any given time point for each well. It is derived from the following equation:

$$CI = \frac{(\Omega_{tn} - \Omega_{t0})}{15\,\Omega}$$

Where Ω_{tn} = resistance at time point being measured and Ω_{t0} = resistance at time point 0 (blank measurement). Each trace was calculated from averaged 2 technical repeats. Traces were normalized to baseline migration for each CIM-16 plate (cell impedance measured for wells with pure media and no C5a gradient) and then averaged. The traces were presented as delta cell index (ΔCI), which shows the fold change relative to cells migrating towards the

media alone over time. Using ΔCI traces recorded over 4 hours, the area under the curve (AUC) was quantified for each trace (n = 2-7 biological repeats for each concentration).

2.11. IncuCyte image acquisition and analysis

BMDMs were imaged at a rate of 3 frames/h (for experiments in dishes) or 2 frames/h (for experiments in plates) using an IncuCyte ZOOM, a live-cell imaging system contained in an incubator (37°C, 5% CO_2) (Sartorius, Gottingen, Germany). To analyse and quantify migration of individual macrophages, cells were tracked using a custom-made particle-tracking algorithm in Fiji. Bright-field images were extracted from the in-built IncuCyte software, stabilized, the median background intensity was subtracted, and particle locations were recorded. Analyses of trajectories to quantify cell velocities, net-to-gross displacement ratio (NGDR), and chemotactic bias were performed in Matlab as previously described (*284*).

2.12. Statistical analysis

All experiments were designed, where possible, to generate groups of equal size. Where possible, blinding and randomization protocols were used. All data is presented as mean ± standard error mean (SEM), of n observations carried across at least 2 independent experiments, where n represents the number of biological repeats or independent values, not technical replicates. Statistical analysis was calculated using GraphPad Prism 9 (GraphPad Software, San Diego, California, USA; RRID:SCR_002798). For comparison of two groups, an unpaired Student's t-test was used. More than two groups of normally distributed data with single variable and no repeated measurements were assessed by a one-way ANOVA followed by Turkey post-hoc test. To compare two variables, a two-way ANOVA followed by Sidak's post-hoc test was used. In all cases a $P < 0.05$ was considered significant.

Chapter 3

Phenotyping of the human CD68 promoter-driven inducible Cre recombinase driver mouse line which allows specific targeting of tissue resident macrophages[2]

3.1. Introduction

3.1.1. Macrophage-identifying markers

Many cell surface markers are readily available to discriminate between myeloid cell types such as neutrophils and monocytes from macrophages or dendritic cells in both the mouse and human; classical macrophage markers are listed in Table 3.1. CD68/macrosialin and F4/80 have been traditionally used to definitively distinguish between macrophages and monocytes or dendritic cells as they are said to be highly and exclusively expressed on all macrophage populations (*285*). Additionally, macrophages have been defined as cells with high expression of CD11b, CSF1R (CD115), CD204, CX3CR1, CD64, Galectin 3, MHC class II (MHCII), and CD45 (*103*, *285–287*). These markers have been used in histological staining and flow cytometry to define macrophage populations, however it is becoming more apparent that their expression is neither uniform across macrophage populations nor exclusive to them. Galectin 3 is considered a primary marker for the Kupffer cells in the liver, while CD169 expressing macrophages are found in the lymph nodes and spleen (*103*, *286*). Peritoneal macrophages, express F4/80 at high levels, whereas capsular macrophages in the liver have relatively low levels of F4/80 (*133*, *149*). Similarly, CD11b is differentially expressed in liver and lung. Monocyte-derived macrophages in the liver and tissue macrophages in the lung express highly levels of CD11b while Kupffer cells in the liver and alveolar macrophages in the lung

[2] Data presented in this chapter has been published in Rumianek *et al.,* 2022 – see Appendix 1, p.259

are only expressing CD11b at medium to low levels (*133*, *142*). Identifying macrophages becomes ever more complex when their 'defining' markers are shared with other myeloid cells. For example, CD115 is a classical flow cytometry marker for monocytes just as much as it is for macrophages while MHCII is one of the defining markers for dendritic cells (*288*, *289*); this overlap in expression is highlighted in Table 3.1. This is most likely due to the common haematopoietic progenitors, which give rise to the common myeloid progenitor, which in turn differentiate into neutrophils and monocytes (*27*). There has also been common progenitor identified for dendritic cells and macrophages which further makes discrimination of these two related cells types difficult (*30*).

Due to these shared expression profiles genetic tools for identifying and distinguishing macrophages from other cells of the myeloid lineage has been challenging. Many groups tried using the genetic regulatory elements of these 'macrophage-specific' markers as drivers for the expression of either fluorescent reporter genes or Cre recombinase (*279*, *290*, *291*). However, the overlap in expression with other myeloid cells and the differences in the expression intensity between the macrophage populations themselves translated into both high levels of lineage non-restricted expression and variable levels of targeting between macrophage populations.

3.1.2 Human CD68 and macrosialin

Human CD68 and its murine homolog, macrosialin (Cd68) are heavily glycosylated type 1 transmembrane proteins that belong to the lysosomal/endosomal-associated membrane glycoprotein family (*292*). Human *CD68* gene is located on chromosome 17 while the mouse *Cd68* gene is located on chromosome 11; they both contain 6 exons (*293*). Its close proximity

to a housekeeping gene *EIF-4A1* suggests that it is in permanently open chromatin region and therefore its myeloid specificity comes from post-transcriptional modulation (*294*).

In humans CD68 intron 1 drives macrophage specificity, however a similar specificity driver has not been found in murine *Cd68* gene yet (*293*). The CD68 gene is highly expressed in mononuclear phagocytes, tissue-resident macrophage populations, such as microglia, Kupffer cells and osteoclasts, and in myeloid dendritic cells (*295*). Its expression is induced by the macrophage colony-stimulating factor and is dependent on transcription factor PU.1 cooperating with C-Jun (*296*). The murine promoter contains regulatory regions at -7 kb and -2.5 kb from the transcription start site, which act as macrophage enhancer regions in myeloid cells and activity repressors in non-myeloid cells (*294*). Macrophages have been classically defined in histochemical staining and flow cytometry using these markers, however their expression is not restricted to macrophages alone. Despite these regions restricting CD68 expression to macrophages, low level CD68 expression has been documented in B cells, CD4 T cells, neutrophils and basophils as well as non-immune cells such as fibroblasts, endothelial cells and arterial smooth muscle cells, which questions the paradigm of it being strictly macrophage-specific marker (*293*).

Human CD68 protein is 354 amino acids long and contains mucin-like domain, proline-rich hinge, LAMP-like domain, transmembrane domain and C-terminal cytosolic tail. Murine macrosialin shares 80% similarity in the amino acid sequence with the human protein and they are both found in the endosomal cell compartment with the main portion of the protein located in the lumen of the endosomes (*293*). Both the human and the mouse proteins are highly glycosylated, which significantly influences their structure and function. Glycosylation

Marker	Macrophage-expression	Other targets
CD11b	Pan-macrophage	All myeloid cells (*285*)
CD64	Pan-macrophage	Neutrophils, DCs (*297*, *298*)
CD68	Pan-macrophage	Monocytes, neutrophils, DCs, basophils, T cells, B cells (*279*, *293*, *295*)
CD115 (CSF1R)	Pan-macrophage	Monocytes (*288*)
CD169	Lymph node, spleen	Monocytes (*299*)
CD204	Pan-macrophage	Monocytes (*300*)
F4/80	Pan-macrophage	Langerhans cells, eosinophils (*285*, *301*)
CX3CR1	Pan-macrophage	Monocytes (*302*)
Galectin-3	Liver	Monocytes, DCs, eosinophils, mast cells, NK cells (*303*)
MHCII	Pan-macrophage	DCs, B cells (*289*)

Table 3.1. Common macrophage-defining markers and their expression in other immune cell types.

becomes upregulated and remodelled in response to inflammatory stimuli as well as during phagocytosis, where it increases ligand binding (*304*).

The exact function of CD68 is not known, however there are several studies exploring the potential contribution it has in inflammatory responses. CD68 is classified as a class D scavenger receptor with its proposed ligand being oxidised LDL (oxLDL). Yoshida *et al.* showed an upregulation of Cd68 expression when murine peritoneal macrophages were treated *ex vivo* with oxLDL while Zeibig *et al.* used a decoy ligand for macrosialin to competitively antagonise oxLDL binding, which resulted in reduced accumulation of oxLDL in the aortic walls of mice (*305*, *306*). However, oxLDL has been disputed as the potential ligand for macrosialin and CD68. De Beer *et al.* showed marked increase in macrosialin expression in livers of both athero-prone and athero-resistant mice fed high fat diet as well as lack of direct oxLDL binding *in vitro* in transfected Cd68-overexpressing cell lines (*307*). Moreover, Song *et al.* observed that primary peritoneal macrophages from Cd68 'knock-out' mice were robustly up-taking oxLDL *ex vivo* further questioning oxLDL as the primary ligand for CD68 receptor (*308*).

CD68 has been shown to be upregulated by pro-inflammatory stimuli such as LPS and IFN-γ in microglia suggesting a potential role in inflammation (*309*). However, Song *et al.* found no evidence for Cd68 involvement in bacterial and viral killing or antigen presentation therefore directly contradicting this view (*308*). Instead they observed that Cd68 'knock-out' cells had increased antigen presentation to CD4 T cells, which suggested Cd68 as a negative regulator of either uptake of antigen or MHCII trafficking. Furthering that hypothesis, Lin *et al.* found CD68 expressed constitutively in small intestinal epithelial cells, which are involved in constant processing and presentation of intestinal antigens (*310*).

However, the exact function of CD68 may also depend on the tissue where it is expressed. Cha *et al.* found that binding of peptide P39 to CD68 inhibits entry of malaria sporozoites to Kupffer cells in the liver (*311*). Cd68 'knock-out' mice were also found to have skeletal abnormalities due to CD68-deficient osteoclasts having reduced bone resorption ability (*170*). Whereas in cancer, high CD68 expression in tumour-associated macrophages present in tumour stroma in patients with oral squamous cell carcinoma was associated with worsened 10-years survival prognosis, higher lymph node metastasis and increased aggressiveness (tumour grade) (*312*).

3.1.3. Principles behind Cre-*loxP* targeting systems

Global genetic ablation models are a useful tool in studying *in vivo* biology but could be more powerful if they were more cell type-specific. The idea of creating conditional, tissue-specific deletions using this principle have emerged in the late 1980s, however it wasn't until 1998 when it was proven that Cre-*loxP* system is adaptable to and reliable in any cellular or tissue environment and can work with any kind of DNA (*313*). Cre recombinase is a 38-kDa DNA recombinase enzyme encoded by *cre* (cyclization recombinase) gene of bacteriophage P1. It recognises specific 34-bp long DNA fragment sequence called *loxP* (locus of x-over, P1) and mediates deletion of DNA fragments embedded between two *loxP* sites (*314*).

Cre-*loxP* systems quickly became the gold standard of tissue-specific gene deletions and targeting, especially in *in vivo* murine models. The principle behind this system is based on creating and mating two separate mouse lines. Firstly, a Cre-driver strain is created where a tissue-specific promoter for the tissue of interest is driving the expression of Cre recombinase (*314*). This ensures that Cre recombinase will only be expressed in the cells of interest, therefore allowing conditional targeting. Secondly, a 'floxed' mouse is created where

the gene of interest, or a STOP cassette, is flanked by *loxP* sites (*314*, *315*). If a gene of interest is embedded between the two *loxP* sequences Cre recombinase activation causes it excision and therefore creates a 'knock-out' mouse (*314*). If a STOP cassette is embedded between the *loxP* sites in the absence of Cre recombinase it inhibits the expression of the gene placed directly after the second *loxP* sequence. However, when Cre recombinase is present it excises the STOP cassette and allows the expression of the gene directly behind it, therefore creating a conditional transgene-expressing mouse (*315*).

The system can be further refined by allowing temporal control of the Cre activation. Inducible Cre-*loxP* systems rely on addition of an external modulator, usually tamoxifen or doxycycline, to activate Cre recombinase, which gives the opportunity to induce the deletion or expression at any desired time point during the experiment (*314*). Tamoxifen-inducible Cre is a one-step system based on modified Cre recombinase which has been fused with the oestrogen receptor containing a mutated ligand binding domain – CreERT (*316*). This fused protein was further improved to CreERT2 version, which increased its sensitivity to 4-hydroxy tamoxifen (a liver metabolite of tamoxifen) ten times and is now the preferable form to use in animal models (*314*, *317*). In its inactive form CreERT2 is located in cytoplasm and chaperoned by heat shock protein 90 (HSP90), however upon binding of tamoxifen it dissociates HSP90 and relocates to the nucleus to excise *loxP* sites and induces the desired transgene expression or 'knock-out' effects (*314*). In this type of system tamoxifen is usually administered by intraperitoneal injection or oral gavage (*318*).

Alternatively, the doxycycline inducible 'tet-On' approach can be used to temporally control Cre recombinase expression. In this two-step system the tissue-specific promoter of interest constitutively expresses reverse tetracycline-controlled transactivator (rtTA). rtTA creates an

active complex upon binding with doxycycline, which binds and activates the 'tet-On' promoter – tetracycline response element (TRE). In this system, TRE is the promoter directly responsible for the expression of Cre recombinase, which can then excise the *loxP* sites (*142*, *314*). Doxycycline is usually administered in food or drinking water (*314*).

By now, hundreds of 'tissue-specific' promoters and have been identified and used for generating Cre driver lines for most of the commonly researched tissues, with varying degree of specificity. Similarly, hundreds of genes have been 'floxed' and multiple lines have been created to allow expression of new genes in target tissues, mainly fluorescent proteins genes such as GFP or tdTomato that allow easy visualisation and phenotyping. The Jackson Laboratory compiled an online repository of commercially available Cre driver mice – Mouse Genome Database, which offers over 300 readily-available and optimised Cre driver lines as well as reporter strains that allow assessment of function of newly created Cre driver strains (*319*).

3.1.4. Human CD68 promoter cassette and its previous uses in *in vivo* macrophage targeting

Transgenic human CD68 (hCD68) promoter has been used as a macrophage driving promoter in cell lines and animals since the 1990s. It exhibits 68% sequence identity to the mouse Cd68 promoter and is identical in almost all key transcription factor binding sites to the macrosialin promoter - except for the -47 PU.1 transcription factor binding site, which is not conserved, and in hCD68 is replaced with a consensus sequence for C/EBPβ transcription factor (*320*). The best expression cassette has been created by combining the hCD68 promoter with 83-bp first intron of the human CD68 gene (IVS-1), which has been shown to act as an enhancer of the macrophage specificity in cell lines and *in vivo* (*279*, *280*). This 2940-bp cassette can be inserted into the genome as a driver of macrophage targeting either to promote constitutive

expression of, for example, a fluorescent reporter gene or to drive the expression of inducible Cre recombinase (*279*, *321*). So far human CD68 promoter cassette has been reported to successfully target macrophages *in vivo* in five separate models - two constitutively-expressing mouse line, one constitutive Cre driver line, one inducible tet-On mouse line and one constitutively-expressing rat line (*279*, *321–323*).

Lang *et al.* used the hCD68 promoter cassette to constitutively overexpress epitope-tagged IL-10 in macrophages specifically – macIL-10tg mice (*323*). Using this model, they showed that overexpression of IL-10 in macrophages causes macrophage deactivation and their inability to efficiently respond to bacterial infections. However, perhaps the most novel finding of that study was the high specificity of hCD68 transgenic cassette in targeting macrophages *in vivo*, which they compared to MHC-II promoter driven mouse line, opening the door for the whole array of hCD68 promote-driven mouse lines.

Iqbal *et al.* created a widely used hCD68 promoter cassette-based mouse line, hCD68-GFP mouse, where constitutively active hCD68 drives the expression of enhanced green fluorescent protein (EGFP) in monocytes and macrophages across the entire organism from development onwards (*279*). Single integration of the hCD68 promoter cassette and the EGFP transgene on chromosome 3 resulted in robust expression of GFP in tissue-resident macrophage populations such as Kupffer cells, microglia and alveolar macrophages, *ex vivo* monocyte-derived macrophages and blood monocytes. The extremely bright signal in the monocytes rendered this model particularly useful for adoptive transfer experiments, where determining the origins of migrated monocytes and macrophages can be achieved by tracing GFP expression alone (*279*, *324*, *325*). Similarly, this mouse line has been used to image macrophages recruited to atherosclerotic lesions thanks to the high signal and therefore easy

detection (*326*, *327*). Recently, analogous system was created by Turner-Stokes *et al.* to perform live imaging of mononuclear phagocytes in rat kidneys (*322*). By using the hCD68-EGFP transgene cassette they were able to trace two separate waves of monocyte recruitment during glomerulonephritis as well as to confirm that rats possess classical and non-classical monocytes homologous to those identified in mice and humans. Importantly, they also proved that the hCD68 expression cassette is a potent driver of monocyte and macrophage specificity across different species (*322*).

Franke *et al*. used the hCD68 expression cassette to create conditional monocyte-specific constitutive Cre driver line – hCD68-Cre mouse (*328*). They used it to create conditional macrophage-specific knock-out of PHD2 - the main isoform of HIF prolyl hydroxylase. Using this model, they were able to show that loss of PHD2 in macrophages causes severe erythropoietin overproduction and resulting erythrocytosis. However, they also highlighted the fact that embryonic activation of hCD68 promoter cassette targets the entire haematopoietic system and, to a much smaller extent, some subsets of epithelial cells (*328*). This has been also noted by Iqbal at al. who showed that blood neutrophils are also highly GFP-expressing (*279*).

Pillai *et al.* aimed to further refine the hCD68 promoter driven macrophage targeting by using tet-On Cre system where the hCD68-driven expression is controlled by doxycycline administration (hCD68-rtTA mouse), therefore adding temporal control to the system (*321*). The main advantage of the inducible macrophage-specific model is the ability to cross the hCD68-rtTA mice with desired tet-On promoter mouse lines and therefore target genes whose constitutive deletion is embryonically lethal or prevents normal development of the immune system (*142*). Pillai et al. used tet-SNARE/GFP mice to phenotype their model and

showed that the GFP expression is limited to F4/80 and MOMA-2-expressing cells. However they also noted that the apparent activity of the hCD68 promoter does not fully overlap with expression of classical macrophage markers or other common macrophage-specific promoters such as CSF1R (*321*). McCubbrey *et al.* used that observation to study the heterogeneity of alveolar macrophages - they showed that hCD68-rtTA mouse targets efficiently alveolar tissue macrophages and recruited macrophages but not the resident macrophages, which reside in the airspaces (*142*). This discrepancy in targeting different sub-populations of macrophages within one tissue suggests that hCD68 promoter cassette may allow us to further refine our understanding of tissue-resident macrophages as well as target them with greater precision.

3.1.5 Conditional mouse lines targeting macrophages and their limitations

Reporter mouse lines are generally published as specific for a certain tissue or a cell type and their phenotyping often focuses on showing the effect size in the desired cell populations whilst omitting comprehensive evaluation of the off-target effects. Jaxon Laboratory's database lists over 30 Cre driver lines which have been postulated to target myeloid cells (*8*, *20*). Of those, there are five which are referred to as 'macrophage-specific' and commonly used to study monocyte and macrophage fate mapping or conditional macrophage-specific deletions (*330*). They are based on 'macrophage-specific' genes that drive the expression of Cre recombinase or constitutive fluorescent reporter genes.

LysM-Cre mouse was developed in 1999 to conditionally target monocytes, macrophages and neutrophils. It utilises *Lyz2* gene that encodes the enzyme lysozyme M (LysM), which is an antimicrobial enzyme produced specifically in myeloid cells (*290*). Clausen *et al.* showed it to be highly efficient in bone marrow-derived macrophages and primary peritoneal

macrophages, however much less efficient in splenic myeloid population (*290*). To further validate the target population for LysM Faust *et al.* developed a constitutively expressing EGFP mouse driven by the LysM promoter (*331*). They confirmed that the GFP expression was limited to the cells of myeloid lineage, however surprisingly the strongest expressing cells were neutrophils. LysM-driven mice are therefore useful for targeting macrophages, however not specific for them. Moreover, the relatively low efficiency of targeting splenic myeloid fraction implies that they might not be the optimal for studying tissue resident macrophages.

CSF1R, or CD115, is a tyrosine kinase receptor for the macrophage colony-stimulating factor, encoded by the *c-fms* gene and thought to be expressed exclusively in monocytes, macrophages and their progenitors (*291*, *330*). Initially, constitutive Csf1r-EGFP reporter mouse has been created to allow macrophage fate mapping (*332*). In their study Sasmono *et al.* showed that the first intron and the conserved FIRE sequence in it were crucial for the expression of the transgene, however it was later shown that this expression cassette has detectable activity in neutrophils and B cells yet poor expression in some key macrophage populations (*291*, *332*). To refine this system a Csf1r-Cre driver line was created by Deng *et al.* and crossed with $STAT3^{fl/fl}$ line to investigate the effects of conditional STAT3 knockout on inflammation-associated colorectal cancer (*333*). They noted high efficiency of targeting the bone marrow-derived macrophages but also observed about 50% of neutrophils and T cells being affected. Grabert *et al.* postulated that the off-target effects and rapid turnover of surface CSF1R, which results in the loss of signal, can be alleviated by inserting the reporter gene into the *Csf1r* locus rather than using a Csf1r promoter (*291*). They introduced a FusionRed (FRed) cassette at the end of the *Csf1r* locus and showed high levels of targeting in macrophages. The main off-target effects were attributed to megakaryocytes and classical

dendritic cells. Interestingly, they also showed that haematopoietic stem cells did not express FRed, which is contradictory to the idea that M-CSF acts through CSF1R to induce myeloid lineage commitment in the stem cells (*291*, *334*).

CX3C chemokine receptor 1 (CX3CR1), or fractalkine receptor, is thought to be exclusively expressed in mononuclear phagocytes and therefore a good target gene for creating macrophage specific Cre driver lines (*330*). Jung *et al.* used the *Cx3cr1* locus to create constitutively expressing EGFP mouse, which enabled them to show that, this receptor was highly expressed on monocytes and macrophages but also dendritic cells and NK cells (*335*). Yona *et al.* further refined this expression cassette by creating a constitutive Cre driver line and a tamoxifen-inducible CreER driver line – Cx3cr1-Cre and Cx3cr1-CreER respectively (*59*). Using these two mice they were able to map the development of tissue-resident macrophages and show that they are established embryonically instead of recruited from blood monocytes. Moreover, they were able to show progression of monocyte development from circulating Ly6C^{high} monocytes to end stage macrophage-like patrolling Ly6C^{low} monocytes (*59*). However, during comparative analysis with other macrophage-specific Cre driver lines constitutive Cx3cr1-Cre was shown to have relatively low efficiency in alveolar and splenic macrophages as well as significant non-macrophage gene targeting in mast cells and dendritic cells (*329*).

CD11b, or integrin alpha M, is a key adhesion molecule upregulated during myeloid development with the highest expression levels seen in mature monocytes, macrophages and neutrophils (*330*, *336*) Ferron *et al*. created a constitutive CD11b-Cre driver line, which showed high efficiency of targeting myeloid cells in the bone marrow and spleen as well as mature osteoclasts, enabling unique insights into early common precursors of osteoclasts and

other tissue-resident macrophages (*336*). However, compared to other macrophage targeting Cre lines, the CD11b-Cre mouse had a low efficiency of targeting in most of the tissue-resident macrophages whilst having high off-target effects in other myeloid cell types. Moreover, there was significant variation in the targeting efficiency between littermates, rendering this line unreliable (*329*).

Lastly, classical tissue-resident macrophage marker F4/80, or EGF-like module-containing mucin-like hormone receptor-like 1, has been used by Schaller *et al.* to generate a constitutive Cre driver mouse line (*337*). Using the IκBα$^{fl/fl}$ mouse they showed macrophage-specific deletion of the IκBα allele. However, later it has been shown that there is a high variability in the expression of F4/80 among different macrophage populations, which resulted in this model being efficient only for certain sub-populations of macrophages (*329*).

3.2 Rationale and experimental aims of this chapter

Attempts at specific genetic targeting of macrophages so far have not been fully successful. Popular 'macrophage-targeting' mouse lines such as LysM-Cre, CX3CR1-Cre, CSF1R-Cre or hCD68-GFP all show marked targeting of other myeloid cells such as monocytes, neutrophils and dendritic cells. In the Greaves lab we hypothesised that inducible Cre recombinase activity would be more restricted to macrophages because it would avoid the early expression of macrophage markers during embryogenesis and haematopoiesis. To test this hypothesis, we established a novel knock-in mouse line hCD68-CreERT2, which expresses tamoxifen inducible CreERT2 recombinase under the control of the human CD68 expression cassette. I crossed it with the commercially available tdTomato$^{fl/fl}$ reporter mouse line to induce tdTomato fluorescence in all cells targeted by the hCD68 expression cassette.

Therefore, the experimental aims for this chapter are:

1. To establish expression profile of tdTomato in tissue resident macrophages as a readout of the efficiency of macrophage targeting in hCD68-CreERT2 mouse line.

2. To establish expression profile of tdTomato in other immune cells as a way of assessing lineage non-restricted expression in hCD68-CreERT2 mice.

3. To compare the expression profile in macrophages and other immune cells between hCD68-CreERT2 mouse and LysM-Cre and hCD68-GFP mouse lines.

4. To induce atherosclerosis in hCD68-CreERT2 mice as a proof-of-concept experiment in using this novel mouse strain for studying macrophages in disease models.

3.3. Results

3.3.1. Generation of hCD68-CreERT2-tdTomato reporter mouse.

Human CD68 expression cassette with engineered DNA construct that encoded a tamoxifen inducible Cre recombinase was inserted into the ROSA26 locus of embryonic stem cells before being injected into albino C57BL/6J blastocysts yielding hCD68-CreERT2 chimeric founders (done in collaboration with Ben Davies at the Wellcome Trust Centre for Human Genetics at the University of Oxford). Mice were fertile and produced an expected Mendelian ratio of transgenic and non-transgenic litter mates with no obvious developmental defects. I confirmed the genotype of the founders by PCR. I mated hCD68-CreERT2 heterozygous males with tdTomato$^{fl/fl}$ heterozygous females to generate double transgenic experimental mice (hCD68-tdTom) (Figure 3.1A) and used littermates carrying no transgenes, or a single transgene as controls throughout this chapter. Using a commercially available fluorescent reporter mouse with a flox/STOP cassette is a standard way of phenotyping new Cre driver lines (*318*, *329*). Out of 444 pups born during this study 109 were heterozygous for both alleles, 101 were heterozygous for hCD68-CreERT2 only, 102 were heterozygous for tdTomato only and 132 mice were wild-type for both alleles, confirming proportional Mendelian inheritance. Principles behind tamoxifen-inducible expression of tdTomato used as a readout for Cre recombinase activation are graphically represented in Figure 3.1B.

3.3.2. Optimization of tamoxifen dosing regime

To establish the most efficient induction of Cre recombinase in our model I tried multiple tamoxifen dosing regimens (Figure 3.2). I based the proposed doses of tamoxifen and the induction periods on published dosing regimens. Tamoxifen is a selective oestrogen receptor (ER) modulator originally licenced as a ER-positive breast cancer drug. CreERT2 is

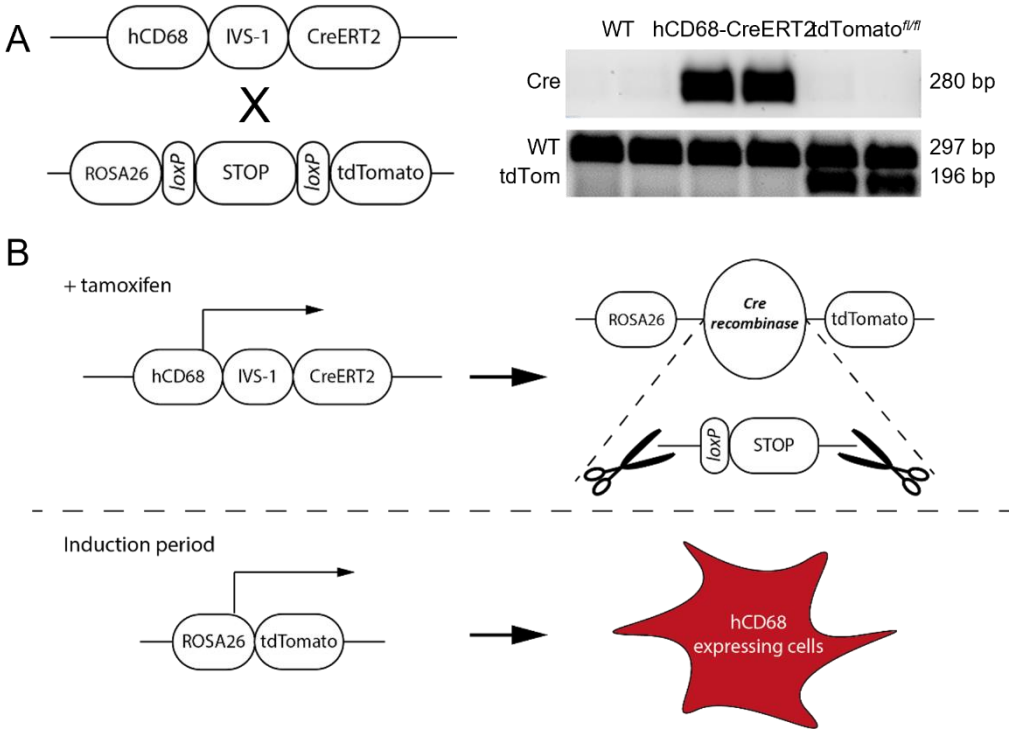

Figure 3.1. Design and generation of the inducible hCD68-CreERT2 model. A) Presence of Cre recombinase and tdTomato genes was confirmed by extracting DNA from ear notches, a standard PCR amplification and running side-by-side on an agarose gel for all genotypes available for het x het breeding strategy. B) Principles of the human CD68 promoter-driven tamoxifen inducible Cre recombinase activation; not to scale.

constitutively expressed in the target cells but becomes translocated to the nucleus upon biding of a tamoxifen's metabolite 4-hydroxy tamoxifen (4-OHT) (*318*). It can act as either agonist or antagonist of the oestrogen receptor depending on the tissue (*338*), which leads to a broad profile of off-target effects that it can cause. For example, it has been shown to negatively affect bones and adipose tissue, which both harbour important tissue-resident macrophage populations, and to cause marked weight loss (*338*, *339*). My goal was therefore to minimise the dose and duration of tamoxifen administered to the mice whilst achieving robust expression of tdTomato in tissue-resident macrophages. Published protocols generally use 1-3 mg of tamoxifen which is either injected intraperitoneally (I.P.) or orally gavaged for 3-5 days, followed by an induction period (*318*, *338–340*). I chose to orally gavage the mice to avoid causing an acute local inflammatory response in the peritoneum due to needle injury or tamoxifen itself and therefore risking a possibility of a disturbance to the resident macrophage population in the peritoneum.

I started with orally gavaging 1 mg of tamoxifen per day for 3 consecutive days, with a 2 days induction period (Figure 3.2A) and chose to look at peritoneal macrophages due to their robust GFP expression in hCD68-GFP mice. However, only a small proportion (~20%) expressed tdTomato after 2 days (Figure 3.3A). Subsequently, I decided to increase the dose of tamoxifen and to extend both the dosing and the induction periods. I chose to use 2 or 3 mg of tamoxifen per day for 5 consecutive days with an induction period of 3-7 days. I also decided to assess the tdTomato expression in splenic and hepatic macrophage populations as well as the bone marrow. As seen in Figure 3.3, using 2 mg/day with 3 days induction period rendered no significant improvement in tdTomato expression in the peritoneal macrophages and had relatively modest effects in all other tissues with 10-30% of macrophages targeted in

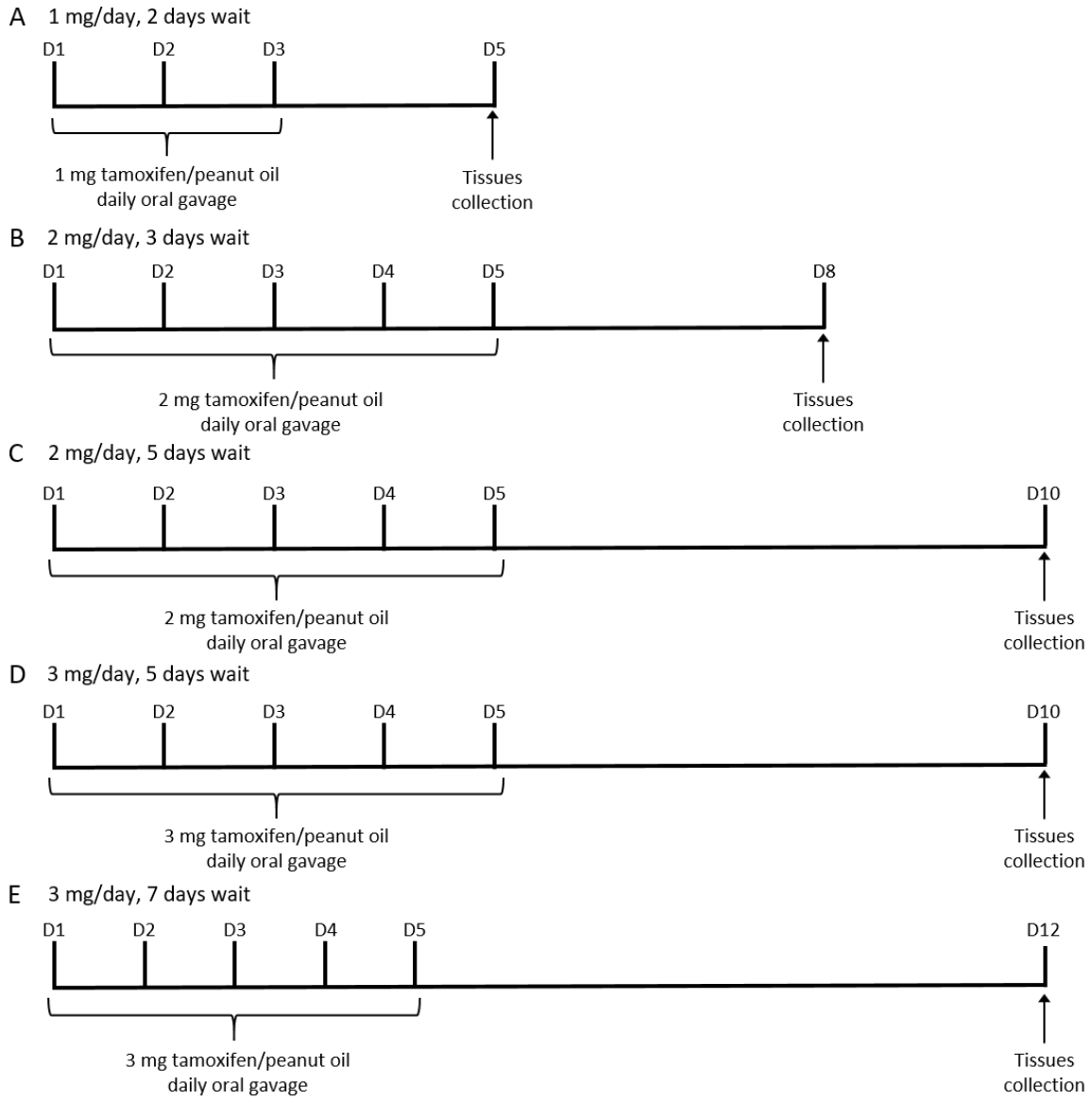

Figure 3.2. Variants of tamoxifen dosing regimens. Activation of Cre recombinase by tamoxifen was tested in 5 different dosing regimens: A) 1 mg of tamoxifen/peanut oil daily for 3 days and 2 days induction period (1 mg/day, 2 days wait). B) 2 mg of tamoxifen/peanut oil daily for 5 days and 3 days induction period (2 mg/day, 3 days wait). C) 2 mg of tamoxifen/peanut oil daily for 5 days and 5 days induction period (2 mg/day, 5 days wait). D) 3 mg of tamoxifen/peanut oil daily for 5 days and 5 days induction period (3 mg/day, 5 days wait). E) 3 mg of tamoxifen/peanut oil daily for 5 days and 7 days induction period (3 mg/day, 7 days wait).

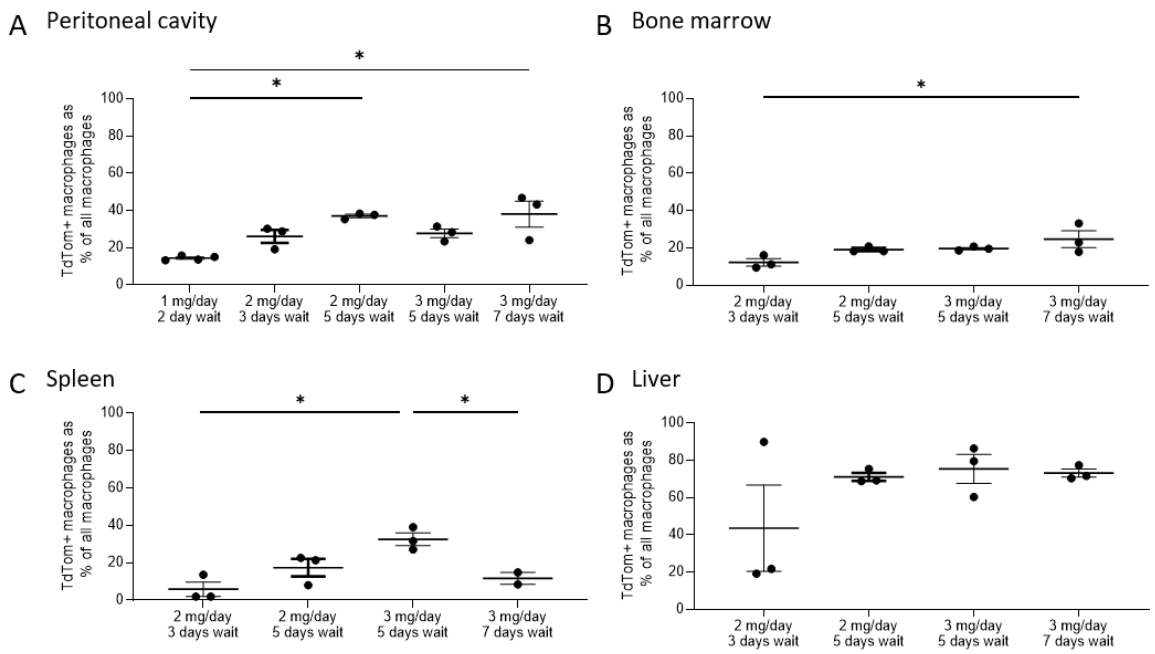

Figure 3.3. Optimisation of tamoxifen dosing regimen. Frequency of tdTomato-expressing macrophages as a proportion of all tissue resident macrophages in (A) peritoneal cavity, (B) bone marrow, (C) spleen and (D) liver; macrophages were defined as CD11b+ and F4/80+ cells by flow cytometry, dosing regiments were defined in Figure 2, one-way ANOVA (* = $p<0.05$).

the peritoneum, spleen and bone marrow. I could not draw any meaningful conclusions from the hepatic macrophages due to extreme spread of data (Figure 3.3D). Extending the induction period to 5 days improved targeting of peritoneal, splenic and bone marrow macrophages and kept it stable in the liver. Further increase in the dose, from 2 mg to 3 mg per day caused an increase in the spleen expression of tdTomato, stable expression in the bone marrow and the liver and a slight decline in the expression of tdTomato in the peritoneum. Extending the induction period from 5 to 7 days also did not cause any significant improvements in any of the tested tissues, however it caused a significant decline in the proportion of tdTomato-expressing splenic macrophages (Figure 3.3.C).

Overall, the highest level of tdTom expression in the peritoneum was seen with '2 mg/day, 5 days wait' protocol and in the spleen with the '3 mg/day, 5 days wait' protocol (Figure 3.3A and 3.3C respectively). Bone marrow macrophages were stably targeted at around 20% efficiency with a slight yet significant rise from '2 mg/day, 3 days wait' protocol to '3 mg/day, 7 days wait' protocol (Figure 3.3B). Hepatic macrophages showed the best targeting efficiency with around 80% targeted with the '2 mg/day, 5 days wait' protocol, which remained stable for the higher tamoxifen dose and the longer induction period (Figure 3.3D). Taken together, this data showed no significant improvement in targeting efficiency from 2 mg/day for 5 days to 3 mg/day for 5 days across all the tissues, which in my opinion did not justify the potential side effects that a higher dose of tamoxifen could cause to the mice. Therefore, I chose to follow the '2 mg/day, 5 days wait' protocol (Figure 3.2C) for the remainder of this study. It produced the overall highest expression in peritoneal macrophages whilst having long enough induction period to also allow for full Cre recombinase activation and minimise the variability in the expression seen in the liver with '2 mg/day, 3 days wait' protocol (Figure 3.3D).

3.3.3. The hCD68 promotor drives inducible Cre-recombinase in tissue resident macrophages

To assess the pattern of inducible Cre activity in tamoxifen treated hCD68-tdTom mice in different tissue resident macrophage populations I used flow cytometry with panels of well characterised monoclonal antibodies. When compared to vehicle treated hCD68-tdTom mice, tamoxifen treated hCD68-tdTom mice had robust expression of tdTomato in $CD11b^{+}F4/80^{+}$ peritoneal resident macrophages with ~30% of peritoneal macrophages expressing tdTom (Figure 3.4A-C). Reassuringly, I found no expression in control mice treated with tamoxifen or hCD68-tdTom mice treated with vehicle, which confirmed the lack of 'leakiness' of the Cre recombinase activation. Having noticed in the dot plots that the expression of tdTomato in peritoneal macrophages seems to be concentrated in cells of bigger size I decided to further investigate the level of tdTomato expression in two known peritoneal macrophage populations – the large and small peritoneal macrophages (LPMs and SPMs respectively, Figure 3.5). I further sub-divided the total macrophages gate to separate them by size (Figure 3.5A). When compared, tamoxifen treated hCD68-tdTom mice had ~40 % of LPMs display tdTomato expression, while only ~20 % of SPMs expressed tdTomato (Figure 3.5B). Moreover, the level of tdTomato expression (MFI) was significantly lower in SPMs compared to LPMs (Figure 3.5C).

Within the spleen of tamoxifen treated hCD68-tdTom mice there was robust expression of tdTomato in $CD11b^{+}F4/80^{+}$ macrophages with ~30 % of splenic macrophages expressing tdTomato (Figure 3.4D-F). As in the peritoneum, no expression was seen in control mice treated with tamoxifen or the hCD68-tdTom mice treated with vehicle.

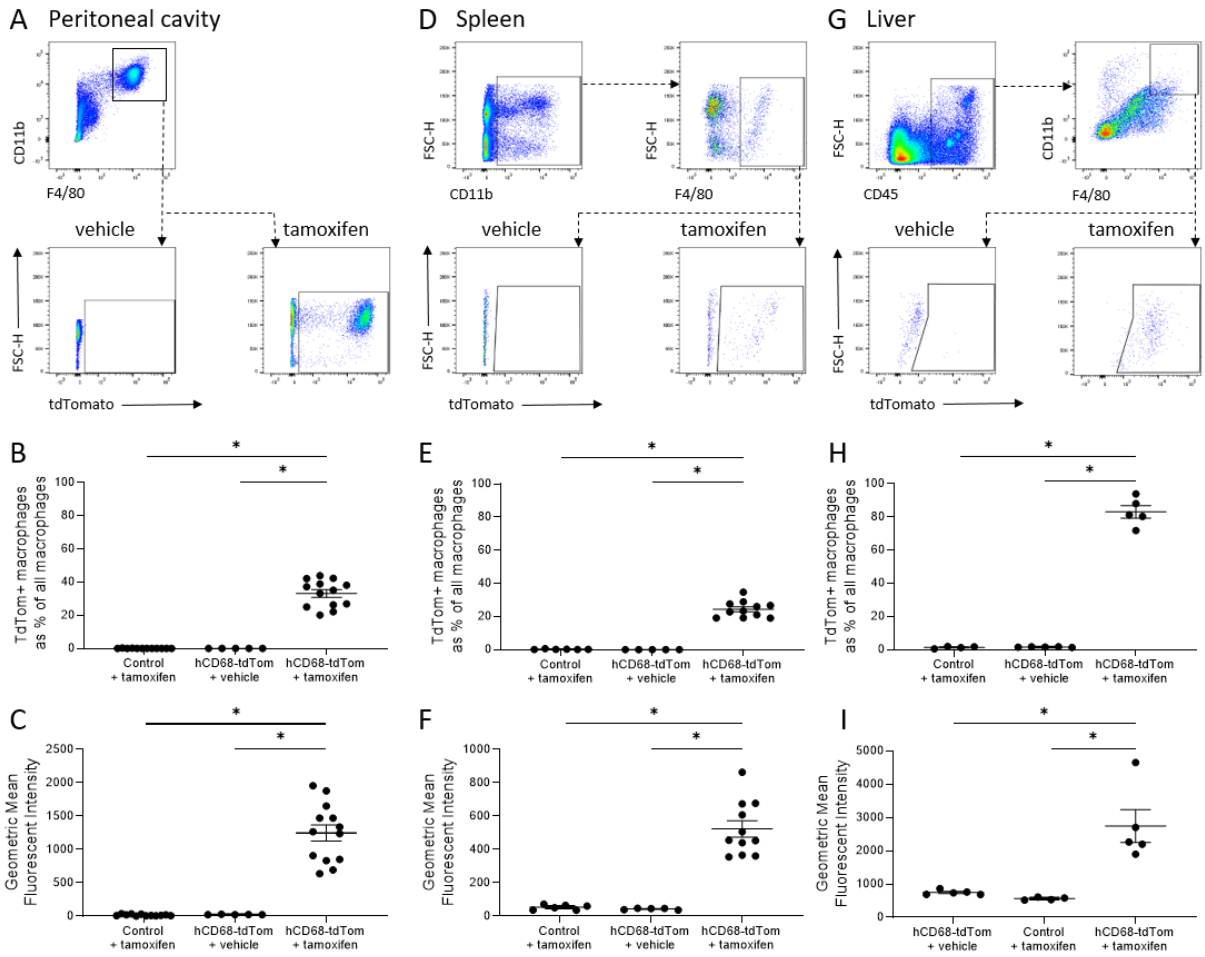

Figure 3.4. The hCD68 promoter driven inducible Cre recombinase has high activity levels in tissue resident macrophages as detected by flow cytometry. Tissue-resident macrophage populations in (A) peritoneal cavity, (D) spleen and (G) liver were defined as CD11b$^+$ and F4/80$^+$ cells (gating strategy shown by representative dot plots with tdTomato$^+$ gate also shown) with the corresponding frequency of tdTomato-expressing macrophages as a proportion of all macrophages shown in (B) peritoneal cavity, (E) spleen and (H) liver and with respective mean fluorescence intensity values of tdTomato expression in the whole macrophage population in (C), (F) and (I); one-way ANOVA (* = $p<0.05$).

The liver has a large and heterogeneous population of tissue resident macrophages with four subtypes readily distinguishable by flow cytometry (*133*). When compared to vehicle-treated hCD68-tdTom mice, tamoxifen treated hCD68-tdTom mice had robust expression of tdTomato in all liver CD11b^{hi}F4/80^{hi} macrophages with ~80% of them expressing high levels of tdTomato (Figure 3.4G-I). However, due to the significant heterogeneity within the liver macrophages I wanted to further investigate hCD68 promoter driven Cre activity within different macrophage subsets (Figure 3.6). I used published studies to design a flow cytometry panel that allowed me to distinguish following populations with the gating strategy presented in Figure 3.6A - lipid-associated macrophages (LAMs; CD11b^{hi}Ly6C^{+}CD11c^{-}MHCII^{+}CLEC4F^{low}), monocyte-derived Kupffer cells (Mono-KCs; CD11b^{hi}Ly6C^{+}CD11c^{-}MHCII^{+}CLEC4F^{+}), capsular macrophages (CMs; CD11b^{low}F4/80^{int}TIM4^{-}MHCII^{+}) and Kupffer cells (KCs; CD11b^{+}F4/80^{hi}CLEC4F^{hi}TIM4^{hi}) (*133*, *341*). All liver macrophage populations in tamoxifen treated hCD68-tdTom mice expressed tdTomato with Kupffer cells showing most efficient targeting (~90% of all KCs; Figure 3.6E), intermediate efficiency in the monocyte-derived populations (~30% of LAMs and ~50% Mono-KCs; Figure 3.6B and 3.6C respectively) and the lowest targeting efficiency in the capsular macrophages (~20%; Figure 3.6D). Interestingly, the expression of tdTomato measured by mean fluorescent intensity was also significantly different between subsets of liver macrophage (Figure 3.6F). Mono-KCs expressed the highest levels of tdTomato, while CMs expressed the lowest level, opening a possibility to distinguish between the assessed hepatic macrophage subsets within the tissue using MFI alone.

To confirm flow cytometry results and extend the range of tissues that I examined for their tdTomato expression I used fluorescent microscopy to visualise endogenous tdTomato

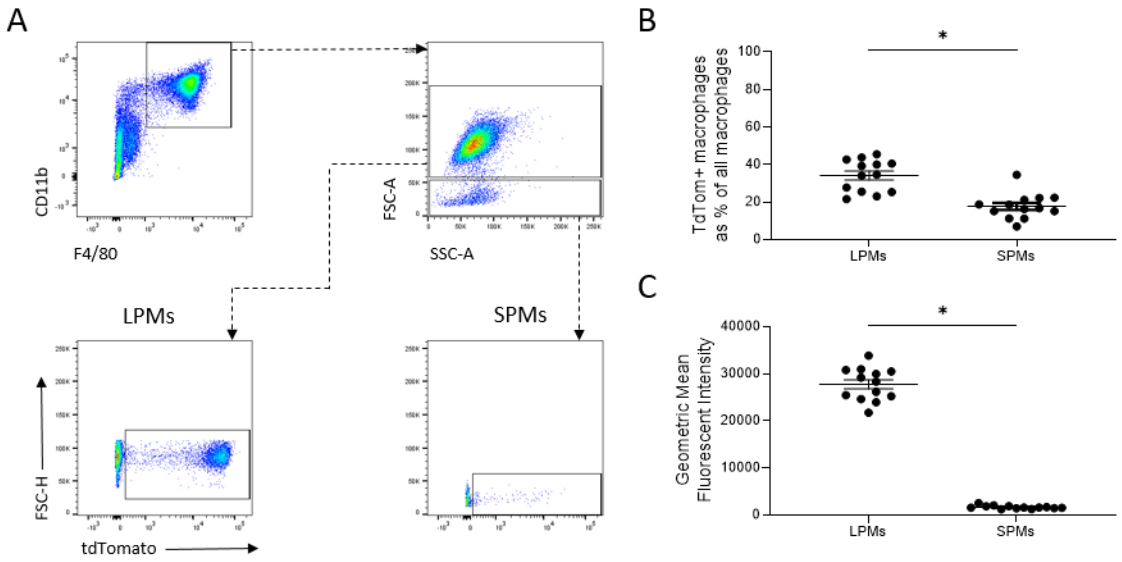

Figure 3.5. hCD68 promoter drives the expression of tdTomato in large and small peritoneal macrophages to a varying degree. A) Representative dot plots of the gating strategy for large peritoneal macrophages (LPMs) and small peritoneal macrophages (SPMs) where forward scatter (FSC-A) has been used to distinguish their size. B) Frequency of tdTomato-expressing large and small peritoneal macrophages as a proportion of all macrophages of the given subtype with corresponding mean fluorescent intensity in (C); student t-test (* = $p<0.05$).

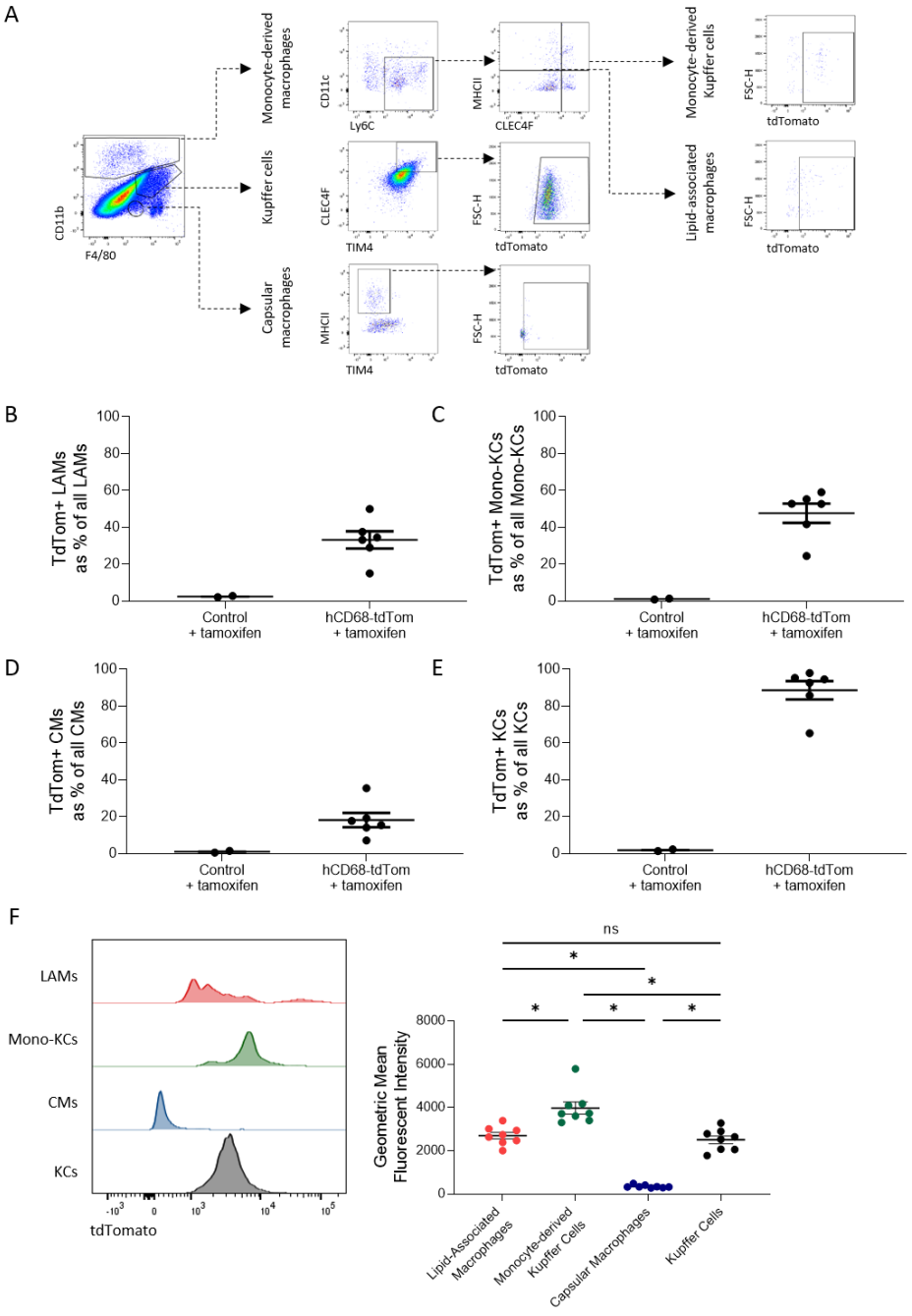

Figure 3.6. hCD68 promoter drives the expression of TdTomato in different macrophage sub-populations in the liver to a varying degree. A) Representative dot plots of the gating strategy for liver monocyte-derived macrophages (CD11bhigh, F4/80low, CD11c-, Ly6C+) sub-divided into monocyte-derived Kupffer cells (Mono-KCs, MHCII+, CLEC4Fhigh) and lipid-associated macrophages (LAMs, MHCII+, CLEC4Flow), Kupffer cells (KCs, CD11bint, F4/80high, CLEC4F+, TIM4+) and capsular macrophages (CMs, CD11b-, F4/80+, MHCII+, TIM4-). B) Frequency of tdTomato-expressing lipid-associated macrophages as a proportion of all lipid-associated macrophages. C) Frequency of tdTomato-expressing monocyte-derived Kupffer cells as a proportion of all monocyte-derived Kupffer cells. D) Frequency of tdTomato-expressing capsular macrophages as a proportion of all capsular macrophages. E) Frequency of tdTomato-expressing Kupffer cells as a proportion of all Kupffer cells. F) Histogram of the mean fluorescent intensity of liver macrophage sub populations with corresponding values graphed and colour-coded on the right; lipid-associated macrophages are represented by red histogram, monocyte-derived Kupffer cells as green, capsular macrophages as blue and Kupffer cells as black, one-way ANOVA or student t-test as appropriate, (* = $p<0.05$).

expression (Figure 3.7). Confirming the cytometry results from Figure 3.4, control spleens (Figure 3.7A) and livers (Figure 3.7B) displayed no expression of tdTomato while tamoxifen treated hCD68-tdTom mice displayed a discrete expression pattern of tdTomato within these tissues. Moreover, I examined the kidney (Figure 3.7C) and the lung (Figure 3.7D) and noted no expression of tdTomato in the control group and a robust discrete pattern of expression in hCD58-tdTom mice dosed with tamoxifen. Whilst the lung showed a fairly uniform distribution of the tdTom expressing cells at 10x magnification (Figure 3.7D) the kidney showed different expression patterns depending on the location (Figure 3.7C). Discrete tdTomato expressing cells in the bottom half of the image were seen in contrast to the top part, where tdTomato expression seems to be distributed in elongated interconnected cells. Since CD68 expression has been reported to be activated in epithelial cells (*328*, *342*), I speculated that the expression pattern seen in the kidney revealed an off-target effect of Cre recombinase induction where glomerular endothelial cells were targeted (top half of the image) alongside tissue-resident macrophages (bottom half of the image and 100x close-up). Unfortunately, since the tissues were co-stained only with DAPI I could not confirm the exact anatomical location within any of the tissues imaged. This is a major limitation of this experiment and it would be of great value to co-stain these tissue samples with macrophage markers such as Gal 3, CD68 and CD169 (to confirm that tdTomato-expressing cells are indeed macrophages) and for other cell types such as endothelium (potential markers could be CD31, CD34 ICAM-1, LYVe-1 or Tie-2).

3.3.4. The hCD68 promoter drives limited inducible Cre-recombinase expression in non-macrophage cells.

Having observed the lineage non-restricted expression of tdTomato in kidney endothelium I set out to extensively examine off-target effects in other tissues. Previously the hCD68

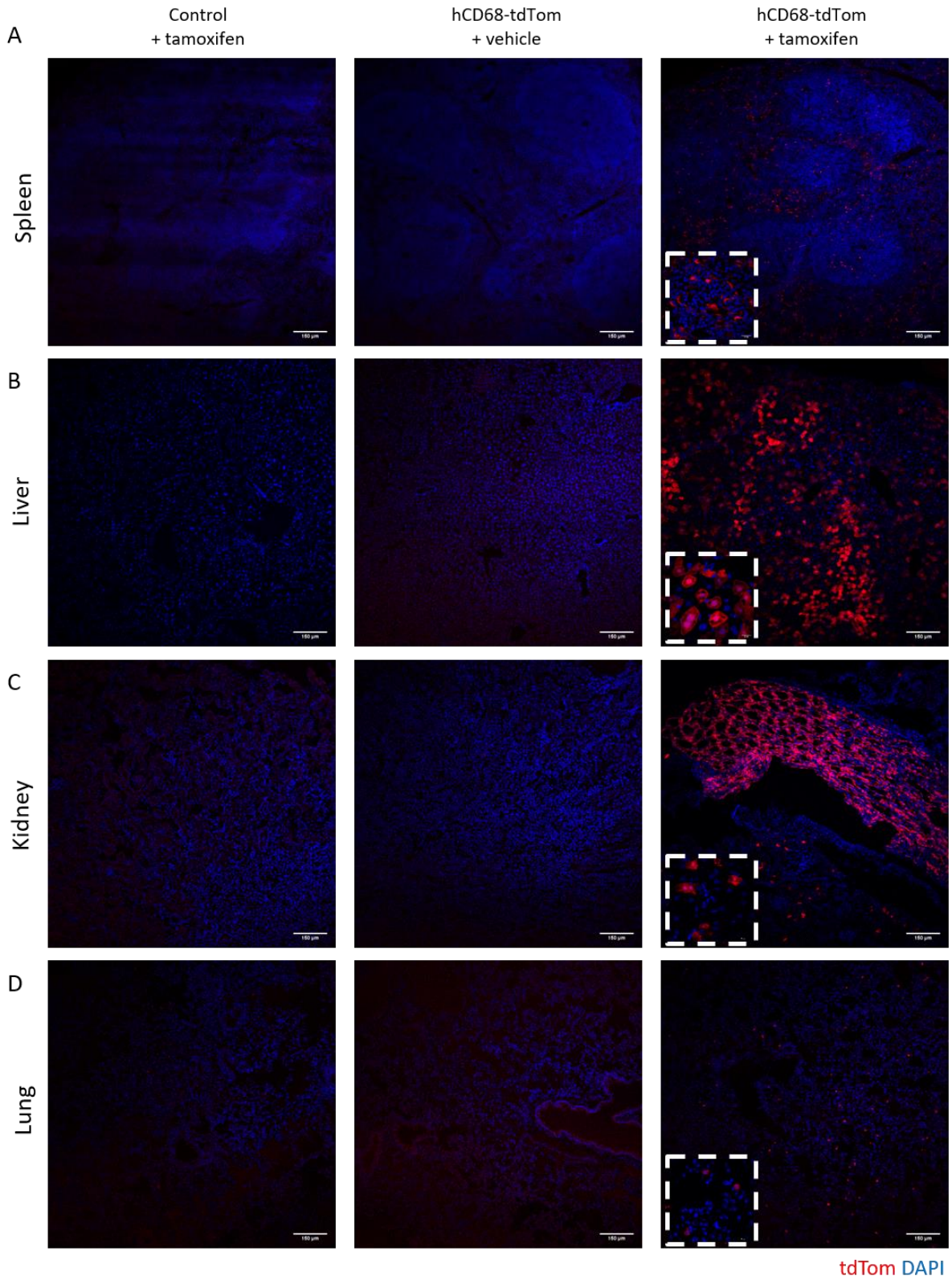

Figure 3.7. The hCD68 promoter-driven inducible Cre recombinase has high activity levels in tissue-resident populations as detected by confocal microscopy. Representative immunofluorescence images of endogenous tdTomato expression in (A) the spleen, (B) the liver, (C) the kidney and (D) the lung at 10x magnification with DAPI in blue and tdTomato in red. Due to lack of co-staining no precise location within the tissue could be determined. Overlaid 100x image of tdTomato-expressing cells is shown in the white dashed panel for each organ in the bottom left corner of the 'hCD68-tdTom + tamoxifen' image; scale bar = 150µm.

expression cassette was used to drive green fluorescent protein and showed robust expression in non-macrophage myeloid cells, mainly monocytes and neutrophils in the blood (*279*). Therefore, I assessed Cre-recombinase activity in circulating myeloid and non-myeloid leukocytes (Figure 3.8). There was no detectable tdTomato expression in circulating $CD11b^{+}CD115^{+}$ monocytes from control mice, however, tamoxifen treated hCD68-tdTom mice had a small but significant increase in the number of tdTomato expressing cells (Figure 3.8B). To further assess this expression pattern, I separated the $Ly6C^{high}$ and $Ly6C^{low}$ monocytes (Figure 3.8A). Interestingly, I only saw evidence of tdTomato expression in $Ly6C^{low}$ monocytes, with 20% of them expressing tdTomato, which suggests that the inducible hCD68 promotor driven Cre-recombinase has activity in patrolling $Ly6C^{low}$ monocytes only (Figure 3.8C and Table 3.2). Since other myeloid Cre driver lines showed significant activity in neutrophils, I wanted to know the level of tdTomato expression in hCD68-tdTom mice in circulating neutrophils (*59*, *290*, *333*). Tamoxifen treated hCD68-tdTom mice had no or very low expression of tdTomato (<2 %) in $CD11b^{+}CD115^{-}Ly6G^{+}$ neutrophils (Figure 3.8D and Table 2). In the other myeloid blood populations, there was <5 % expression of tdTomato in dendritic cells from tamoxifen treated hCD68-tdTom mice and <1 % tdTomato expression in eosinophils from tamoxifen treated hCD68-tdTom mice (Table 3.2 and Figure 3.8F and 3.8G respectively). Additionally, there was no more than 1.5% of tdTomato expression in $CD4^{+}$ and $CD8^{+}$ T cells or in circulating B-cells in tamoxifen treated hCD68-tdTom mice (Table 3.2 and Figure 3.8I, 3.8J and 3.8K respectively). Statistical analysis showed significant increases in the hCD68-tdTom mice dosed with tamoxifen when compared to control mice dosed with tamoxifen as well as hCD68-tdTom mice dosed with the vehicle in most of the blood immune cell populations, however looking at the overall values, apart from the $Ly6C^{low}$ monocytes, they are highly unlikely to have significant biological effects when using hCD68-CreERT2 mice

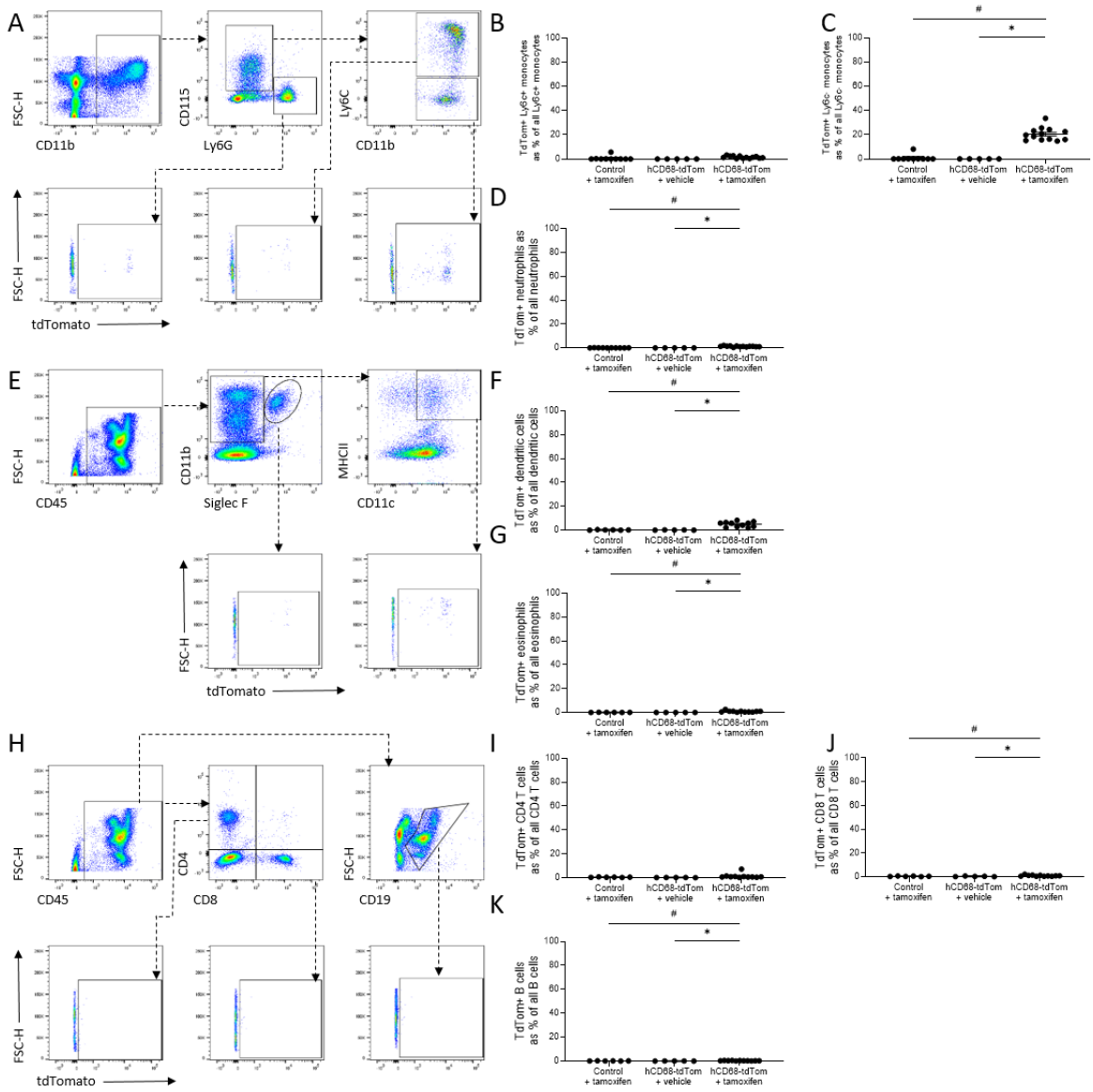

Figure 3.8. The hCD68 promoter driven inducible Cre recombinase has limited activity in circulating leukocytes. A) Representative dot plots of the gating strategy for neutrophils (CD115$^-$, Ly6G$^+$), total monocytes (CD115$^+$, Ly6G-), Ly6C^{high} and Ly6C^{low} monocytes (CD115$^+$, Ly6G$^-$, Ly6C$^+$ and CD115$^+$, Ly6G$^-$, Ly6C$^-$ respectively). B) Frequency of tdTomato-expressing monocytes as a proportion of all monocytes. C) Frequency of tdTomato-expressing Ly6C^{high} and Ly6C^{low} monocytes. D) Frequency of tdTomato-expressing neutrophils as a proportion of all neutrophils. E) Representative dot plots of the gating strategy for dendritic cells (CD45$^+$, CD11b$^+$, Siglec F$^-$, MHCII$^+$, CD11c$^+$) and eosinophils (CD45$^+$, CD11b$^+$, Siglec F$^+$). F) Frequency of tdTomato-expressing dendritic cells as a proportion of all dendritic cells. G) Frequency of tdTomato-expressing eosinophils as a proportion of all eosinophils. H) Representative dot plots of the gating strategy for CD4 T cells (CD45$^+$, CD4$^+$, CD8$^-$), CD8 T cells (CD45$^+$, CD4$^-$, CD8$^+$) and B cells (CD45$^+$, CD19$^+$). I) Frequency of tdTomato-expressing CD4 T cells as a proportion of all CD4 T cells. J) Frequency of tdTomato-expressing CD8 T cells as a proportion of all CD8 T cells. K) Frequency of tdTomato-expressing B cells as a proportion of all B cells; one-way ANOVA (# = $p<0.05$ for 'Control + tamoxifen' vs 'hCD68-tdTom + tamoxifen'; * = $p<0.05$ for 'hCD68-tdTom + vehicle' vs 'hCD86-tdTom + tamoxifen').

Population	Control + tamoxifen	hCD68-tdTom + vehicle	hCD68-tdTom + tamoxifen
Ly6C^{high} monocytes	0.63 ± 0.56	0.02 ± 0.01	1.54 ± 0.27
Ly6C^{low} monocytes	0.85 ± 0.80	0.01 ± 0.01	20.49 ± 1.49#*
Neutrophils	0.07 ± 0.02	0.06 ± 0.01	1.28 ± 0.12#*
Dendritic cells	0.22 ± 0.09	0.11 ± 0.05	4.93 ± 0.66#*
Eosinophils	0.08 ± 0.03	0.00 ± 0.00	0.91 ± 0.20#*
CD4 T cells	0.48 ± 0.07	0.24 ± 0.03	1.41 ± 0.60
CD8 T cells	0.51 ± 0.08	0.47 ± 0.11	1.05 ± 0.16#*
B cells	0.16 ± 0.03	0.09 ± 0.01	0.33 ± 0.04#*

Table 3.2. tdTomato expression in circulating leukocyte populations. Percentage of tdTomato-expressing blood leukocytes represented as mean ± SEM; one-way ANOVA (# = $p<0.05$ for 'Control + tamoxifen' vs 'hCD68-tdTom + tamoxifen'; * = $p<0.05$ for 'hCD68-tdTom + vehicle' vs 'hCD86-tdTom + tamoxifen').

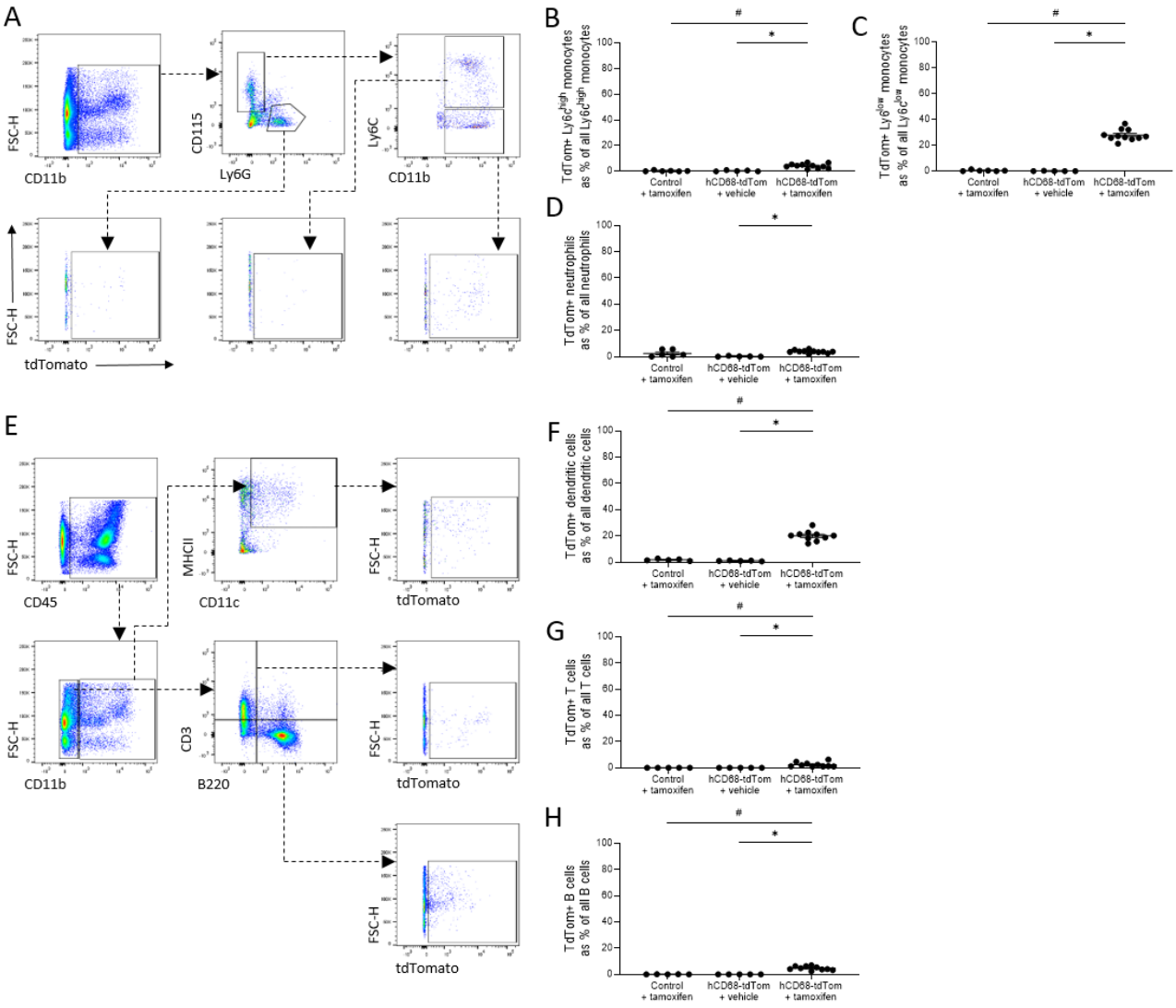

Figure 3.9. TdTomato expression in spleen non-macrophage populations. A) Representative dot plots of the gating strategy for splenic neutrophils ($CD11b^+$, $CD115^-$, $Ly6G^+$), $Ly6C^{high}$ monocytes ($CD11b^+$, $CD115^+$, $Ly6G^-$, $Ly6C^+$) and $Ly6C^{low}$ monocytes ($CD11b^+$, $CD115^+$, $Ly6G^-$, $Ly6C^-$). B) Frequency of tdTomato-expressing $Ly6C^{high}$ monocytes as a proportion of all $Ly6C^{high}$ monocytes. C) Frequency of tdTomato-expressing $Ly6C^{low}$ monocytes as a proportion of all $Ly6C^{low}$ monocytes. D) Frequency of tdTomato-expressing neutrophils as a proportion of all neutrophils. E) Representative dot plots of the gating strategy for splenic dendritic cells ($CD45^+$, $CD11b^+$, $MHCII^+$, $CD11c^+$), T cells ($CD45^+$, $CD11b^-$, $CD3^+$, $B220^-$) and B cells ($CD45^+$, $CD11b^-$, $CD3^-$, $B220^+$). F) Frequency of tdTomato-expressing dendritic cells as a proportion of all dendritic cells. G) Frequency of tdTomato-expressing T cells as a proportion of all T cells. H) Frequency of tdTomato-expressing B cells as a proportion of all B cells; one-way ANOVA (# = $p<0.05$ for 'Control + tamoxifen' vs 'hCD68-tdTom + tamoxifen'; * = $p<0.05$ for 'hCD68-tdTom + vehicle' vs 'hCD86-tdTom + tamoxifen').

Population	Control + tamoxifen	hCD68-tdTom + vehicle	hCD68-tdTom + tamoxifen
Ly6C^{high} monocytes	0.39 ± 0.17	0.39 ± 0.20	4.25 ± 0.54*#
Ly6C^{low} monocytes	0.45 ± 0.22	0.07 ± 0.07	27.91 ± 1.30*#
Neutrophils	2.42 ± 1.06	0.22 ± 0.13	3.86 ± 0.34*
Dendritic cells	1.78 ± 0.33	1.03 ± 0.13	20.08 ± 1.21*#
T cells	0.03 ± 0.005	0.03 ± 0.003	2.40 ± 0.58*#
B cells	0.07 ± 0.02	0.03 ± 0.003	4.72 ± 0.47*#

Table 3.3. tdTomato expression in spleen non-macrophage populations. Percentage of tdTomato-expressing splenic immune non-macrophage populations represented as mean ± SEM; one-way ANOVA (# = $p<0.05$ for 'Control + tamoxifen' vs 'hCD68-tdTom + tamoxifen'; * = $p<0.05$ for 'hCD68-tdTom + vehicle' vs 'hCD86-tdTom + tamoxifen').

for macrophage targeting. Taken together, these results demonstrate that hCD68 driven inducible Cre recombinase is highly selective for macrophage populations *in vivo* and has little activity in circulating myeloid and lymphoid cell populations.

As the spleen is a reservoir for multiple immune cell types, I quantified tdTomato expression in non-macrophage immune cell populations within the spleen (Figure 3.9 and Table 3.3). Monocytes were sub-divided into Ly6C^{hi} (CD11b^{+}CD115^{+}Ly6C^{hi}) and Ly6C^{low} (CD11b^{+}CD115^{+}Ly6C^{low}) (Figure 3.9A). Importantly, <5 % of Ly6C^{hi} monocytes had tdTomato expression while ~28 % of the splenic Ly6C^{low} monocytes expressed tdTomato (Figure 3.9B and 3.9C respectively and Table 3.3). On the other hand, less than 4 % of neutrophils (CD11b^{+}CD115^{-}Ly6G^{+}) expressed tdTomato (Figure 3.9A/D and Table 3.3). I also found that ~20 % of splenic dendritic cells (CD45^{+}CD11c^{+}MHCII^{+}) had tdTomato expression (Figure 3.9E/F and Table 3.3). In the non-myeloid cells ~2.5 % of splenic T-cells (CD45^{+}CD11b^{-}CD3^{+}) (Figure 3.9E/G and Table 3.3) and under 5 % B-cells (CD45^{+}CD11b^{-}B220^{+}) expressed tdTomato (Figure 3.9E/H and Table 3.3). Overall, I found very limited evidence for Cre recombinase activation in non-macrophage cells in the liver, with the exception of Ly6C^{low} monocytes and dendritic cells.

3.3.5. The human CD68 promoter has higher macrophage specificity compared to endogenous murine Cd68 expression.

Having shown that hCD68 driven inducible Cre recombinase has selective activity in macrophage populations but not in other myeloid cell populations, I hypothesised that this could mirror variable levels of the endogenous murine Cd68 expression in different immune cell types. Even though all CD11b^{+}F4/80^{+} tissue resident peritoneal macrophages (Figure 3.10A) express murine Cd68 (Figure 3.10D/E), only around ~30 % of the same population express tdTomato (Figure 3.10B/C). In the circulation (Figure 3.10F), murine Cd68

was highly expressed by all myeloid cell types: neutrophils ($CD11b^{+}CD115^{-}Ly6G^{+}$; Figure 3.10G), $Ly6C^{high}$ ($CD11b^{+}CD115^{+}Ly6G^{-}Ly6C^{+}$, Figure 3.10H) and $Ly6C^{low}$ ($CD11b^{+}CD115^{+}Ly6G^{-}Ly6C^{+}$, Figure 3.10I) monocytes, but, apart from $Ly6C^{low}$ monocytes, they expressed low to undetectable levels of tdTomato. Since CD68 has never been reported to be expressed this highly in neutrophils I wanted to confirm that the antibody binding was

specific. Therefore, in Figure 3.10J, I compared the representative histograms for fluorescence minus one control, isotype control and a positive sample to show that the binding of PE-mCD68 antibody to neutrophils and monocytes was specific. Overall, these results show that the human CD68 expression cassette has increased lineage specificity for macrophages compared to expression of the murine macrosialin.

3.3.6. TdTomato expression in tissue resident macrophages is maintained for at least 6 weeks after Cre recombinase activation

To test the stability of tdTom expression following hCD68 driven Cre recombinase induction I extended the induction period by 6 weeks on top of the usual protocol. tdTom expression was determined 5 days after the last tamoxifen dose and a second group of mice '+ 6 weeks' was harvested 6 weeks later (Figure 3.11A). I assessed tdTomato expression in macrophage populations within the peritoneal cavity, spleen and liver at baseline and + 6 weeks. There was no decrease in the number of tdTomato expressing macrophages in the peritoneal cavity (Figure 3.11B), spleen (Figure 3.11D) and liver (Figure 3.11F) in the +6 weeks group, however, there was increase in the intensity of tdTomato expression in the tdTomato-expressing macrophages present the peritoneal cavity (Figure 3.11C) and spleen (Figure 3.11E) compared to baseline.

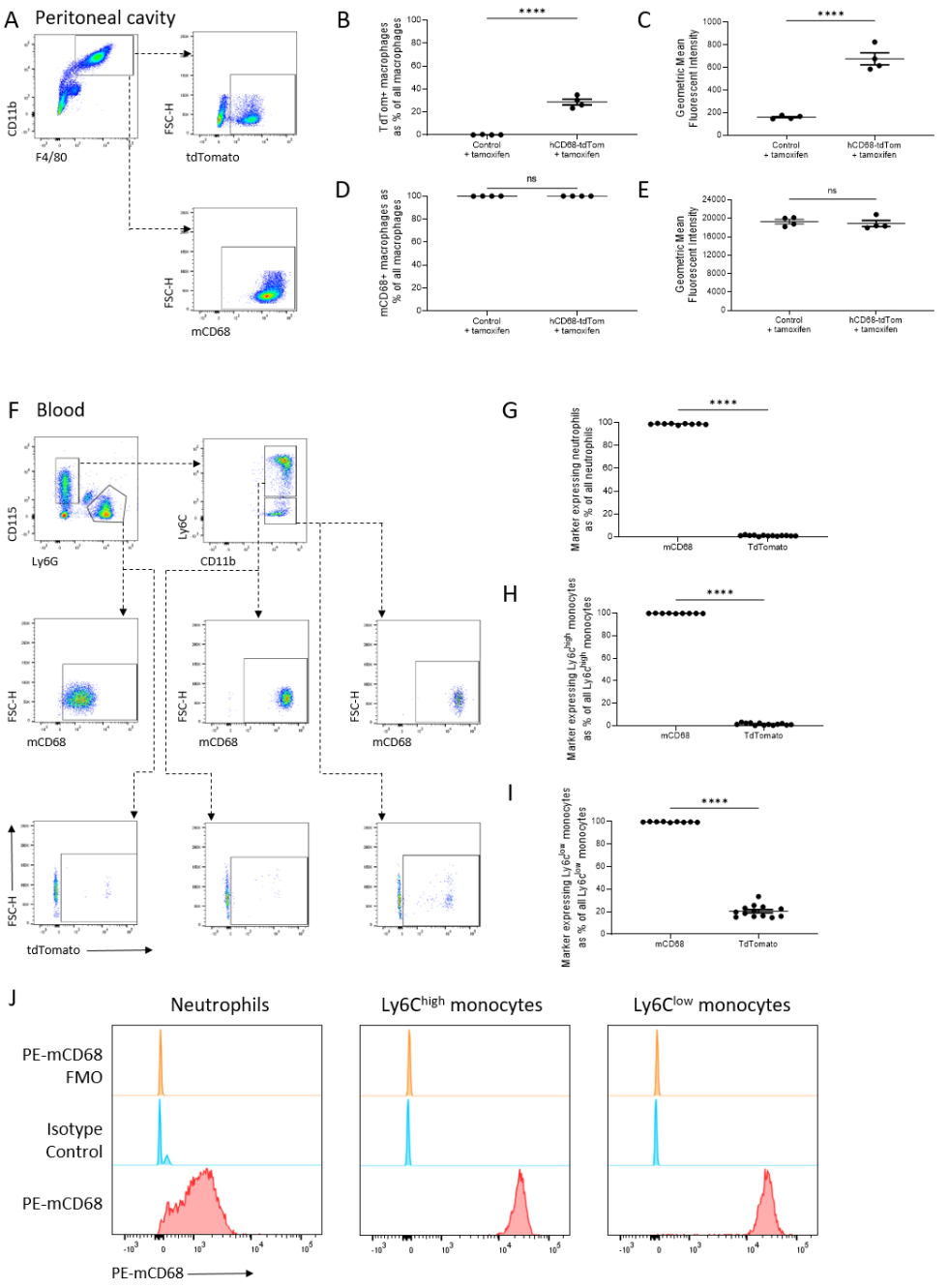

Figure 3.10. The transgenic human CD68 promoter has higher macrophage specificity compared to endogenous murine Cd68 expression. A) Representative dot plots of the gating strategy for peritoneal macrophages ($CD11b^+$, $F4/80^+$) and their expression of tdTomato and murine CD68 (mCD68). B) Frequency of tdTomato-expressing peritoneal macrophages as a proportion of all peritoneal macrophages with corresponding mean fluorescence intensity in (C). D) Frequency of mCD68-expressing macrophages as a proportion of all macrophages with corresponding mean fluorescence intensity in (E). F) Representative dot plots of the gating strategy for blood neutrophils ($CD115^-$, $Ly6G^+$), $Ly6C^{high}$ and $Ly6C^{low}$ monocytes ($CD115^+$, $Ly6G^-$, $Ly6C^+$ and $CD115^+$, $Ly6G^-$, $Ly6C^-$ respectively) and their expression of tdTomato and mCD68. G) Comparison of frequency of neutrophils expressing mCD68 and tdTomato. H) Comparison of frequency of $Ly6C^{high}$ monocytes expressing mCD68 and tdTomato. I) Comparison of frequency of $Ly6C^{low}$ monocytes expressing mCD68 and tdTomato. J) Representative histograms (normalised to mode) for the mCD68 expression in neutrophils, $Ly6C^{high}$ monocytes and $Ly6C^{low}$ monocytes show for fluorescence minus one (FMO) control, isotype control and positive sample; for panels (G), (H) and (I) mCD68 was quantified for control mice without tamoxifen, tdTom was measured for hCD68-tdTom + tamoxifen mice, student t-test (**** = $p<0.0001$).

To ensure that the longer induction period does not change the macrophage targeting profile, I assessed tdTomato expression in circulating leukocytes and splenic non-macrophage populations (Table 3.4 and Figure 3.12). Interestingly, after additional 6 weeks there was no tdTomato expression in any leukocyte populations in the blood (Table 3.4). Within circulating immune cell populations after 6 weeks there was a significant reduction of tdTomato expression in circulating neutrophils, Ly6C^{high} and Ly6C^{low} monocytes, dendritic cells, eosinophils and CD8^{+} T cells in the hCD68-tdTom mice dosed with tamoxifen. On the other hand, all splenic non-macrophage populations apart from Ly6C^{low} monocytes maintained similar proportion of tdTomato expressing cells (Figure 3.12) when compared to the baseline expression. However, the expression levels measured by the MFI have significantly decreased in both the neutrophils and Ly6C^{low} monocytes (Figure 3.12B and 3.12F respectively). Interestingly, the MFI value for B cells increased significantly after 6 weeks of induction even though the proportion of tdTomato expressing B cells did not change significantly (Figure 3.12 I/J). Taken together this data demonstrated that hCD68-CreERT2 driver mouse line can be used for studies where prolonged targeting of tissue-resident macrophages is required. The already relatively low off-target effects in the blood are completely abolished after additional 6 weeks of induction period, which reflects short half-life and high turnover of circulating immune cells in comparison to the tissue-resident macrophages. In splenic tissue, non-macrophage expression of tdTomato remains low, either at a level comparable to the baseline expression or significantly decreased, with the exception of B cells where the expression intensity increases but the proportion of targeted cells remains stable.

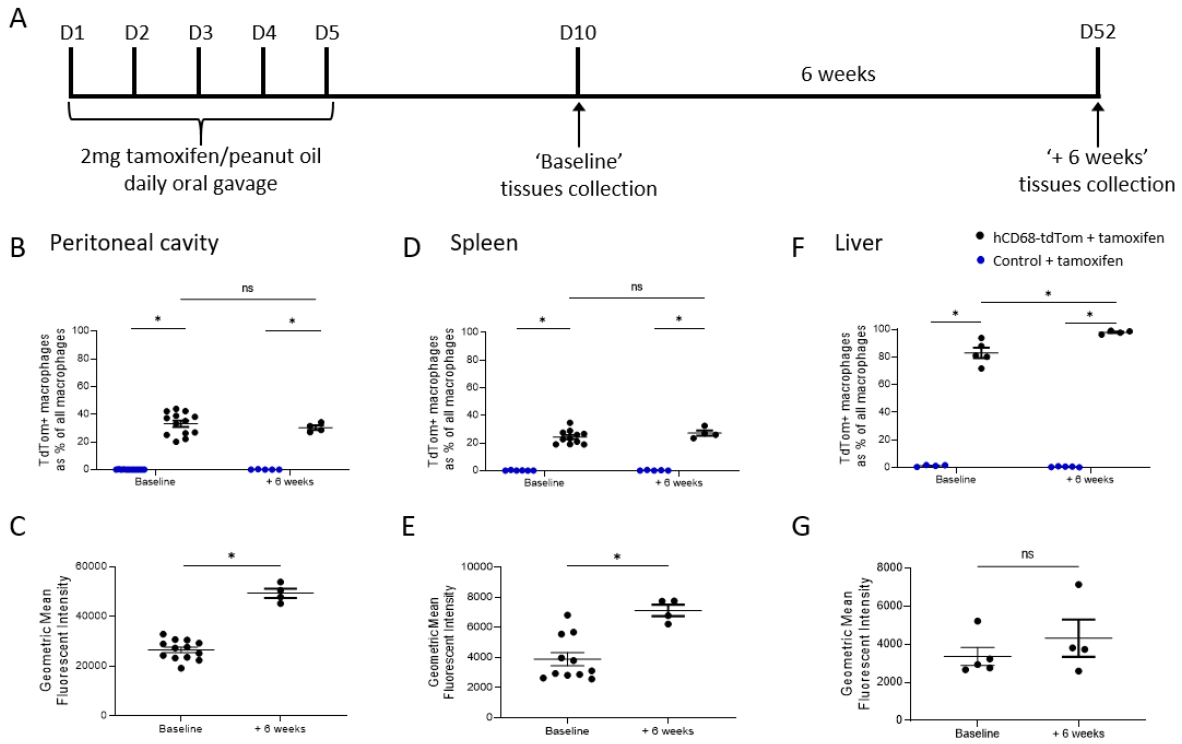

Figure 3.11. TdTomato expression in tissue resident macrophages is maintained for at least 6 weeks after Cre recombinase activation. In all panels control + tamoxifen mice are marked as blue dots; hCD68-tdTom + tamoxifen mice are marked as black dots. In all panels mice with the usual 5 days wash out period are marked 'Baseline', while mice with an additional 6 weeks wait are marked '+ 6 weeks'. A) Tamoxifen dosing protocol for induction of Cre recombinase activity and assessment of targeting efficiency 6 weeks post-induction in hCD68-CreERT2 model. Frequency of tdTomato-expressing macrophages as a proportion of all macrophages in (B) peritoneal cavity (D) spleen and (F) liver with corresponding mean fluorescence intensity of tdTomato$^+$ macrophages for 'Baseline' and '+6 weeks' groups in (C), (E) and (G); two-way ANOVA in panels (B), (D) and (F), student t-test in panels (C), (E), (G), (* = $p<0.05$).

Population	Baseline	+ 6 weeks
Ly6C^{high} monocytes	1.54 ± 0.27	0.03 ± 0.03*
Ly6C^{low} monocytes	20.49 ± 1.49	0.05 ± 0.05*
Neutrophils	1.28 ± 0.12	0.06 ± 0.02*
Dendritic cells	4.93 ± 0.66	0.10 ± 0.10*
Eosinophils	0.91 ± 0.20	0.12 ± 0.04*
CD4 T cells	1.41 ± 0.60	0.53 ± 0.14
CD8 T cells	1.05 ± 0.16	0.30 ± 0.11*
B cells	0.33 ± 0.04	0.20 ± 0.04

Table 3.4. tdTomato expression in circulating leukocytes declines 6 weeks after Cre recombinase activation. hCD68-tdTom mice with the standard 5 days wash out period are marked 'Baseline', while mice with an additional 6 weeks wait are marked '+ 6 weeks' (as per Figure 3.11). Percentage of tdTomato-expressing blood leukocytes represented as mean ± SEM; student t-test (* = $p<0.05$).

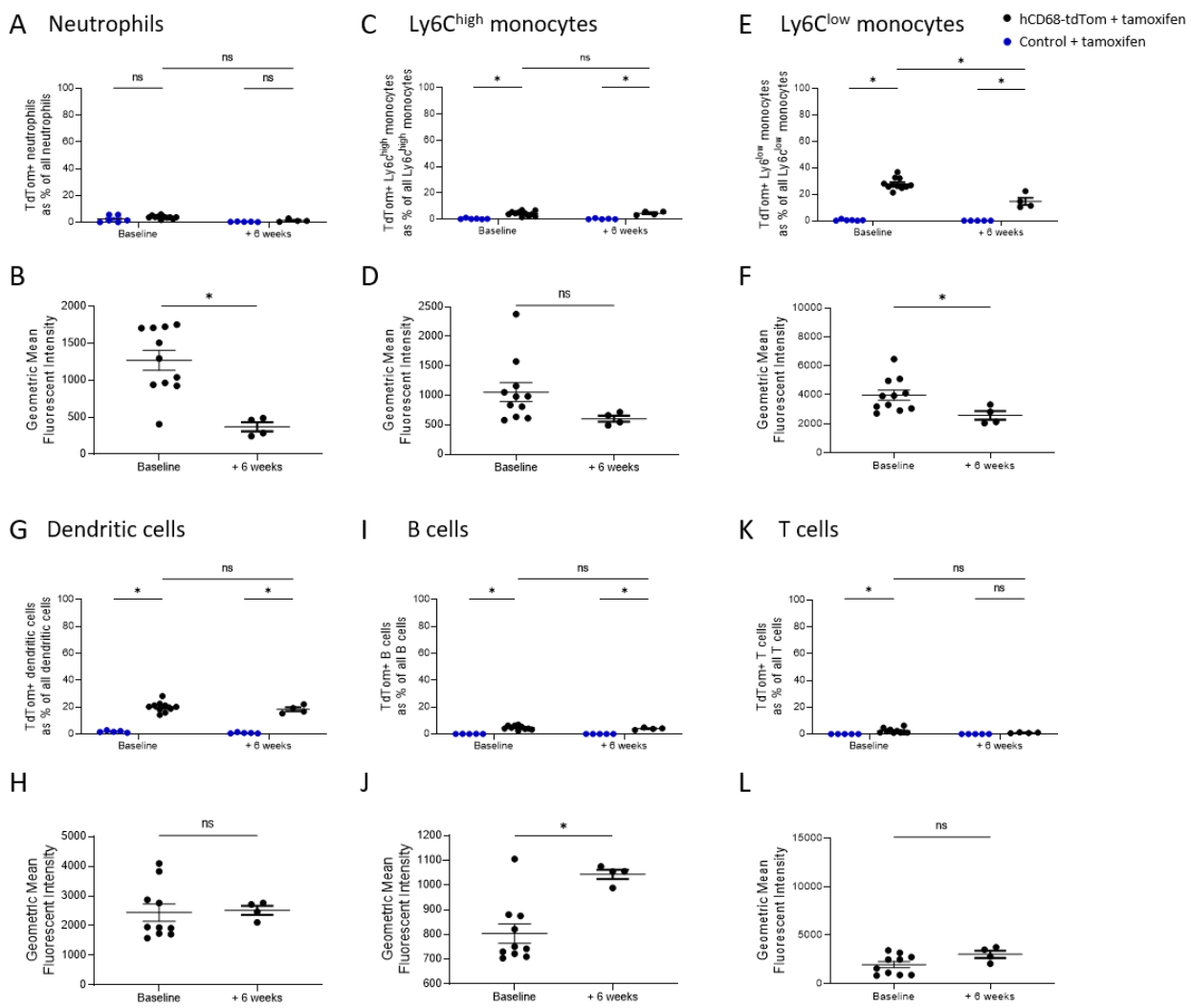

Figure 3.12. tdTomato expression in non-macrophage spleen populations remains low 6 weeks after Cre recombinase activation. In all panels control + tamoxifen mice are marked as blue dots; hCD68-tdTom + tamoxifen mice are marked as black dots. In all panels mice with the standard 5 days wash out period are marked 'Baseline', while mice with an additional 6 weeks wait are marked '+ 6 weeks'. Frequency of tdTomato-expressing splenic (A) neutrophils, (C) Ly6C^{high} monocytes, (E) Ly6C^{low} monocytes, (G) dendritic cells, (I) B cells and (K) T cells as a proportion of all cells of the given type with corresponding mean fluorescence intensity of tdTomato+ cells for 'Baseline' and '+6 weeks' groups in (B), (D), (F), (H), (J) and (L); two-way ANOVA in panels (A), (C), (E), (G), (I) and (K), student t-test in panels (B), (D), (F), (H), (J) and (L), (* = $p<0.05$).

3.3.7. The comparison between the human CD68 promoter-driven inducible Cre recombinase mouse line and LysM-Cre driver line.

The LysM-Cre is one of the most widely used macrophage-targeting Cre driver mice. Therefore, I wanted to compare the targeting profile of hCD68-CreERT2 mouse to constitutively active LysM-Cre mouse, so I crossed both lines with the same tdTomato$^{fl/fl}$ reporter mouse line. Because I used the same tdTom reporter mouse I was able to use the same cytometer settings, which allowed me to compare not just the proportion of cells targeted but also the mean fluorescence intensity between the two strains. Constitutive Cre activation in LysM-tdTom mice resulted in higher proportion of tdTomato expressing cells in macrophage populations in the peritoneal cavity (Figure 3.13A) and spleen (Figure 3.13C) but lower efficiency of targeting in the liver (Figure 3.13E) compared to hCD68-tdTom mice.

Peritoneal cavity macrophages from LysM-Cre-tdTom mice also had higher levels of tdTom expression (Figure 3.13B), while no difference in MFI was seen in splenic or hepatic macrophages (Figure 3.13D and 313F respectively). Fluorescent microscopy to visualise the endogenous tdTomato expression confirmed flow cytometry results in the spleen (Figure 3.13G) and liver (Figure 3.13H) with cells endogenously expressing tdTomato seen in both strains. Interestingly, despite no changes in fluorescence intensity detected by flow cytometry between the strains, the LysM-Cre mice appeared dimmer than hCD68-CeERT2 mice in both organs, which may be due to high background fluorescence or the endogenous expression of tdTom being bleached to a greater extend while processing the organs.

I next wanted to compare the specificity of the hCD68-CreERT2 and LysM-Cre targeting by assessing tdTomato expression in circulating leukocyte populations. I demonstrated that tamoxifen treated hCD68-tdTom mice have almost no expression of tdTomato on blood neutrophils while ~90 % of circulating neutrophils in LysM-tdTom mice expressed tdTom

(Figure 3.14A). A similar result was seen in blood Ly6C^{high} monocytes with only ~2.5 % of Ly6C^{high} monocytes in tamoxifen treated hCD68-tdTom expressed tdTomato, compared to ~66 % of Ly6C^{high} monocytes from LysM-tdTom mice (Figure 3.13B). Additionally, ~20 % of Ly6C^{low} monocytes from tamoxifen treated hCD68-tdTom expressed tdTomato compared to ~83% of Ly6C^{low} monocytes from LysM-tdTom mice (Figure 3.13C). In the other myeloid blood populations ~5% of hCD68-tdTom dendritic cells were targeted in comparison to ~60% of LysM-tdTom dendritic cells (Figure 3.14D). In the eosinophil population less than 1% of hCD68-tdTom cells were targeted, compared to ~20% of LysM-tdTom cells (Figure 3.14E). When looking at lymphocyte populations in the blood, almost no expression was seen in either CD4^{+} T cells, CD8^{+} T cells or B cells in the hCD68-tdTom mice while 10-20% of cells were targeted in those population in LysM-tdTom mice (Figure 3.14F, 3.14G and 3.14H respectively).

Given that spleen harbours multiple immune populations and proved to be the main source of lineage non-restricted expression in hCD68-CreERT2 mice I wanted to assess and compare the expression levels of non-macrophage immune compartment in the spleens of hCD68-tdTom and LysM-tdTom mice (Figure 3.15). LysM-Cre mice showed significant increase of tdTomato expression and efficiency of targeting in all immune cell types assessed. Particularly, neutrophils and Ly6C^{high} and Ly6c^{low} monocytes showed a marked increase in efficiency of targeting and in the levels of expression, from ~5% to ~60% in neutrophils, ~5% to ~80% in Ly6c^{high} monocytes and ~30% to about 90% in Ly6c^{low} monocytes (Figure 3.15A, 3.15C and 3.15E respectively). All of these cell types also showed a significant increase in the expression of tdTomato in LysM-cre mice in comparison to hCD68-CreERT2 mice (Figure 3.15B/D/F). Dendritic cells, B cells and T cells also showed a smaller but significant

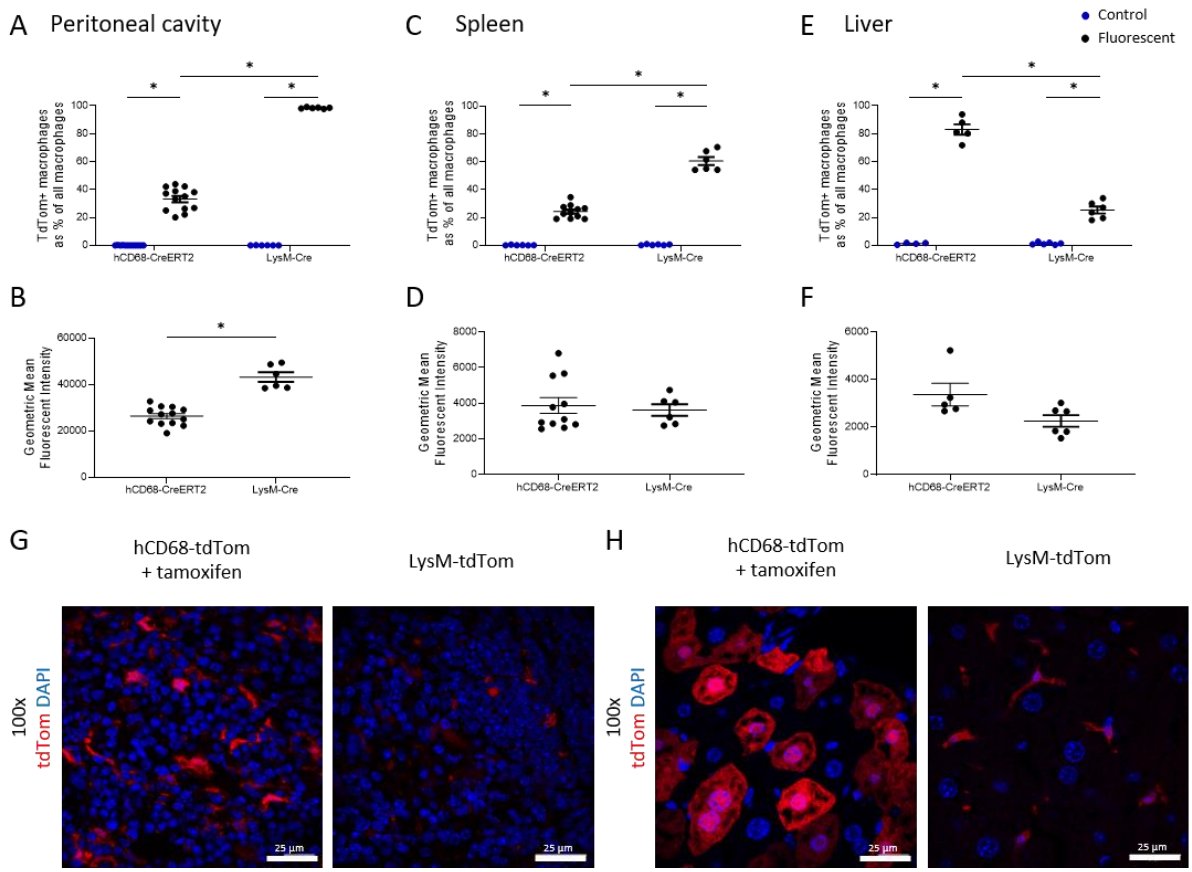

Figure 3.13. The hCD68 promoter driven inducible Cre recombinase improves targeting of liver macrophages compared to LysM-Cre. In all panels control mice (littermates of hCD68-tdTom mice that were given tamoxifen or littermates of LysM-tdTom mice) are marked as blue dots; Fluorescent mice (hCD68-tdTom + tamoxifen or LysM-tdTom mice) are marked as black dots. Frequency of tdTomato-expressing macrophages as a proportion of all macrophages in (A) peritoneal cavity (C) spleen and (E) liver with corresponding mean fluorescence intensity of tdTomato+ macrophages for hCD68-CreERT2 and LysM-Cre mice in (B), (D) and (F). Representative immunofluorescence images of endogenous tdTomato expression in (G) the spleen and (H) the liver of hCD68-tdTom and LysM-tdTom mice at 100x magnification with DAPI in blue and tdTomato in red; scale bar = 25µm; two-way ANOVA in panels (A), (C) and (E), student t-test in panels (B), (D) and (F), (* = $p<0.05$).

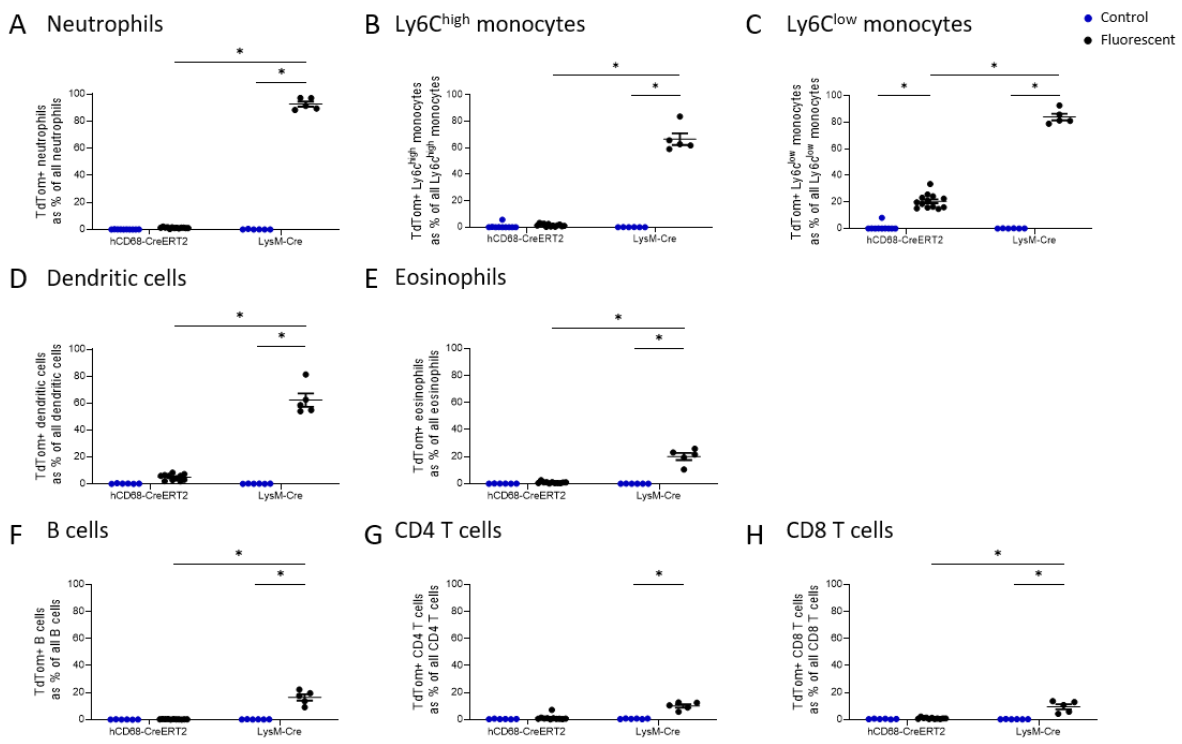

Figure 3.14. The hCD68 promoter driven inducible Cre recombinase reduces lineage non-restricted expression of tdTomato in blood compared to LysM-Cre. In all panels control mice (littermates of hCD68-tdTom mice that were given tamoxifen or littermates of LysM-tdTom mice) are marked as blue dots; Fluorescent mice (hCD68-tdTom + tamoxifen or LysM-tdTom mice) are marked as black dots. Frequency of tdTomato-expressing blood (A) neutrophils, (B) Ly6C^{high} monocytes, (C) Ly6C^{low} monocytes, (D) dendritic cells, (E) eosinophils, (F) B cells, (G) CD4 T cells and (H) CD8 T cells as a proportion of all blood leukocytes of the given type for hCD68-CreERT2 and LysM-Cre mice; two-way ANOVA, (* = $p<0.05$).

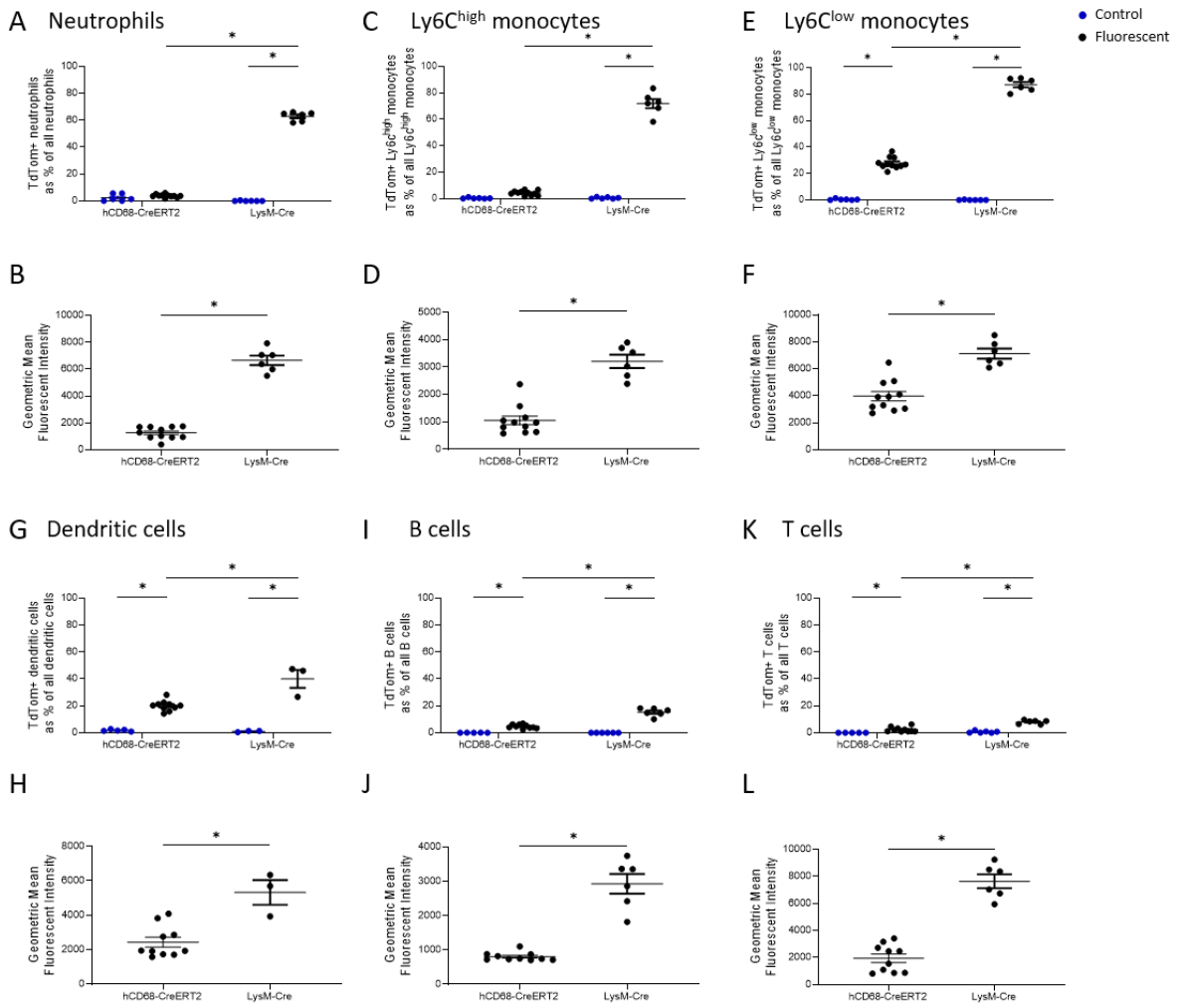

Figure 3.15. The hCD68 promoter driven inducible Cre recombinase reduces lineage non-restricted expression of tdTomato in spleen compared to LysM-Cre. In all panels control mice (littermates of hCD68-tdTom mice that were given tamoxifen or littermates of LysM-tdTom mice) are marked as blue dots; Fluorescent mice (hCD68-tdTom + tamoxifen or LysM-tdTom mice) are marked as black dots. Frequency of tdTomato-expressing spleen (A) neutrophils, (C) Ly6C^{high} monocytes, (E) Ly6C^{low} monocytes, (G) dendritic cells, (I) B cells and (K) T cells as a proportion of all cells of the given type with corresponding mean fluorescence intensity of tdTomato+ cells for hCD68-CreERT2 and LysM-Cre mice in (B), (D), (F), (H), (J) and (L); two-way ANOVA in panels (A), (C), (E), (G), (I) and (K), student t-test in panels (B), (D), (F), (H), (J) and (L), (* = $p<0.05$).

increase in the efficiency of targeting with ~20% to ~40% in DCs, ~5% to ~15% in B cells and ~5% to ~10% in T cells (Figure 3.15G, 3.15I and 3.15K respectively). This increase in the proportion of targeted cells also corresponded to the expression levels with all three cell types showing a marked increase in expression from hCD68-CreERT2 mice to LysM-Cre mice (Figure 3.15H/J/L). Overall, I showed that hCD68-CreERT2 mouse has a more macrophage-specific phenotype of expression compared to the constitutive LysM-Cre mouse line, which carries across all the tissues. Additionally, the hCD68-CreERT2 mouse is significantly more efficient at targeting tissue-resident macrophages in the liver compared to the LysM-Cre driver mouse.

3.3.8. The comparison between the human CD68 promoter-driven inducible Cre recombinase mouse line and constitutively active GFP line.

Since hCD68-GFP mouse line was developed in the Greaves lab and uses the same hCD68 expression cassette (*279*) I wanted to compare its expression profile with the inducible hCD68-CreERT2 driver line. I was able to show that hCD68-CreERT2 mouse targets the same tissue-resident macrophage populations as hCD68-GFP mouse (Figure 3.16). hCD68-GFP mouse targeted higher proportion of peritoneal and splenic macrophages when compared to hCD68-CreERT2 mouse (Figure 3.16A and 3.16C respectively). Since the endogenous fluorescence was induced by different fluorescent constructs, and therefore excited by different lasers, I was not able to compare the expression of endogenous fluorescence between the two strains directly – to confirm the relatively high expression profiles in the peritoneum and spleen I show representative histograms of the tdTomato and GFP expression relative to the FMO control for each of them in Figure 3.16B and 3.16D respectively. I also used fluorescent microscopy to visualise the endogenous tdTomato and GFP expression in the spleen (Figure 3.16E) and liver (Figure 3.13F). I was not able to process

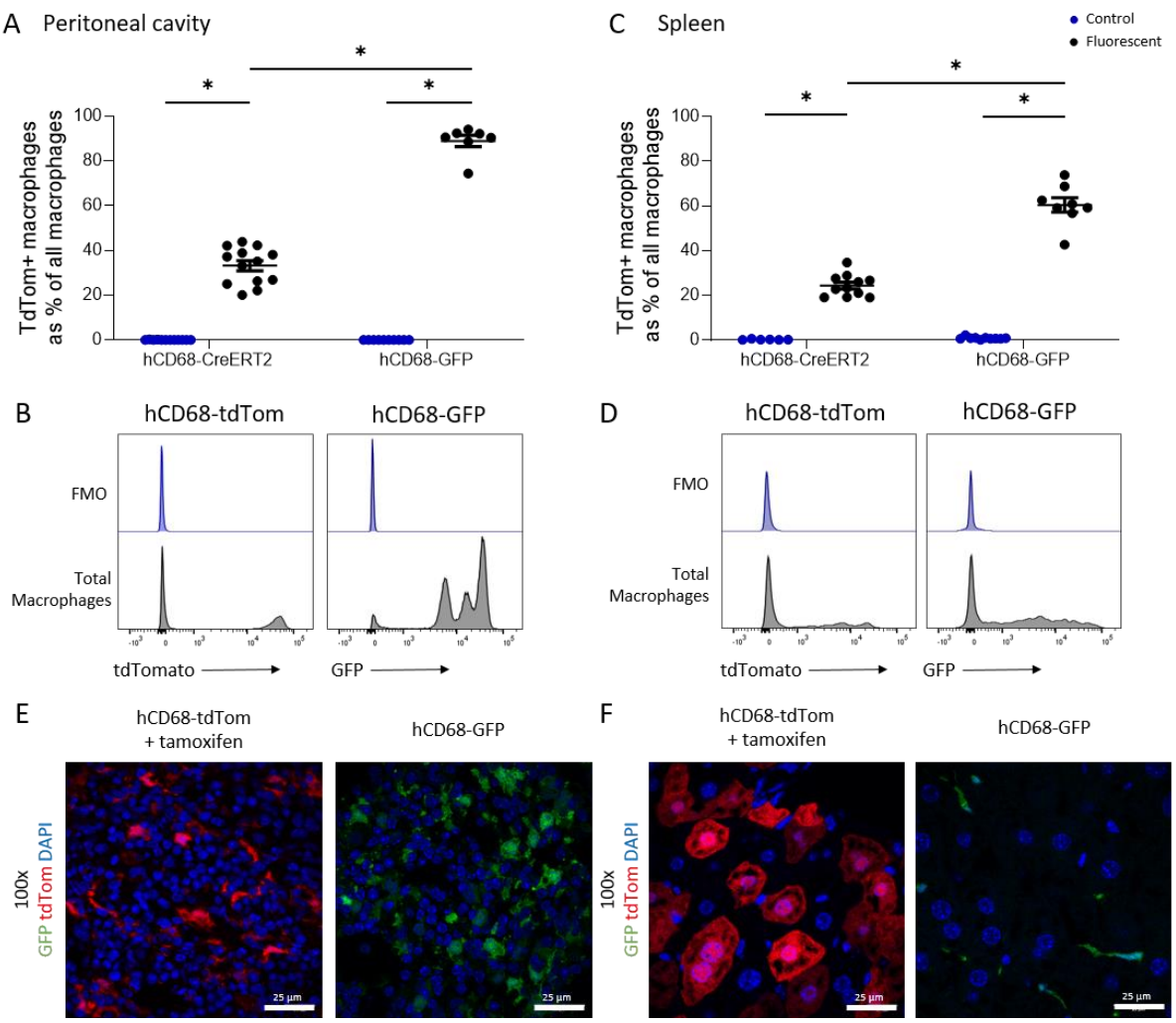

Figure 3.16. The hCD68 promoter driven inducible Cre recombinase targets the same macrophage populations as hCD68-GFP mouse. In all panels control mice (littermates of hCD68-tdTom mice that were given tamoxifen or WT littermates of hCD68-GFP mice) are marked as blue dots; fluorescent mice (hCD68-tdTom + tamoxifen or hCD68-GFP mice) are marked as black dots. Frequency of tdTomato or GFP-expressing macrophages as a proportion of all macrophages in (A) peritoneal cavity and (C) spleen with the corresponding representative histograms of the fluorescence minus one (FMO) control and a positive sample in (B) and (D) respectively; two-way ANOVA, (* = $p<0.05$). Representative immunofluorescence images of endogenous tdTomato and GFP expression in (E) the spleen and (F) the liver of hCD68-tdTom and hCD68-GFP mice at 100x magnification with DAPI in blue, tdTomato in red and GFP in green; scale bar = 25µm.

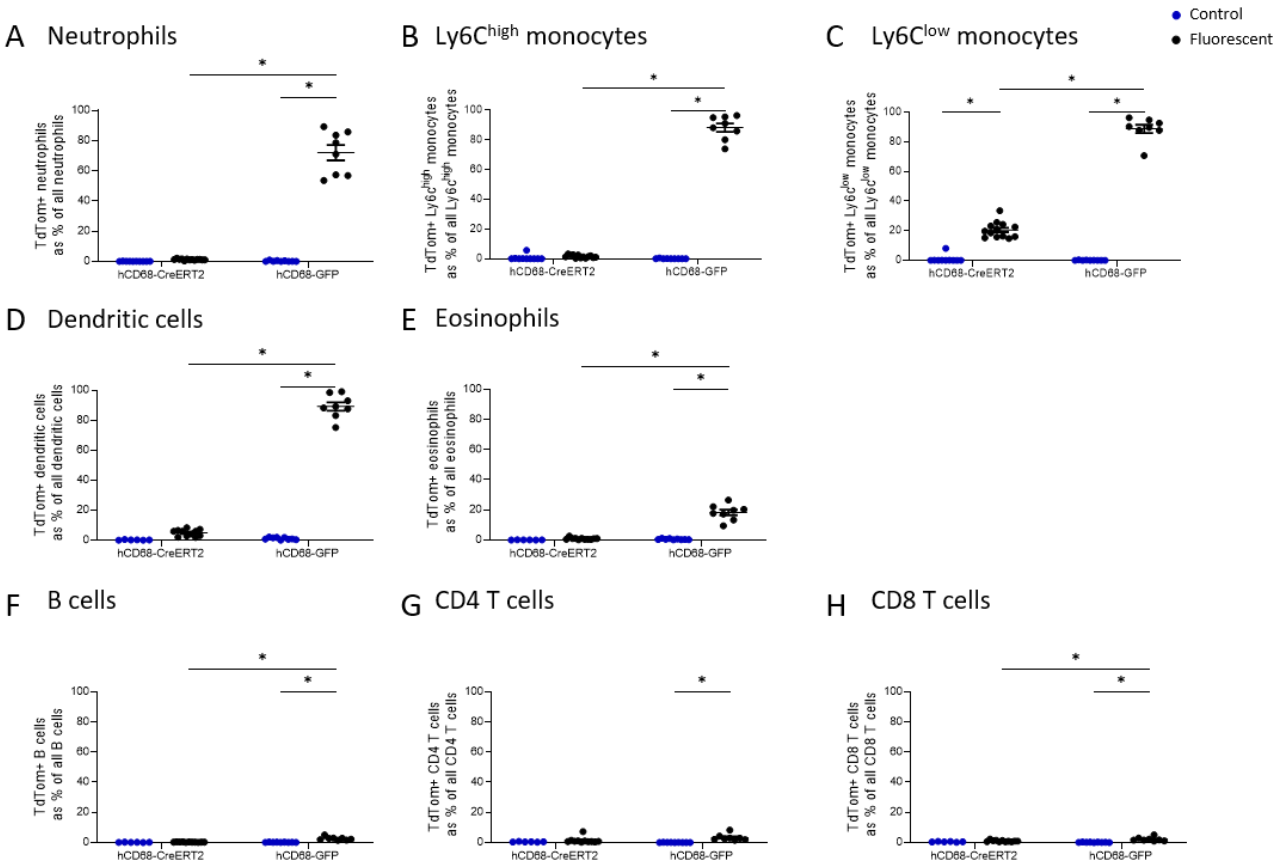

Figure 3.17. The hCD68 promoter driven inducible Cre recombinase reduces lineage non-restricted fluorescence in blood compared to hCD68-GFP mouse. In all panels control mice (littermates of hCD68-tdTom mice that were given tamoxifen or WT littermates of hCD68-GFP mice) are marked as blue dots; fluorescent mice (hCD68-tdTom + tamoxifen or hCD68-GFP mice) are marked as black dots. Frequency of tdTomato or GFP-expressing blood (A) neutrophils, (B) Ly6C^{high} monocytes, (C) Ly6C^{low} monocytes, (D) dendritic cells, (E) eosinophils, (F) B cells, (G) CD4 T cells and (H) CD8 T cells as a proportion of all blood leukocytes of the given type for hCD68-CreERT2 and hCD68-GFP mice; two-way ANOVA, (* = $p<0.05$).

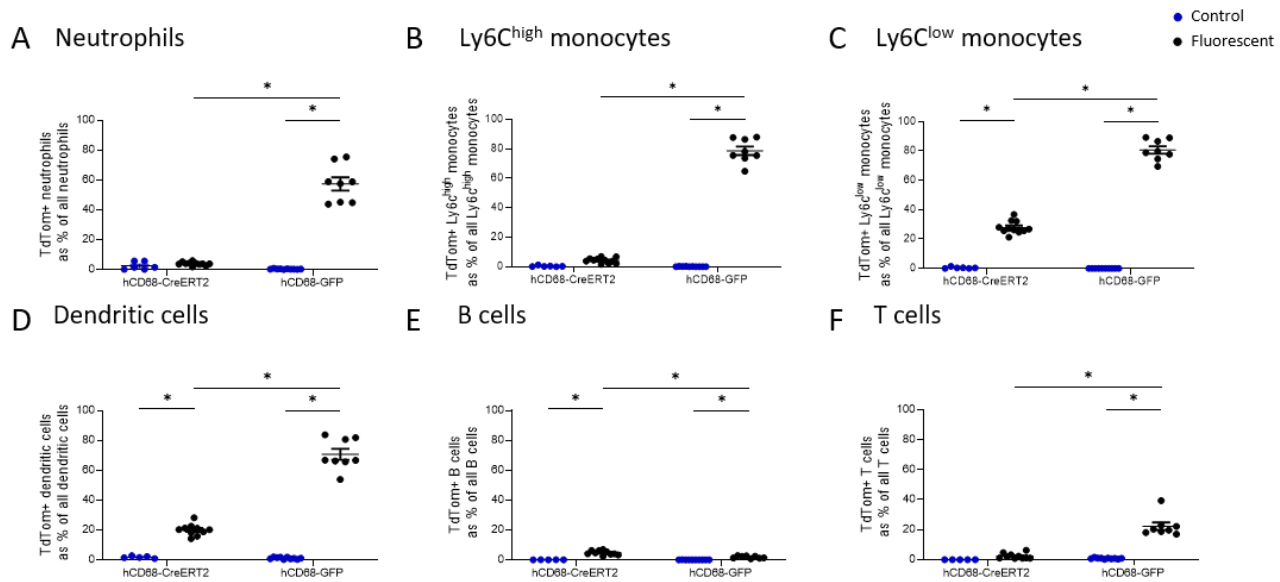

Figure 3.18. The hCD68 promoter driven inducible Cre recombinase reduces lineage non-restricted fluorescence in spleen compared to hCD68-GFP mouse. In all panels control mice (littermates of hCD68-tdTom mice that were given tamoxifen or WT littermates of hCD68-GFP mice) are marked as blue dots; fluorescent mice (hCD68-tdTom + tamoxifen or hCD68-GFP mice) are marked as black dots. Frequency of tdTomato-expressing spleen (A) neutrophils, (B) Ly6C^{high} monocytes, (C) Ly6C^{low} monocytes, (D) dendritic cells, (E) B cells and (F) T cells as a proportion of all cells of the given type; two-way ANOVA, (* = $p<0.05$).

the livers in the flow cytometry analysis due to extremely high auto-fluorescence levels in the hCD68-GFP mice, which interfered with the GFP detection therefore making my data unreliable for this tissue.

Next, I wanted to compare the specificity of the hCD68-CreERT2 and hCD68-GFP targeting by assessing tdTomato expression in circulating leukocyte populations. I demonstrated that tamoxifen treated hCD68-tdTom mice have almost no expression of tdTomato on blood neutrophils while ~70 % of circulating neutrophils in hCD68-GFP mice expressed GFP (Figure 3.17A). A similar result was seen in blood Ly6C^{high} monocytes with only ~2.5 % of Ly6C^{high} monocytes in tamoxifen treated hCD68-tdTom expressed tdTomato, compared to ~90 % of Ly6C^{high} monocytes from hCD68-GFP mice being fluorescent (Figure 3.17B). Additionally, ~20 % of Ly6C^{low} monocytes from tamoxifen treated hCD68-tdTom expressed tdTomato compared to ~90% of Ly6C^{low} monocytes from hCD68-GFP mice being fluorescent (Figure 3.17C). In the other myeloid blood cell populations ~5% of hCD68-tdTom dendritic cells were targeted in comparison to ~90% of hCD68-GFP dendritic cells (Figure 3.17D). In the eosinophil population less than 1% of hCD68-tdTom cells were targeted, compared to ~20% of hCD68-GFP cells (Figure 3.17E). When looking at lymphocyte populations in the blood, almost no expression was seen in either CD4^{+} T cells, CD8^{+} T cells or B cells in the hCD68-tdTom mice and the hCD68-GFP mice, yet there was a modest but significant increase in the proportion of B cells and CD8^{+} T cells targeted by hCD68-GFP mouse when compared to hCD68-tdTom mouse (Figure 3.17F and 3.14H respectively).

I also wanted to assess and compare the expression levels of non-macrophage immune compartment in the spleens of hCD68-tdTom and hCD68-GFP mice (Figure 3.18). hCD68-GFP mice showed significant increase in efficiency of targeting in all immune cell types assessed.

Particularly, neutrophils and Ly6C^{high} and Ly6c^{low} monocytes showed a marked increase in efficiency of targeting and in the levels of expression, from ~5% to ~60% in neutrophils, ~5% to ~80% in Ly6c^{high} monocytes and ~30% to about 80% in Ly6c^{low} monocytes (Figure 3.18A, 3.18C and 3.18E respectively). Dendritic cells and T cells also showed a smaller but significant increase in the efficiency of targeting with ~20% to ~70% in DCs and ~5% to ~20% in T cells (Figure 3.18D and 3.18F respectively). B cells were targeted at very low levels in both mouse lines, with small but significant decrease in targeting efficiency between the hCD68-tdTom and hCD68-GFP mice (Figure 3.18E). Overall, I showed that hCD68-CreERT2 mouse has a more macrophage-specific phenotype of expression compared to the constitutive hCD68-GFP mouse line, which carried across all the tissues.

3.3.9. The human CD68 promoter-driven inducible Cre recombinase targets recruited macrophages in atherosclerotic lesions

Lipid laden macrophages within arterial walls are a key driver of the pathophysiology in cardiovascular disease. To induce hyperlipidaemia hCD68-tdTom and control mice were injected with a gain-of-function mutant PCSK9 adeno-associated virus vector (AAV) or a control viral vector (*343*). Mice given a single intravenous injection of AAV8-mPCSK9 or control AAV were placed on a high fat diet (HFD). After 16 weeks of HFD feeding hCD68-tdTom mice or control were given tamoxifen to induce Cre recombinase activity (Figure 3.19A). As expected, mice given a single injection of AAV8-mPCSK9 but not a control AAV developed atherosclerotic lesions in the aortic sinus as shown by increased Oil Red O staining (Figure 3.19B). I next looked for tdTomato expression within atherosclerotic lesions in tamoxifen treated hCD68-tdTom mice. AAV8-mPCSK9 injected hCD68-tdTom mice treated with tamoxifen expressed high levels of tdTomato within the atherosclerotic plaque. (Figure 3.19C). TdTomato expressing macrophages were distinguishable from auto

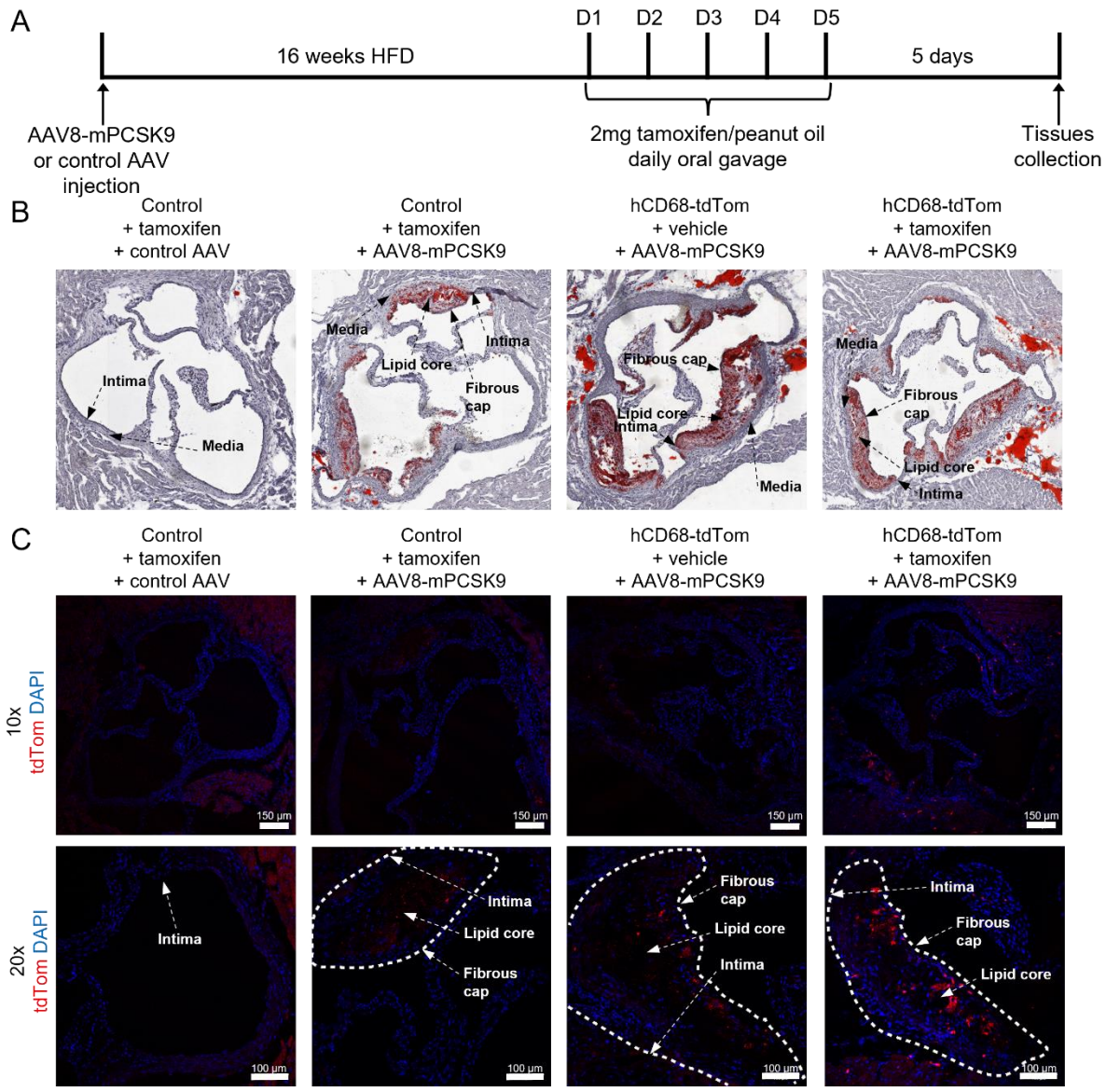

Figure 3.19. The hCD68 promoter driven inducible Cre recombinase targets recruited macrophages in atherosclerotic lesions. A) Timeline of the PCSK9 atherosclerosis model and induction of Cre recombinase in hCD68-CreERT2 mice. B) Representative images of Oil Red O staining of the aortic roots confirm the induction of atherosclerotic plaques in the AAV8-mPCSK9 injected groups with the anatomy of the plaques labelled. C) Representative immunofluorescence images of endogenous tdTomato expression in the aortic roots at 10x (whole aortic root) and 20x (plaque close-up with plaque edges outlined with the dashed white line, anatomy of plaque labelled) magnification with DAPI in blue and tdTomato in red; scale bar = 150 µm in 10x images and 100 µm in 20 x images.

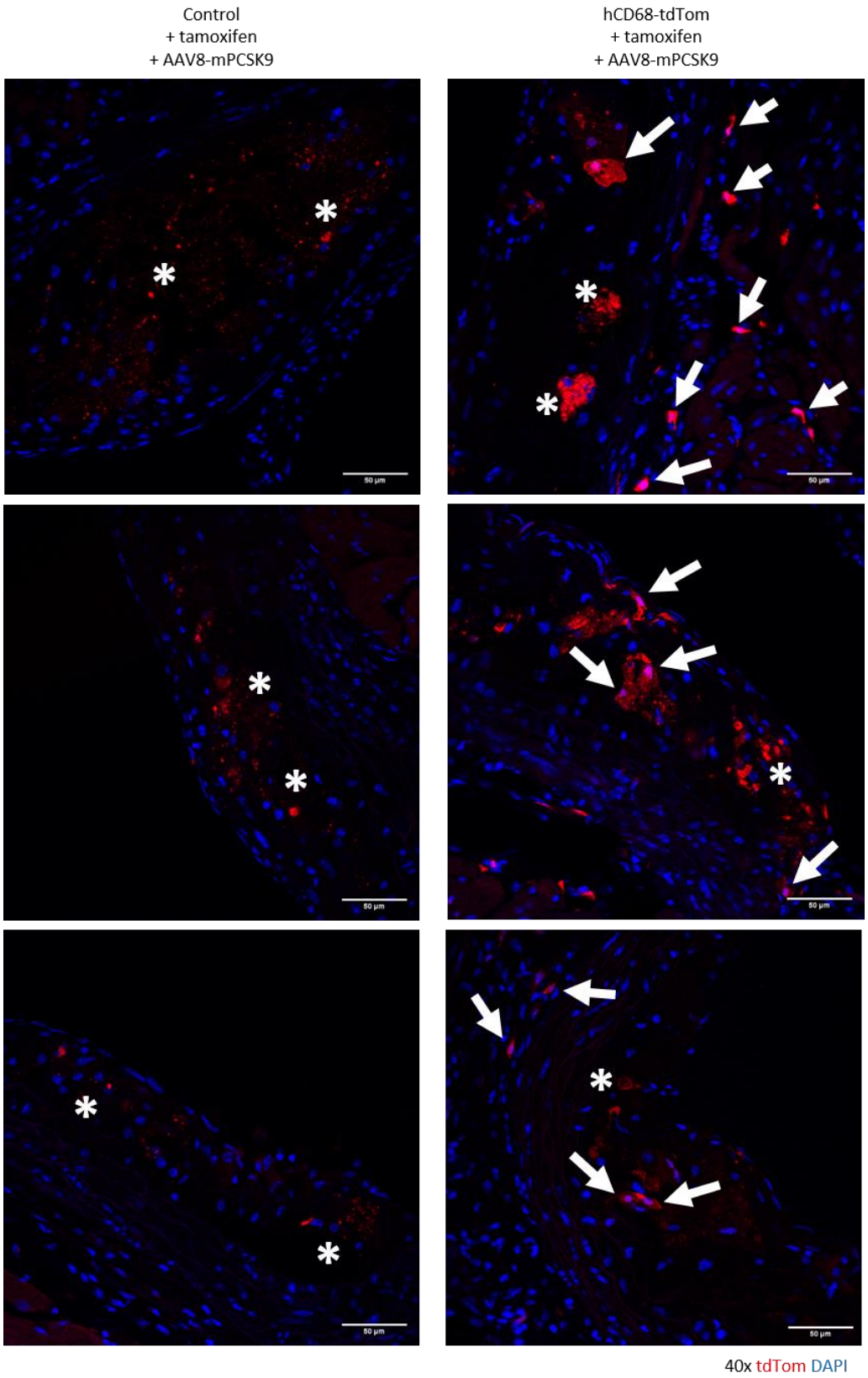

Figure 3.20. tdTomato-expressing cells in the atherosclerotic lesions are detected alongside auto-fluorescent lipid droplets. Representative immunofluorescence images of endogenous tdTomato expression in cells (marked with white arrows) and auto-fluorescent lipid droplets (marked with white asterisks) in the atherosclerotic plaques at 40 x magnification with DAPI in blue and tdTomato in red; scale bar = 50 µm, n=3 technical repeats for each group consisting of 3 biological repeats.

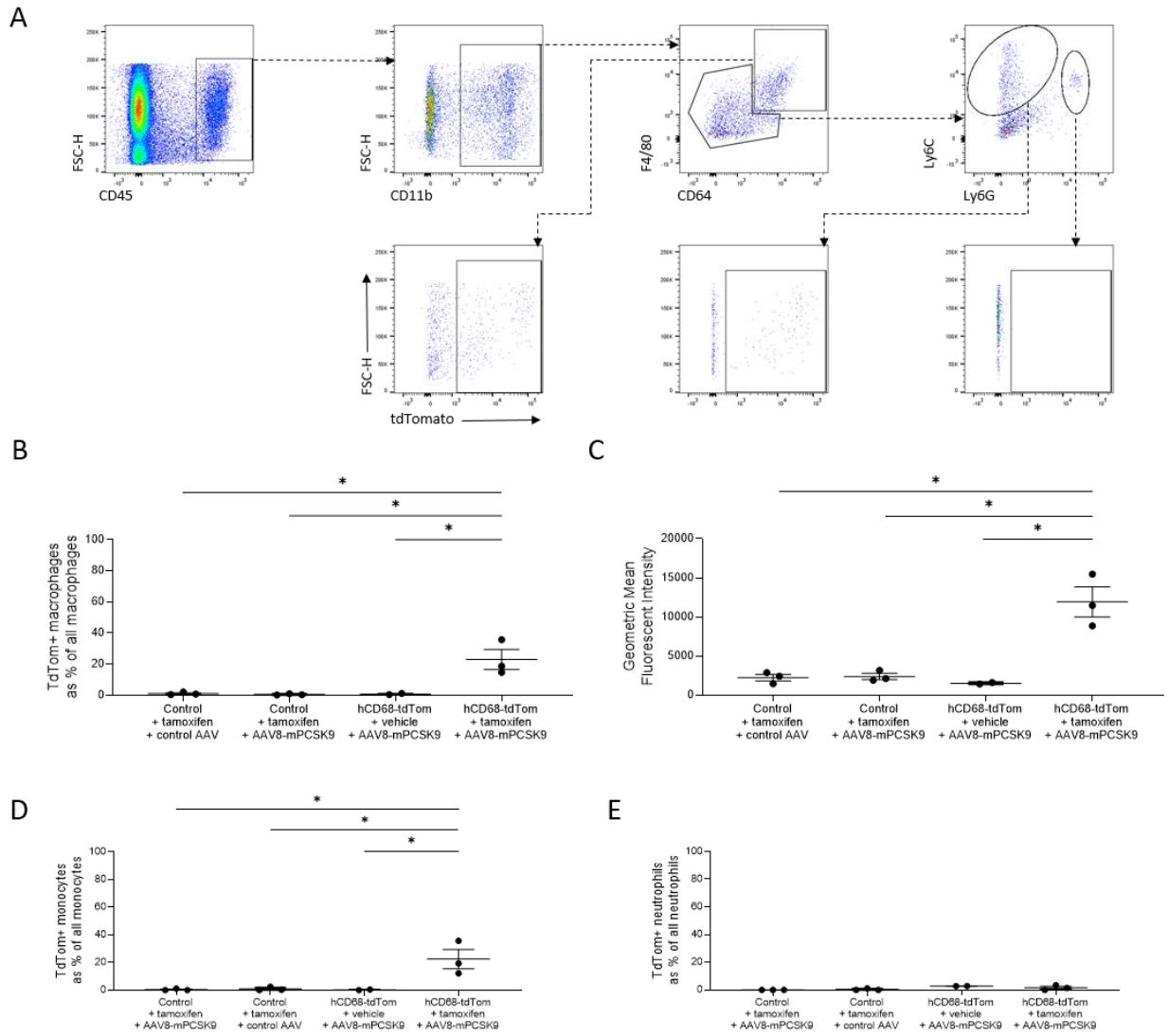

Figure 3.21. hCD68 promoter driven activation of TdTom expression in the aorta as detected by flow cytometry. A) Representative dot plots of the gating strategy for aortic macrophages ($CD45^+$, $CD11b^+$, $F4/80^+$, $CD64^+$), monocytes ($CD45^+$, $CD11b^+$, $F4/80^-$, $CD64^-$, $Ly6C^+$, $Ly6G^-$) and neutrophils ($CD45^+$, $CD11b^+$, $F4/80^-$, $CD64^-$, $Ly6C^+$, $Ly6G^+$). B) Frequency of tdTomato-expressing aortic macrophages as a proportion of all aortic macrophages with the corresponding mean fluorescent intensity of total aortic macrophages in (C). D) Frequency of tdTomato-expressing aortic monocytes as a proportion of all aortic monocytes. E) Frequency of tdTomato-expressing aortic neutrophils as a proportion of all aortic neutrophils; one-way ANOVA (* = $p<0.05$).

fluorescent lipid drops, due to the proximal co-localisation of DAPI stained nuclei (Figure 3.20).

To further assess the tdTom expression in the immune cells compartment of the atherosclerotic lesion I preformed aortic digests followed by flow cytometry (Figure 3.21B). As expected, there was a large population of $CD11b^{+}F4/80^{+}CD64^{+}$ macrophages in AAV8-mPCSK9 injected mice (Figure 3.21A). Importantly, when these mice were treated with tamoxifen to induce Cre recombinase activity there was significant induction in expression of tdTomato (Figure 3.21B/C). I also observed tdTomato expression in ~25 % of all $Ly6C^{+}$ monocytes within in the atherosclerotic lesion (Figure 3.21D), and reassuringly there was no tdTomato expression in recruited neutrophils (Figure 3.21E). Collectively, these results demonstrated that the human CD68 promoter-driven inducible Cre recombinase can specifically target macrophages with atherosclerotic lesions, with limited targeting to plaque associated neutrophils.

3.3.10. Administration of 4-hydroxy tamoxifen does not improve tdTomato expression in tissue-resident macrophage populations.

CreERT2 construct becomes activated by a liver metabolite of tamoxifen called 4-hydroxy tamoxifen (*318*). Since I saw the highest efficiency of targeting in the liver, I hypothesised that it might be due to the bioavailability of 4-OHT being the highest there, as it is its production site. Therefore, I set out to dose the hCD68-tdTom mice with 4-hydroxy tamoxifen to compare the expression of tdTomato in tissue-resident macrophage populations reasoning that bypassing the need for metabolising tamoxifen in the liver will improve the bioavailability of 4-OHT across all tissues and will result in increased targeting of peritoneal and splenic macrophage populations. I used the same flow cytometry panels and settings to conduct a

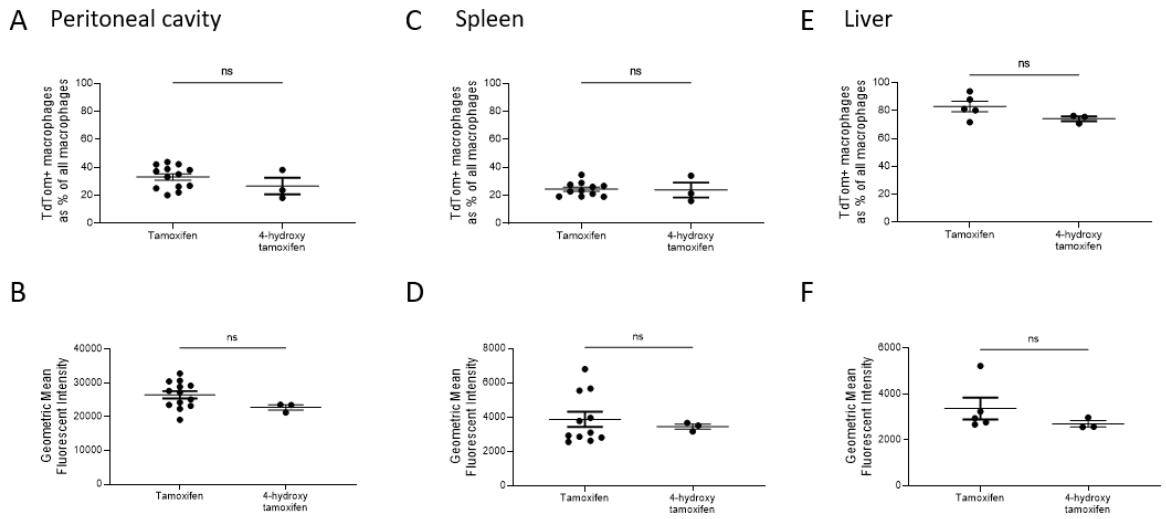

Figure 3.22. Administration of 4-hydroxy tamoxifen does not improve tdTomato expression in tissue-resident macrophage populations. Frequency of tdTomato-expressing macrophages in hCD68-tdTom mice treated with tamoxifen or 4-hydroxy tamoxifen as a proportion of all macrophages in (A) peritoneal cavity (C) spleen and (E) liver with corresponding mean fluorescence intensity of tdTomato+ macrophages in (B), (D) and (F); student t-test.

head-to-head comparison between tamoxifen and 4-hydroxy tamoxifen (Figure 3.22), which showed no significant improvement in either efficiency of targeting or overall expression of tdTomato in tissue resident macrophages in the peritoneal cavity (Figure 3.22A/B), spleen (Figure 3.22C/D) and the liver (Figure 3.22E/F). Given the much higher cost of buying 4-OHT than tamoxifen, I concluded that there was no justification in dosing the mice with 4-hydroxy tamoxifen instead of tamoxifen.

3.3.11. Sex of the mouse does not significantly influence the expression of tdTomato in tissue-resident macrophage populations

Sex is often overlooked as a variable in immunological research and in creating genetic tools for it despite many pathologies having a clear sex bias, for example autoimmune diseases. Sex has also been shown as an important factor in influencing the replenishment of tissue-resident peritoneal macrophages (*344*). Cre-ERT2 systems are based on the Cre recombinase protein fused with oestrogen receptor, which physiologically has different functions in males and females (*317*). In female mice, tamoxifen administration has been shown to stimulate longitudinal bone growth but also atrophy of the myometrium while in male mice it was shown to alter Leydig cell function which led to decreased levels of testosterone in the serum and in testicles (*338*). Given that tamoxifen was shown to have sex-dependent effects and that sex was a factor influencing tissue-resident macrophages I wanted to see if sex influences the expression of tdTomato in the hCD68-CreERT2 mice.

I analysed the expression of tdTomato in tissue resident macrophages in male and female mice (Figure 3.23). I found no sex-dependent difference in the efficiency of targeting in tissue-resident peritoneal, splenic or hepatic macrophages (Figure 3.23A, 3.23C and 3.23E respectively). I also saw no difference in expression of tdTom (measured by mean fluorescence intensity) between males and females in splenic and hepatic macrophages

(Figure 3.23D and 3.23F respectively), however, I found a small but significant decrease in tdTomato MFI value of female mice as compared to the male mice in the peritoneal tissue-resident macrophages (Figure 3.23B). Having seen a significant difference in a population of interest, I set out to investigate whether sex influenced any of the off-target effects (Tables 3.5 – 3.8). I found no significant differences in the efficiency of targeting of in either the blood or the splenic non-macrophage immune populations (Table 3.5 and 3.6 respectively). There was also no difference in the expression levels (measured by MFI) in the splenic non-macrophage immune populations (Table 3.8). In the blood there was a significant increase in the expression level of tdTomato in the eosinophils of female mice as compared to male mice with no other circulating leukocyte exhibiting any significant differences (Table 3.7).

It was reassuring to find no sex-dependent difference in the efficiency of targeting any of the immune cells populations I had assessed across four different tissues. The differences seen in the level of expression of tdTomato between males and females that I found in the peritoneal macrophages and blood eosinophils are important to note yet hard to interpret. There was no consistency between the two patterns of expression with female peritoneal macrophages expressing less tdTom than males but female eosinophils expressing more. The change in the peritoneal macrophages was significant yet small while females had double the expression of tdTomato in their eosinophils when compared to males. But given the fact that only around 1% of all eosinophils is targeted in the hCD68-CreERT2 mice the biological relevance of that increase is minimal. Moreover, none of the other tissue-resident macrophage populations or blood leukocyte populations showed any significant differences. Therefore, I concluded that despite these observed changes there were no general sex-specific differences in the expression patterns in male and female hCD68-CreERT2 mice.

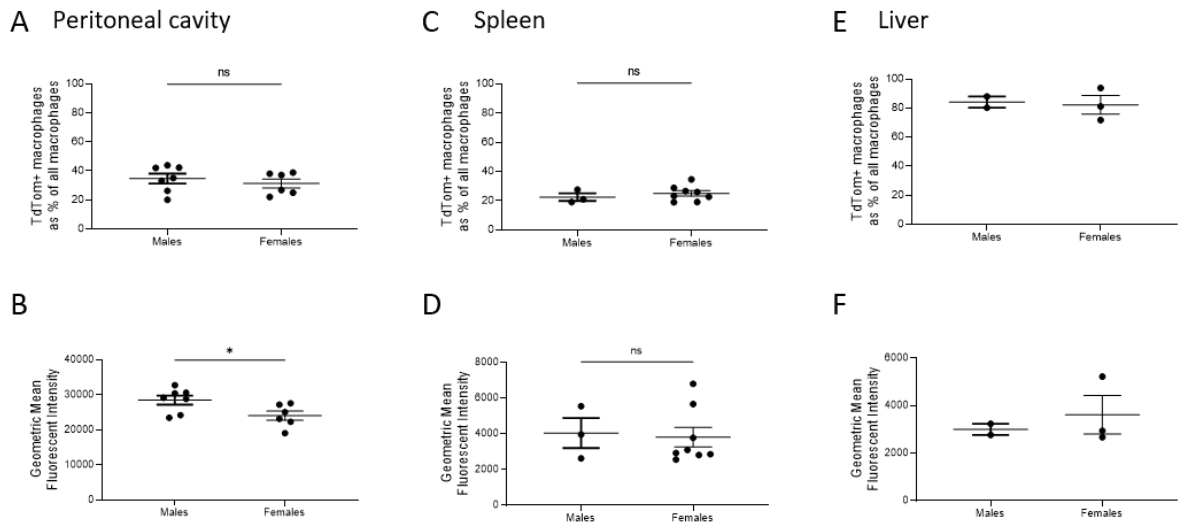

Figure 3.23. Sex of the mouse does not significantly influence the expression of tdTomato in tissue-resident macrophage populations. Frequency of tdTomato-expressing macrophages in male and female hCD68-tdTom mice as a proportion of all macrophages in (A) peritoneal cavity (C) spleen and (E) liver with corresponding mean fluorescence intensity of tdTomato+ macrophages in (B), (D) and (F); student t-test (* = $p<0.05$) for biological repeats of n = 2-7.

Population	Males	Females
Ly6C^{high} monocytes	1.83 ± 0.40	1.20 ± 0.33
Ly6C^{low} monocytes	20.60 ± 2.52	20.37 ± 1.62
Neutrophils	1.27 ± 0.21	1.28 ± 0.15
Dendritic cells	3.33 ± 1.34	5.53 ± 0.70
Eosinophils	0.35 ± 0.10	1.11 ± 0.23
CD4 T cells	2.70 ± 2.32	0.93 ± 0.10
CD8 T cells	0.96 ± 0.24	1.09 ± 0.21
B cells	0.32 ± 0.11	0.34 ± 0.04

Table 3.5. Comparison of frequency of tdTomato expression in blood leukocyte populations between sexes. Percentage of tdTomato-expressing blood leukocytes in male and female hCD68-tdTom mice represented as mean ± SEM; student t-test for biological repeats of n = 3-8.

Population	Males	Females
Ly6C^{high} monocytes	4.34 ± 1.53	4.22 ± 0.57
Ly6C^{low} monocytes	26.23 ± 0.32	28.54 ± 1.77
Neutrophils	4.16 ± 0.54	3.75 ± 0.43
Dendritic cells	20.80 ± 0.50	19.90 ± 1.52
T cells	2.72 ± 1.86	2.05 ± 0.44
B cells	5.02 ± 1.23	4.64 ± 0.54

Table 3.6. Comparison of frequency of tdTomato expression in splenic non-macrophage populations between sexes. Percentage of tdTomato-expressing splenic immune populations in male and female hCD68-tdTom mice represented as mean ± SEM; student t-test for biological repeats of n = 2-8.

Population	Males	Females
Ly6C^{high} monocytes	5660 ± 755.5	6045 ± 533.1
Ly6C^{low} monocytes	8709 ± 767.1	8001 ± 549.2
Neutrophils	8722 ± 1214	10496 ± 969.9
Dendritic cells	6171 ± 1142	6004 ± 332.3
Eosinophils	3558 ± 1458	7143 ± 715.4*
CD4 T cells	1708 ± 331.9	2089 ± 376.4
CD8 T cells	1157 ± 355.7	1958 ± 490.5
B cells	2281 ± 643.2	2664 ± 229.3

Table 3.7. Comparison of expression of tdTomato in blood leukocyte populations between sexes. Geometric mean fluorescent intensity values of tdTomato-expressing blood leukocytes in male and female hCD68-tdTom mice represented as mean ± SEM; student t-test (* = $p<0.05$) for biological repeats of n = 3-8.

Population	Males	Females
Ly6C^{high} monocytes	791.7 ± 184.4	1154 ± 200.8
Ly6C^{low} monocytes	3432 ± 262.8	4169 ± 452.4
Neutrophils	1019 ± 377.9	1365 ± 125.4
Dendritic cells	2291 ± 581.0	2475 ± 347.3
T cells	2669 ± 498.5	2598 ± 197.4
B cells	792.5 ± 82.5	806.9 ± 47.33

Table 3.8. Comparison of expression of tdTomato in splenic non-macrophage populations between sexes. Geometric mean fluorescent intensity values of tdTomato-expressing splenic immune populations in male and female hCD68-tdTom mice represented as mean ± SEM; student t-test for biological repeats of n = 2-8.

3.4. Discussion

In this chapter, I have set out following experimental aims to phenotype the novel transgenic reporter human CD68 promoter cassette driven mouse line. Firstly, I wanted to establish the expression profile in tissue resident macrophages and other immune cell types in the peritoneal cavity, blood, spleen and liver in order to determine how macrophage-restricted and long-lasting the expression of the inducible Cre recombinase is. Secondly, I wanted to compare this novel mouse line to existing macrophage-targeting lines – constitutive LysM-Cre and hCD68-GFP mice. And lastly, I wanted to conduct a proof-of-concept disease model study to assess how this new Cre driver line will perform alongside other interventions, for which purpose I chose the inducible PCSK9 atherosclerosis model.

3.4.1. Assessment of expression profile of Cre recombinase in the hCD68-CreERT2 mouse

To assess the efficiency of Cre recombinase activation I crossed the hCD68-CreERT2 mice with commercially available TdTomato$^{fl/fl}$ mice, a standard methodology for phenotyping new transgenic Cre driver lines. In this method TdTomato fluorescence serves as a readout of the Cre recombinase activation. To optimise the fluorescence signal I tested five different dosing protocols for tamoxifen (Figure 3.2 and 3.3). I wanted to achieve highest possible signal without causing any side effects of tamoxifen to the mice. Despite some evidence that intraperitoneal injections might achieve better expression than oral administration (*318*), I chose to use oral gavage as a delivery method for tamoxifen to avoid any disturbances to the peritoneal population of macrophages. After assessing macrophage populations in the peritoneal cavity, bone marrow, spleen and liver I chose to dose the mice with 2 mg of tamoxifen per day for 5 consecutive days and allow 5 days induction period before the samples collection. In my opinion this protocol showed evidence of robust tdTomato

induction, approaching the highest achievable expression in the protocols tested whilst avoiding potential side effects and increased mortality rate caused by doses of 3 mg per day and above, which were documented by Donocoff *et al.* (*318*).

Using the optimised protocol, I detected TdTomato-expressing cells using flow cytometry and confocal microscopy in resident macrophage populations in the peritoneal cavity, spleen and liver (Figure 3.4 and 3.7). Detailed analysis showed that inducible tdTomato expression is restricted to tissue-resident macrophages, absent from the circulating leukocytes, limited in non-macrophage immune populations in the spleen and independent from murine Cd68 expression (Figures 3.8 - 3.10 respectively). I tested turnover of tdTomato labelled cells by allowing 6 weeks wash-out period following the usual dosing protocol and showed no decline in tdTomato expression in tissue-resident macrophage populations (Figures 3.11-3.13). Additionally, I tested the use of 4-hydroxy tamoxifen as a potential way to improve the efficiency of tdTomato expression and observed no significant advantage of 4-OHT over tamoxifen (Figure 3.22). Lastly given the reported sex-specific functions of oestrogen receptor and of tamoxifen administration, I compared the expression of tdTomato across all tested tissues between male and female hCD68-tdTom mice and found no sex-biased expression profile in any of the tissues (Figure 3.23 and Tables 3.5-3.8).

The search for a truly 'macrophage-specific' transgene targeting has so far been unsuccessful, most likely due to all myeloid cells expressing very similar markers at various stages of development (*26*, *345*). CD68 is a classical macrophage-defining marker, frequently used to identify macrophages in histological sections (*285*). This is a crucial difference to the mouse line previously published by the lab, where hCD68 expression cassette drove constitutive expression of green fluorescent protein in neutrophils, monocytes and macrophages

alike (*279*). In the new inducible mouse line, tdTomato expression in circulating leukocytes of myeloid origins (neutrophils, monocytes and dendritic cells) is extremely low (Figure 3.8 and Table 3.2). The only appreciable expression is detected in Ly6C^{low} monocytes which may be explained by the fact that they are the end-stage of development of blood vessels-dwelling monocytes and have been previously suggested to be the equivalent of circulatory macrophages (*59*). I hypothesised that the difference in transgene expression might result from differential expression of murine Cd68 across the myeloid populations in the blood. Contrary to my hypothesis, I saw that macrosialin was highly expressed in all myeloid populations in the peritoneum and blood, including the neutrophils (Figure 3.10). It has been previously reported that monocytes and a subset of human blood neutrophils can express CD68, but not to the extent we saw in our study (*346*). The human CD68 promoter and IVS-1 intron expression cassette has been shown to be a very potent driver for macrophage targeting when used in a constitutive GFP transgenic mouse (*279*). However, due to the nature of this cassette, when activated embryonically it targets other myeloid cell types with efficiency comparable to macrophage targeting, in line with Cd68 being expressed by other myeloid cell types. Similar results have been seen in other inducible hCD68 promoter-driven mice models, where reported expression in blood leukocytes was lower than in other macrophage targeting Cre lines (*7*, *45*). This suggests that human CD68 promoter cassette when activated in adult animals is highly specific for mature tissue resident macrophages, unlike the endogenous expression pattern of murine Cd68.

hCD68-CreERT2 mice achieved the highest efficiency of targeting in the liver, which might be due to tamoxifen being metabolised in that organ to its active form (4-hydroxy tamoxifen) and therefore having the highest bioavailability in that tissue (*340*). To test that, I dosed the

mice with equal doses of tamoxifen and 4-hydroxy tamoxifen (2 mg per day for 5 days with 5 days induction period), however I saw no appreciable difference in the tdTomato expression in any of the key tissue-resident macrophage populations (Figure 3.22). In my experiments, I was able to discriminate between different sub-populations of liver macrophages and show that Cre recombinase activation varies between them in terms of efficiency of targeting as well as intensity of expression (Figure 3.6). Kupffer cells were the highest expressers of tdTomato in the liver with much lower values in the monocyte-derives sub-populations and in capsular macrophages, reinforcing the idea that hCD68-CreERT2 mouse line preferentially targets tissue resident macrophages. Moreover, I was able to distinguish between macrophage subsets based on significant differences in their mean fluorescence intensity values (*133*). To further my conclusions, when I gated separately on the large and small peritoneal macrophages I saw that the efficiency of tdTomato expression and its intensity were both higher in the embryonically derived LPMs compared to monocyte-derived SPMs (*149*). Given that tissue-resident macrophages are believed to have a slow turnover in tissues (*95*), I wanted to test how long after the tamoxifen dosing I will be able to detect the tdTomato expression. Encouragingly, I saw no decline in tdTomato expression 6 weeks post-targeting (Figures 3.11-3.13), which further points to the specific targeting of tissue-resident macrophages. In contrast, after the 6 weeks wash-out period there was no expression of tdTomato in the blood at all, since circulating blood cells tend to be short-lived (*347*).

3.4.2. Comparison of hCD68-CreERT2 mice with constitutive LysM-Cre and hCD68-GFP lines

Cre driver mouse lines which are referred to as macrophage-targeting are driven by five main gene expression cassettes, LysM, Csf1r, Cx3cr1, CD11b and F4/80, however none of them are truly macrophage-specific. I wanted to compare the hCD68-CreERT2 mouse to another well

established and commercially available macrophage-targeting Cre driver line as well as another mouse line using the same hCD68 expression cassette.

Therefore, I performed a side-by-side comparison with LysM-Cre mice (crossed the same tdTomato$^{fl/fl}$ mouse as hCD68-tdTom mice) and the constitutive hCD68-GFP mice (Figures 3.13-3.18). When compared to LysM-Cre, I showed better macrophage lineage-restricted targeting in hCD68-CreERT2 model (Figures 3.13-3.15). Specifically, hCD68-CreERT2 mouse showed no expression of tdTomato in blood leukocytes apart from Ly6C^{low} monocytes whereas LysM-Cre mouse had high expression in all blood leukocytes of myeloid lineage (Figure 3.14). Similarly, in the splenic non-macrophage populations there was a significant improvement of lineage non-restricted tdTom expression between hCD68-CreERT2 mice and LysM-Cre mice (Figure 3.15). Even though peritoneal and splenic macrophages were targeted worse than in LysM-Cre mice, hCD68-CreERT2 mouse achieved significant improvement of targeting hepatic macrophages (Figure 3.13). These results are expected, given that LysM driven mice have been reported to have poor expression in tissue-resident macrophage but high efficiency of targeting neutrophils (*290*, *331*). They also reinforce the idea that hCD68 expression cassette induced in adult mice is more macrophage-specific than other macrophage-targeting drivers.

I obtained very similar results when comparing the hCD68-CreERT2 mice with hCD68-GFP mice (Figures 3.16 - 3.18). Both peritoneal and splenic tissue-resident macrophage populations were targeted to a lesser extent (Figure 3.16), however the expression profile in the blood and non-macrophage splenic immune cells suggests higher macrophage specificity of hCD68-CreERT2 than hCD68-GFP (Figures 3.17 and 3.18). Unfortunately, I was not able to do a head-to-head comparison between liver macrophages due to the high auto-fluorescence

in the organ interfering with the flow cytometry detection. For the same reason the immunofluorescence image of the liver in Figure 3.16F looks like there is barely any expression of GFP in the organ. In their original paper, Iqbal *et al.* encountered the same problem, which they solved by bleaching the endogenous florescence and applying an anti-GFP antibody followed by a fluorescent secondary antibody to precisely image the cells that expressed GFP under hCD68 promoter (*279*). In hindsight, that would have been the better approach for this study as well, however then the technique for imaging the two mice lines would have been different and less of a direct comparison. Overall, comparing hCD68-CreERT2 mouse to hCD68-GFP mouse reinforced my idea that specificity for tissue-resident macrophages driven by hCD68 expression cassette is due to adult onset of expression.

3.4.3. Use of hDC68-CreERT2 mouse in experimental model of atherosclerosis

Next, I wanted to assess the utility of hCD68-CreERT2 mice and the tamoxifen induction protocol in disease models, since ultimately fate mapping or studying macrophage biology in homeostatic state are not the end goal for creating new transgenic mice. As a proof-of-concept experiment I chose to induce atherosclerotic lesions in hCD68-tdTom mice using the PCSK9 model (*343*) because macrophages are known to be important in atherosclerosis and have been previously targeted using the hCD68 expression cassette (*348*). I was able to show that aortic-resident macrophages and macrophages present in atherosclerotic plaques expressed tdTomato, proving the possibility of using hCD68-CreERT2 system to study macrophage biology in pathological states (Figures 3.19-3.21). The relatively high level of monocyte targeting compared to homeostatic state in other tissues and in blood could be because monocytes that have migrated into the aortic tissue have most likely started the phenotypic shift towards macrophages and therefore upregulated the expression of hCD68 promoter cassette. Importantly, tdTomato expression was still absent in neutrophils further

confirming the specificity of targeting. Therefore, in the future, hCD68-CreERT2 mice could be used for studying specific gene deletions and inductions at various stages of atherosclerosis. Alleles of interest could be floxed then crossed with the hCD68-CreERT2 mice and their deletion induced at specific time points in the disease model, which will give the opportunity to study them in early or late atherogenesis or during regression.

3.4.4. Limitations and possible improvements of this study

The main limitation of hCD68-CreERT2 transgenic model lies in the fact that it does not achieve full targeting in all tissue resident macrophage populations. This is however unsurprising given that none of the previously published macrophage targeting inducible Cre models achieved full expression in desired cell populations (*291*, *321*, *349*). I tried improving efficiency of targeting by dosing with 4-hydroxy tamoxifen rather than tamoxifen, which did not change the efficiency of targeting (Figure 3.22), however I could also improve the preparation of 4-hydroxy tamoxifen itself. To make a direct comparison with tamoxifen I dissolved 4-OHT in ethanol, which is a poor solvent for it, which resulted in having to go through multiple rounds of sonication and leaving it in a 37^{o}C shaker overnight. Afterwards, it looked less translucent than the dissolved tamoxifen, which makes me question how good the preparation was and whether it influenced the potency of my 4-OHT. In hindsight, I should have used DMSO for this preparation and prioritised the quality of the drug preparation over the direct comparison with my usual tamoxifen preparation. Additionally, all mice were dosed with the same dose of tamoxifen, 2 mg per day for 5 days, regardless of their age and weight. Even though it is a common practice, it is also a limitation of my study, especially that I was using both males and females and mice of different age which introduced greater variability to the weight range. To further optimise my dosing regime, I should have dosed the mice with 80 mg/kg of tamoxifen per day (equivalent of 2 mg per day for an average 25g mouse), which

would take into account their different weights. Another way I could have tried to improve the efficiency of targeting in the hCD68-CreERT2 mice is using intraperitoneal injections of tamoxifen as well as the oral administration, given that there is some evidence from Donocoff *et al.* that I.P. injections give better results (*318*).

Given this already low expression level, it would be crucial to cross hCD68-CreERT2 mouse line with a 'floxed' mouse strain that is not a reporter gene as the efficiency of knocking-out a gene could be even lower than tdTomato expression I observed. This is because deletion of a 'floxed' STOP codon to induce expression of a reporter gene, such as tdTomato, is relatively simple and error-free as the STOP codon is short and therefore easier to excise; moreover, only one copy of the reporter gene is activated. On the other hand, deletion of a gene to create a 'knock-out' mouse is much more complicated and prone to errors, which further reduce the efficiency of targeting. Firstly, the common practice is to excise only a part of the gene of interest, usually the first exon, as smaller DNA fragments are easier to excise (*350*). If the gene of interest possess any internal transcription start sites or can undergo alternative splicing this can reduce the efficiency of the gene deletion. Secondly, it is possible to delete exons that encode for the functionally most important part of the protein, such as those that control its catalytic activity (*350*). However, using this method there is a risk of generating truncated proteins which may not be functionally neutral and prevent activation of other similar proteins in ways that can be difficult to predict and control. Thirdly, the efficiency with which Cre recombines loxP sites is affected by their genomic position and the distance between them – recombination efficiency decreases with increasing genetic distance (*351*). Therefore, hCD68-CreERT2 mouse could cut different loxP-flanked alleles with different efficiencies. Additionally, most studies require complete deletion of the gene of interest,

which requires breeding the Cre mice with homozygous *flox/flox* mice. As a result, the Cre recombinase and the floxed allele of the gene of interest are found together in the germline, where unexpected recombination is common and can also change expression pattern compared to the reporter mouse such as tdTomato$^{fl/fl}$ (*352*).

hCD68-CreERT2 transgenic cassette was inserted into the Rosa26 locus in this mouse strain, which is a common practice in creating new mouse lines as Rosa26 locus is considered a 'genomic safe harbour' (*353*). Rosa26 locus is ubiquitously transcriptionally active in embryonic and adult mice, which ensures great stability of cassette insertion and subsequent gene expression and has a high rate of success in designing new transgenic mice (*350*). The main advantages of using Rosa26 locus for cassette insertion are stable, single-copy insertion of the gene of interest and no disruption to either the endogenous gene or any other gene. However, insertion into Rosa26 is a limitation in itself as it cannot recapitulate the broader gene regulation of the endogenous locus. Insertion of the transgene to the endogenous locus instead could be advantageous as it would retain all the cis-regulatory elements such as enhancers and possibly further improve the specificity of targeting and maintain more physiological expression levels of the gene of interest. Even though this approach would be able to capture broader gene regulation and more accurately mirror the real expression of the endogenous gene, insertion of the transgenic cassette into the endogenous locus comes with its own caveats. Most importantly, the expression level of reporter gene may be low or variable due to weak or transient endogenous promoter activity, resulting in lower signal-to-background ratio that may cause problems in reliable detection of the signal (*354*). Secondly, disruption of endogenous locus may cause cell viability or function defects which will change the observed phenotype (*354*). Finally, from a pragmatic point of view, creating new mouse

lines where using endogenous locus is much more difficult, lengthy and costly than inserting the transgenic cassette into Rosa26 locus.

Additionally, I only looked at a few specific populations of tissue-resident macrophages. Given that the expression levels vary between tissues I would have liked to expand my flow cytometry panels to look at other tissues that harbour macrophage populations, mainly the brain and the lung. I believe that lung would have been especially important, given that I have seen robust expression of tdTomato in my microscopy images (Figure 3.7) and that McCubbrey *et al.* noted that using hCD68 expression cassette in a tet-On system allowed them to distinguish between three separate lung macrophage populations (*142*).

To further validate my flow cytometry data across all tissues, I would like to include co-staining for macrophages, dendritic cells and monocytes as well as for non-immune cell types such as endothelial cells in the microscopy images. That would allow me to confirm that the tdTomato expression is restricted to macrophages, DCs and Ly6c^{low} monocytes (as seen in the flow cytometry data) as well as determine precise anatomical location of macrophage populations in the organs studied. Given the evidence from the kidney images where I observed tdTomato in, what I suspect are, endothelial cells (Figure 3.7), it would be beneficial to further expand my flow cytometry panels and include markers for non-immune cells as well as co-staining tissue slices. That would allow me to include even more in-depth analysis of the off-target effects that hCD68 expression cassette drives in this model.

In this study I only looked at tissue-resident macrophages *in vivo*, however I have seen conflicting evidence whether that is the only population of macrophages that is being targeted. Evidence from flow cytometry data in small peritoneal macrophages and liver macrophage sub-populations suggests that hCD68-CreERT2 mouse does not target

monocyte-derived macrophages efficiently. However, given that most macrophages in atherosclerotic plaques are believed to be derived from monocytes (*189*), the atherosclerosis study showed possible evidence of targeting in monocyte-derived macrophages in the atherosclerotic plaques which suggest that these cells could be targeted in hCD68-CreERT2 in certain contexts. Given this discrepancy, I would like to perform an experiment where I induce macrophage recruitment with either thioglycollate or BioGel alongside the tamoxifen dosing and check whether the elicited macrophages express tdTomato. To further look into possible targeting of monocyte-derived macrophages I would like to extract bone marrow from hCD68-tdTom mice, grow bone-marrow derived macrophages (BMDMs) *ex vivo* and try to induce tdTomato expression with 4-OHT in petri dishes, similarly to the experiment done by McNeill *et al*. (*348*). I briefly tried doing this experiment and imaging the growth of BMDMs in the IncuCyte, however I could not detect any red fluorescence. I suspect that this was either due to my *ex vivo* tamoxifen dosing protocol being sub-optimal or IncuCyte being unable to detect the fluorescence due to high background fluorescence. If I had more time, I would like to optimise the 4-OHT dosing and use flow cytometry instead of IncuCyte to look at the fluorescence readout in BMDMs.

Lastly, I would have liked to look at the expression of the Cre recombinase enzyme in more detail *in vitro*. When I tried looking for commercial antibodies and qPCR primers for Cre recombinase I was surprised by the lack of them, given how popular Cre-*loxP* systems are. I found a western blotting and a flow cytometry antibody, however I was not able to detect any binding with either of them. I suspect that it might be due to our system using the CreERT2 fused protein, rather than the original Cre recombinase. If the epitope detected by the antibody happened to be in the fused region, the antibodies would not be able to bind and

detect the Cre recombinase, which is exactly what happened in my experiments. I also could not find any commercially available RT-qPCR primers to quantify tissue mRNA expression of the Cre recombinase. I tried designing my own based on the genotyping primers which I had but they failed to detect Cre recombinase mRNA and I run out of time to follow up with the optimisation.

3.4.5. Summary

As we are gaining a better understanding of tissue-resident macrophages, their origins and ways to replenish them, it is crucial to develop more macrophage specific models that can be used for in vivo investigations. So far, the most detailed descriptions of heterogeneous macrophage populations have come from single cell studies, which have their own limitations and constraints in terms of availability to researchers and experimental design. Currently available macrophage-targeting mouse models offer little reassurance that circulating monocytes and neutrophils will not be equally well targeted.

In this study I present a novel human CD68 promoter cassette driven inducible CreERT2 mouse model with the potential to improve tissue resident macrophage targeting *in vivo*. At the steady state, I showed improved specificity of targeting macrophages and minimal off-target effects in the blood, compared to other published mouse Cre driver lines. Moreover, I showed stable targeting over long periods of time and that it is possible to induce the Cre recombinase expression in disease models without disrupting the model itself. I believe that the hCD68-CreERT2 mice will find multiple applications in studying tissue-resident macrophage populations and their heterogeneity in health and disease.

Even though hCD68-CreERT2 mouse presents an advancement in targeting specificity of macrophages *in vivo* it does not solve the longstanding problem of off-target expression in

monocytes and dendritic cells. As such, further refinement can be achieved by using the newly developed sequential intersectional genetics approach, where Dre-rox controls Cre recombinase expression and therefore Cre activity is restricted within, and defined by, the intersection of 2 gene expression domains. Dre recombinase catalyses recombination between rox sites, analogous to Cre recombinase recombining loxP sites. Sequential intersectional genetics utilises tamoxifen-inducible CrexER where 2 rox sites were inserted to flank the oestrogen receptor (ER) of the original CreER cDNA (*355*). This strategy ensures sequential recombination where Dre recombinase, which is under the control of one promoter, drives the excision of ER part of the Cre recombinase, which activates the enzyme to recombine the desired *loxP* sites. Alternatively, Dre recombinase can excise STOP codon between the CreER recombinase and its promoter, allowing for tamoxifen-inducible activation of Cre recombinase (*356*). In both cases, Cre recombinase is under the control of a second promoter and only expressed in the cells where this promoter is active. Therefore, the Cre recombinase activity can only be detected in cells which express both the first and the second promoter, enabling enhanced specificity of targeting (*355*). Even though this system was initially implemented for specifically targeting vascular endothelial cells in different tissues, the range of Dre lines is expanding to other cell types and tissues, such as adipose tissue (*355*, *357*). Recently, cavity macrophages have been targeted using this system by combining CD45 Dre driver mouse with GATA6-CreER mouse to target specifically cavity macrophages, whilst avoiding monocyte-derived and tissue-resident macrophages (*356*). Using CD45-driven Dre mouse, which is a haematopoietic promoter not a macrophage-specific one, was possible in this study because cavity macrophages are the only immune cells expressing GATA6 (other expressors include hepatocytes and cardiomyocytes),however for general macrophage targeting this system would have to be further refined. Taking into

consideration ‘macrophage-specific’ markers from Table 3.1 and their co-expression profiles, it is still difficult to find a combination of two promoters which would ensure truly macrophage specificity without targeting either monocytes or dendritic cells. The only marker that should not target monocytes or DCs is F4/80, however previous attempts at using it for mouse lines showed that it has poor expression profile and is not uniformly expressed across macrophage populations (please refer to section 3.1.5 of this thesis). Therefore, sequential intersectional genetic approach brings a great promise in targeting specific sub-populations of macrophages within organs with well-defined markers (e.g. splenic marginal zone macrophages, which are the only expressors of CD169 in that organ), specific targeting of whole macrophage population still presents a technical challenge.

Chapter 4

Fluid-walled chemotaxis assay to study macrophage migration *in vitro*[3]

4.1. Introduction[4]

4.1.1. Historic perspective on chemotaxis assays

Since the advent of chemotaxis research in the 1800s until mid-20th century most researchers used naturally thin and translucent membranes in live animals (frog's mesentery, tadpole's tails and rabbit ear membranes) to study leukocyte movement (*358*, *359*). In 1841 Addison and in 1873 Cohnheim observed cells emigrating from the blood into the inflamed tissue, however it was Leber in 1888 who noted the directionality of cell movement and proposed that leukocytes may undergo chemotaxis. He injected guinea pig corneas with moulds to observe leukocyte infiltration under the microscope, which he noted was directional towards the injection site (*359*, *360*). Building on that observation, Theodor Leber himself as well as other groups in the early 20th century were able to establish that leukocytes were attracted and moved directionally towards bacteria and tissue breakdown products, which was widely accepted by the scientific community by 1940s.

Despite the significant increases in understanding of cell migration that resulted from those early experiments, the experimental techniques did not advance as fast in the chemotaxis field as they did in other aspects of cell biology. That apparent stagnation led Henry Harris in 1953 and 1954 to voice a critique of the whole field and expose poor experimental design, lack of appropriate controls and outdated techniques, which questioned the validity and reproducibility of all the previous findings (*359*, *361*). He argued that most of the previous

[3] Data presented in this chapter has been published in Deroy, Rumianek *et al.*, 2022 – see Appendix 1, p.259
[4] Introduction to this chapter has been adapted Rumianek & Greaves, 2020 – see Appendix 1, p.259

experiments were badly controlled and the accumulation of leukocytes at inflammation sites in the membranes could be explained by non-specific trapping of cells rather than directional migration and he pointed out the need for actual recording of cell movement in an isolated system that would prove the directionality and specificity of the migration (*359*). Harris therefore designed a system where cells were trapped in a film of clotted plasma between a slide and a coverslip and clumps of bacteria were introduced. Using dark-field microscopy and long exposures of a single photographic film he was able to track the cell paths through time and prove that cell movement is directional and induced by the addition of bacteria (*361*). His chemotaxis assay was soon followed by a new "transwell" setup designed by Stephen Boyden in 1962, which simplified and standardised chemotactic experiments whilst opening a possibility of quantification (*362*). Boyden's chamber was widely discussed and with time became one of the most popular chemotaxis assays, paving the way for the rapid expansion and an increase in popularity of cell migration assays. Modified versions of the original transwell assay are still some of the most widely used chemotaxis platforms.

4.1.2 Harris' criteria and the search for the 'ideal' chemotaxis assay

To highlight the poor experimental design and strengthen his argument against the early methods of studying chemotaxis, Harris proposed a set of conditions that should be fulfilled by an 'ideal chemotaxis assay' to ensure the highest quality of research. The 'ideal assay' that Harris proposed would allow detection of both chemotaxis and fugetaxis, testing of enhancers and inhibitors of cell migration as well as precise distinction of different signal-dependent movement types (*359*). Harris' criteria were collected together by Bignold in 1988 and recited over the years to judge all the novel techniques appearing in published papers and are now considered the gold standard of chemotaxis research (*363*, *364*).

According to Harris, the 'ideal chemotaxis assay' should:

1. Have no passive movement of cells to ensure that any change in the position of the cells is because of its active motion.

2. Ensure that if soluble factors are being tested, sufficient concentration of the chemoattractant reaches the experimental chamber.

3. Be able to control the concentration gradients of chemoattractants from their source until they reach the cells, especially by preventing any convection currents.

4. Enable cells to move both towards (chemotaxis) and away from (fugetaxis) the chemoattractant source in a homogenous environment.

5. Ensure that if a test object is introduced it is possible to distinguish between active cell migration and trapping of cells around the given object due to their random movement.

6. Be free from sampling error (*359*, *363*, *364*).

As common-sense and reasonable as those criteria seem they have proven to be much harder to put into practice than even Harris himself expected. In his original *in vitro* chemotaxis assay for blood leukocytes he failed to achieve sufficient localisation of soluble factors to his experimental chamber (*363*). None of the current chemotaxis assays fulfil all of these criteria and the whole field adopted the view that 'the more assays the better' while largely ignoring the limitations that omitting some of above points creates (summarised in Table 4.1). While most of the popular assays can detect enhancers and inhibitors of chemotaxis, it has proven much harder to distinguish between chemotaxis, chemokinesis and fugetaxis (*364*).

Additionally, as the field evolved and adapted to ever-increasing pace of science new considerations such as throughput and single cell versus population studies became important in choosing and designing chemotaxis assays. In their 2004 review Frow *et al*. assessed most popular assays based on how low-to-high throughput they are versus how much information can be obtained about cell movement behaviour at a single cell level (*364*). Since their goal was to find an optimal method for anti-inflammatory drug discovery projects they favoured the high throughput-low information assays such as transwell assays as good candidates for drug screens, while noting that transwell assays and under-agarose assays provide also the middle ground that can be useful for basic science studies (*364*). Including these new considerations, the modern 'ideal chemotaxis assay' should therefore allow high-throughput studies that can also inform on cell behaviour on a single-cell level (while maintaining the ability to look at whole populations of cells) and also fulfilling Harris' original criteria.

Isolated *in vitro* systems, such as the ones shown in table 4.1, have multiple advantages for assaying cellular behaviour in isolation, however, they come with their own caveats and limitations beyond their technical capabilities. They are designed to be reductionist systems, where typically only one cell type can be studied in a highly controlled, single-variable environment. As such, they cannot recapitulate *in vivo* situation where multiple cell types interact and constantly signal to each other and migrating cells are exposed to multiple shifting and ever-changing gradients at any given time point. Moreover, another area of cell migration research where current chemotaxis assays are lacking is haptotaxis. All the widely used chemotaxis assays rely on soluble chemoattractant gradients, however *in vivo* cells are most likely to encounter a mixture of soluble and surface-bound chemoattractants. While

attempts have been made to create easy and robust haptotaxis assays, further development in this area will be crucial in understanding macrophage migration (*235*, *237*).

Ex vivo co-culture and organoid migration assays are being developed to counteract the aforementioned limitations of the isolated *in vivo* systems. Co-culture set-ups can be achieved by adapting already existing technologies, such as 3D gel invasion assays, microfluidics and transwell assays (*365*–*368*). Co-culture migration assays can either allow transmission of soluble factors from one cell population to the other or actual physical interactions between two or more cell types, which mimics the *in vivo* situation more closely (*367*, *369*). Macrophage migration have been studied in co-cultures for with fibroblasts, tumour cells and skeletal muscle, offering a better insight into processes of tissue repair and tumour-associated macrophage migration such as the fact that macrophage motility and directionality is improved by the presence of fibroblasts and that presence of both aids skeletal muscle tissue repair (*365*, *366*, *369*). Organoids are artificially grown 3D masses of cells or tissues that resemble an organ and are therefore thought to provide more structural similarity to the actual tissue as well as give the possibility to use human-derived cells that recapitulate human organs to a greater extent than human-derived cell monolayers alone. Chakrabarti et al. used human-derived gastric organoids to show the importance of Sonic Hedgehog in BMDM chemotaxis to gastric epithelium and that this mechanism, which they have previously shown to be important in mice, can be recapitulated in human-like tissue (*370*). Even though those systems resemble the *in vivo* conditions more closely, in such systems the gradients created by different cell types cannot be precisely measured and controlled and therefore isolated *in vitro* chemotaxis assays and co-culture/organoid chemotaxis assays are useful for answering different questions about cell migration.

4.1.3. Transwell assays – from Boyden chamber to real-time recordings

The invention of the Boyden chamber in 1962 was a turning point in the chemotaxis field (*362*). Despite its limitations, the simplicity of the assay design allowed for well-controlled and reproducible *in vitro* studies of cell migration and it quickly became the standard technique in all cell migration research. The basic design of a Boyden chamber consists of a well filled with a chemoattractant solution and an insert that gets submerged into it. The inside of the insert ('top well') is separated from the bottom well by a porous membrane. Therefore, when cells are seeded into the insert concentration gradient of a chemoattractant is created by diffusion and cells can migrate through the pores in the membrane to the chemoattractant chamber (*362*).

One of the main advantages of transwell assays is the ability to clearly distinguish between chemotaxis and chemokinesis, without the need of single cell tracking, thanks to checkerboard analysis. In checkerboard analysis chemoattractant is placed both in the bottom and top wells at varying concentrations to create a range of gradients with different steepness and direction. In checkerboard analysis increased migration in wells where there is a shallow gradient, or no gradient, is a hallmark of chemokinetic movement while lack of migration in shallow gradients accompanied by increased migration in steep chemoattractant gradients signifies chemotactic movement (*364*) Transwell assay design fulfils most of Harris' criteria, except for allowing the cells to migrate away from the source of the chemoattractant. Although there is no precise way to control the gradient the physical barrier of the porous membrane prevents convection currents from flushing the cells through. In early experiments high inter-well variability and relatively high volumes were the main disadvantages to the technique (*371*). However, the assay's simple readout was ideal for studies where the

	Transwell assays	Dunn & Zigmond chambers	Under agarose assay	Traditional microfluidics
Stable gradients	+	+/-	-	+
Single cell tracking	-	+	+	+
Fugetaxis detection	+	-	+	+
Distinction between chemotaxis & chemokinesis	+	+	+/-	+
High throughput	+/-	-	-	+
Specialised equipment needed	+/-	-	-	+
Real-time observation	+	+	+	+
Multiple cell types simultaneously	-	-	+/-	+/-
Patterning cells	-	-	-	+/-
Multiple chemoattractants simultaneously	-	-	+	+
Easy system reconfiguration	-	-	-	-

Table 4.1. Comparison of traditional chemotaxis assays. Commonly used chemotaxis assays are compared based on Harris' criteria and other desirable features.

research question was about the overall difference in migratory potential of the whole population rather than differences in cells' migratory behaviour such as velocity, directionality or mode of movement.

Falk *et al.* improved the Boyden chamber by creating ChemoTx 96-well plates. They replaced individual inserts with a porous membrane covering the whole plate and placed a drop of the required cell suspension directly over the porous membrane, which required lower volumes (*372*). Another major improvement came with the xCELLigence system which used gold microelectrodes attached to the lower surface of the porous membrane to record real-time migration data by measuring impedance of the cells as they attach to the bottom of the membrane (*272*). To overcome the problem of migrated cells detaching from the membrane and therefore influencing the reading, IncuCyte created a chemotaxis assay where real-time phase microscopy photos of the top of the membrane are used to measure how many cells have pushed through the membranes instead (*267*).

Transwell assays can be used to compare two separate populations of cells on one plate, however they cannot look at mixed populations in one well such as whole blood due to different pore sizes required for different cell types as well as inability to easily distinguish different cell types once added into the system. Moreover, transwell assays cannot distinguish an inhibitor of chemotaxis from a chemorepellent since both such agents would result in reduced migration through the membrane. Transwell assays are primarily short-term studies and therefore unable to investigate processes such as how transendothelial migration of monocytes can influence their maturation into macrophages. Therefore, despite being probably the most widely used cell migration assays, transwell systems do not fulfil all of

Harris' criteria of the 'ideal chemotaxis assay' and they are limited in their capacity to investigate complex migratory behaviours such as cellular decision making.

4.1.4. Zigmond and Dunn Chambers

The Zigmond chamber was developed in 1977 with the aim of improving stability of soluble chemoattractant gradients in comparison to transwell assays (*373*). Also called an orientation chamber, it consists of a slide with two channels separated by a raised barrier. When one channel contains pure buffer and the other contains chemoattractant solution and the narrow passage that the barrier creates supports formation of a stable chemoattractant gradient. Cells of interest are attached to a cover slip that is inverted over the wells and the passage so that cells can sense the gradient and migrate in any direction on the cover slip; hence their movement can be recorded.

Despite theoretically creating a stable chemoattractant gradient the fact that Zigmond chamber was an open system in practice meant that convection currents were disturbing the gradients. To overcome that problem Zicha and Dunn created a novel closed chemotaxis system in 1991 (*374*). They replaced the channels with two concentric wells separated by a raised barrier. The circular design meant that inverting a coverslip with the cells over it sealed the system making it a closed circuit and therefore ensuring stability of the gradient. They demonstrated gradient stability for up to 30 hours by both mathematical modelling and experiments with dyes (*374*). However, the Dunn chamber is impractical to use for testing chemotaxis inhibitors and enhancers. The system is a low throughput one for pharmacological studies and is often used alongside more efficient systems such as transwell assays (*364*).

4.1.5. 'Under Agarose' Migration Assay

The basic principle behind under agarose assay is that cell-impermeable agarose gel is laid over a glass or plastic slide and a row of 3 wells are punched out in the gel. Cells are seeded in the middle well while small volumes of buffer or chemoattractant solution are added to the side wells. Solutions diffuse through the agarose gel to create a chemoattractant gradient (*375*). Cells can then detect the chemoattractant and move up the concentration gradient under the agarose gel. The assay is typically single time point – at the end of the experiment the agarose gel is removed, cells are fixed and stained on the slide and the distribution pattern is used to quantify the movement (*375*). Popular quantification methods include counting the number of cells that left the middle well or dividing the distance between the wells into serial 'slices' and looking at distribution of cells across the slices. Despite theoretically having the potential to include multiple wells in practice concentration gradients are difficult to reliably control in multiple comparison setting. Under agarose migration fulfils most of Harris' criteria, however it is rarely used for testing modulators of migration as it is a low throughput method (*364*). Moreover, chemokinetic agents may not be detected in this system because an increase in random movement without the incentive to migrate under the agarose may result in increased movement only within the well, which would not be detected in a single time point assay.

4.1.6. TAXIScan and ibidi µ-slides – early application of microfluidics technology

Microfluidics chemotaxis assays bring promise to fulfil all the criteria of the 'ideal chemotaxis assay', however they tend to be hard to reproduce and are not yet commercially available.

TAXIScan and ibidi tried to overcome this limitation by introducing commercially available real time chemotaxis assays based on simplified microfluidics designs.[5]

TAXIScan consists of a small metal chip with 12 wells connected in pairs by narrow (8μm wide) channels (*277*). Cells are injected into one of the wells while chemoattractant is injected into the second well. When cells migrate into the channel and towards the chemoattractant, their movement is recorded in real time using phase microscopy. Ibidi μ-slides operate on a similar principle where two triangular reservoirs are connected by a narrow observation area that contains cells of interest (*376*). However, the advantage of ibidi μ-slides lies in the ability to seed the observation area with an ECM matrix creating a 3D assay as well as ability to seed cells as a source chemoattractant into one of the reservoirs.

Both systems have reported the establishment of stable concentration gradients for up to 48h, but they both rely on passive diffusion of the chemoattractant gradient. The main difference lies in the fact that TAXIScan's narrow channel allows effectively only one cell to pass at one time while ibidi's observation area is 1 mm wide therefore allows unconstrained cell passage. Since macrophage movement was shown to depend on the constrictions of their extracellular environment lack of a narrow channel may be advantageous (*273*). The main disadvantage of both systems is the cost and requirements for specialised equipment to perform the experiments.

4.1.7. Gel invasion – *in vitro* 3D migration assay

Macrophage migration *in vivo* happens almost exclusively in 3D tissue environments therefore it can be argued that all 2D chemotaxis systems have limited physiological

[5] TAXIScan is no longer commercially available but was included in this chapter because of important contributions to the field this technology enabled.

relevance. Collagen, fibrin or ECM mixtures (such as Matrigel) gels are used to create 3D migration environments with different rigidity and porosity with the aim of mimicking different types of tissue (*273*). Chemoattractants can diffuse through the gels either directly from a reservoir or by setting up adjacent gels. They can also be seeded in the top chamber of a transwell assay (*112*), Cells can be either fixed and counted at a single time point or monitored continuously. As the gels are translucent cell movement through the matrix can be recorded and analysed for velocity, displacement, directionality and cell shape changes. Another common method of quantification is seeding the cells on top of the gel and counting how many of them enter the matrix.

Despite having the advantage of a 3D environment, gel invasion assays have limited ability to answer basic biological questions because of the impact of the artificial matrix itself on cell movement. Moreover, the assay is only reversible if cells are seeded directly into the gel and can move both away from and towards the source of the chemoattractant – when they are seeded on top of the gel the assay becomes a one-way system.

4.1.8. Microfluidics assays

Microfluidics chemotaxis devices are usually generated when a 3D-printed plastic construct, typically made of polydimethylsiloxane (PDMS), is attached to a glass or plastic slide and movement of cells through the system is recorded in real time (*377*). Theoretically, their main advantage is the ability to design and print the systems specifically to test a given hypothesis. In practice microfluidics devices are not easily manipulated and each study uses a unique design. Microfluidic circuits rely mainly on passive diffusion of chemoattractant solution through the system to establish the gradient. However, complex maze-like structures, where chemoattractant solution is mixed with pure buffer, are used to control the steepness of the

gradient at different points of the circuits and expose cells to areas of different intensity gradients (*378*).

Active flow of chemoattractant solutions is also possible, which provides the most stable exposure of cells to chemoattractants. Both passive mazes and active flow give better control over the gradient but may be prone to convection currents. Microfluidics circuits can be used to address more complex questions about cell migration, for the first time giving researchers a platform that can be modulated to answer specific scientific question rather than having to find a research question that fits the assay. Because of that they can be designed to fulfil Harris' criteria as well as incorporate Frow's new requirements. In practice however, microfluidics is still in its infancy and 90% of all published microfluidics chemotaxis appear in specialised engineering journals therefore rarely reaching the biologists that could benefit from the systems (*379*). Additionally, most biomedical laboratories do not have the resources and expertise to design and print their own circuits while the published ones are not commercially available. Moreover, PDMS has been shown to be cytotoxic which raises questions about the impact of the system itself on the cell biology (*377*).

4.1.9. Principles of open microfluidics

One approach to overcoming the PDMS toxicity and making microfluidics devices more accessible to biologists was introduction of open microfluidics, where at least one of the walls, usually the top of the device, is removed and replaced by a layer of immiscible oil that maintains sterility whist allowing easier access to the sample and preventing evaporation (*380*). This ensures that systems can be loaded and manipulated with normal pipettes, removing the need for specialised equipment such as syringe pumps. Until now such systems were either 'semi-open' (inlets were fully open but the actual channels were fully enclosed)

and using surface tension to create flow through the system or 'open-space' where the whole of the system top has been replaced with immiscible oil and the flow was either manual or due to capillary forces (*380*). Yu *et al.* created one such system to study macrophage conditioning in tumour development, both in passive conditioning cultures and in flowing ones, and compared it to using transwell assays for similar purposes (*381*). However, they did not test their system for chemotaxis research.

Walsh *et al.* took open microfluidics a step further and removed plastic moulds altogether (*382*). Instead, they created 'fluid walls' by using hydrophobic forces between an immiscible fluorocarbon oil FC40 and cell culture media to create fully fluid designs on common tissue-culture petri dishes. The system, which they called 'Freestyle Fluidics' (FF), allows complete freedom of design and printing of cell culture media onto petri dishes therefore allowing creation of complex patterns (circuits) as well as 'well-plates' confided within 60 mm dish (*26*, *27*). Fluid dynamics within the system are based on differences in pressure between different chambers as well as passive diffusion throughout. Deroy *et al.* carefully experimentally examined and modelled these dynamics to predict flow depending on variables such height of the circuits (dependent itself on the volume of media added), shear stress on the interface between FC40 and the media as well as bifurcating and merging branches within the circuits (*385*). These pilot studies ensured that this system is adaptable to any desired shape and application, however so far it has mainly been used for miniaturising and speeding up workflows in molecular biology such as complex feeding and plating protocols during clonal selection of cells (*383*).

4.1.10. Use of chemotaxis assays in macrophage migration studies

Different chemotaxis assays are appropriate for asking different research questions and this diversity has been reflected in macrophage chemotaxis research. In general 2D systems were used for molecular and kinetic studies while 3D gel invasion assays were used for distinguishing transitions between mesenchymal and amoeboid movement and the impact of ECM on macrophage migration (*273*). The most popular research tool has been transwell systems, which were used to understand the involvement of different molecular mechanisms involved in macrophage migration, from PI3K/Akt axis to the control of lamellipodia formation and focal complexes (*265*, *266*). Transwell assays' simple readout has been preferred for studies, where the research question was about the overall difference in migratory potential of the whole population rather than single cell migratory behaviour. Transwell assays have been used to study molecular components of the migratory pathways (thanks to the use of inhibitors and knock-out cells), as well as for drug testing. Single time point transwell systems have been important in discovering modulators of macrophage migration such as leptin and NFκB (*268*, *271*). The advent of real-time recordings added much needed kinetic data highlighting that different populations of macrophages have different migratory profiles. Iqbal *et al.* explored the heterogeneity of migration kinetics between thioglycolate- and biogel-elicited macrophages as well as bone marrow-derived macrophages and resident peritoneal macrophages (*272*). Each population displayed different migratory profiles towards common macrophage chemoattractants such as CCL2, CCL3 and CCL5. Given the general 'one size fits all' approach in discussing leukocyte migration the study by Iqbal *et al.* is an important reminder of the danger of generalising biological processes in such heterogeneous and plastic cell populations such as macrophages. This issue has been followed up by Cui *et al*. who used 3D gel migration assay to look into molecular mechanisms

behind those differences as well as between different polarisation states and concluded that the difference lies in expression of CD11a, CD11b, CD11c and CD11d integrins and their adhesion to the ECM (*112*). However, given the differences between 2D and 3D systems those studies are not directly comparable.

While transwell systems are popular for confirming intracellular components of chemotactic pathways and finding modulators of chemotaxis, TAXIScan and Dunn chamber have been used to go a step further in elucidating those mechanisms. Both have been particularly useful in looking at morphology of cell migration (*261*, *277*). Wheeler *et al.* used Dunn chamber to investigate the morphology of migrating bone marrow derived macrophages (*261*). Using this system, alongside transwell assays, they were able to show that members of Rho GTPases family Rac1 and Rac2 are responsible for the formation of lamellipodia and podosomes, but not migration itself. Vogel *et al.* used TAXIScan to investigate differences in migration and adhesion between non-polarised (M0) and M1/M2 polarised monocyte-derived primary human macrophages (*277*). They were able to show that M0 and M2 anti-inflammatory macrophages could migrate further than M1 macrophages. They attributed the difference in migratory capacity to non-polarised and M2 macrophages being able to rearrange their cytoskeleton more efficiently and forming multiple filopodia, while M1 macrophages remained more spherical in shape resulting in less migration (*277*). Moreover, TAXIScan has been used to compare morphology of pseudopodia formation across different eukaryotic migratory cells to understand evolution of the migratory mechanisms (*249*).

Even though microfluidics platforms have been used for discovery of novel macrophage chemotaxis modulators, such systems have been mainly used to understand chemotactic gradients and how cells detect and respond to them (*237*, *386*). Most of the current

chemotaxis research in microfluidic systems has been done on dendritic cells, which have a very defined and well understood responses to the CCL19/CCL21 chemotaxis axis, making them a more controlled experimental chemotaxis model (*237*). Research questions studied in DCs are relevant to macrophage research, such as cellular decision-making during migration in heterogenous environments with different pore sizes (*278*). Even though such questions have been studied in 3D gel migration assays the carefully designed microfluidics systems which combine different widths of the channel in one system have a clear advantage over comparing the same cell population in different gels with different (worse controlled) porosity (*273*, *278*).

Despite having the advantage of a 3D environment, gel invasion assays have limited ability to answer basic biological questions because of the impact of the artificial matrix itself on cell movement Cui *et al.* showed the ability to use 3D *in vitro* systems for molecular studies that inform not only on the molecular pathways involved in migration but also the shape changes that macrophages undergo and their ability to switch between amoeboid and mesenchymal migration (*112*). Pakshir *et al.* demonstrated the that 3D gel invasion assays can be also used to study cell-to-cell interactions in real time (*387*). They successfully implemented video microscopy to show that macrophage directional migration in a 3D matrix can be induced by mechanosensing of physical changes that contractile fibroblasts create in the ECM, independently of soluble chemoattractants.

4.2 Rationale and experimental aims of this chapter

The sustained popularity of transwell assays, despite their limitations, and the lack of better alternatives highlights the need for a technological advancement in the chemotaxis field. While the advent of microfluidics, paired with computerised image processing, brought a great promise to find this 'ideal chemotaxis assay' it also created new challenges such as inter-lab reproducibility and the rising cost and complexity of producing and obtaining the assay setups. The current goal in the field is therefore finding an assay that can fulfil all of Harris' criteria while being relatively straightforward and inexpensive enough to achieve reproducibility and popularity comparable to transwell assays or under agarose assays.

Given the flexibility of design whilst using common tissue culture reagents, technology invented by Walsh *et al.* is the perfect candidate to create such an 'ideal' macrophage chemotaxis assay. Therefore, I engaged in an interdisciplinary collaboration with the Walsh Lab at the Engineering Science Department at the University of Oxford to adapt their Freestyle Fluidics technology to study macrophage migration. Since all the experiments presented in this chapter were done in collaboration with Dr Cyril Deroy from the Walsh Lab, for the purpose of results and discussion I will use 'we' as the primary pronoun in this chapter.

Therefore, our experimental aims for this study were:

1. To adapt the Freestyle Fluidics platform for studying macrophage chemotaxis by designing systems where bone marrow-derived macrophages can be exposed to stable soluble gradients of chemoattractant C5a in both passively diffusing and actively flowing circuits.

2. To develop a method of reliably imaging and analysing the movement of macrophages within our experimental system.

3. To test our circuits against Harris' criteria in the hope that they will fulfil all the requirements of the 'ideal' chemotaxis assay.

4. To investigate the migratory behaviour of single macrophage within macrophage populations within our circuits and establish their patterns of movement depending on the cell's location within the population and the chemoattractant gradient that they are exposed to.

4.3. Results

4.3.1. Principles of printing circuits and depositing cells using Freestyle Fluidics platform

Since Freestyle Fluidics has never been adapted for studying eukaryotic cell migration we undertook extensive optimisation to ensure that the assay we designed is of the best achievable quality. In general, circuits can be printed on standard 60 mm or 35 mm Petri dishes using a custom-built 'printer' as described previously (*388*). Initially, we printed circuits on 60 mm dishes and imaged them at discrete time points with a benchtop phase microscope. However, to minimise the disturbance of the gradient and cells by moving of the dishes out of the incubator and to the microscope, and to achieve higher resolution of imaging, we eventually decided to use IncuCyte Zoom which is an automated microscope adapted to incubator conditions. That way we only needed to move the dishes once and they were kept in 37^{o}C, 5% CO_2 at all times. Almost all the circuits shown in this chapter were printed on 35 mm Petri dishes in order to utilise the IncuCyte Zoom's 'whole well' imaging mode (available only for well plates and 35 mm Petri dishes), which allowed us freedom to analyse custom areas of interest in each experiment according to circuit design.

The custom FF printer consists of a 3-axis traverse that holds a dispensing needle used to add/remove liquids (Figure 4.1A). There are multiple ways of printing the circuits (*384*), however in this study we used only two modes: 'forward printing' in the early phases of development, which was replaced by 'jetting' during optimisation. Forward printing (Figure 4.1B) consists of two steps. Firstly, media is deposited in any desired shape on a Petri dish (e.g. Figure 4.1D) and held in place due to interfacial forces between the media and the dish, similarly to a drop of rain hanging onto the window against gravity forces. Secondly, immiscible and bio-inert fluorocarbon oil called FC40 is gently manually overlaid onto the dish

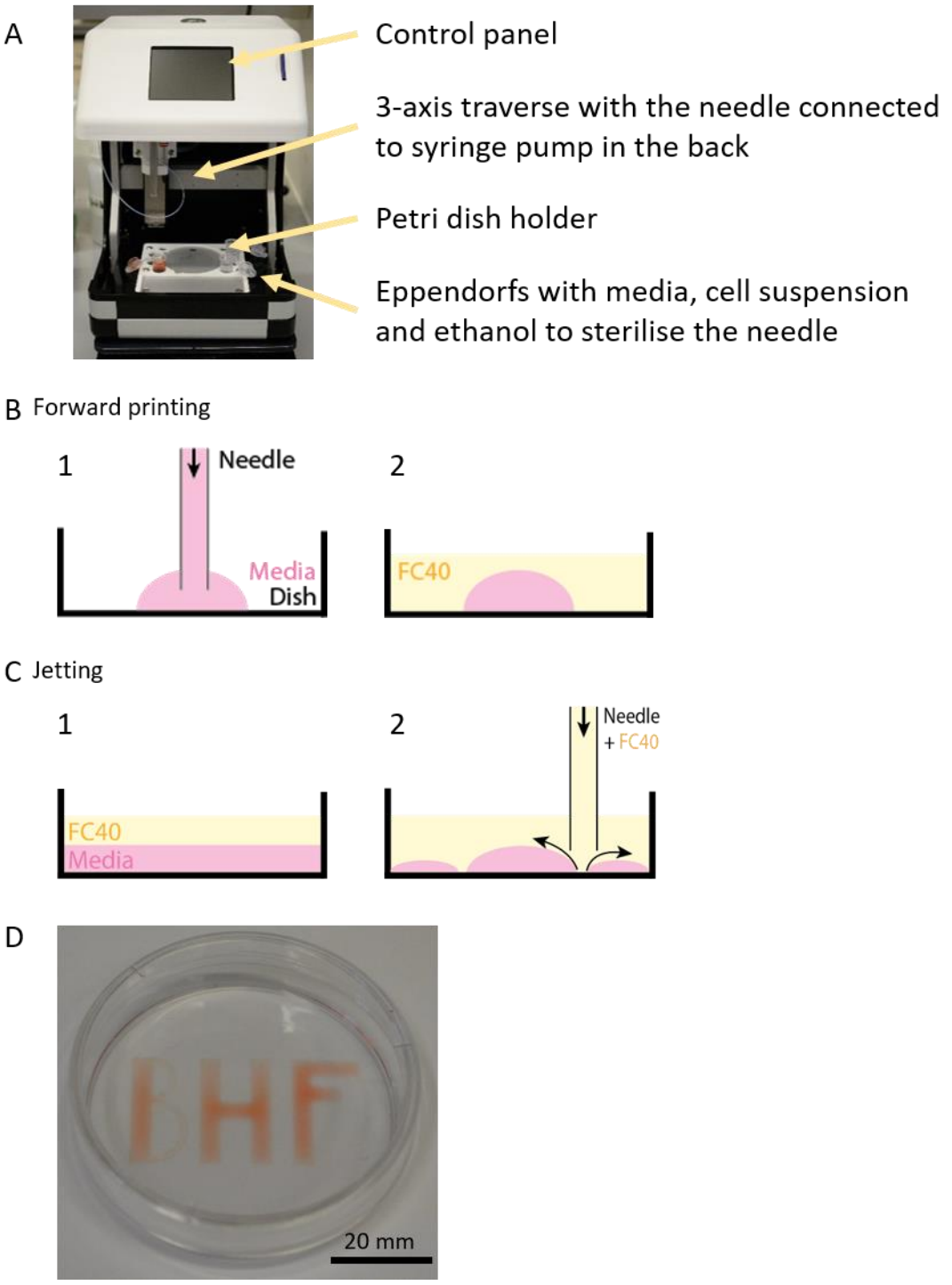

Figure 4.1. Principles of freestyle fluidics (FF) printing. A) Photograph of the custom FF printer with key components highlighted. B) Principles of 'forward printing' the circuits 1. Needle infuses media on a dish; moving the needle laterally deposits the media in the desired pattern aka circuit. 2. FC40 (2 mL) is gently manually overlaid onto the patterned media to create the pinning lines aka fluid walls of the circuit; diagrams not to scale. C) Principles of 'jetting' the circuits. 1. The bottom of the dish is covered with media which is immediately removed to leave ~50 µL in a thin layer, followed by gently manually overlaying FC40 (2 mL). 2. A needle loaded with FC40 is lowered into FC40 until just above the media and 'jetted', or forcefully ejected, FC40 on to the dish to replace media with FC40 that remains locally stuck to the dish. Moving the jetting needle laterally around cells creates a continuous isolating FC40 wall and therefor the desired circuit walls; diagrams not to scale. D) Example of the flexibility of pattern design and printing on a 60 mm Petri dish using the 'forward printing' method on the custom FF printer; scale bar 20 mm.

and the circuit. Aqueous media and the oil cannot mix, however FC40 is more adherent to the plastic than media, which creates 'pinning lines' – the fluid walls of the circuit which are held in place by the hydrophobic and interfacial forces between the media, FC40 and the Petri dish. However, forward printing is limited by the width of the dispensing needle (25 gauge), ~500 µm, which becomes the smallest dimension any circuit can have.

Jetting became the preferred method of circuit printing in our experiments because it overcomes the width limitation of forward printing and therefore allows for more precise pattern creation (Figure 4.1C). Small volume of media is added to the Petri dish to wet the bottom of it and then immediately poured out, leaving extremely thin layer of media behind (~ 50 µL in a 35 mm Petri dish). FC40 is then carefully manually overlaid on top of the thin media layer. The dispensing needle is inserted just above the thin media layer and jets a stream of FC40 through the thin layer of medium onto the bottom of the dish. This pushes medium aside so FC40 locally contacts – and adheres to – the bottom of the dish. The traverse then moves the jetting needle above the dish along a path that will define the footprint of the pinning lines- this process reshapes the interface between medium and fluorocarbon to create the desired fluid walls.

Cells can be deposited into the circuits either by adding them post-printing or by building the circuits around plated cells (Figure 4.2). Initially, we forward printed or jetted our circuits and added the cells afterwards by infusing cell suspension into one of the chambers of the circuit (Figure 4.2A). This created a concentric pattern around the location of the dispensing needle, meaning unequal distribution across the chamber and cells concentrated in the centre with a cell-free zone around the edges. Moreover, using this technique we were not able to infuse any cells into the conduits of our circuits. Plating the cells in the desired pattern and then

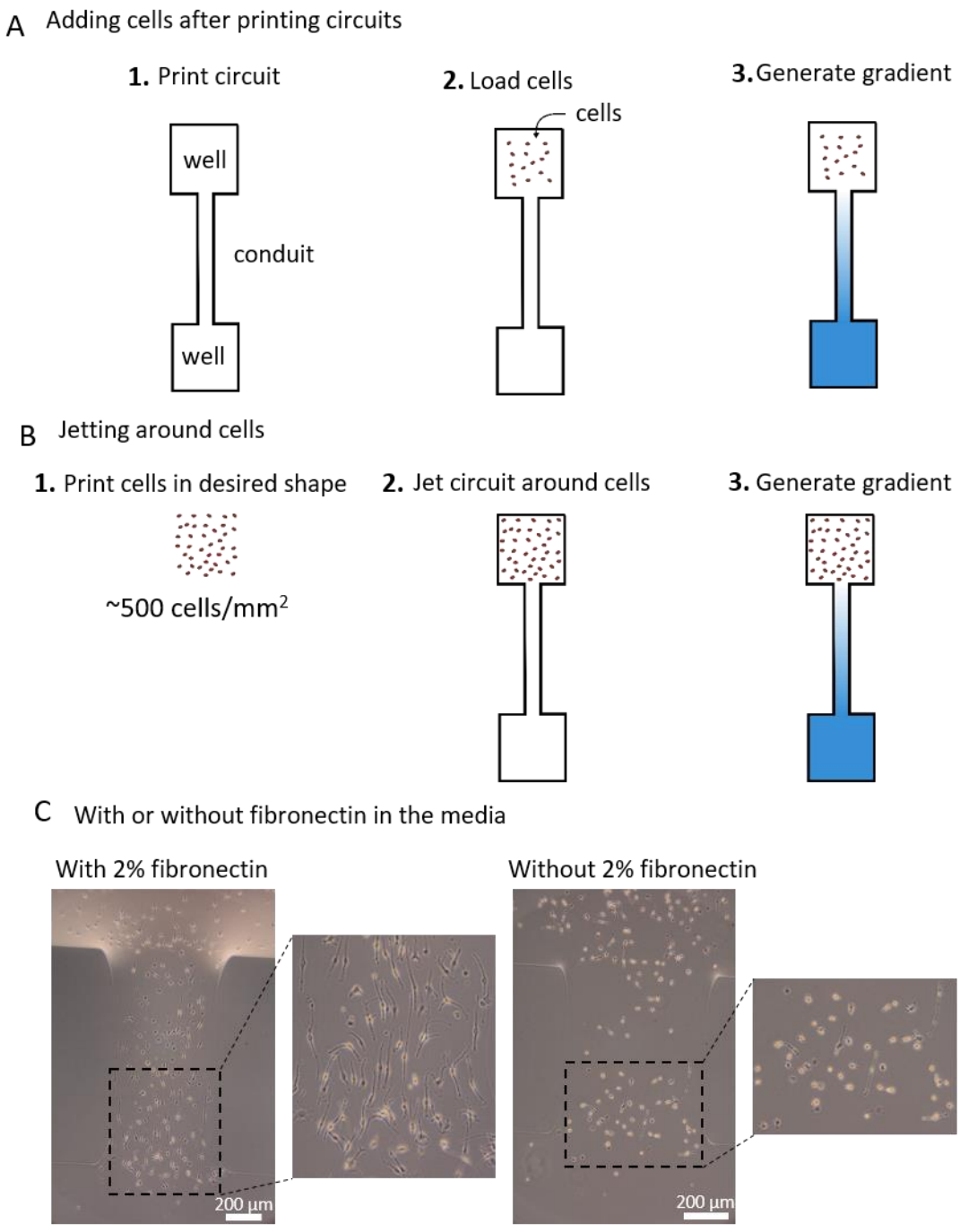

Figure 4.2. Possible methods of depositing cells into the passive circuits. A) Adding cells after printing circuits. 1. Circuits are forward printed or jetted in the desired patterns. 2. Cells are deposited at the desired location within the circuit and left to attach. 3. Diffusion gradient is created by addition of chemoattractant into the desired chamber of the circuit. B). Jetting around cells. 1. Cells are printed in the shape of the required chamber at ~500 cell per 1 mm2. 2. Circuit are jetted around the patterned cells. 3. Diffusion gradient is created by addition of chemoattractant into the desired chamber of the circuit. C) Adding cells with or without 2% fibronectin in the media. Representative 10 x images showing cells that were added to a circuit chamber as per method A of this figure after 48 h in 10nM C5a gradient in circuits with or without 2% fibronectin in the media. 138 cells migrated into the conduit after 48 h when 2% fibronectin was present while 77 cells migrated into the conduit at the same time point when fibronectin was absent; zoomed in images show cell morphology, scale bar = 200 µm.

building the circuits around them created a much more uniform distribution of cells in the circuit (Figure 4.2B). Firstly, we forward printed the circuits at ~500 cells/mm^2 density (infusion with 1000 cells/µL suspension) in the desired pattern. We found this density to be an optimal middle point because they were sparsely populated enough for the tracking algorithm was able to reliably determine cell paths whilst being dense enough to keep the culture alive; we found that BMDMs that were deposited into the circuits at low densities died within the first 24h in the circuits. Thanks to jetting, we were then able to create the conduits around the cells as well as pattern cells in precise locations within the circuits, as seen in Figure 4.8 and Figure 4.11 respectively.

During the early phases of optimisation, we considered introducing extracellular matrix coating of the Petri dishes to aid macrophage migration. We chose to coat the dishes with fibronectin as it has been previously shown to aid macrophage migration in 2D systems (*389*). However, pre-coating of the dishes caused negative changes to the interfacial forces between the media, FC40 and the dish, causing the pinning lines to collapse. Therefore, we tried adding 2% fibronectin to the media that the cells are suspended in and the circuits are drawn with (Figure 4.2C). We compared cell migration with and without fibronectin in the media and observed that when fibronectin was added more cells migrated in the circuits. Additionally, we observed changes in morphology of migrating BMDMs – when fibronectin was present their cytoskeleton remodelling was more extensive, with extremely long pseudopodia being extended up to 48 hours within the circuits. In comparison, cells that migrated without any fibronectin were rounder and formed much smaller pseudopodia. Therefore, we decided to add 2% fibronectin to the media we used for creating the circuits. This solution provided

enough support and stimulation for the BMDMs to improve their migratory response and aid their cytoskeleton remodelling without causing the collapsing pinning lines.

Therefore, our overall protocol for creating chemotactic circuits using Freestyle Fluidics platform and a standard culture of bone marrow-derived macrophages became as follows. We first printed BMDMs in any desired 2D pattern by infusing culture medium containing suspended cells and 2% fibronectin through the dispensing needle and on to the surface of a dish (1000 cells/µL suspension, needle suspended 300 µm above dish surface). The dish was placed in an incubator for 5 min so cells attach, and the bottom of the dish was then gently and completely covered with 1mL of medium with 2% fibronectin; as macrophages are strongly adherent, they remained firmly attached to the dish where originally deposited. Most of the medium was then removed to leave a thin layer (~50 µL), which was immediately covered with 1mL of FC40. After returning the dish to the printer in the original orientation, the circuits were jetted around the cells (needle 500 µm above the dish surface) and the circuits were infused with more media to provide additional nutrients for the BMDMs.

4.3.2. Considerations in chemotactic circuit design

As we were the first group to try and establish chemotaxis circuits using the Freestyle Fluidics platform, we opted for simpler designs that would mimic Boyden chamber principles over more complicated mazes that are often created using traditional microfluidics (*278*, *390*). The overarching idea for the passive circuits was to create two separate chambers connected by narrow conduits so that BMDMs can be deposited in one of the chambers and the chemoattractant solution into the other. That way a gradient could be established through the conduits without flushing the cells with the chemoattractant upon addition. Initially, we started with one large circuit per 60 mm Perti dish, which consisted of two rectangular

chambers connected by 7 narrow conduits (Figure 4.3A). Conduits were ~500 µm in width as they were forward printed and therefore made with a single motion of 25G needle. Cells were deposited into one of the chambers post-printing causing an unequal distribution across the chamber. Seven conduits ensured sufficient diffusion across and into the cell chamber, fulfilling the requirement for sufficient chemoattractant localisation in the experimental chamber, however multiple entry points of the gradient meant there was less control over the chemoattractant gradient. Nonetheless, we were able to observe directional migration of cells into the conduits and therefore we were able to demonstrate that Freestyle Fluidics circuits could be used as a macrophage chemotaxis platform. However, due to cell and gradient distribution the migration was uneven across the conduits with most cells moving across the three middle conduits and very few through the side ones.

The advantage of the chamber/conduit design was the possibility of easy circuit manipulations by adding and removing either the chambers or conduits. To introduce the ability to run controls and parallel conditions within the circuits we therefore added a third parallel chamber. Simultaneously we reduced the number of conduits to 3 per each side to further control the diffusion through them (Figure 4.3B), especially since the four side conduits supported very little migration in the previous design. We decided to add cells to the middle chamber so that the other chambers could be used either for pure media and chemoattractant solution, therefore creating an in-built negative control within the system, or two different chemoattractants, one in each chamber, therefore allowing cellular decision making/competition studies. We were able to run experiments with the in-built negative control, however the large dimensions of the circuit and multiple channels were still

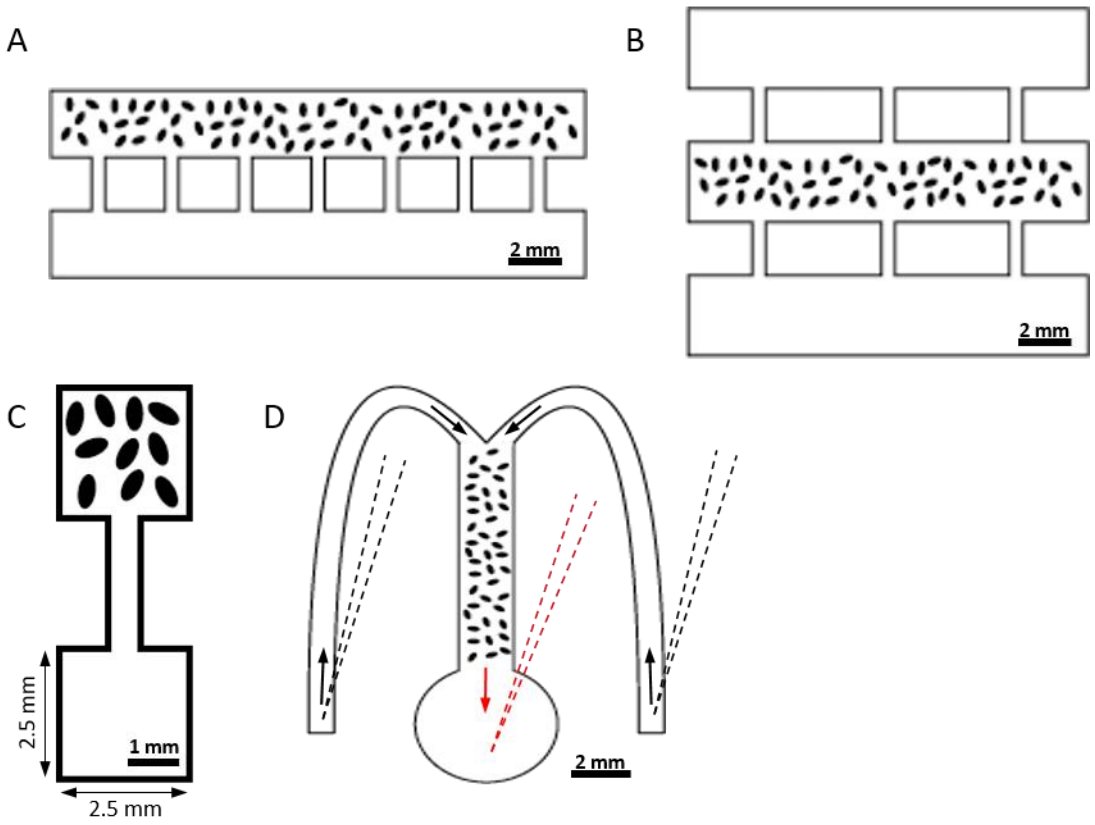

Figure 4.3. Evolution of the circuit design. A) Initial design consisted of two rectangular chambers with seven uniformly spread conduits connecting the chambers, cells were deposited into one of the chambers while chemoattractant would be added to the second chamber to create diffusion gradient. B) The circuit was extended to incorporate three parallel chambers with the middle chamber connected to each of the side chambers by three conduits; cells were deposited in the middle chamber and exposed to two distinct gradients created in the side chambers. C) Circuit was minimised to allow multiple technical repeats printed onto a dish, two 2.5 mm x 2.5 mm square chambers were connected by single conduit (600 µm width, 1.5 mm length) with cells deposited into one of the chambers; up to 12 such circuits can be fitted onto a standard 35 mm Petri dish. This design was further modified to allow more flexible experimental designs. D) Active 'm'-shaped circuit was created by connecting two separate arms into one bigger conduit (1.8 mm width, 5 mm length) with cells deposited in it and a round 'sink' where the flowed media would be collected; using syringe pumps a needle was inserted into the end of each of the arms to continuously infuse media (needles represented in black dashed lines with the direction of flow indicated by black arrows) with or without a chemoattractant and a separate needle and syringe pump were inserted into the 'sink' to withdraw the excess media (needle represented by red dashed lines with red arrow indicating direction of flow).

suboptimal for reliably controlling the gradients. Given that we were able to fit only one circuit per 60 mm Petri dish it was also a very low throughput solution.

To increase throughput and further simplify the design we reconfigured the passive circuits to a 'dumbbell' shape, which consists of two square chambers (footprints 2.5 x 2.5 mm) connected by a thin conduit (600 µm wide, 1.5 mm long), as shown in Figure 4.3C. We were able to fit 12 of those circuits in each 35 mm Petri dish significantly increasing the assay throughput. Despite having no in-built controls we were able to run multiple conditions in parallel thanks to 12 circuits being available on each dish and therefore we could include the controls as well as technical repeats for each experiment. Single conduit allowed us to fully control, and therefore mathematically model the gradient. The simplicity of this design made it extremely easy to manipulate; we tested different lengths of the conduit as well as added another chamber for comparative studies (Figure 4.11 and Figure 4.12 respectively). That version of the circuit connected three parallel chambers (also 2.5 mm x2.5 mm) to two conduits (600 µm wide, 1.5 µm long), however due to larger circuit dimensions, only 6 circuits were printed in each 35 mm dish.

Since passive gradients change over time, we wanted to establish a second system where active pumping would ensure unchanging gradient profile over time. For flow-generated gradients, we used 'm'-shaped circuits (Figure 4.3D). These circuits consist of two arms that join into a conduit that ends in a large circular sink (7 mm wide). Cells were deposited in the central conduit (6 mm long, 1.8 mm wide), and side arms were used to perfuse media or chemoattractant solutions. Needles attached to a syringe pumps were inserted into each end of the side arms, as illustrated in black dashes lines in Figure 4.3D, while a separate needle

with a separate syringe pump is inserted into the sink to retrieve excess of the flowed media (red dashed lines in Figure 4.3D).

4.3.3. Generation and maintenance of gradients in passive circuits

In passive circuits, reagents are pipetted directly through the fluid walls into the circuit – either manually or robotically on the printer – before gradients are established by diffusion. It is therefore essential that this pipetting does not induce flows that distort chemoattractant gradients. This was achieved as illustrated in Figure 4.4A. Initially, pressures in the passive dumbbell circuit described in Figure 4.3C were at equilibrium. Then, medium (1 µL) was added to the top chamber (represented by red dye in Figure 4.4A) to increase its Laplace pressure (defined as $\Delta P = \frac{\gamma}{R}$, where $\gamma =$ interfacial tension, $R =$ radius of curvature, and $P_{top} = 20$ Pa); consequently, medium started to flow towards the bottom chamber. Next, a smaller volume of chemoattractant (0.5 µL) was added to the bottom chamber (represented by blue dye in Figure 4.4A; $P_{bottom} = 11$ Pa). This increased the Laplace pressure in that chamber decreases the pressure gradient in the whole system ($\Delta P_{circuit} = 9$ Pa). Once 0.25 µL medium entered the bottom chamber (shown as red dye entering the bottom chamber in Figure 4.4A, panel t = 5min), the system reached equilibrium. This procedure ensured that the pressure in the conduit is greater than P_{bottom} after adding the chemoattractant, so that no attractant can flow out of the bottom chamber into the conduit. Instead, upon reaching equilibrium, attractant simply diffused out of the bottom chamber to create a gradient from the bottom to the top of the conduit (Figure 4.4A, t = 1h).

As passive circuits were prepared on the printer and moved to the microscope for imaging, movement-induced advective flows could perturb gradients. Therefore, we monitored gradient uniformity during our protocol. We printed twelve circuits and loaded them with

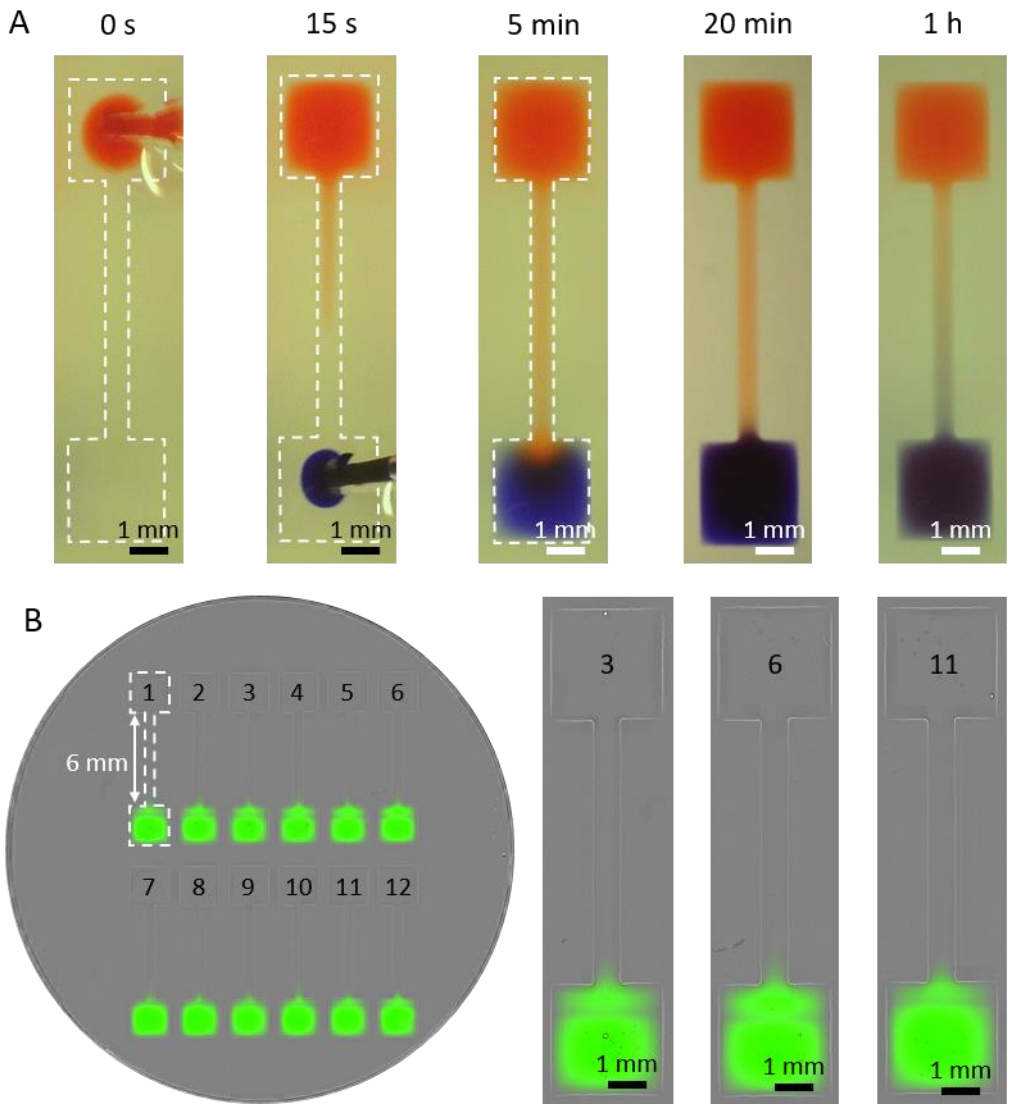

Figure 4.4. Gradient generation and maintenance in passive circuits. A) Establishing gradients in a passive dumbbell circuit, from left to right: 1 µL of red dye was manually pipetted into the top chamber at t = 0 sec. Resulting pressure differences induced advective flow down the conduit. A volume of blue dye too small to reverse this flow (0.5 µL) was pipetted into the bottom chamber immediately after (t = 15 sec). At t = 5 min, red dye has entered the bottom chamber, the system equilibrated and diffusion now started establishing the gradient of the blue dye. At t = 20 min, blue dye started to diffuse up the conduit. After 1 h, linear concentration gradient of each dye was established; scale bars = 1 mm, dashed lines - wall footprints. B) Gradients in dumbbells remained undistorted as dishes are moved from printer to microscope. Left: Image of a whole 35 mm dish containing 12 identical dumbbells formed by stitching together smaller images. Medium ± fluorescein was loaded into upper and lower chambers as in (A) by the FF printer, the dish manually transferred to a microscope, images were collected after 20 min to assess gradient disturbance across the circuits. Incorrect stitching by the software yielded apparently fluorescein-free lines at the top of lower chambers. Right: Close-ups of 3 circuits.

fluorescein on the printer (in a biosafety cabinet to ensure sterility), moved the dish to an imaging system (an IncuCyte ZOOM in an incubator), and imaged for their fluorescence readout - fluorescent fronts in all conduits were located in essentially the same places, consistent with little or no advective perturbation (Figure 4.4B). To further illustrate uniformity of gradient formation despite moving the dish, three of the twelve circuits printed are shown in the zoomed-in images at the right side of panel in Figure 4.4B.

Gradients generated in passive circuits change over time as diffusion drives the system to equilibrium. To account for that, we wanted to establish their dynamics over time to be able to determine the concentration of chemoattractant that the cells are exposed to at any time-point and location. The narrow conduit provided the perfect conditions to assess and model gradient dynamics over time as it is linear, with very defined dimensions and pressure and starts directly at the source of the chemoattractant gradient. We decided to use 10 nM C5a as the main chemoattractant concentration in our studies and therefore all the calculations were performed for that compound. Diffusion is described by Fick's second law, which correlates concentration, time, distance and the diffusion coefficient (dependent on the molecular weight of the compound). We arbitrarily decided that the system reached equilibrium when the attractant concentration at the top of the conduit (opposite to its source) reaches 15% of the initial concentration in the bottom chamber; time needed to achieve this was marked as t_{ss}. After reaching steady state, the gradient in the conduit was linear and set to vary from 0 to 10 nM ($c_{max} = 10$ nM). Using Fick's second law we established that doubling conduit length (x) quadrupled t_{SS} (e.g., for C5a in our system, if $x = 2$ mm, $t_{SS} \approx 1.5$ h; if $x = 4$ mm, $t_{SS} \approx 6$ h; Table 4.2). Knowing the time required for the diffusion

to reach equilibrium was crucial for calculating the concentration of the chemoattractant that the cells respond to.

We next determined the rate of mass transfer through a conduit from Fick's first law of diffusion (correlating mass flow rate and area) to assess the duration of these stable gradients (and predict maximum experimental runtimes). We defined the maximum experimental runtime as the time needed for the 10 nM C5a to be evenly distributed across the system, assuming the concentration gradient remains approximately constant until 5% of the chemoattractant's initial concentration c_{max} reaches the top chamber where it becomes evenly distributed ($c_{end} = 0.05\ x\ c_{max}\ @\ t_{end}$). Since in our system conduits have fixed widths, area and therefore t_{end} varied proportionally with conduit length (e.g., for $x = 2$ mm, $t_{end} \approx 15$ days; for $x = 4$ mm, $t_{end} \approx 30$ days; Table 4.2). Given that primary BMDMs would not survive such long experimental runtimes their lifespan became a limiting factor – we observed that fully differentiated BMDMs survived up to 72 h in our system so we run our experiments in the passive circuits for 48 hours.

4.3.4. Generation and maintenance of gradients in active circuits

The passive circuits have the advantage of being simple to set up and do not require external pumps; however, their gradients change over time as diffusion drives the system to equilibrium. In contrast, gradients generated by diffusion between two laminar streams flowing continuously through one conduit remain stable and unchanging for as long as flow continues. Stable gradients in the active 'm'-shaped circuits (Figure 4.3D) were thus established. Briefly, two needles were inserted separately into left and right arms of the circuit; needles were filled with media with or without C5a and were connected via polytetrafluoroethylene (PTFE) tubing to two syringes on one syringe pump. The syringes

Conduit length (mm)	**1.5**	**2**	**3**	**4**	**5**	**6**	**7**
t_{ss} (hours)	0.9	1.5	3.4	6	9.5	13.6	18.6
t_{end} (days)	11.5	15	23	30	38	45	53

Table 4.2. Conduit length as a variable in gradient establishment. Dumbbell shaped circuits were designed to have their conduit length vary between 1.5 – 7 mm. Dynamics of the gradient onset were theoretically calculated for tss = hours needed for the steady state of the gradient to establish and for tend = longest possible amount of days that the steady state of the gradient can be maintained given the length of the conduit and the volumes in the system.

were infusing at a constant flow rate, so media (represented by the red dye added in Figure 4.5A) and media + attractant (represented by blue dye in Figure 4.5A) met as laminar streams in the central conduit. Diffusion then created a stable concentration gradient across the width of the conduit. The steepness of this gradient was controlled by varying the overall flow rate in the conduit (lower rates yield shallower gradients as represented by dyes in Figure 4.5A).

Unlike traditional microfluidic devices with fixed geometries, fluid-walled conduits have flexible interfaces that morph with changes in pressure; as a result, conduit height decreases in the flow direction due to decreasing pressure. Furthermore, conduits have cross-sections that are sections of a circle. Thus, the average velocity in a conduit varied as a function of conduit length, x, and conduit width, z (*385*).To predict the shape of the concentration gradient in conduits where streams meet along the conduit centreline, we determined the average velocity, u_{mean}, along the centreline over the entire conduit length (in increments $\Delta x = 6$ μm). From these values, we inferred the time t a particle spends in the conduit at any given location to obtain the local concentration. Flow velocities at any point in fluid-walled conduits can be predicted using a simplified power law if the geometry of the conduit footprint, flow rate, and fluid properties of perfusing medium are known (*385*). We thus determined flow velocities to transform the time-dependent diffusion solution into a distance along the device substitution using $t = \frac{x}{u_{mean}}$, where u_{mean} is the mean flow velocity at a given x-location.

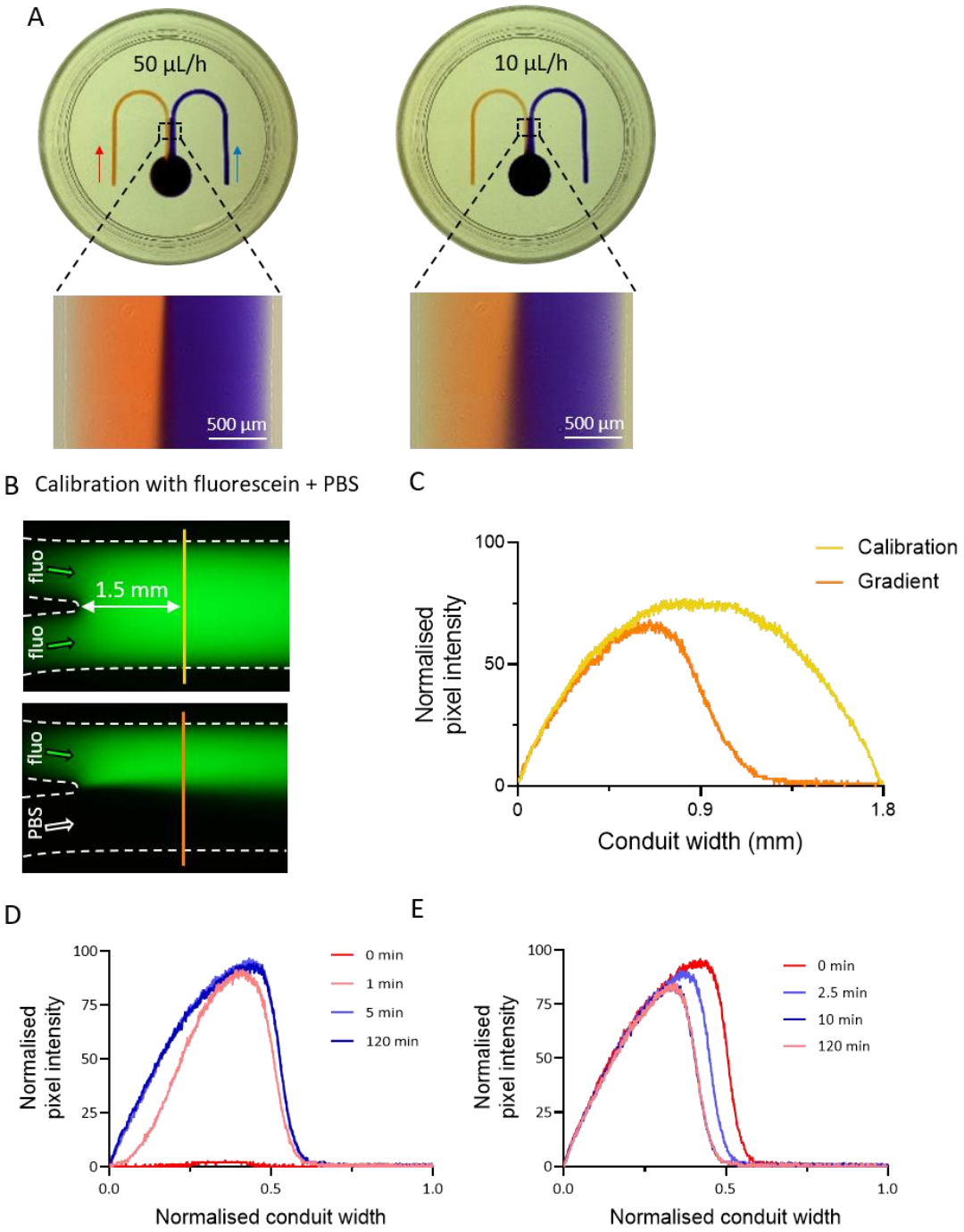

Figure 4.5. Gradient generation and maintenance in active circuits. A) Establishing gradients in an active 'm'-shaped circuit. Images of circuits as dyes were infused continuously through the arms at a rate of either 25 µL/h in each arm (left) or 5 µL/h in each arm (right) to create diffusion gradient down the central conduit. Zoomed images: gradient width increased depending on the flow rate with shallower gradient created by slower infusion rate; scale bar = 500 µm. B) Calibration of gradient modelling using fluorescein. Top: fluorescein was infused through both arms of the m-shaped circuit (labelled with yellow and called 'Calibration'). Bottom: fluorescein was infused through one arm of the circuit while PBS was infused into the other to create a gradient (labelled with orange and called 'Gradient'). C) Normalised fluorescence intensity profile across the width of the conduit for the conditions in (B). D) Imaging gradient establishment and stability using fluorescein/PBS infusion from panel (B) over the course of 120 min. E) Established fluorescein/PBS gradient (t = 0 min) is abruptly shifted by 200 µm and its re-establishment and stability are imaged for 120 min.

Additionally, gradients can be shifted by varying the ratio of flow rate between input streams Q_1 and Q_2. Using the previously established semi-analytical solution to predict conduit heights in flowing systems, we applied the same method to determine flow rate ratios required to shift gradients by a fixed distance (*385*). Determining the required flow rates for each arm depended on maximum conduit height, viscosity of the media flown, conduit half width and interfacial tension. Since shifting gradients brings the centreline closer to the conduit edge where flow velocities are lower due to conduit curvature, we adapted our model to account for these changing velocities.

To validate our assumptions for predicting the location and steepness of the concentration gradients in active circuits, we flowed fluorescein through the system. To calibrate the recording, we flowed it through both arms of the 'm' shaped circuit – predictably the highest fluorescence intensity was detected in the middle of the conduit (Figure 4.5B and 4.5C). When fluorescein was infused only through one arm and PBS through the other, a gradient was established at the interface of the two (Figure 4.5B and 4.5C, Movie 4.1). The recordings showed that the gradient was located in the middle of the conduit, fully established within the first 5 minutes of the active pumping and remained stable over the course of 2 hours (Figure 4.5D). When flows were abruptly altered to shift the gradient by 200 µm, fluorescein recording showed that the gradient stably re-established at the new location within 10 minutes of the change and remained stable for 2 hours (Figure 4.5E, Movie 4.2).

4.3.5. Bone marrow-derived macrophage migratory response to complement C5a and chemokine CXCL12

Next we wanted to establish the optimal dose of complement C5a to use during the validation of our system. Complement C5a is a very potent macrophage chemoattractant therefore an ideal candidate for validating a new chemotaxis system (*267*). We decided to use xCELLigence

chemotaxis assay for establishing a dose-response curve to C5a and showed that in this transwell assay 10 nM of C5a elicited the highest possible migratory response of bone marrow derived macrophages (Figure 4.6B). We therefore assumed that 10 nM C5a would be able to elicit the highest possible response in the Freestyle Fluidics circuits and decided to use this concentration during the validation process.

Chemokine CXCL12 is another known macrophage chemoattractant (*268*), which we wanted to use during the validation process. However, in the xCELLigence assay the maximal BMDM migratory response it elicited was 7 times lower than the one to C5a (Figure 4.6D). Additionally, the variation in the responses to each of the concentrations were much greater than to C5a, probably due to the lower potency of CXCL12 compared to C5a. To further compare the two chemoattractants, we looked at the normalised traces of cell impedance produced in the assay. All the responses to C5a, regardless of the concentration, followed a predictable pattern where delta cell index would steadily increase within the first hour of recording until reaching the maximum response and plateau after (Figure 4.6A). By 4 hours all the concentrations have plateaued. Contrarily, CXCL12 responses did not follow similar pattern (Figure 4.6C). Traces did not show a steady increase in delta cell index within the first hour, some of them even registered negative normalised values, which means that the migration in experimental wells was lower than in the control wells with no CXCL12. Moreover, they never plateaued suggesting that the registered response was not stable. We therefore concluded that CXCL12 is not a reliable BMDMs chemoattractant for *in vitro* studies and decided not to test it in the FF circuits.

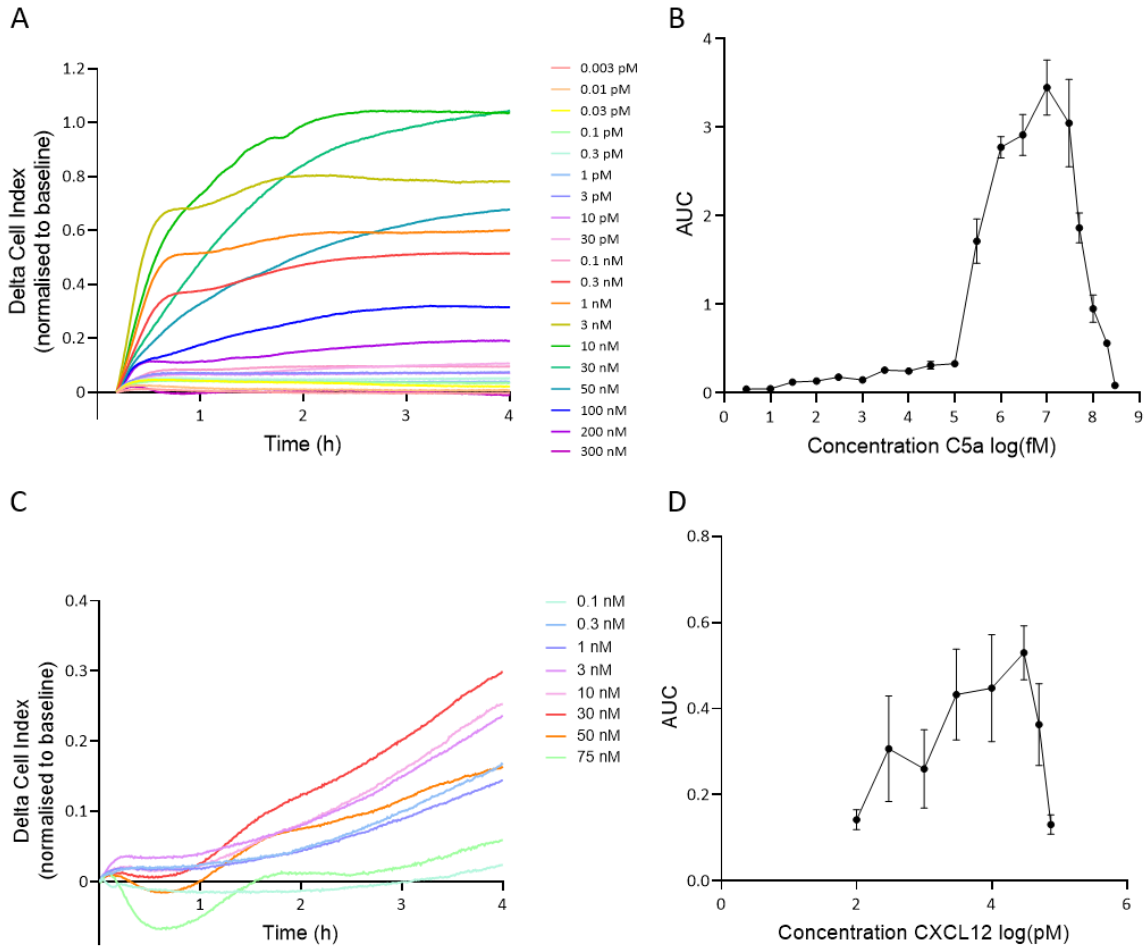

Figure 4.6. Dose-response curves of bone marrow derived macrophages in validated xCELLigence system. A) Mean traces of the impedance measurements of BMDM migration towards C5a registered every 40 seconds for 4 hours were normalised to baseline for each plate. B) The area under the curve (AUC) quantified for the traces in A to establish dose-response curve of BMDMs to C5a concentrations ranging from 0.003 pM – 300 nM. (n = 3-7 biological repeats per each concentration). C) Mean traces of the impedance measurements of BMDM migration towards CXCL12 registered every 40 seconds for 4 hours were normalised to baseline for each plate. D) The area under the curve (AUC) was quantified for the traces in C to establish dose-response curve of BMDMs to CXCL12 concentrations ranging from 0.1 nM – 75 nM. (n = 2-5 biological repeats per each concentration).

4.3.6. Detection of chemotaxis and chemokinesis in passive circuits

In our system, macrophages moved by mesenchymal mode of migration i.e., extending pseudopodia that pull the cell over the substrate. Pseudopodia extending towards an attractant were early visible markers of chemotaxis (*391*). For the purpose of analysis, we needed to determine the time of onset of chemotaxis. We chose to analyse morphological changes in BMDMs that are characteristic of cell migration. As BMDMs extend pseudopodia to move across surfaces and sense chemical stimuli (*260*), we determined the time required for these pseudopodia to first become apparent around cells (Figure 4.7A). For each cell that was detected as migratory over the course of 48 hours exposure to the gradient, the first image of the IncuCyte recording where pseudopodia were extended in the direction of C5a source was noted as the initiation of chemotactic response. The time at which that happened then provided a window during which cells were activated, and corresponding concentrations and gradient strengths were determined using the distance of cells to the C5a chamber and the theoretical model of C5a distribution across the conduit.

On the other hand, it was important to distinguish dead cells from alive cells in the circuits. We used observed morphology in the phase-contract images as well as cell velocity to recognise dead cells. As seen in the example image in Figure 4.7B, cells which died in the circuits were much smaller and rounder than alive macrophages, with no protrusions extending out of the cell bodies. Additionally, they showed no random movement characteristic of macrophages scanning their environment.

To validate the possibility of chemotaxis and chemokinesis detection in the Freestyle Fluidics circuits, we exposed BMDMs to a gradient of C5a that varied from 0 to 10 nM and monitored their responses in the dumbbell shaped circuits (Figure 4.8 and Figure 4.9). Initially, we

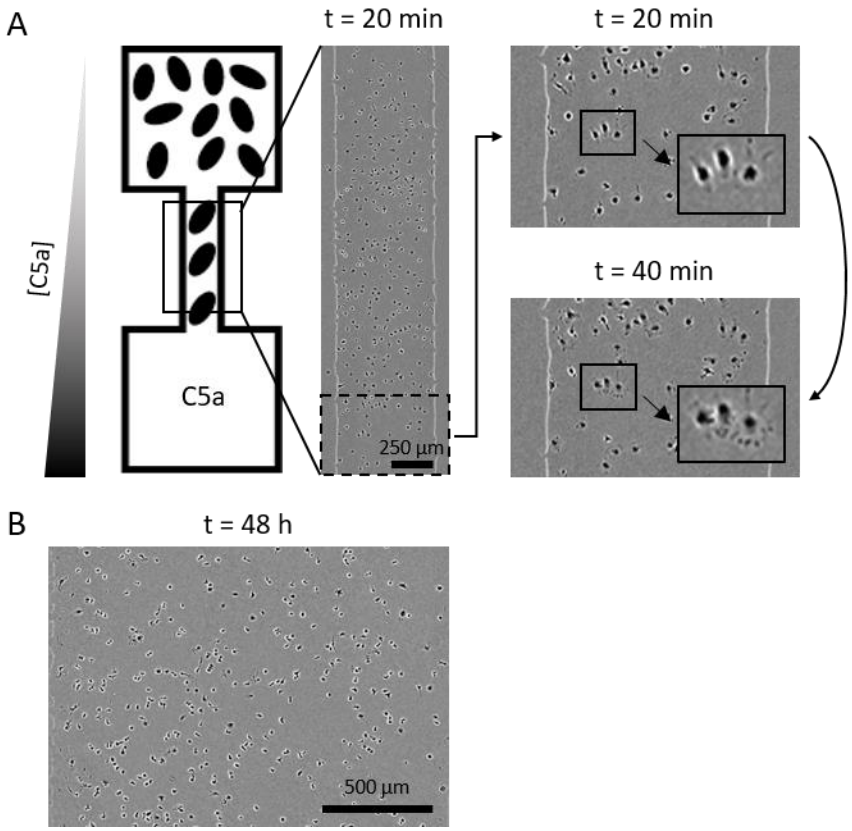

Figure 4.7. Establishing onset of chemotactic response in the circuits. A) The cartoon (left) shows the experimental setup. Centre: image showing the conduit at t = 20 min after C5a addition. Top right: image showing that cells are mostly round at t = 20 min. Bottom right: cells extended pseudopodia directionally towards the C5a source at t = 40 min, which was considered as the onset of chemotactic response; scale bar = 250 µm. B) Representative image of cells that did not survive in the circuit at t = 48h – cells were considered dead when no movement was registered and cells were small and round as per this representative image; scale bar = 500 µm.

deposited all cells in the top chamber of a dumbbell-shaped circuit (Figure 4.8A) and we added C5a diluted in the media (calculated to make up c_{max} = 10 nM in the chamber) into the bottom chamber; we collected images every 20 min for 48 hours to create a time-lapse movie (Movie 4.3). Almost no cells were seen in the conduit at first (Figure 4.8A, t = 20 min). As the gradient became established ($t_{SS} = 0.9$ h for the 1.5 mm conduit), cells entered the conduit and after 48 hours some even reached the bottom chamber (Figure 4.8A, t = 48 h). Tracks of individual cell trajectories were derived by analysing successive images in the time-lapse recording; these tracks showed a biased movement of cells towards C5a (Figure 4.8A; blue tracks indicate movement towards C5a, red ones away from it, and black dots show static cells). Trajectories were also binned according to angle and displayed as rose plots (blue segments indicate tracks moving towards C5a, and red ones away from it, with segment length reflecting the number of trajectory points per bin). We also quantified cells' average drift velocity in the direction of the attractant (v_{taxis}, average y-velocity) for each condition. v_{taxis} was calculated by averaging the y-velocities of each trajectory (positive velocities towards the top chamber, negative velocities towards the bottom chamber). Thus, in a gradient, negative values of v_{taxis} indicated biased movement towards C5a.

Next, we built circuits around cells initially located in the conduit and examined the response of these cells to the same gradient (Figure 4.8B; Movie 4.4). Given that we could precisely model the C5a gradient in the conduit, we were able to investigate cell response to C5a more precisely when the cells were initially present in the conduit. Tracks of individual cell trajectories were recorded across the entire conduit and showed more diverse migratory profile than cells recorded in Figure 4.8A. Most of the trajectories were still biased towards C5a (Figure 4.8B) and the v_{taxis} was lower yet still negative, confirming chemotactic response

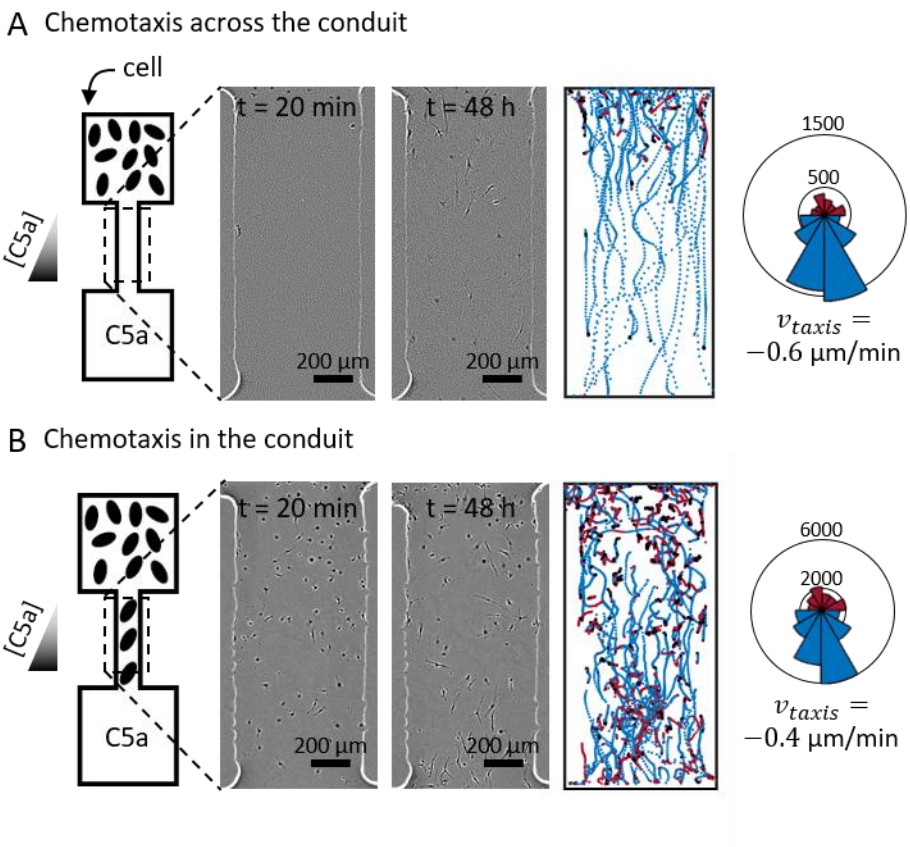

Figure 4.8. Demonstrating chemotaxis in passive circuits. C5a (10 nM) was added to the bottom chamber, trajectories of individual cells tracked over 48h and rose plots generated (n = 3 biological repeats for each condition, blue = towards C5a, red = away from C5a, black = stationary). A) Left to right: migration of cells initially present only in the top chamber (as illustrated by the cartoon). Images of conduit at t = 20 min and t = 48 h showed that cells migrated into an empty conduit. Cell trajectories and a colour-coded rose plot with the circles indicating number of trajectory points falling into each bin and measurement of vtaxis (directional speed). B) Left to right: migration of cells initially present in the conduit (as illustrated by the cartoon and images of conduit at t = 20 min and t = 48 h). Cell trajectories and a colour-coded rose plot with the circles indicating number of trajectory points falling into each bin and measurements of vtaxis (directional speed); scale bars = 200 µm.

of cells. However, there was a greater proportion of cells recorded with the red tracks, which fell into the red bins of the rose plot (away from the C5a source); in other words, across the entire population of BMDMs in the conduit only some cells migrated directionally.

One of the key criteria that Harris proposed for the 'ideal' chemotaxis assay was the ability to distinguish between chemotaxis and chemokinesis. Therefore, we tested the ability to detect chemokinesis in our system by creating dumbbell circuits with cells in the chamber and in the conduit that were either exposed to media only (Figure 4.9A, Movie 4.5) or to 10 nM C5a everywhere in the circuit (Figure 4.9B, Movie 4.6). Tracked cell trajectories and rose plots showed no clear bias towards or away from the bottom end of the conduit in either condition (Figure 4.9A and Figure 4.9B). In both conditions in the circuits with no gradient, $v_{taxis} = 0$ µm/min, confirming the absence of chemotactic bias.

To assess our ability to distinguish between chemotaxis and chemokinesis we measured average cell velocities and the net-to-gross displacement ratio (NGDR) for each condition The NGDR is defined as the straight-line distance between start and end points of a trajectory divided by the total distance travelled along the path of the trajectory (see for instance Oliveira *et al.* (*284*)). Therefore, an NGDR of 1 indicates a cell travels in a straight line from start to finish irrespective of whether it is towards or away from attractant, while progressively lower values point to decreased directedness. There was no significant change in velocity between any of the conditions presented in Figures 4.8A, 4.8B, 4.9A and 4.9B (Figure 4.9C), however there was a significant increase in the NGDR value in the presence of the C5a gradient (conditions from Figure 4.8) as compared to the lack of gradient (conditions from Figure 4.9), as shown in Figure 4.9D. Given the bias indicated by the rose plots and v_{taxis}

values from Figure 4.8 we could conclude that the increase in the NGDR value was due to directional migration towards the C5a source.

To ensure that the chemokinetic movement that we recorded in the conduit was not induced by the conduit itself, we decided to perform bias experiments to establish the effect of the circuit itself on the random migration of BMDMs in it. Fluid-walled conduits have cross-sections that are sections of a circle, and conduit height decreases from the centreline to the wall. Consequently, cells growing in such conduits have varying volumes of media above them depending on their location in the conduit. Therefore, we investigated the effect of cell position on cell behaviour using passive dumbbell-shaped circuits with uniform distribution of cells across the entire area of the circuits, to assess whether these changing heights biased cell behaviour. We exposed cells in the circuits to either cell culture media alone or uniform distributions of 10 nM C5a (no gradient) and imaged them over 48 h. We then segmented circuits into 19 distinct regions and compared cell velocities in each (Figure 4.10). In this way, we showed that average cell velocities throughout circuits were nearly identical and thus that changing heights did not impact cell behaviour. There was no significant difference recorded between media alone or C5a in each of the regions. Moreover, one-way ANOVA performed to assess the difference between the 19 regions showed no significance for either media alone ($P = 0.9805$, $F = 0.3977$) or the 10 nM C5a ($P>0.9999$, $F = 0.1171$).

4.3.7. Cell patterning as a way of investigating properties of macrophages migrating in a population

Thus far, we have imaged short conduits (length 1.5 mm) initially containing no cells, or those where cells are uniformly distributed everywhere. However, having observed that not all of the cells initially present in the conduit were migrating towards C5a-containing well, we wanted to investigate this phenomenon further. We hypothesized that macrophages will

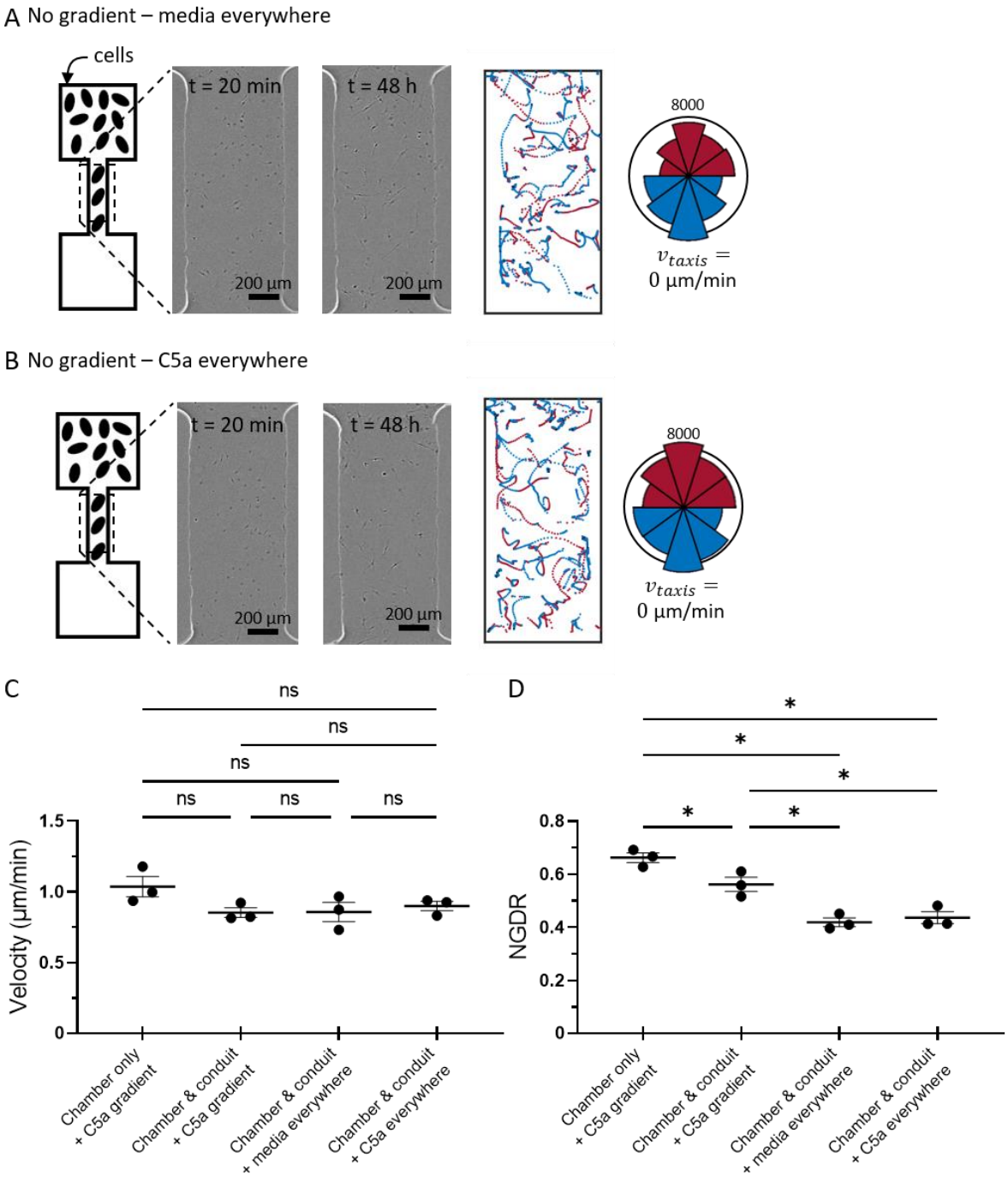

Figure 4.9. Distinguishing chemotaxis and chemokinesis in passive circuits. Left to right: migration of cells initially present in the conduit (as illustrated by the cartoons and images of conduits at t = 20 min and t = 48 h) in circuits where A) no C5a was introduced or B) media containing 10 nM C5a media was used everywhere in the circuit. Cell trajectories and colour-coded rose plots where blue bins are towards the empty chamber and red bins are away from it the with the circles indicating number of trajectory points falling into each bin and measurements of vtaxis (directional speed); scale bar = 200 µm. C) Average velocity measured for cells in the conduit between the conditions in Figure 7 and Figure 8. D) Mean net-to-gross displacement ratio (NGDR) for cells in the conduit measured for the conditions in Figure 7 and Figure 8; ±SEM, n = 3 biological replicates, one-way ANOVA, *p<0.05.

change their chemotactic response based on their position in the circuit (as they will all be exposed to a different concentration of C5a) We decided to compare responses of cells distributed in 4 different patterns in longer 6 mm conduits (chosen to improve resolution and allow better ways to pattern the cells, but note that t_{ss} changed to 13.6 h). Initially, cells occupied either the whole conduit (Figure 4.11A, Movie 4.7), or just the top of the conduit (Figure 4.11B, Movie 4.8), middle (Figure 4.11C, Movie 4.9), or bottom third (Figure 4.11D, Movie 4.10). Since all 4 conduits had the same dimensions and as bottom chambers were filled with the same C5a concentration, diffusion established identical gradients in all conduits that developed similarly over time. Unexpectedly, trajectories of cells at equivalent points along the y axis in the 4 conduits differed. In Figure 4.11A, the conduit initially filled uniformly with cells, only cells in the bottom third yield long blue trajectories and a biased rose plot, whilst those above them do not. This might have been expected since responders were closest to the highest attractant concentration, and non-responders far from it. However, in the other three panels (Figures 4.11B-D) the front closest to C5a was also always rich in responders, regardless of the distance from the lower chamber. In other words, migratory responses of macrophages in this system seemed to depend more on the position of the cells at the front of the population, and not on the absolute C5a concentration expected at that point in the conduit.

Having observed that the BMDMs initiated migration at different location within the conduit we next wanted to determine the lowest C5a concentration eliciting chemotaxis (c_{min}) in each of the four circuits described in Figure 4.11A-D. Therefore, we used the time-lapse movies generated from our recordings to trace cells yielding the long blue trajectories back

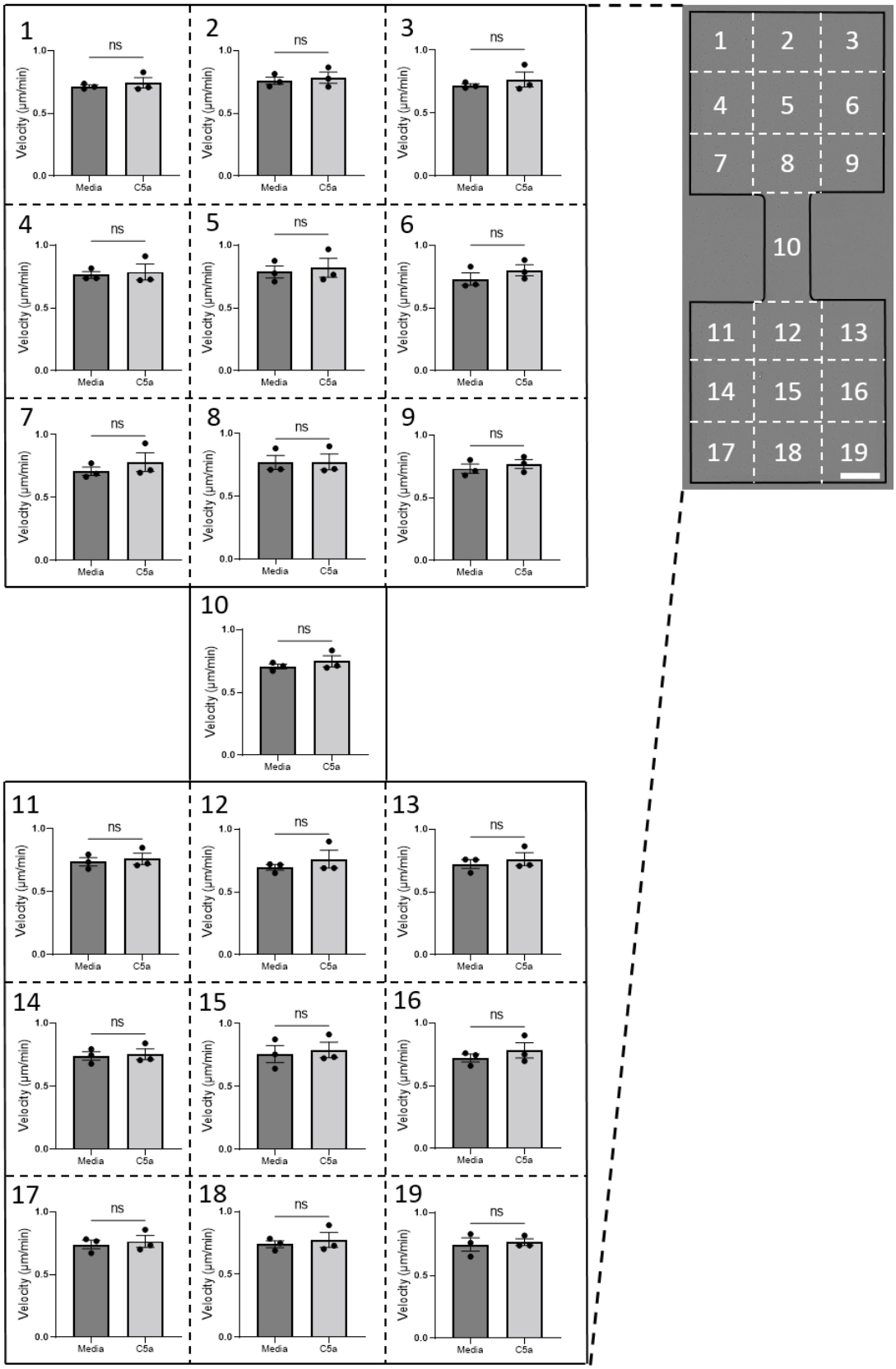

Figure 4.10. Location within a circuit has no effect on velocity of BMDM movement. Cells were deposited throughout the entire circuit to identify potential biases in cell behaviour at various circuit locations. Each circuit was arbitrarily divided into 19 regions as shown in diagram on the right. Average cell velocities over 48 h were analysed in each region containing only medium (dark grey) or uniform distributions of 10 nM C5a (light grey); scale bar = 250 µm, n = 3 biological replicates for each condition, separate t-test for each.

in time to identify when and where they first extend pseudopodia towards attractant, as per Figure 4.7A. From that we calculated the local C5a concentration present at that time and place. Because these movies were collected using a framerate of 20 min, temporal resolution was limited. Therefore, we recognize the calculated concentration as $c_{min_{obs}}$, present in the earliest frame in which such pseudopodia are seen and therefore this is an upper limit of the actual c_{min}. In movies 4.8 and 4.11 (corresponding to Figure 4.11A and Figure 4.11D), marker pseudopodia were seen at the bottom of the conduit in the first frame, and $c_{min_{obs}}$ was ~1 nM for both patterns (Figure 4.11E). In movies 4.9 and 4.10 (corresponding to Figure 4.11B and Figure 4.11C), marker pseudopodia were seen in the second frame, and values for $c_{min_{obs}}$ were 0.1 pM and 79 pM respectively (Figure 4.11E; comparable to the minimum concentration eliciting a response in xCELLigence transwell assays from Figure 4.6). This gave a thousand-fold range in the lowest C5a concentration eliciting a response. As these gradients were so shallow, and if a macrophage is 0.1 mm in length, this makes it likely that the first responders in Figure 4.11B experienced a C5a concentration of c_{min} at one end of their body and zero at the other. Such low concentrations of $c_{min_{obs}}$ suggest high sensitivity of this assay, which combined with the theoretical calculations provided new ways of confidently studying chemoattractant gradients in ranges lower than previously reported (*45*, *46*).

4.3.8. Passive circuit reconfigurations to study multiple cell populations

We next designed and implemented circuits with 3 chambers that enabled comparison of chemotactic responses of two distinct cell populations without requiring distinguishing cell labels (Figure 4.12). The middle chamber served as a C5a reservoir, while chambers and conduits above and below contain different cell types. As seen in Figure 4.12A, to establish

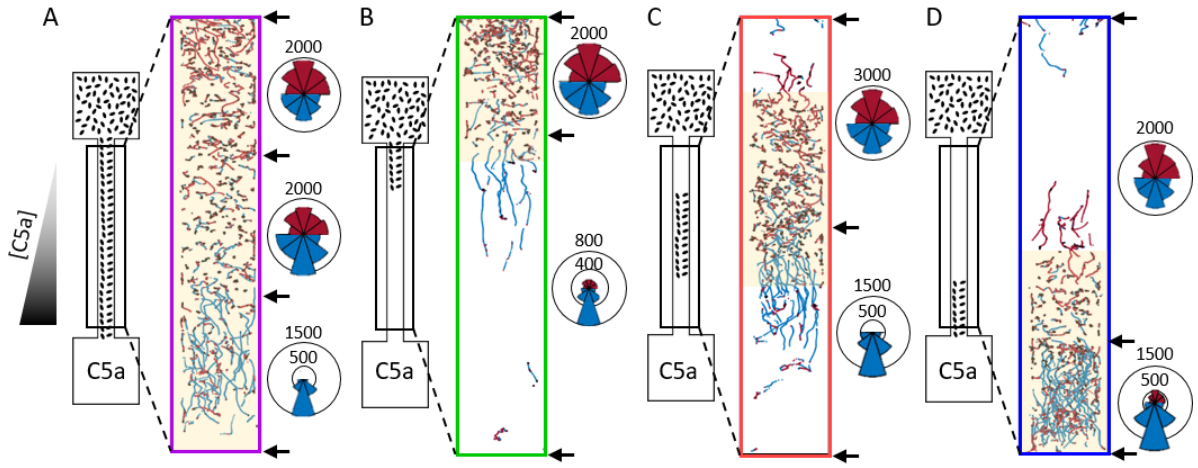

E

	Whole (A)	Top (B)	Middle (C)	Bottom (D)
$Cmin_{obs}$ (nM)	1.01 ± 0.29	0.00012 ± 0.000018	0.079 ± 0.0063	1.8 ± 0.06

Figure 4.11. Cell patterning reveals properties of collective macrophage migration independent of absolute amount of chemoattractant. BMDMs were printed in different patterns, C5a gradients established (0-10 nM), and cells imaged for 48 h. Cartoons illustrating circuits set-up (conduit length 6 mm), cell starting positions, trajectories from a single experiment (blue – towards C5a, red – away from C5a, black – stationary) and rose plots (blue – towards C5a, red – away from C5a with circles indicating number of trajectory points falling into each bin) are shown for cells initially located A) across the entire conduit, B) top of the conduit only, C) middle of the conduit only and D) bottom of the conduit only; yellow shading - initial position of cells, n = 3 biological repeats. E) Table of theoretically calculated minimum C5a concentration at which the cells initiate migration ($Cmin_{obs}$) depending on their initial position in the circuits.

gradients, medium was first added to the top chamber (1 µL, $P_{top} = 20$ Pa), a smaller volume to the bottom one (0.9 µL, $P_{bottom} = 18.5$ Pa), and an even smaller volume of C5a to the middle one (0.6 µL, $P_{middle} = 13$ Pa). This created pressure gradients that drove medium into the C5a chamber as seen at t = 3 min (Figure 4.12A, red dye represents medium, blue represents medium + C5a) until the system reaches equilibrium at t = 10 min. Then, diffusion created a steady gradient of C5a along both conduits (Figure 4.12A, t = 1 h). To validate this approach, C5a-receptor 1 knock-out BMDMs (KO) were deposited in the top chamber, wild-type BMDMs on the appropriate Balb/c background (WT) at the bottom, and 10 nM C5a in the middle (Figure 4.12B, Movie 4.11). As expected, KO cells exhibited mostly unbiased movement in the upper conduit (Figure 4.12B, rose plot in top inset), while WT cells had a stronger chemotaxis response to C5a (Figure 4.12B, rose plot in bottom inset). Since a small proportion of KO cells migrate directionally towards C5a, we next investigated the efficiency of genetic knock-out of C5aR1 in the BMDMs using flow cytometry. We saw that almost 100% of WT BMDMs expressed CD88 (C5aR1) while a significantly smaller proportion of $C5a^{-/-}$ cells expressed CD88 (Figure 4.12C). Notably, there was a high inter-experimental variation in CD88 expression on the knock-out cells which was absent in the WT cells (two separate experiments were marked with filled-in and hollow black dots in Figure 4.12C). However, the overall expression of CD88 (as measured by the mean fluorescent intensity values) was unchanged between the experiments and significantly lower in the C5a knock-out cells (Figure 4.12D). To ensure that the apparent expression of CD88 on the knock-out cells was not due to unspecific binding or fluorescent spill-over from other channels into CD88 channel, we run fluorescent minus one (FMO) and isotype controls, which are shown in Figure 4.12E. Nonetheless, we cannot be certain that the specific CD88 antigen bind site of the antibody that we used was not binding any off-target epitopes. Overall, we showed a possibility of

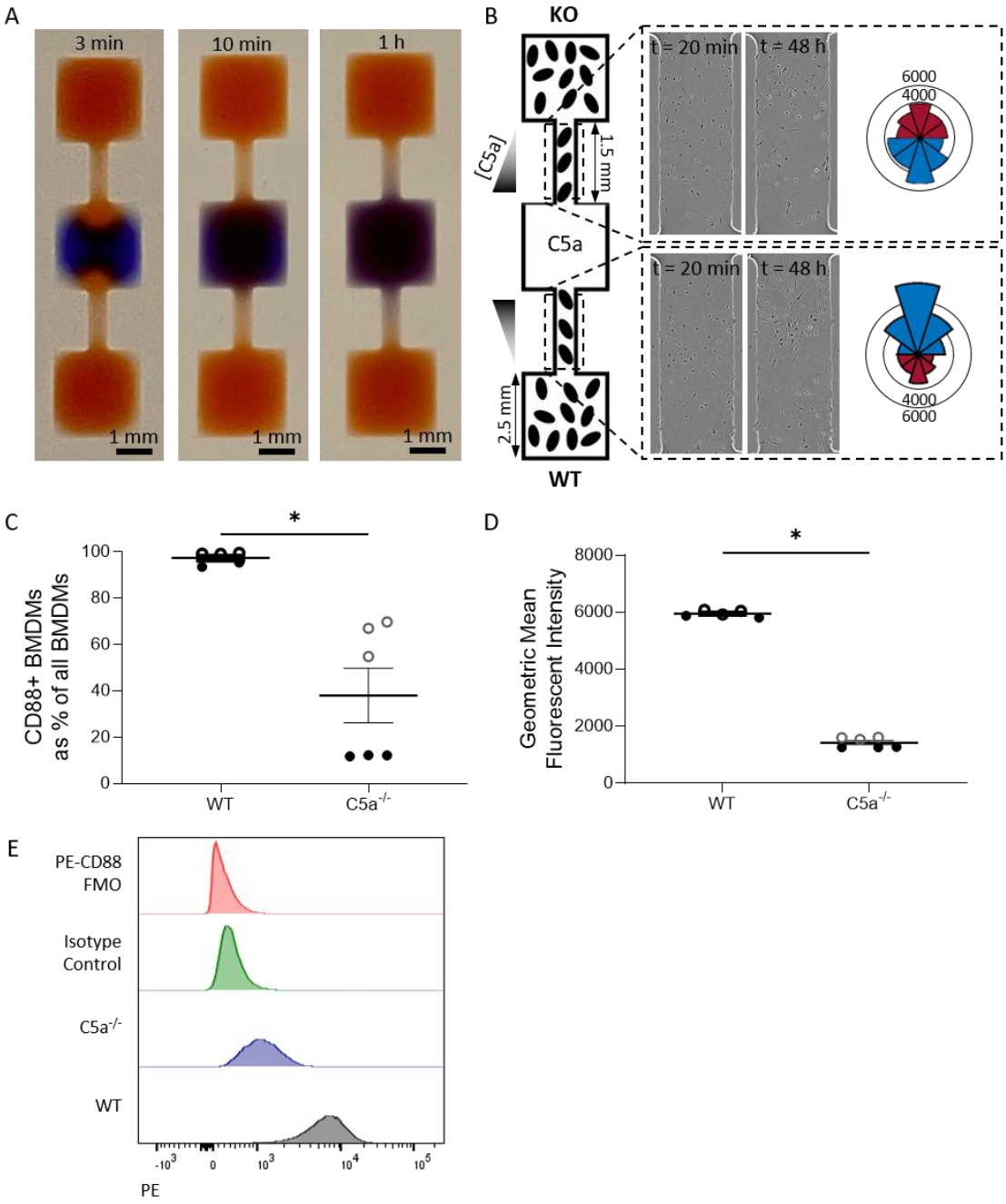

Figure 4.12. Passive circuits can be reconfigured to study multiple macrophage populations. A) At t = 0, dyes were pipetted manually into chambers – first 1 µL red into the top chamber, 0.9 µL red into the bottom one, and finally 0.6 µL blue into the middle one of a 3-chamber circuit with 2.5 mm x 2.5 mm square chambers and 600 µm x 1.5 mm conduits (not shown). At t = 3 min, the induced pressure difference drove red dye into the middle chamber, and pressures equilibrated. After 10 min, blue dye diffused throughout the middle chamber. At t = 1 h, blue dye diffused equally into both conduits to create steady gradients; scale bar = 500 µm. B) Circuits were built around wild-type Balb/c BMDMs (WT) in the bottom chamber, and the C5aR1-/- BMDMs on Balb/c background (KO) in the top one at density of ~500 cells/mm2. Gradients were established as in (A) by adding medium ± C5a (equivalent to red and blue dyes respectively), and images collected for 48 h with t = 0 h and t = 48 h showed in close-ups next to plus rose plots (n = 3 biological replicates). C) Frequency of CD88+ cells in WT and KO BMDM cultures with the corresponding mean fluorescence intensity in (D); two separate experiments are marked with filled-in and hollow black dots. E) Representative histograms of PE intensity for PE-CD88 FMO control, isotype control for the PE-CD88 antibody on the C5a-/- cells, C5a-/- sample and WT sample; student t-test, *p<0.05.

adapting the FF platform for analysing multiple cell populations in a single microfluidic system without the need for cell labelling.

4.3.9. Passive circuit reconfigurations to increase throughput of the system

Given that one of the new considerations in designing chemotaxis assays proposed by Frow et al. was the ability to perform high-throughput screens (*364*), we decided to test if our passive circuits could be scaled down to fit and perform the assay on well plates. To achieve this, we used a custom-built pro-printer - three axis traverse that is larger than the printer used before and can fit microplates but works using the exact same principles as the usual FF printer. Therefore, we printed 12 identical dumbbell circuits in each well of a 6-well microplate (1.5 mm conduits, 72 circuits in total; Figure 4.13C). As before, gradients of chemoattractant were generated and circuits imaged to analyse cellular response. We thus compared the response of BMDMs cultured in the top chamber of circuits and exposed to gradients of 10 nM C5a, to that of BMDMs plated everywhere in circuits with uniform distributions of 10 nM C5a or in the absence of C5a. As expected we saw a significant increase in the mean NGDR in the circuits where gradient was established compared to media or C5a everywhere (Figure 4.13B), similarly to circuits drawn on 35 mm Petri dishes (Figure 4.9D). Interestingly, the average cell velocity was significantly different between all the conditions (Figure 4.13A), which was not the case in the same dumbbell circuits drawn in well plates (Figure 4.9C). Specifically, addition of 10 nM C5a either as a gradient or everywhere in the circuit caused a significant increase in velocity compared to media alone (Figure 4.13A). This would suggest that the directional movement is unchanged when circuits are printed on well plates, however either chemokinesis in response to C5a is stronger in the well-plates or the non-stimulated cells are more stationary.

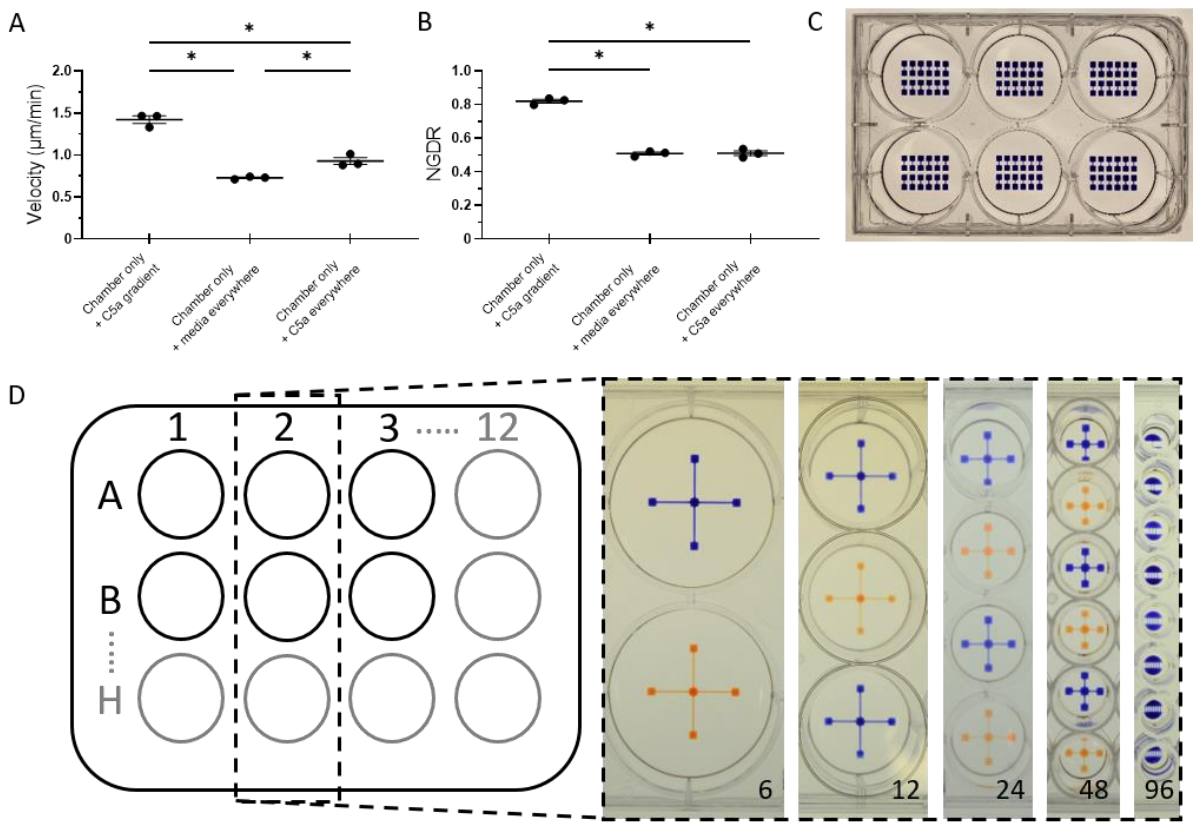

Figure 4.13. Passive circuits can be reconfigured to increase throughput by printing onto well plates. A) Mean velocity in circuits printed onto a 6-well plate with cells. B) Mean net-to-gross displacement ratio (NGDR) in circuits printed onto a 6-well palate; ± SEM, n = 3 biological repeats, one-way ANOVA, *p<0.05. C) Representative image of a 6-well plate containing 72 identical dumbbells (1.5 mm long conduits). Blue dye is added to aid visualization. D) Example of reconfiguration of the circuits to fit into various size well plates. Images show a column from each plate. In 6- to 48-well plates, circuits have 5 chambers and conduit length decreases as wells become smaller. In the 96-well plate, each circuit has 2 chambers with 1-8 connecting conduits.

The flexibility of the approach allows circuits with various shapes to be shrunk to fit inside wells of 12- to 96-well plates (Figure 4.13D). We modified dumbbell circuits to fit into any well plate with example designs drawn inside of differently sized wells in Figure 4.13D. Such designs could be used to compare more cell types or increase throughput by adding two additional chambers and conduits, allowing comparison of response of four different cell types to one attractant, without requiring additional cell labels. In this case, changes in shape are mainly implemented by changing the length of the conduits. Circuits could also be shrunk to fit inside each well of a 96-wellplate, and we illustrated this by printing a series of dumbbell circuits with increasing numbers of interconnecting conduits (1 – 8 conduits from top to bottom in the last panel of Figure 4.13D).

4.3.10. Detection of chemotaxis in active circuits

Given that passive gradients change over time we wanted to establish an actively flowing circuit where BMDMs would be exposed to stable gradients of C5a over the entire course of the experiment. We used 'm' shaped circuits to exploit the properties of diffusion gradients created by two laminar flows merging, as explained in Figure 4.5. As before, we recorded cell movement over 48 h to follow chemotaxis of BMDMs across the central channel in the 'm'-shaped circuit. As seen in Figure 4.14, many cells migrated from the left to the centre, leaving behind a cell-depleted zone - individual trajectories and a rose plot (segment length indicates the number of trajectories per bin) confirmed chemotaxis towards 10 nM C5a (Movie 4.12). Importantly, the cell band just to the right of this depleted zone is enriched in taxing cells superimposed on non-responsive ones that were initially present there. We mapped a theoretical prediction of the normalized concentration gradient onto the image of cells at 48 h (right-most panel in Figure 4.14) with colours depicting local normalised concentrations of C5a from 0 to 1 (corresponding to 0-10 nM C5a) and the over-imposed curves showing the

gradient contours (red line – 5 nM, with black lines correspond to 10-fold decrease in concentrations). The leftmost black line was drawn to represent the minimum concentration triggering a response and mapped onto the leftmost edge of the depleted region (equivalent to $c_{max} \times 10^{-5} = 0.1$ pM). While the diameter of a murine macrophage is typically ~20 µm (*394*), their length can be >100 µm when extending pseudopodia and moving. As a result, cells in this region of the conduit easily sense one to two orders of magnitude difference in C5a concentration across their body. In contrast to the passive circuits, it was cells far from the front that responded, while those at the front did not. The predicted C5a concentrations around responsive cells in both flow-free and flowing circuits were comparable to the lowest concentrations eliciting taxis in the xCELLigence assay (Figure 4.6), thus validating our findings. To our knowledge, the response of macrophages to such low concentrations of C5a has not been shown before.

4.3.11. Abruptly shifting gradient as a factor driving macrophage migration

Given our previous result, we hypothesised that we could induce further shift in the position of migrating BMDMs by shifting the active stable gradient to a new location. To test this hypothesis, we attempted to control cell movement by shifting the gradient by 200 µm to the right in order to recruit more responsive cells in specified regions of the conduit (Figure 4.15, Movie 4.13). First, we generated a 10 nM gradient of C5a over cells cultured in the conduit of an 'm'-shaped circuit as before, and imaged the conduit in the IncuCyte (first panel in Figure 4.15). As expected, after 24 h, a band of BMDMs have migrated into the central region of the conduit (second panel Figure 4.15). The gradient was then abruptly shifted 200 µm to the right by increasing the flow rate of the left stream (from 5 to 7.15 µL/h) and decreasing the flow rate of the right one (from 5 to 2.85 µL/h) while keeping the overall flow rate in the

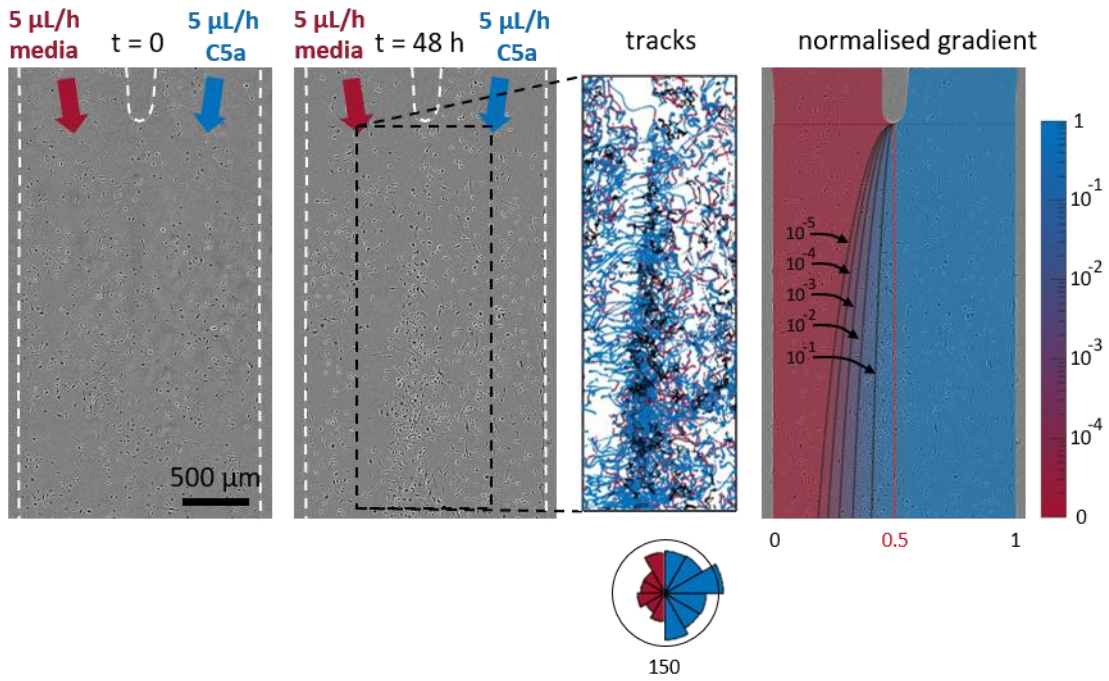

Figure 4.14. Tracking chemotaxis in active circuits. Left to right: Two representative frames illustrating BMDMs in the central conduit of 'm'-shaped circuits that were exposed to laminar streams of medium and medium + 10 nM C5a over 48h. At t = 0, cells are randomly distributed; at t = 48 h, some cells accumulate in a vertical band (leaving a region depleted of BMDMs behind). Cell trajectories in region indicated and the overlaid rose plot with the circle indicating the number of trajectories that fall into each bin. Normalized concentration gradient overlaid on frame at t = 48 h (concentrations of 1 and 0 equal 10 and 0 nM C5a). Contours indicate 10-fold decreases in C5a concentrations; the leftmost one marks the left of the depleted zone and so the minimum concentration inducing migration; for cell trajectories and the rose plots blue = towards C5a, red = away from C5a, black = stationary, scale bar = 500 µm, dotted white lines = fluid walls.

conduit unchanged (10 µL/h). Cells were then imaged for an additional 24 h. Analysis of cell trajectories and a rose plot revealed that the band of cells distributed along the centre of the conduit shifted in the direction of C5a, indicating a bias towards the newly positioned gradient (final panel in Figure 4.15; note the large proportion of blue tracks towards C5a, and enlarged blue segment in the rose plot). Therefore, we confirmed that by shifting the gradient we were able to induce further migration of BMDMs across the conduit of an 'm'-shaped circuit.

4.3.12. Gradually shifting gradient does not drive macrophage migration

Since BMDMs followed a gradient of C5a when abruptly shifted, we decided to investigate whether cells can follow a continuously shifting gradient. As before, BMDMs were exposed to a 10 nM gradient of C5a and imaged over 24 h (as in Figure 4.15), during which a sub-population of cells migrate from the left to the centre of the conduit where the concentration of C5a was higher (Figure 4.16, Movie 4.14). Over the following 24 h, we shifted the gradient continuously from the centre of the conduit to 150 µm from the right edge, by gradually increasing the flow rate through the left arm (from 5 to 9.98 µL/h) and decreasing the flow rate through the right one (from 5 to 0.02 µL/h) which was performed using the 'ramp' function of the syringe pump. Analysis of cell trajectories during this 24-48h period revealed that BMDMs did not follow the gradient as efficiently, only the cells at the initial location of the gradient kept chemotaxing, while the cells that were swept across with the moving gradient stayed stationary, which reduced the chemotactic bias (rose plots under third panel in Figure 4.16). However, when the gradient remained stationary for an additional 24 h, chemotaxis became stronger, and a new cell band appeared on the right (final panel in Figure 4.16). This confirmed that cells remained competent to chemotax throughout the whole 72 h, and that sweeping the gradient across more cells – at least at the pace chosen in this experiment – did not significantly recruit more cells into the enriched band.

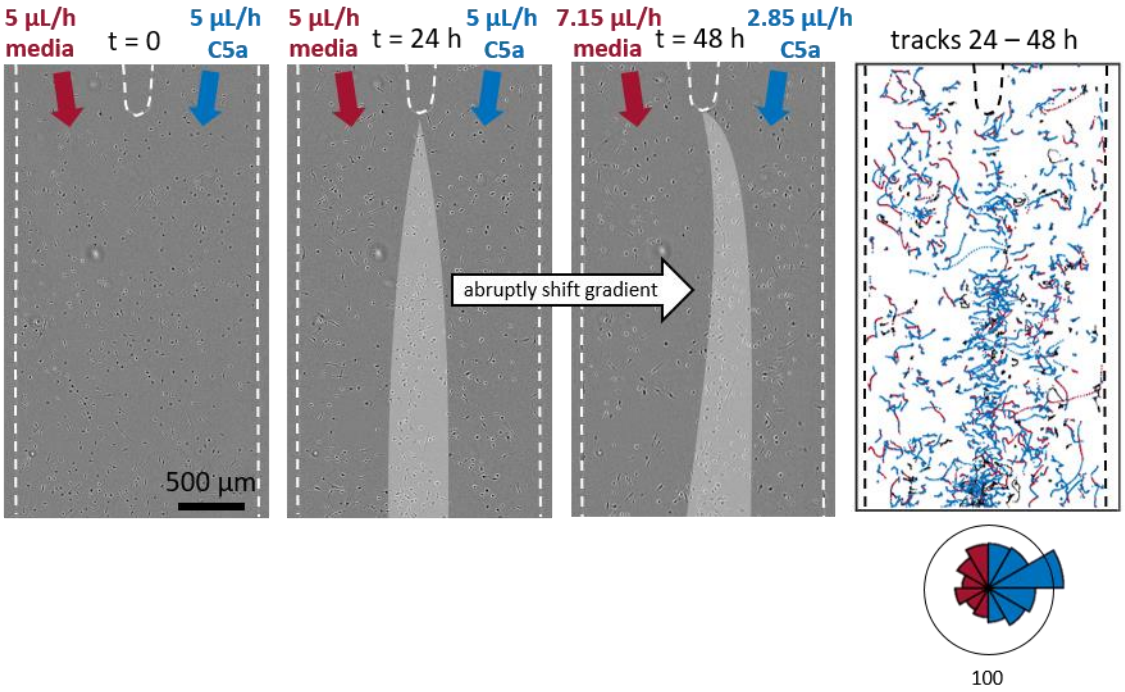

Figure 4.15. Abrupt shift of gradient location drives further chemotaxis. Left to right: Three representative images illustrating BMDMs in the central conduit of 'm'-shaped circuits that were exposed to laminar streams of medium and medium + 10 nM C5a, so diffusion created a stationary gradient for 24 h followed by an abrupt shift to the right by ~200 µm, and then a stationary gradient in the new position for 24 h (equal inputs from both arms were abruptly changed after 24 h to 7.15 µL/h on the left and 2.85 µL/h on the right). Cell trajectories (24-48 h) and overlaid rose plot with the circle indicating number of trajectories falling into each bin; for cell trajectories and the rose plots blue = towards C5a, red = away from C5a, black = stationary; scale bar = 500 µm, dotted white lines = fluid walls, n = 3 biological repeats.

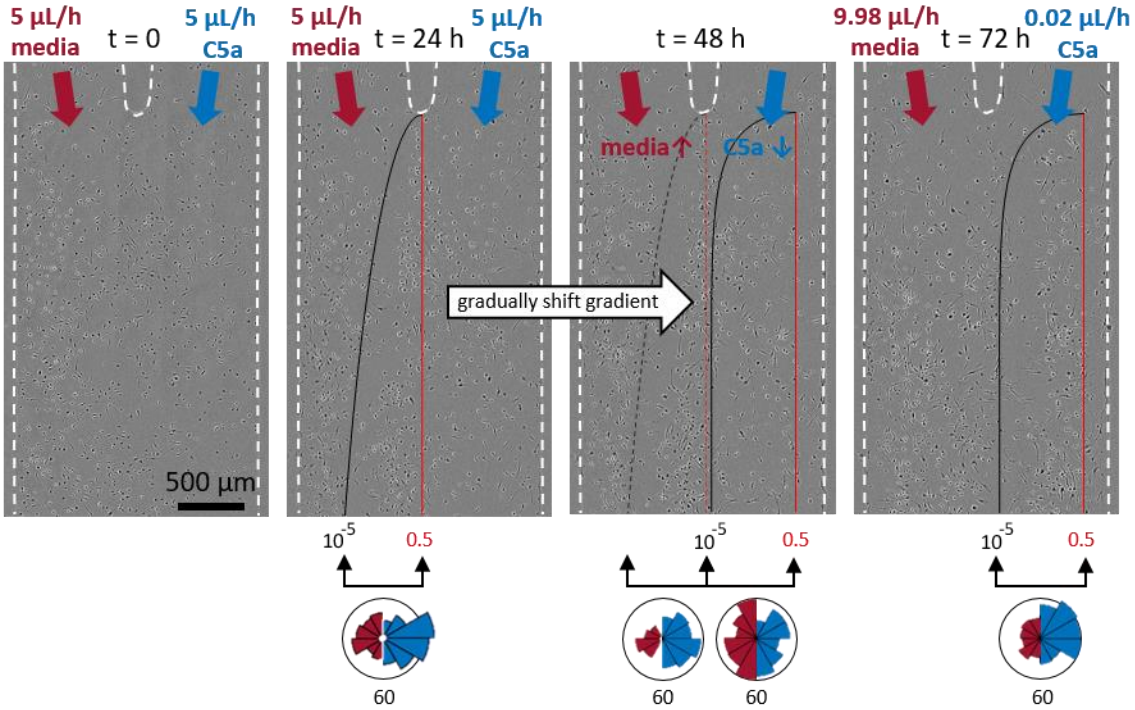

Figure 4.16. BMDMs do not follow gradually shifting gradients. Left to right: Four representative images illustrating BMDMs in the central conduit of 'm'-shaped circuits that were exposed to laminar streams of medium and medium + 10 nM C5a, so diffusion created a stationary gradient for 24 h (equal inputs), shifted steadily by 750 µm to the right over 24 h (by progressively increasing/decreasing flows into left/right inputs), and stationary for 24 h (as existing inputs held steady). Rose plots underneath each image with the circle indicating number of trajectories falling into each bin; blue = towards C5a, red = away from C5a, black = stationary; scale bar = 250 µm, dotted white lines = fluid walls, n = 3 biological repeats.

4.4. Discussion

In this chapter, I set out to adapt the Freestyle Fluidics platform to study macrophage chemotaxis. With my collaborators, we designed and executed fluid-walled circuits that can reliably support formation of active and passive chemoattractant gradients and proved that we can reliably track and quantify chemotaxis as well as chemokinesis. We tested technical capabilities of this new system against Harris' original criteria as well as newer considerations such as high throughput and single cell recordings. Finally, we investigated previously unknown properties of macrophage migration – their coordinated migratory response in a population as well as response to changes in chemoattractant gradient.

4.4.1. Adaptation of the Freestyle Fluidics platform to study macrophage migration

Previously, the Freestyle Fluidics platform has been mainly used for creating grids that support cell culture in clonal selection (*383*). However, we developed a suite of chemotaxis assays designed using reconfigurable circuits built around living primary cells on standard Petri dishes (as exemplified in Figure 4.3) and applied them to investigate the complex interactions involved in the chemotaxis of primary murine macrophages to C5a. Taking advantage of properties of circuits with fluid walls, this method addressed many limitations of traditional chemotaxis assays, as listed in Table 4.3. We considered different methods of printing the circuits (Figure 4.1) and depositing cells into them (Figure 4.2) and decided that jetting around previously plated cells, all in media containing 2% fibronectin, was the most optimal solution. We considered and tested multiple possible geometries for the passive circuits but ultimately we decided that the simplest design where two square 2.5 x 2.5 mm chambers are connected by a single conduit was the most optimal due to the ability to control and model the gradient by controlling conduit length as well as easily change its dimensions

	Transwell assays	Dunn & Zigmond chambers	Under agarose assay	Traditional microfluidics	Freestyle Fluidics
Stable gradients	+	+/-	-	+	+
Single cell tracking	-	+	+	+	+
Fugetaxis detection	+	-	+	+	+
Distinction between chemotaxis & chemokinesis	+	+	+/-	+	+
High throughput	+/-	-	-	+	+
Specialised equipment needed	+/-	-	-	+	+/-
Real-time observation	+	+	+	+	+
Multiple cell types simultaneously	-	-	+/-	+/-	+
Patterning cells	-	-	-	+/-	+
Multiple chemoattractants simultaneously	-	-	+	+	+
Easy system reconfiguration	-	-	-	-	+

Table 4.3. Comparison of traditional chemotaxis assays with the Freestyle Fluidics chemotaxis assay presented in this chapter. Commonly used chemotaxis assays and Freestyle Fluidics are compared based on Harris' criteria and other desirable features.

and the number of chambers in it (Figure 4.3). Additionally, in both passive and active circuits, we detected macrophages responding to far lower concentrations than previously reported (~0.1 pM), which we validated using the real-time xCELLigence transwell assay (Figure 4.6). We established C5a gradients in flow-free (passive) dumbbell-shaped circuits, which could be theoretically modelled to predict local C5a concentrations at any given time (Figure 4.4 and Table 4.2), therefore proving sufficient localisation of our soluble gradient to the experimental chamber. Moreover, we showed that the gradients remained stable and undisturbed by convection currents even when moved from the FF printer to the microscope. Given that bone marrow-derived macrophages are relatively slow moving cells, we were able to use IncuCyte, an automated microscope adapted for incubator conditions, to image the cells at a rate of 3 frames per hour (every 20 min) and still be able to create time-lapse movies where cells could be reliably tracked and their velocity, directionality and net-to-gross displacement ratio quantified. Thanks to that quantification we were able to distinguish between chemotaxis and chemokinesis (Figure 4.8 and Figure 4.9) – one of key criteria of an 'ideal' chemotaxis assay according to Harris. We also showed that BMDMs behaved the same across the entire circuit (Figure 4.10), which ensured the lack of sampling error due to looking at the cells present exclusively in the conduits. Due to the flexibility of modifying the passive FF chemotaxis circuits, we were able to deposit cells in precise patterns across the 6 mm conduits, which revealed previously unappreciated properties of macrophages migrating in a population.

Additionally, we performed a proof-of-concept experiment in a modified 3-chamber circuit that compared the chemotactic response of WT and C5a KO cells (without any cell labels) and was able to shows that, as expected, WT cells migrated towards C5a more efficiently than KO ones (Figure 4.12). Unexpectedly, the commercially available knock-out mouse line we used,

C.129S4(B6)-C5ar1tm1Cge/J, showed a reduction in CD88 expression (a knock down) rather than a full knock-out with BMDMs derived from homozygous mice still expressing C5aR1. However, the proportion of cells expressing CD88 had a high inter-experimental variation suggesting that C5aR1 might have been unintentionally primed to a pro-inflammatory state during one of the experiments. Reassuringly, there was no change in the mean fluorescence value of the CD88, which is a proportional measure of the actual expression on the cell surface. Given a more than 3-fold difference in expression between the WT and 'KO' cells even if a high proportion of the 'KO' cells were able to upregulate their expression of CD88, it was still at a very low level. Given this apparent variation in proportion of cells labelled another plausible explanation is the fact that the antibody was not binding specifically. We run isotype control and fluorescence minus one control to check for and minimise the impact of non-specific binding of the antibody, which allowed us to control for non-specific binding of the isotype and for fluorescence spill-over into CD88 channel, however we cannot be certain that the specific CD88 antigen bind site of the antibody was not binding any off-target epitopes. Overall, the tree chamber approach gave us an advantage over the previous systems in the fact that it did not require cell labelling, as many of the cell labelling dyes are cytotoxic and cannot be used for experiments as long as 48 hours.

To further test the flexibility of this platform, we build our usual 'dumbbell' passive circuits on well plates to increase throughput (12 circuits in each well of a 6-well plate; Figure 4.13). We showed that downscaling the passive circuits changed the average velocity of cells between the circuits, however, had no effects on the directionality detected, which is perhaps the key readout of chemotaxis. Despite not performing any chemotactic assays, we successfully designed and printed a series of circuits that could fit even smaller wells, such as

the ones in 96-well plates, which opened up a possibility of further increase in throughput. Such increase in throughput will allow performing extensive drug screen in the future.

Finally, we generated stable active gradients, which were ten-fold steeper than the ones in flow-free circuits. We used external syringe pumps to drive input flows through the arms of 'm'-shaped circuits (Figure 4.14). We managed to control cell movement by shifting gradients from the centre of the conduit to the right-hand wall (by 200 or 750 µm) either abruptly or continuously (Figure 4.15 and Figure 4.16 respectively). Interestingly, cells did not efficiently follow a continuously shifting gradient, although they did so once the gradient stops moving. In other words, cells seemed to sense the presence of C5a in both time and space.

4.4.2. Migration of macrophages is governed by population dynamics

We obtained unexpected results by comparing responses of cells initially occupying different parts of 4 identical conduits – either the whole conduit, or just the top, middle, or bottom third (Figure 4.11). We expected cells to respond according to their position and so to predicted C5a concentration gradient. Instead, responders were the ones closest to the highest C5a concentration irrespective of the position in the conduit. This phenomenon could be caused by a mixture of the following observations. Firstly, in the absence of cells gradients would develop identically in circuits with the same dimensions. However, in Figure 4.11, cells at equivalent points along the 4 conduits (and so experiencing similar C5a concentrations and gradients) responded in some cases, but not in others. This suggests that C5a concentration gradient cannot be the only trigger of cell migration. Secondly, there is clear evidence that cells can distort pre-existing gradients, and even generate ones from a uniform field of attractant by binding, internalizing, or degrading attractant around them (*395*). Macrophages also change their migration when other cells further up a gradient distort the concentrations

behind them (*236*, *269*). Moreover, self-generated gradients can guide cells robustly over longer distances than pre-existing ones, with responding cells always being the ones at the front (*236*, *395*). This is consistent with what we observed in passive patterned circuits - migrating cells were at the front, irrespective of predicted C5a concentration. Thirdly, responding cells can emit signals to near neighbours that amplify an initial response, and reduce a late one – for example neutrophils can initially signal to each other to swarm towards infecting bacteria, and later they reduce excessive swarming and so reduce inflammation (*396*). Although such paracrine signalling has not been shown in chemotaxing macrophages, tissue-resident macrophages can coordinate extension of their pseudopodia to cloak microlesions and so must signal to each other (*397*). Therefore, a population of macrophage coordinating its response to an inflammatory stimulus is not unexpected, however their ability to initiate migration at different levels of C5a was only possible to observe due to unique flexibility of the 'dumbbell' passive circuits.

4.4.3. Macrophage response to changes in chemoattractant gradients

It is widely accepted that eukaryotic cells regulate their responses to concentration gradients by spatial sensing (*398*). Additionally, migrating myeloid cells (dendritic cells and neutrophils) were shown to sense temporal dynamics of chemoattractant concentrations and respond to rising concentrations of CCL19 and CXCL12 – a behaviour that contrasts with C5a (*399*). Moreover, neutrophils migrate further towards shifting gradients of interleukin-8 than static ones (*400*). While there is an opportunity for paracrine signals to diffuse between cells in the passive circuits, flow of the media flushes away any possible secreted signals in the active circuits as media in the conduit is wholly replaced every minute (Figure 4.14). Then, it is no longer surprising that responders are at the front in the passive gradients (Figure 4.11), but not in flowing ones (Figures 4.14-16) where inter-cellular signalling becomes impossible.

Therefore, our findings suggest that macrophages can sense C5a both spatially and temporally, and that shifting gradients modulate what is already a complex response. To our best knowledge, the difference in macrophage response to abrupt and continuously shifting gradients has not been reported before and is a feature detectable exclusively using our novel approach. This behaviour was consistent with cells responding poorly when their leading edges sense falling attractant concentrations despite the presence of a gradient across their whole bodies; then, they only migrate actively once the gradient stops moving.

4.4.4. Limitations and possible improvements of this study

The main technical limitation of the current study resulted from the low temporal resolution of recordings and therefore limited estimation of the minimum concentration (c_{min}) eliciting chemotaxis in passive circuits. The IncuCyte machine used in this study does not allow choosing a region of interest during recordings so whole-well images had to be taken, which takes considerably longer than imaging only areas of interest. When we tried to increase frame rate the machine was overheating, which was dangerous for the equipment but also the high temperature killed the cells. Using an alternative live cell imaging equipment could improve the temporal resolution, however given that macrophages are slow at migrating we decided to stay with the in-house equipment due to convenience and the fact that it was located in the same room as the tissue culture hoods where the circuits were printed and therefore the dishes didn't have to be moved far.

We chose to work with bone-marrow derived macrophages as they are primary cells, reasonably quick and easy to grow and their robust migratory response to C5a is well documented (*267*). However, this system is theoretically adaptable to any adherent migratory cell type that can detect soluble gradients. This is something that I would have liked to test if

we had more time. Potential cell types that we could have used are bone marrow-derived dendritic cells, U937 macrophage cell line or fibroblasts such as a L929 cell line, which all have migratory capability and are readily available (*278*, *401*, *402*). The main consideration in that case would be optimising the cell density individually for each cell type. Similarly, we used only C5a gradients because it is the most potent chemoattractant for the BMDMs, however using other types of macrophages, such as Biogel elicited or thioglycolate recruited ones would have allowed us to study wider range of chemoattractants, especially since Iqbal *et al.* showed the possibility of using CCL2, CCL3 and CCL5 with those cell types in the xCELLigence assay (*272*).

BMDMs in our time-lapse recordings appeared to migrate exclusively via mesenchymal migration mode, greatly changing their shape and extending multiple, sometimes extremely long pseudopodia. This initially proved to be challenging when tracking the cells as most algorithms could not detect macrophages that extensively remodelled their cytoskeleton as cells at all or the same cells as in the previous frame. Initially we tried using BMDMs derived from hCD68-GFP mouse, however since the GFP was located in the cytoplasm it did not help in avoiding the problem of changes in cell shape. Commercially available nuclear dyes tend to kill cells within 24 hours and therefore were also not possible to use in our experiment given our 48 hours' runtime. Eventually, we adapted an algorithm that was designed specifically to recognise cell bodies in cells that extend pseudopodia, therefore allowing tracking and quantification of the BMDM movement. However, this algorithm is specific for macrophages and therefore might not be applicable for other cell types tested in the circuits.

We chose to add 2% fibronectin to the media when printing the cells and the circuits to aid the migration of macrophages for reasons discussed earlier. However, we have not tested

other extracellular matrix components that could have given better results or even allowed coating of the dishes. Moreover, fibronectin has been shown to induce macrophage activation and chemotaxis (*403*). This itself could have contributed to a higher baseline or non-directional migration in our system. Since the optimisation of fibronectin happened very early in the development process, when our imaging and analysis were not advanced enough yet to track single cells and quantify their velocity, we made a simple assessment of the improvement in migration with fibronectin (Figure 4.2C). We never revisited that issue, however in hindsight it would have been advantageous to try multiple ECM components as scaffolding for the migrating BMDMs.

We considered cells as dead when they appeared small, rounded, and exhibited no movement throughout 48 hours of recoding (as seen in Figure 4.7B). However, we never quantified cell death in the system, nor did we look at rates of cell death outside of the conduits. In hindsight, we should have tried monitoring cell death, at least at t = 48 hours to assess how well our macrophages are surviving in the circuits. Given the freedom to add more fluids through the fluid walls of the circuits, addition of Trypan Blue would have been sufficient to assess live/dead cell ratio.

Finally, throughout this study we used L929-conditioned media in the circuits, the same medium we used for BMDM differentiation from bone marrow. We tried using DMEM with various concentrations of foetal bovine serum and 1% penicillin/streptozotocin as well as chemotaxis buffer used in the xCELLigence assay, however the cells never survived being re-suspended in and added to circuits in media different to the one used for differentiation. We could never explain this finding, however we speculated that it might be due to extremely unusual conditions and low volumes that this system exposes the BMDMs to, leaving very

little room for them to adapt to changes in environment. Other such small factors have proven extremely important, for example media being properly warmed up when added to the circuits (even marginally too cold media killed cells due to temperature shock in a few experiments). However, using L929-conditioned media in experimental chambers had some major caveats, mainly that BMDMs can keep differentiating and dividing under constant exposure to M-CSF. In our time-lapse recording we did not observe any evidence of further cell division. We could not test the phenotype of the cells in our circuits after 48 hours but ideally, we would like to confirm the expression of key macrophage markers such as F4/80 and CD11b on a sample population of cells prior to the addition to the circuits and then retrieve them perform the same analysis after 48 hours in the system to ensure that no phenotypic switch occurred after 48 hours of being in the circuits.

4.4.5. Summary

Freestyle Fluidics provided a unique platform for creating macrophage chemotaxis assay. In this study, we developed circuits based on passive and active diffusion gradients of C5a that allow reliable tracking of macrophage migration. In line with the criteria of an 'ideal' chemotaxis assay proposed by Harris in the 1950s we showed that cells did not migrate directionally in the absence of a chemoattractant gradient. Using fluorescein and mathematical modelling we showed that the chemoattractant gradients localise sufficiently to the conduits and experimental chambers. We were able to precisely control the gradients by either changing the conduit length in the passive circuits or changing flow speed in the arms of the 'm'-shaped active circuit. Cells were able to move both towards and away from the C5a source, as seen in the rose plots and tracked trajectories and their movement was solely based on the gradient they were exposed to, not their position in the circuit. Given the more recent considerations in the search for an 'ideal' chemotaxis assay, we showed that our

passive circuits can be adapted for well plates, including 96-wel plates, to increase throughput (for example for screening studies). Our algorithm was able to track the cells at a single cell level, with the movies providing details on the morphology of migrating cells in real-time. However, our patterning experiments showed that population behaviours of macrophages can be also studied in the FF circuits.

Perhaps the key technical advancement, which was never attempted in the previous chemotaxis assays, was the precise control and shift in position of the active gradients. *In vivo*, gradients of chemokines are likely evolving over time and therefore this new platform has the potential to facilitate our understanding of macrophage response to changing inflammatory landscape in tissues. Given the flexibility of this system, it will be also possible to study cellular decision making in response to multiple chemoattractant gradients present at the same time as well as isolate cells of interest for further analysis. We thus hope that this study provides new ways of evaluating chemotaxis and spatio-temporal sensing in adhesive mammalian cells and opens new avenues of chemotaxis research, particularly into the molecular basis of such sensing as well as the paracrine signalling in a population of migrating macrophages.

4.5. Appendix

4.5.1. List of movies used in the chapter

Movie 4.1. Establishing a stable fluorescein gradient in an 'm'-shaped conduit. Fluorescein was infused through one arm of the conduit (top) at 5 µL/h and PBS through the other arm (bottom) at 5 µL/h. Dashed white lines show the conduit pinning lines. After 5 min, the concentration gradient of fluorescein was fully developed and stable across the conduit centerline; the conduit was imaged over 1 h just below the junction.

Movie 4.2. Abruptly shifting a fluorescein gradient in an 'm'-shaped conduit. The stable fluorescein gradient of Movie 1 was shifted 200 µm from the centerline towards the top side of the conduit (fluorescein side) by increasing the flowrate of PBS to 7.15 µL/h and decreasing the flowrate of fluorescein to 2.85 µL/h (as in Figure 15). The gradient was then seen rapidly shifting to its new location to become stable after ~6 min, and the conduit was imaged for a further 30 min

Movie 4.3. Macrophages in the top chamber of a dumbbell circuit chemotaxing in a 10 nM gradient of C5a (as in Figure 8A). Cells were initially contained within the top chamber (not visible), and few could be seen at the top of the conduit (length = 1.5 mm). Cells chemotaxed through the conduit over 48 h towards the C5a chamber at the bottom.

Movie 4.4. Macrophages in the conduit of a dumbbell circuit chemotaxing in a 10 nM gradient of C5a (as in Figure 8B). Cells were initially uniformly distributed in the conduit (length = 1.5 mm). Most cells in the bottom half of the conduit chemotaxed over 48 h towards the C5a chamber (bottom). However, most cells in the top half did not chemotax and were chemokinetic.

Movie 4.5. Macrophages in the conduit of a dumbbell circuit with medium everywhere (as in Figure 9A). Cells were initially uniformly distributed in the conduit (length = 1.5 mm). In the absence of a gradient, cells were chemokinetic and moved randomly over 48 h.

Movie 4.6. Macrophages in the conduit of a dumbbell circuit with uniform distribution of 10 nM C5a (as in Figure 9B). Cells were uniformly distributed in the conduit (1.5 mm). In the absence of a C5a gradient (uniform distribution of C5a), the cells were chemokinetic and moved randomly over 48 h.

Movie 4.7. Macrophages in 6 mm conduit chemotaxing in a 10 nM gradient of C5a (as in Figure 11A). Cells were initially uniformly distributed in the conduit (length = 6 mm). Only cells initially at the bottom of the conduit chemotaxed over 48 h towards the C5a chamber; cells initially located behind this band of responding cells did not chemotax and were chemokinetic.

Movie 4.8. Macrophages in top third of a 6 mm conduit chemotaxing in a 10 nM gradient of C5a (as in Figure 11B). Cells were initially distributed in the top third of the conduit (length = 6 mm). Seven cells at the front closest to C5a chemotaxed over 48 h towards the attractant; cells behind these ones did not chemotax and were chemokinetic.

Movie 4.9. Macrophages in middle third of a 6 mm conduit chemotaxing in a 10 nM gradient of C5a (as in Figure 11C). Cells were initially distributed in the middle third of the conduit (length = 6 mm). Only cells at the front chemotaxed over 48 h towards the C5a chamber; cells behind these ones did not chemotax and were chemokinetic.

Movie 4.10. Macrophages in bottom third of a 6 mm conduit chemotaxing in a 10 nM gradient of C5a (as in Figure 11D). Cells were initially distributed in the bottom third of the

conduit (length = 6 mm). Only cells at the front chemotaxed over 48 h towards the C5a chamber; cells behind these ones did not chemotax and were chemokinetic.

Movie 4.11. Macrophages in the conduits of a 3-well dumbbell circuit in a 10 nM gradient of C5a (as in Figure 12). Bone marrow derived macrophages that are $C5a^{-/-}$ (right panel, C5a source at the bottom) or WT (left panel, C5a at the top) recorded in their separate conduits of a 3-well dumbbell circuit in a 10 nM gradient of C5a.; cells were uniformly distributed in the conduits (length = 1.5 mm) and their movement registered over 48 hours.

Movie 4.12. Macrophages in 'm'-shaped circuit under a steady gradient of 10 nM C5a (as in Figure 14). Cells plated in the central conduit of an 'm'-shaped circuit were exposed to a steady gradient of C5a over 48 h. Medium was perfused through the left arm (5 µL/h) and C5a through the right (5 µL/h). A gradient was established across the center of the conduit, and cells chemotaxed from into this region from the left, leaving behind a cell-deplete zone.

Movie 4.13. Macrophages in 'm'-shaped circuit under a gradient of 10 nM C5a shifted abruptly to the right (as in Figure 15). Cells plated in the central conduit of an 'm'-shaped circuit were exposed to a steady gradient of C5a over 24 h; medium was perfused through the left arm (5 µL/h) and C5a through the right (5 µL/h). Cells on the left chemotaxed into the center of the conduit to leave behind a cell-deplete zone. After 24 h, the gradient was shifted abruptly 200 µm to the right by increasing medium flow (7.15 µL/h) and decreasing C5a flow (2.85 µL/h), and then flow was kept steady for an additional 24 h. Cells in the center of the conduit responded by chemotaxing further to the right.

Movie 4.14. Macrophages in 'm'-shaped circuit under a gradient of 10 nM C5a shifting continuously to the right (as in Figure 16). Cells plated in the conduit of an 'm'-shaped circuit

were exposed to a steady gradient of C5a over 24 h. Medium was perfused through the left arm (5 µL/h) and C5a through the right (5 µL/h). Cells on the left chemotaxed into the center of the conduit to leave behind a cell-deplete zone. After 24 h, the gradient was shifted continuously over the next 24 h by 750 µm to the right, by gradually increasing medium flow (from 5 to 9.98 µL/h) and decreasing C5a flow (from 5 to 0.02 µL/h). During this time, cells chemotaxed but not as strongly as previously. At the end of the continuous shift, the gradient was kept steady in the new location (150 µm from the right wall) for an additional 24 h. A new band of cells then responded by chemotaxing strongly into this region, creating a cell-deplete zone in the right half of the conduit.

Chapter 5

Summary of the thesis and final discussion

At the beginning of my graduate studies, I identified the unmet need for introducing new *in vivo* and *in vitro* techniques that could capture the intricacies of macrophage biology. My initial plan was to pursue only the *in vitro* technique development path which was going to complement my biological pursuits. However, due to the COVID-19 pandemic and the restriction associated with it, I decided to focus this thesis purely on technology development and added an *in vivo* arm to my studies.

5.1. Key Findings

The first aim of my thesis was to phenotype the novel tamoxifen-inducible hCD68-CreERT2 mouse. With regard to this aim I made the following key findings:

- The hCD68-CreERT2 mouse showed robust expression of Cre recombinase activity (detected as tdTomato fluorescence) in key tissue-resident macrophage populations in the peritoneal cavity, spleen and the liver.

- Different populations of tissue-resident macrophages within the peritoneum and the spleen showed differential activation of Cre recombinase and could be distinguished by differences in tdTomato fluorescence intensity.

- Leukocyte populations in the circulation showed negligible activation of tdTomato, apart from Ly6C^{low} monocytes.

- Non-macrophage populations in the spleen showed limited activation of Cre recombinase with the main 'off-target' effects observed in dendritic cells and Ly6C^{low} monocytes.

- Tissue-resident macrophages were efficiently targeted for at least 6 weeks after tamoxifen dosing with no observed decline in tdTomato fluorescence.

The second aim of my thesis was to validate the hCD68-CreERT2 mouse line in an experimental model of macrophage-driven disease and to compare it to existing mouse lines that are commonly used to target macrophages, namely hCD68-GFP mouse and constitutive LysM-Cre mouse. In regard to this aim, I made the following key findings:

- hCD68-CreERT2 mice showed lower efficiency of targeting peritoneal and splenic tissue-resident macrophages, however improved efficiency of targeting liver macrophages when compared to constitutive LysM-Cre mice.

- hCD68-CreERT2 mice showed lower efficiency of targeting peritoneal and splenic tissue-resident macrophages as well as significantly lower targeting of splenic non-macrophage populations when compared to hCD68-GFP mice.

- Activation of Cre recombinase in circulating leukocytes was significantly lower in hCD68-CreERT2 mice when compared to either LysM-Cre or hCD68-GFP mice.

- Tamoxifen-induces tdTomato fluorescence could be detected in macrophages and monocytes within the atherosclerotic plaques of hCD68-CreERT2 mice which were subjected to inducible PCSK9 virus-driven model of hyperlipidaemia.

The third aim of my thesis was to create and validate an *in vitro* chemotaxis assay, using the Freestyle Fluidics platform. In regard to this aim, my collaborators and I made following key findings:

- We designed and optimised custom passive and active circuits that could support the migration of bone marrow-derived macrophages in defined chemoattractant gradients and proved that we can detect both chemotaxis and chemokinesis in the system.

- We demonstrated the stability and controllability of gradients in both passive and active circuits and derived models to mathematically calculate the exact concentration of the chemoattractant at any given location and time within the conduits.

- We showed that our chemotaxis system is flexible and easily scalable by introducing a multiple-comparison design as well as printing our passive circuits on well plates.

The fourth and final aim of my thesis was to use this novel Freestyle Fluidics chemotaxis *in vitro* assay to study macrophage response to changes in chemoattractant gradient. In regard to this aim my collaborators and I made following key findings:

- We showed that migration of macrophages is controlled by their position in the population rather than the absolute chemoattractant concentration that they are exposed to.

- We showed that BMDMs can follow a stable chemoattractant gradient that shifted its position in an abrupt manner.

- In contrast, we showed that macrophages are unable to follow a slowly shifting gradient sweeping across them until the gradient becomes stabilised.

5.2. The hCD68-CreERT2 mouse and its possible future uses in *in vivo* macrophage targeting

Genetic tools to investigate macrophage biology *in vivo* have always lacked in cell-type specificity. The hCD68-CreERT2 mouse introduces a new tool into the collection of already available models. Its main advantage lies in the ability to avoid targeting most myeloid cell populations in the blood, a major improvement on the previous mouse lines. Additionally, the CreERT2 fusion enzyme allows inducible targeting and avoids the embryonic activity of the Cre enzyme, which would result in embryonic activation of the reporter gene. This is an advantage over the hCD68-GFP mice since we previously suggested that embryonic activation of hCD68 promoter leads to the non-macrophage targeting in the hCD68-GFP mouse (*404*). The advantage in using oestrogen receptor-fused Cre recombinase over the already published tet-On system lies in the one step activation which reduces the risk of erroneous activation or the lack of it (*321*).

I believe that this new *in vivo* macrophage targeting tool will enable researchers to address questions about macrophage heterogeneity in a range of tissues and their role in pathology with improved precision. Given that I observed differential expression of tdTomato in different sub-populations of liver and peritoneal macrophages it is reasonable to postulate that the hCD68-CreERT2 mouse line could be used to study functional differences between

sub-populations of macrophages within tissues, something that until now has been mainly investigated using single cell transcriptomic approaches and, to a certain degree, flow cytometry. However, this system still does not provide full macrophage specificity as I observed significant tdTomato expression in dendritic cells in the spleen, which has been a long-standing critique for most other published *in vivo* macrophage targeting models. Given how much macrophages and DCs overlap in their expression of surface markers and their plasticity, it remains a challenge how to reliably separate those two cell types *in vivo* in experiments that do not include single cell transcriptomics.

Another important direction, which I have not explored is the embryonic activation of Cre recombinase in this system. Even though they could not fully prove the origin of different embryonic macrophage populations, hCD68-CreERT2 mice could be used to study the macrophages in embryonic tissues and to infer their likely origins based on relative timings of contribution from known sources such as the yolk sac and the foetal liver. One of the key future experiments would be exploration of the targeting profile of myeloid cells in embryos which would include tamoxifen dosing of pregnant dams and imaging of embryonic distribution of tdTomato labelled cells at different stages of development.

Additionally, aortic tissue-resident macrophages have been shown to contribute to the macrophage pool in murine atherosclerotic plaques and have been hypothesised to locally proliferate there (*405*, *406*). Building on my work with the inducible PCSK9 model of atherosclerosis, a crucial experiment to test this hypothesis would be to induce Cre recombinase expression before the starting the inducible atherosclerosis model (to label aortic resident macrophages) and to look for the presence of tdTomato expressing macrophages inside the plaques. Furthermore, a Cre driver mouse line is only as good as its

ability to be crossed with 'floxed' strains. Considering the atherosclerosis model I have already successfully implemented using the hCD68-CreERT2 mice, the ideal candidate gene for floxing would be LYVE-1, which is expressed on aortic tissue-resident macrophages (*407*). LYVE-1^{+} macrophages have been shown inside murine atherosclerotic plaques and are associated with lower stability of the plaques (*405*). Therefore, genetic ablation of LYVE-1^{+} macrophages during early stages of atherosclerosis development should improve the disease progression. Importantly, depletion of LYVE-1^{+} macrophages before the onset of the plaques have been shown to increase arterial stiffness and collagen deposition in the adventitia, both associated with worsened atherosclerosis, which suggests that inducing the deletion at an appropriate time point would be crucial for this experiment (*407*). The only caveat of this approach is that a LYVE-$1^{fl/fl}$ mouse has not been developed yet and therefore further technology advancement is needed to study this gene in macrophage population.

5.3. Freestyle Fluidics as a contender for the 'ideal' *in vitro* macrophage chemotaxis assay and migration questions for the future

We set out to adapt the Freestyle Fluidics platform for a chemotaxis assay bearing in mind Harris' criteria for an 'ideal' chemotaxis assay listed in section 4.1.2. of this thesis. To address the first criterion, we successfully showed that there is no directional displacement of cells without a gradient present. To address the second and third criteria, we used dyes to visualise the gradient formation and diffusion over time in both passive and active circuits and showed that indeed the cells were reliably exposed to a stable gradient. In the case of passive circuits, we were able to calculate the gradient dynamics and control them by changing the length of the conduit. In active circuits, we showed that we could reliably control the steepness and the position of the gradient by changing the infusion rates through the circuit arms. Cells in

circuits were tracked in all directions and we showed a proportion of them migrating against the gradient direction, therefore fulfilling the fourth criterion. Lastly, to ensure lack of any sampling error, we tracked bias in the system and showed the position of the cells in the circuit does not influence their movement. In regard to the more modern considerations, we addressed the issue of throughput by showing the possibility to print passive circuits on well plates. We also showed that we could reliably do single-cell tracking and combine it with analysing behaviour of the entire macrophage population. Since FF comes with its own limitations, such as the need for the custom printer and relatively intricate set up we would not go as far as saying that it is an 'ideal' chemotaxis assay. However, we believe that by considering all the aforementioned criteria in our assay design, we created a system that improves on the currently available ones and allows to appreciate the unique nature of macrophage migration.

This assay has already allowed us to identify previously unknown properties of macrophage migration, such as the ability to sense and react to rapid and gradual changes in chemoattractant gradients over time, due to the ability of precisely controlling the gradient. This previously unappreciated temporal sensing during macrophage migration should be investigated further to uncover the molecular machinery driving that process. G protein-coupled receptor kinase 3 (GRK3) has been implicated in temporal sensing of dendritic cells and neutrophils and has been shown to be expressed in macrophages (*399*, *408*). GRK3 has not been studied in the context of macrophage migration, however deletion of another member of the same receptor family, GRK2, has been shown to increase macrophage mobilisation (*409*). Therefore, GRK3 could be a potentially interesting target for genetic

ablation or pharmacological modulation to try and uncover the molecular basis of the temporal chemoattractant sensing we have observed in macrophages.

Another interesting future avenue for using the FF chemotaxis platform would be establishing drug screenings for migration modulators in the higher throughput passive circuits printed on well plates. Firstly, this would be a beneficial approach because of the number of circuits fitted per dish, but also because this assay could easily detect both enhancers and inhibitors of chemotaxis without the need for complete recalibration of the system itself. Using drug repurposing approaches, commercial libraries of tool compounds or FDA-approved drugs could be efficiently screened for their previously unknown abilities to modulate chemotaxis of macrophages. Given the importance of defective macrophage migration in pathologies such as atherosclerosis and the lack of therapies that target it, this approach could provide an efficient alternative to *de novo* drug development.

Finally, the only mode of macrophage migration we observed in our system is the mesenchymal movement, which is typically associated with 3D assays. We did not investigate why that is, however one might speculate that the presence of fibronectin in the media induced the mesenchymal mechanism in macrophages. As such, it would be interesting to further investigate this mechanism and determine whether it is indeed the porosity of the environment that governs the migration mode of macrophages or whether it is exposure to certain ECM components (*273*). Moreover, despite exposing all the BMDMs to migration-inducing concentrations of C5a in our active system only a proportion of them migrated in all experiments. It would be crucial to investigate whether that is because of an inherent property of those cells or whether there were some environmental cues that differentiated the migratory macrophages from the static ones. The flexibility of our system allows isolation

and retrieval of cells and therefore the 'migrators' could be separated from the static cells and their transcriptomic profiles could be investigated for changes in gene expression that could indicate the reason for this difference.

5.4. How can new *in vivo* and *in vitro* tools drive macrophage research forward?

As Henry Harris pointed out in the 1950s in his critique of the chemotaxis field, stagnation in technical development can lead to false scientific conclusions (*359*). Assumptions and current experimental designs are often driven by the available techniques, therefore rather than addressing the scientific questions that need answering, researchers often address the questions that can be asked with the tools they possess. Macrophages have definitely fallen victims of this, often being grouped with other immune cells like monocytes or dendritic cells instead of being appreciated as a separate and highly dynamic cell type. With the advent of single cell transcriptomics and highly selective monoclonal antibodies for surface markers, the scientific community is realising the breadth and diversity of macrophage populations and functions both in tissue homeostasis and pathology. Knowing this, we need to strive to adapt the existing technologies, or design new ones, that can capture this without relying on assumptions that were true for other leukocytes. This thesis adds another set of *in vivo* and *in vitro* tools to aid that process with systems that are designed with diverse macrophages in mind. It is by no means a replacement for the current systems, or the ultimate macrophage-specific toolkit, however it opens a discussion about what else we do not know about macrophages because of the assays we have been using to study them.

References

1. R. Medzhitov, Origin and physiological roles of inflammation. *Nat. 2008 4547203*. **454**, 428–435 (2008).

2. D. Furman, J. Campisi, E. Verdin, P. Carrera-Bastos, S. Targ, C. Franceschi, L. Ferrucci, D. W. Gilroy, A. Fasano, G. W. Miller, A. H. Miller, A. Mantovani, C. M. Weyand, N. Barzilai, J. J. Goronzy, T. A. Rando, R. B. Effros, A. Lucia, N. Kleinstreuer, G. M. Slavich, Chronic inflammation in the etiology of disease across the life span. *Nat. Med. 2019 2512*. **25**, 1822–1832 (2019).

3. A. J. Iqbal, E. A. Fisher, D. R. Greaves, Inflammation—a Critical Appreciation of the Role of Myeloid Cells. *Microbiol. Spectr.* **4**, 1–17 (2016).

4. G. B. Ryan, G. Majno, Acute inflammation. *Am. J. Pathol.* **86** (1977), pp. 183–276.

5. E. Kolaczkowska, P. Kubes, Neutrophil recruitment and function in health and inflammation. *Nat. Rev. Immunol. 2013 133*. **13**, 159–175 (2013).

6. I. Mellman, R. M. Steinman, Dendritic Cells: Specialized and Regulated Antigen Processing Machines. *Cell*. **106**, 255–258 (2001).

7. D. Gilroy, R. De Maeyer, New insights into the resolution of inflammation. *Semin. Immunol.* **27**, 161–168 (2015).

8. T. A. Wynn, L. Barron, Macrophages: Master regulators of inflammation and fibrosis. *Semin. Liver Dis.* **30**, 245–257 (2010).

9. J. Savill, I. Dransfield, C. Gregory, C. Haslett, A blast from the past: clearance of apoptotic cells regulates immune responses. *Nat. Rev. Immunol. 2002 212*. **2**, 965–975 (2002).

10. A. C. Doran, A. Yurdagul, I. Tabas, Efferocytosis in health and disease. *Nat. Rev. Immunol. 2019 204*. **20**, 254–267 (2019).

11. C. Nathan, A. Ding, Nonresolving inflammation. *Cell*. **140**, 871–82 (2010).

12. G. M. Barton, A calculated response: control of inflammation by the innate immune system. *J. Clin. Invest.* **118**, 413–420 (2008).

13. H. Iwasaki, K. Akashi, Myeloid lineage commitment from the hematopoietic stem cell. *Immunity*. **26**, 726–40 (2007).

14. T. H. Mogensen, Pathogen recognition and inflammatory signaling in innate immune defenses. *Clin. Microbiol. Rev.* **22**, 240–273 (2009).

15. T. Kawasaki, T. Kawai, Toll-like receptor signaling pathways. *Front. Immunol.* **5**, 461 (2014).

16. S. R. El-Zayat, H. Sibaii, F. A. Mannaa, Toll-like receptors activation, signaling, and targeting: an overview. *Bull. Natl. Res. Cent. 2019 431*. **43**, 1–12 (2019).

17. J. Rehwinkel, M. U. Gack, RIG-I-like receptors: their regulation and roles in RNA sensing. *Nat. Rev. Immunol. 2020 209*. **20**, 537–551 (2020).

18. A. Zahid, H. Ismail, B. Li, T. Jin, Molecular and Structural Basis of DNA Sensors in Antiviral Innate Immunity. *Front. Immunol.* **11**, 3094 (2020).

19. Y. Zhong, A. Kinio, M. Saleh, Functions of NOD-Like Receptors in Human Diseases. *Front. Immunol.* **0**, 333 (2013).

20. V. Motta, F. Soares, T. Sun, D. J. Philpott, Nod-like receptors: Versatile cytosolic sentinels. *Physiol. Rev.* **95**, 149–178 (2015).

21. M. G. Netea, J. Quintin, J. W. M. Van Der Meer, Trained Immunity: A Memory for Innate Host Defense. *Cell Host Microbe*. **9**, 355–361 (2011).

22. M. G. Netea, J. Domínguez-Andrés, L. B. Barreiro, T. Chavakis, M. Divangahi, E. Fuchs, L. A. B. Joosten, J. W. M. van der Meer, M. M. Mhlanga, W. J. M. Mulder, N. P. Riksen, A. Schlitzer, J. L. Schultze, C. Stabell Benn, J. C. Sun, R. J. Xavier, E. Latz, Defining trained immunity and its role in health and disease. *Nat. Rev. Immunol. 2020 206*. **20**, 375–388 (2020).

23. J. Dominguez-Andres, M. G. Netea, Long-term reprogramming of the innate immune system. *J. Leukoc. Biol.* **105**, 329–338 (2019).

24. C. S. Benn, M. G. Netea, L. K. Selin, P. Aaby, A small jab – a big effect: nonspecific immunomodulation by vaccines. *Trends Immunol.* **34**, 431–439 (2013).

25. A. Christ, P. Günther, M. A. R. Lauterbach, P. Duewell, D. Biswas, K. Pelka, C. J. Scholz, M. Oosting, K. Haendler, K. Baßler, K. Klee, J. Schulte-Schrepping, T. Ulas, S. J. C. F. M. Moorlag, V. Kumar, M. H. Park, L. A. B. Joosten, L. A. Groh, N. P. Riksen, T. Espevik, A. Schlitzer, Y. Li, M. L. Fitzgerald, M. G. Netea, J. L. Schultze, E. Latz, Western Diet Triggers NLRP3-Dependent Innate Immune Reprogramming. *Cell*. **172**, 162-175.e14 (2018).

26. M. Guilliams, A. Mildner, S. Yona, Developmental and Functional Heterogeneity of Monocytes. *Immunity*. **49**, 595–613 (2018).

27. H. Iwasaki, K. Akashi, Hematopoietic developmental pathways: on cellular basis. *Oncogene 2007 2647*. **26**, 6687–6696 (2007).

28. S. J. Purohit, R. P. Stephan, H. G. Kim, B. R. Herrin, L. Gartland, C. A. Klug, Determination of lymphoid cell fate is dependent on the expression status of the IL-7 receptor. *EMBO J.* **22**, 5511 (2003).

29. K. Akashi, D. Traver, T. Miyamoto, I. L. Weissman, A clonogenic common myeloid progenitor that gives rise to all myeloid lineages. *Nat. 2000 4046774*. **404**, 193–197 (2000).

30. D. K. Fogg, C. Sibon, C. Miled, S. Jung, P. Aucouturier, D. R. Littman, A. Cumano, F. Geissmann, A clonogenic bone harrow progenitor specific for macrophages and dendritic cells. *Science (80-.).* **311**, 83–87 (2006).

31. A. Yáñez, S. G. Coetzee, A. Olsson, D. E. Muench, B. P. Berman, D. J. Hazelett, N. Salomonis, H. L. Grimes, H. S. Goodridge, Granulocyte-Monocyte Progenitors and Monocyte-Dendritic Cell Progenitors Independently Produce Functionally Distinct Monocytes. *Immunity*. **47**, 890-902.e4 (2017).

32. Y. P. Zhu, G. D. Thomas, C. C. Hedrick, 2014 Jeffrey M. Hoeg Award Lecture: Transcriptional Control of Monocyte Development. *Arterioscler. Thromb. Vasc. Biol.* **36**, 1722–1733 (2016).

33. P. F. Rodrigues, L. Alberti-Servera, A. Eremin, G. E. Grajales-Reyes, R. Ivanek, R. Tussiwand, Distinct progenitor lineages contribute to the heterogeneity of plasmacytoid dendritic cells. *Nat. Immunol. 2018 197*. **19**, 711–722 (2018).

34. T. N. Mayadas, X. Cullere, C. A. Lowell, The multifaceted functions of neutrophils. *Annu. Rev. Pathol. Mech. Dis.* **9**, 181–218 (2014).

35. A. Sheshachalam, N. Srivastava, T. Mitchell, P. Lacy, G. Eitzen, Granule protein processing and regulated secretion in neutrophils. *Front. Immunol.* **5**, 448 (2014).

36. T. Fulop, A. Larbi, N. Douziech, C. Fortin, K. P. Guérard, O. Lesur, A. Khalil, G. Dupuis, Signal transduction and functional changes in neutrophils with aging. *Aging Cell*. **3**, 217–226 (2004).

37. C. M. Gaillard, T. A. Tokuyasu, E. Passegué, S. C. Kogan, PML-RARα Deregulates an Unexpectedly Small Number of Genes in Pre-Leukemic Promyelocytes. *Blood*. **120**, 3526 (2012).

38. C. Gaillard, T. A. Tokuyasu, G. Rosen, J. Sotzen, A. Vitaliano-Prunier, R. Roy, E. Passegué, H. De Thé, M. E. Figueroa, S. C. Kogan, Transcription and methylation analyses of preleukemic promyelocytes indicate a dual role for PML/RARA in leukemia initiation. *Haematologica*. **100**, 1064 (2015).

39. M. D. Bjerregaard, J. Jurlander, P. Klausen, N. Borregaard, J. B. Cowland, The in vivo profile of transcription factors during neutrophil differentiation in human bone marrow. *Blood*. **101**, 4322–4332 (2003).

40. N. Hu, H. Mora-Jensen, K. Theilgaard-Mönch, B. Doornbos-van Der Meer, M. G. Huitema, C. A. Stegeman, P. Heeringa, C. G. M. Kallenberg, J. Westra, Differential Expression of Granulopoiesis Related Genes in Neutrophil Subsets Distinguished by Membrane Expression of CD177. *PLoS One*. **9**, e99671 (2014).

41. Y. Zhang, Q. Wang, C. R. Mackay, L. G. Ng, I. Kwok, Neutrophil subsets and their differential roles in viral respiratory diseases. *J. Leukoc. Biol.* **111**, 1159–1173 (2022).

42. J. G. de M. Monteiro Júnior, D. de Oliveira Cipriano Torres, D. C. S. Filho, Hematological Parameters as Prognostic Biomarkers in Patients with Cardiovascular Diseases. *Curr. Cardiol. Rev.* **15**, 274–282 (2019).

43. Y. P. Zhu, L. Padgett, H. Q. Dinh, P. Marcovecchio, A. Blatchley, R. Wu, E. Ehinger, C. Kim, Z. Mikulski, G. Seumois, A. Madrigal, P. Vijayanand, C. C. Hedrick, Identification of an Early Unipotent Neutrophil Progenitor with Pro-tumoral Activity in Mouse and Human Bone Marrow. *Cell Rep.* **24**, 2329-2341.e8 (2018).

44. Y. Katahira, H. Higuchi, H. Matsushita, T. Yahata, Y. Yamamoto, R. Koike, K. Ando, K. Sato, K. I. Imadome, A. Kotani, Increased Granulopoiesis in the Bone Marrow following Epstein-Barr Virus Infection. *Sci. Reports 2019 91*. **9**, 1–9 (2019).

45. J. F. Deniset, P. Kubes, Neutrophil heterogeneity: Bona fide subsets or polarization states? *J. Leukoc. Biol.* **103**, 829–838 (2018).

46. K. Matsuo, A. Lin, J. L. Procter, L. Clement, D. Stroncek, Variations in the expression of granulocyte antigen NB1. *Transfusion*. **40**, 654–662 (2000).

47. G. Zhou, L. Yu, L. Fang, W. Yang, T. Yu, Y. Miao, M. Chen, K. Wu, F. Chen, Y. Cong, Z. Liu, CD177+ neutrophils as functionally activated neutrophils negatively regulate IBD. *Gut*. **67**, 1052–1063 (2018).

48. S. N. Clemmensen, C. T. Bohr, S. Rørvig, A. Glenthøj, H. Mora-Jensen, E. P. Cramer, L. C. Jacobsen, M. T. Larsen, J. B. Cowland, J. T. Tanassi, N. H. H. Heegaard, J. D. Wren, A. N. Silahtaroglu, N. Borregaard, Olfactomedin 4 defines a subset of human neutrophils. *J. Leukoc. Biol.* **91**, 495–500 (2012).

49. A. Welin, F. Amirbeagi, K. Christenson, L. Björkman, H. Björnsdottir, H. Forsman, C. Dahlgren, A. Karlsson, J. Bylund, The Human Neutrophil Subsets Defined by the Presence or Absence of OLFM4 Both Transmigrate into Tissue In Vivo and Give Rise to Distinct NETs In Vitro. *PLoS One*. **8**, e69575 (2013).

50. M. N. Alder, A. M. Opoka, P. Lahni, D. A. Hildeman, H. R. Wong, Olfactomedin 4 is a Candidate Marker for a Pathogenic Neutrophil Subset in Septic Shock. *Crit. Care Med.* **45**, e426 (2017).

51. S. Massena, G. Christoffersson, E. Vågesjö, C. Seignez, K. Gustafsson, F. Binet, C. H. Hidalgo, A. Giraud, J. Lomei, S. Weström, M. Shibuya, L. Claesson-Welsh, P. Gerwins, M. Welsh, J. Kreuger, M. Phillipson, Identification and characterization of VEGF-A–responsive neutrophils expressing CD49d, VEGFR1, and CXCR4 in mice and humans. *Blood*. **126**, 2016–2026 (2015).

52. G. Christoffersson, E. Vågesjö, J. Vandooren, M. Lidén, S. Massena, R. B. Reinert, M. Brissova, A. C. Powers, G. Opdenakker, M. Phillipson, VEGF-A recruits a proangiogenic MMP-9–delivering neutrophil subset that induces angiogenesis in transplanted hypoxic tissue. *Blood*. **120**, 4653–4662 (2012).

53. F. Veglia, M. Perego, D. Gabrilovich, Myeloid-derived suppressor cells coming of age. *Nat. Immunol. 2018 192*. **19**, 108–119 (2018).

54. S. Rørvig, C. Honore, L.-I. Larsson, S. Ohlsson, C. C. Pedersen, L. C. Jacobsen, J. B. Cowland, P. Garred, N. Borregaard, Ficolin-1 is present in a highly mobilizable subset of human neutrophil granules and associates with the cell surface after stimulation with fMLP. *J. Leukoc. Biol.* **86**, 1439–1449 (2009).

55. G. T. Nguyen, E. R. Green, J. Mecsas, Neutrophils to the ROScue: Mechanisms of NADPH oxidase activation and bacterial resistance. *Front. Cell. Infect. Microbiol.* **7** (2017), doi:10.3389/FCIMB.2017.00373/ABSTRACT.

56. V. Brinkmann, U. Reichard, C. Goosmann, B. Fauler, Y. Uhlemann, D. S. Weiss, Y. Weinrauch, A. Zychlinsky, Neutrophil Extracellular Traps Kill Bacteria. *Science (80-.).* **303**, 1532–1535 (2004).

57. T. S. Kapellos, L. Bonaguro, I. Gemünd, N. Reusch, A. Saglam, E. R. Hinkley, J. L. Schultze, Human

monocyte subsets and phenotypes in major chronic inflammatory diseases. *Front. Immunol.* **10**, 2035 (2019).

58. C. L. Tsou, W. Peters, Y. Si, S. Slaymaker, A. M. Aslanian, S. P. Weisberg, M. Mack, I. F. Charo, Critical roles for CCR2 and MCP-3 in monocyte mobilization from bone marrow and recruitment to inflammatory sites. *J. Clin. Invest.* **117**, 902–909 (2007).

59. S. Yona, K.-W. W. Kim, Y. Wolf, A. Mildner, D. Varol, M. Breker, D. Strauss-Ayali, S. Viukov, M. Guilliams, A. Misharin, D. A. Hume, H. Perlman, B. Malissen, E. Zelzer, S. Jung, Fate Mapping Reveals Origins and Dynamics of Monocytes and Tissue Macrophages under Homeostasis. *Immunity*. **38**, 79–91 (2013).

60. L. M. Carlin, E. G. Stamatiades, C. Auffray, R. N. Hanna, L. Glover, G. Vizcay-Barrena, C. C. Hedrick, H. T. Cook, S. Diebold, F. Geissmann, Nr4a1-Dependent Ly6C low Monocytes Monitor Endothelial Cells and Orchestrate Their Disposal. *Cell*. **153**, 362–375 (2013).

61. K. Ley, C. Laudanna, M. I. Cybulsky, S. Nourshargh, Getting to the site of inflammation: the leukocyte adhesion cascade updated. *Nat. Rev. Immunol. 2007 79*. **7**, 678–689 (2007).

62. T. Gerhardt, K. Ley, Monocyte trafficking across the vessel wall. *Cardiovasc. Res.* **107**, 321–330 (2015).

63. E. B. Finger, K. D. Purl, R. Alon, M. B. Lawrence, U. H. von Andrian, T. A. Springer, Adhesion through L-selectin requires a threshold hydrodynamic shear. *Nat. 1996 3796562*. **379**, 266–269 (1996).

64. M. B. Lawrence, G. S. Kansas, E. J. Kunkel, K. Ley, Threshold Levels of Fluid Shear Promote Leukocyte Adhesion through Selectins (CD62L,P,E). *J. Cell Biol.* **136**, 717–727 (1997).

65. J. R. Chan, S. J. Hyduk, M. I. Cybulsky, Chemoattractants Induce a Rapid and Transient Upregulation of Monocyte α4 Integrin Affinity for Vascular Cell Adhesion Molecule 1 Which Mediates ArrestAn Early Step in the Process of Emigration. *J. Exp. Med.* **193**, 1149–1158 (2001).

66. R. E. Gerszten, E. A. Garcia-Zepeda, Y. C. Lim, M. Yoshida, H. A. Ding, M. A. Gimbrone, A. D. Luster, F. W. Luscinskas, A. Rosenzwelg, MCP-1 and IL-8 trigger firm adhesion of monocytes to vascular endothelium under flow conditions. *Nature*. **398**, 718–725 (1999).

67. P. Von Hundelshausen, K. S. C. Weber, Y. Huo, A. E. I. Proudfoot, P. J. Nelson, K. Ley, C. Weber, RANTES deposition by platelets triggers monocyte arrest on inflamed and atherosclerotic endothelium. *Circulation*. **103**, 1772–1777 (2001).

68. A. R. Schenkel, Z. Mamdouh, W. A. Muller, Locomotion of monocytes on endothelium is a critical step during extravasation. *Nat. Immunol.* **5**, 393–400 (2004).

69. J. Millán, A. J. Ridley, Rho GTPases and leucocyte-induced endothelial remodelling. *Biochem. J.* **385**, 329–337 (2005).

70. W. A. Muller, Leukocyte-endothelial-cell interactions in leukocyte transmigration and the inflammatory response. *Trends Immunol.* **24**, 326–333 (2003).

71. J. Millán, L. Hewlett, M. Glyn, D. Toomre, P. Clark, A. J. Ridley, Lymphocyte transcellular migration occurs through recruitment of endothelial ICAM-1 to caveola- and F-actin-rich domains. *Nat. Cell Biol.* **8**, 113–123 (2006).

72. J. Banchereau, R. M. Steinman, Dendritic cells and the control of immunity. *Nat. 1998 3926673*. **392**, 245–252 (1998).

73. M. Dalod, R. Chelbi, B. Malissen, T. Lawrence, Dendritic cell maturation: functional specialization through signaling specificity and transcriptional programming. *EMBO J.* **33**, 1104 (2014).

74. M. Hubo, B. Trinschek, F. Kryczanowsky, A. Tuettenberg, K. Steinbrink, H. Jonuleit, Costimulatory molecules on immunogenic versus tolerogenic human dendritic cells. *Front. Immunol.* **4**, 82 (2013).

75. J. C. Mbongue, H. A. Nieves, T. W. Torrez, W. H. R. Langridge, The role of dendritic cell maturation in the induction of insulin-dependent diabetes mellitus. *Front. Immunol.* **8**, 327 (2017).

76. H. F. Rosenberg, K. D. Dyer, P. S. Foster, Eosinophils: changing perspectives in health and disease. *Nat. Rev. Immunol. 2012 131*. **13**, 9–22 (2012).

77. Y. M. Park, B. S. Bochner, Eosinophil survival and apoptosis in health and disease. *Allergy. Asthma Immunol. Res.* **2**, 87–101 (2010).

78. K. R. Acharya, S. J. Ackerman, Eosinophil Granule Proteins: Form and Function. *J. Biol. Chem.* **289**, 17406–17415 (2014).

79. P. C. Fulkerson, M. E. Rothenberg, Targeting eosinophils in allergy, inflammation and beyond. *Nat. Rev. Drug Discov. 2013 122*. **12**, 117–129 (2013).

80. M. F. Gurish, K. F. Austen, Developmental Origin and Functional Specialization of Mast Cell Subsets. *Immunity*. **37**, 25–33 (2012).

81. S. N. Abraham, A. L. St. John, Mast cell-orchestrated immunity to pathogens. *Nat. Rev. Immunol. 2010 106*. **10**, 440–452 (2010).

82. D. M. Mosser, K. Hamidzadeh, R. Goncalves, Macrophages and the maintenance of homeostasis. *Cell. Mol. Immunol. 2020 183*. **18**, 579–587 (2020).

83. A. Viola, F. Munari, R. Sánchez-Rodríguez, T. Scolaro, A. Castegna, The Metabolic Signature of Macrophage Responses. *Front. Immunol.* **10**, 1462 (2019).

84. F. Ginhoux, M. Guilliams, Review Tissue-Resident Macrophage Ontogeny and Homeostasis (2016), doi:10.1016/j.immuni.2016.02.024.

85. C. C. Bain, C. A. Hawley, H. Garner, C. L. Scott, A. Schridde, N. J. Steers, M. Mack, A. Joshi, M. Guilliams, A. M. I. Mowat, F. Geissmann, S. J. Jenkins, Long-lived self-renewing bone marrow-derived macrophages displace embryo-derived cells to inhabit adult serous cavities. *Nat. Commun. 2016 71*. **7**, 1–14 (2016).

86. D. A. Hume, The mononuclear phagocyte system. *Curr. Opin. Immunol.* **18**, 49–53 (2006).

87. R. W. Crofton, M. M. C. Diesselhoff-Den Dulk, R. Van Furth, The origin, kinetics, and characteristics of the kupffer cells in the normal steady state. *J. Exp. Med.* **148**, 1–17 (1978).

88. R. Van Furth, M. M. C. Diesselhoff-Den Dulk, Dual origin of mouse spleen macrophages. *J. Exp. Med.* **160**, 1273–1283 (1984).

89. J. Y. Bertrand, A. Jalil, M. Klaine, S. Jung, A. Cumano, I. Godin, Three pathways to mature macrophages in the early mouse yolk sac. *Blood*. **106**, 3004–3011 (2005).

90. I. Klein, J. C. Cornejo, N. K. Polakos, B. John, S. A. Wuensch, D. J. Topham, R. H. Pierce, I. N. Crispe, Kupffer cell heterogeneity: functional properties of bone marrow derived and sessile hepatic macrophages. *Blood*. **110**, 4077–4085 (2007).

91. L. Chorro, A. Sarde, M. Li, K. J. Woollard, P. Chambon, B. Malissen, A. Kissenpfennig, J. B. Barbaroux, R. Groves, F. Geissmann, Langerhans cell (LC) proliferation mediates neonatal development, homeostasis, and inflammation-associated expansion of the epidermal LC network. *J. Exp. Med.* **206**, 3089–3100 (2009).

92. B. Ajami, J. L. Bennett, C. Krieger, W. Tetzlaff, F. M. V. Rossi, Local self-renewal can sustain CNS microglia maintenance and function throughout adult life. *Nat. Neurosci.* **10**, 1538–1543 (2007).

93. S. J. Jenkins, D. Ruckerl, P. C. Cook, L. H. Jones, F. D. Finkelman, N. Van Rooijen, A. S. MacDonald, J. E. Allen, Local macrophage proliferation, rather than recruitment from the blood, is a signature of TH2 inflammation. *Science*. **332**, 1284–1288 (2011).

94. C. Schulz, E. G. Perdiguero, L. Chorro, H. Szabo-Rogers, N. Cagnard, K. Kierdorf, M. Prinz, B. Wu, S. E. W. Jacobsen, J. W. Pollard, J. Frampton, K. J. Liu, F. Geissmann, A lineage of myeloid cells independent of myb and hematopoietic stem cells. *Science (80-.).* **335**, 86–90 (2012).

95. D. Hashimoto, A. Chow, C. Noizat, P. Teo, M. B. Beasley, M. Leboeuf, C. D. Becker, P. See, J. Price, D.

Lucas, M. Greter, A. Mortha, S. W. Boyer, E. C. Forsberg, M. Tanaka, N. van Rooijen, A. García-Sastre, E. R. Stanley, F. Ginhoux, P. S. Frenette, M. Merad, Tissue-Resident Macrophages Self-Maintain Locally throughout Adult Life with Minimal Contribution from Circulating Monocytes. *Immunity*. **38**, 792–804 (2013).

96. K. M. Summers, D. A. Hume, Identification of the macrophage-specific promoter signature in FANTOM5 mouse embryo developmental time course data. *J. Leukoc. Biol.* **102**, 1081–1092 (2017).

97. C. C. Bain, A. Bravo-Blas, C. L. Scott, E. Gomez Perdiguero, F. Geissmann, S. Henri, B. Malissen, L. C. Osborne, D. Artis, A. M. I. Mowat, Constant replenishment from circulating monocytes maintains the macrophage pool in the intestine of adult mice. *Nat. Immunol. 2014 1510*. **15**, 929–937 (2014).

98. P. Italiani, D. Boraschi, Development and functional differentiation of tissue-resident versus monocyte-derived macrophages in inflammatory reactions. *Results Probl. Cell Differ.* **62**, 23–43 (2017).

99. J. Sheng, C. Ruedl, K. Karjalainen, Most Tissue-Resident Macrophages Except Microglia Are Derived from Fetal Hematopoietic Stem Cells. *Immunity*. **43**, 382–393 (2015).

100. E. Mass, I. Ballesteros, M. Farlik, F. Halbritter, P. Günther, L. Crozet, C. E. Jacome-Galarza, K. Händler, J. Klughammer, Y. Kobayashi, E. Gomez-Perdiguero, J. L. Schultze, M. Beyer, C. Bock, F. Geissmann, Specification of tissue-resident macrophages during organogenesis. *Science (80-.).* **353** (2016), doi:10.1126/SCIENCE.AAF4238/SUPPL_FILE/MASS.SM.PDF.

101. L. Honold, M. Nahrendorf, Resident and Monocyte-Derived Macrophages in Cardiovascular Disease. *Circ. Res.* **122**, 113–127 (2018).

102. S. Gordon, A. Plüddemann, Tissue macrophages: heterogeneity and functions. *BMC Biol. 2017 151*. **15**, 1–18 (2017).

103. L. C. Davies, S. J. Jenkins, J. E. Allen, P. R. Taylor, Tissue-resident macrophages. *Nat. Immunol.* **14**, 986 (2013).

104. M. W. Barth, J. A. Hendrzak, M. J. Melnicoff, P. S. Morahan, Review of the macrophage disappearance reaction. *J. Leukoc. Biol.* **57**, 361–367 (1995).

105. M. Liu, A. Silva-Sanchez, T. D. Randall, S. Meza-Perez, Specialized immune responses in the peritoneal cavity and omentum. *J Leukoc Biol*. **109**, 717–729 (2021).

106. K. Liddiard, M. Rosas, L. C. Davies, S. A. Jones, P. R. Taylor, Macrophage heterogeneity and acute inflammation. *Eur. J. Immunol.* **41**, 2503–2508 (2011).

107. A. A. Cassado, M. R. D'Império Lima, K. R. Bortoluci, Revisiting mouse peritoneal macrophages: Heterogeneity, development, and function. *Front. Immunol.* **6**, 225 (2015).

108. A. Vega-Pérez, L. H. Villarrubia, C. Godio, A. Gutiérrez-González, L. Feo-Lucas, M. Ferriz, N. Martínez-Puente, J. Alcaín, A. Mora, G. Sabio, M. López-Bravo, C. Ardavín, Resident macrophage-dependent immune cell scaffolds drive anti-bacterial defense in the peritoneal cavity. *Immunity*. **54**, 2578-2594.e5 (2021).

109. C. Atri, F. Z. Guerfali, D. Laouini, Role of Human Macrophage Polarization in Inflammation during Infectious Diseases. *Int. J. Mol. Sci.* **19** (2018), doi:10.3390/IJMS19061801.

110. Y. Liu, R. Xu, H. Gu, E. Zhang, J. Qu, W. Cao, X. Huang, H. Yan, J. He, Z. Cai, Metabolic reprogramming in macrophage responses. *Biomark. Res.* **9**, 1–17 (2021).

111. A. J. Freemerman, A. R. Johnson, G. N. Sacks, J. J. Milner, E. L. Kirk, M. A. Troester, A. N. Macintyre, P. Goraksha-Hicks, J. C. Rathmell, L. Makowski, Metabolic Reprogramming of Macrophages: GLUCOSE TRANSPORTER 1 (GLUT1)-MEDIATED GLUCOSE METABOLISM DRIVES A PROINFLAMMATORY PHENOTYPE. *J. Biol. Chem.* **289**, 7884–7896 (2014).

112. K. Cui, C. L. Ardell, N. P. Podolnikova, V. P. Yakubenko, Distinct migratory properties of M1, M2, and resident macrophages are regulated by αdβ2 and αmβ2 integrin-mediated adhesion. *Front. Immunol.* **9**, 2650 (2018).

113. G. Lu, R. Zhang, S. Geng, L. Peng, P. Jayaraman, C. Chen, F. Xu, J. Yang, Q. Li, H. Zheng, K. Shen, J. Wang, X. Liu, W. Wang, Z. Zheng, C. F. Qi, C. Si, J. C. He, K. Liu, S. A. Lira, A. G. Sikora, L. Li, H. Xiong, Myeloid cell-derived inducible nitric oxide synthase suppresses M1 macrophage polarization. *Nat. Commun.* **6**, 1–14 (2015).

114. T. Lucas, A. Waisman, R. Ranjan, J. Roes, T. Krieg, W. Müller, A. Roers, S. A. Eming, Differential roles of macrophages in diverse phases of skin repair. *J. Immunol.* **184**, 3964–3977 (2010).

115. S. Iqbal, A. Kumar, Characterization of In vitro Generated Human Polarized Macrophages. *J. Clin. Cell. Immunol.* **06** (2015), doi:10.4172/2155-9899.1000380.

116. C. D. Mills, K. Kincaid, J. M. Alt, M. J. Heilman, A. M. Hill, M-1/M-2 Macrophages and the Th1/Th2 Paradigm. *J. Immunol.* **164**, 6166–6173 (2000).

117. M. Stein, S. Keshav, N. Harris, S. Gordon, Interleukin 4 potently enhances murine macrophage mannose receptor activity: a marker of alternative immunologic macrophage activation. *J. Exp. Med.* **176**, 287–292 (1992).

118. W. Xu, X. Zhao, M. R. Daha, C. van Kooten, Reversible differentiation of pro- and anti-inflammatory macrophages. *Mol. Immunol.* **53**, 179–186 (2013).

119. A. A. Tarique, J. Logan, E. Thomas, P. G. Holt, P. D. Sly, E. Fantino, Phenotypic,functional,and plasticity features of classical and alternatively activated human macrophages. *Am. J. Respir. Cell Mol. Biol.* **53**, 676–688 (2015).

120. P. J. Murray, J. E. Allen, S. K. Biswas, E. A. Fisher, D. W. Gilroy, S. Goerdt, S. Gordon, J. A. Hamilton, L. B. Ivashkiv, T. Lawrence, M. Locati, A. Mantovani, F. O. Martinez, J. L. Mege, D. M. Mosser, G. Natoli, J. P. Saeij, J. L. Schultze, K. A. Shirey, A. Sica, J. Suttles, I. Udalova, J. A. vanGinderachter, S. N. Vogel, T. A. Wynn, Macrophage Activation and Polarization: Nomenclature and Experimental Guidelines. *Immunity*. **41**, 14–20 (2014).

121. M. Nahrendorf, F. K. Swirski, Abandoning M1/M2 for a Network Model of Macrophage Function. *Circ. Res.* **119**, 414–7 (2016).

122. N. Haider, L. Boscá, H. R. Zandbergen, J. C. Kovacic, N. Narula, S. González-Ramos, M. Fernandez-Velasco, S. Agrawal, M. Paz-García, S. Gupta, K. DeLeon-Pennell, V. Fuster, B. Ibañez, J. Narula, Transition of Macrophages to Fibroblast-Like Cells in Healing Myocardial Infarction. *J. Am. Coll. Cardiol.* **74**, 3124–3135 (2019).

123. A. J. Mouton, K. Y. DeLeon-Pennell, O. J. Rivera Gonzalez, E. R. Flynn, T. C. Freeman, J. J. Saucerman, M. R. Garrett, Y. Ma, R. Harmancey, M. L. Lindsey, Mapping macrophage polarization over the myocardial infarction time continuum. *Basic Res. Cardiol.* **113**, 1–18 (2018).

124. Y. Y. Wang, H. Jiang, J. Pan, X. R. Huang, Y. C. Wang, H. F. Huang, K. F. To, D. J. Nikolic-Paterson, H. Y. Lan, J. H. Chen, Macrophage-to-Myofibroblast Transition Contributes to Interstitial Fibrosis in Chronic Renal Allograft Injury. *J. Am. Soc. Nephrol.* **28**, 2053–2067 (2017).

125. J. X. Rong, M. Shapiro, E. Trogan, E. A. Fisher, Transdifferentiation of mouse aortic smooth muscle cells to a macrophage-like state after cholesterol loading. *Proc. Natl. Acad. Sci. U. S. A.* **100**, 13531–13536 (2003).

126. G. Charrière, B. Cousin, E. Arnaud, M. André, F. Bacou, L. Pénicaud, L. Casteilla, Preadipocyte Conversion to Macrophage: Evidence of Plasticity. *J. Biol. Chem.* **278**, 9850–9855 (2003).

127. L. S. Shankman, D. Gomez, O. A. Cherepanova, M. Salmon, G. F. Alencar, R. M. Haskins, P. Swiatlowska, A. A. C. Newman, E. S. Greene, A. C. Straub, B. Isakson, G. J. Randolph, G. K. Owens, KLF4-dependent phenotypic modulation of smooth muscle cells has a key role in atherosclerotic plaque pathogenesis. *Nat. Med. 2015 216*. **21**, 628–637 (2015).

128. Y. Lavin, D. Winter, R. Blecher-Gonen, E. David, H. Keren-Shaul, M. Merad, S. Jung, I. Amit, Tissue-Resident Macrophage Enhancer Landscapes Are Shaped by the Local Microenvironment. *Cell*. **159**, 1312–1326 (2014).

129. N. Schaum, J. Karkanias, N. F. Neff, A. P. May, S. R. Quake, T. Wyss-Coray, S. Darmanis, J. Batson, O. Botvinnik, M. B. Chen, S. Chen, F. Green, R. C. Jones, A. Maynard, L. Penland, A. O. Pisco, R. V. Sit, G. M. Stanley, J. T. Webber, F. Zanini, A. S. Baghel, I. Bakerman, I. Bansal, D. Berdnik, B. Bilen, D. Brownfield, C. Cain, M. Cho, G. Cirolia, S. D. Conley, A. Demers, K. Demir, A. de Morree, T. Divita, H. du Bois, L. B. T. Dulgeroff, H. Ebadi, F. H. Espinoza, M. Fish, Q. Gan, B. M. George, A. Gillich, G. Genetiano, X. Gu, G. S. Gulati, Y. Hang, S. Hosseinzadeh, A. Huang, T. Iram, T. Isobe, F. Ives, K. S. Kao, G. Karnam, A. M. Kershner, B. M. Kiss, W. Kong, M. E. Kumar, J. Y. Lam, D. P. Lee, S. E. Lee, G. Li, Q. Li, L. Liu, A. Lo, W. J. Lu, A. Manjunath, K. L. May, O. L. May, M. McKay, R. J. Metzger, M. Mignardi, D. Min, A. N. Nabhan, K. M. Ng, J. Noh, R. Patkar, W. C. Peng, R. Puccinelli, E. J. Rulifson, S. S. Sikandar, R. Sinha, K. Szade, W. Tan, C. Tato, K. Tellez, K. J. Travaglini, C. Tropini, L. Waldburger, L. J. van Weele, M. N. Wosczyna, J. Xiang, S. Xue, J. Youngyunpipatkul, M. E. Zardeneta, F. Zhang, L. Zhou, P. Castro, D. Croote, J. L. DeRisi, C. S. Kuo, B. Lehallier, P. K. Nguyen, S. Y. Tan, B. M. Wang, H. Yousef, P. A. Beachy, C. K. F. Chan, K. C. Huang, K. Weinberg, S. M. Wu, B. A. Barres, M. F. Clarke, S. K. Kim, M. A. Krasnow, R. Nusse, T. A. Rando, J. Sonnenburg, I. L. Weissman, Single-cell transcriptomics of 20 mouse organs creates a Tabula Muris. *Nat. 2018 5627727*. **562**, 367–372 (2018).

130. K. M. Summers, S. J. Bush, D. A. Hume, Network analysis of transcriptomic diversity amongst resident tissue macrophages and dendritic cells in the mouse mononuclear phagocyte system. *PLOS Biol.* **18**, e3000859 (2020).

131. E. Evren, E. Ringqvist, K. P. Tripathi, N. Sleiers, I. C. Rives, A. Alisjahbana, Y. Gao, D. Sarhan, T. Halle, C. Sorini, R. Lepzien, N. Marquardt, J. Michaëlsson, A. Smed-Sörensen, J. Botling, M. C. I. Karlsson, E. J. Villablanca, T. Willinger, Distinct developmental pathways from blood monocytes generate human lung macrophage diversity. *Immunity*. **54**, 259-275.e7 (2021).

132. A. D. Hildreth, F. Ma, Y. Y. Wong, R. Sun, M. Pellegrini, T. E. O'Sullivan, Single-cell sequencing of human white adipose tissue identifies new cell states in health and obesity. **22**, 639–653 (2021).

133. C. Blériot, F. Ginhoux, Understanding the Heterogeneity of Resident Liver Macrophages. *Front. Immunol.* **10** (2019), , doi:10.3389/fimmu.2019.02694.

134. L. Beattie, A. Sawtell, J. Mann, T. C. M. Frame, B. Teal, F. de Labastida Rivera, N. Brown, K. Walwyn-Brown, J. W. J. Moore, S. MacDonald, E. K. Lim, J. E. Dalton, C. R. Engwerda, K. P. MacDonald, P. M. Kaye, Bone marrow-derived and resident liver macrophages display unique transcriptomic signatures but similar biological functions. *J. Hepatol.* **65**, 758–768 (2016).

135. F. Sierro, M. Evrard, S. Rizzetto, M. Melino, A. J. Mitchell, M. Florido, L. Beattie, S. B. Walters, S. S. Tay, B. Lu, L. E. Holz, B. Roediger, Y. C. Wong, A. Warren, W. Ritchie, C. McGuffog, W. Weninger, D. G. Le Couteur, F. Ginhoux, W. J. Britton, W. R. Heath, B. M. Saunders, G. W. McCaughan, F. Luciani, K. P. A. MacDonald, L. G. Ng, D. G. Bowen, P. Bertolino, A Liver Capsular Network of Monocyte-Derived Macrophages Restricts Hepatic Dissemination of Intraperitoneal Bacteria by Neutrophil Recruitment. *Immunity*. **47**, 374-388.e6 (2017).

136. S. Daemen, A. Gainullina, G. Kalugotla, L. He, M. M. Chan, J. W. Beals, K. H. Liss, S. Klein, A. E. Feldstein, B. N. Finck, M. N. Artyomov, J. D. Schilling, Dynamic Shifts in the Composition of Resident and Recruited Macrophages Influence Tissue Remodeling in NASH. *Cell Rep.* **34**, 108626 (2021).

137. M. P. Soares, I. Hamza, Macrophages and Iron Metabolism. *Immunity*. **44**, 492–504 (2016).

138. M. Haldar, M. Kohyama, A. Y. L. So, W. Kc, X. Wu, C. G. Briseño, A. T. Satpathy, N. M. Kretzer, H. Arase, N. S. Rajasekaran, L. Wang, T. Egawa, K. Igarashi, D. Baltimore, T. L. Murphy, K. M. Murphy, Heme-Mediated SPI-C Induction Promotes Monocyte Differentiation into Iron-Recycling Macrophages. *Cell*. **156**, 1223–1234 (2014).

139. F. K. Swirski, M. Nahrendorf, M. Etzrodt, M. Wildgruber, V. Cortez-Retamozo, P. Panizzi, J. L. Figueiredo, R. H. Kohler, A. Chudnovskiy, P. Waterman, E. Aikawa, T. R. Mempel, P. Libby, R. Weissleder, M. J. Pittet, Identification of splenic reservoir monocytes and their deployment to inflammatory sites. *Science (80-.).* **325**, 612–616 (2009).

140. L. Martinez-Pomares, S. Gordon, CD169+ macrophages at the crossroads of antigen presentation. *Trends*

Immunol. **33**, 66–70 (2012).

141. I. C. M. MacLennan, Germinal centers. *Annu. Rev. Immunol.* **12** (1994), pp. 117–139.

142. A. L. Mccubbrey, L. Barthel, K. J. Mould, M. P. Mohning, E. F. Redente, W. J. Janssen, Selective and inducible targeting of CD11b mononuclear phagocytes in the murine lung with hCD68-rtTA transgenic systems. *Am J Physiol Lung Cell Mol Physiol*. **311**, 87–100 (2016).

143. U. A. Maus, M. Audrey Koay, T. Delbeck, M. Mack, M. Ermert, L. Ermert, T. S. Blackwell, J. W. Christman, D. Schlöndorff, W. Seeger, J. Lohmeyer, Role of resident alveolar macrophages in leukocyte traffic into the alveolar air space of intact mice. *Am. J. Physiol. - Lung Cell. Mol. Physiol.* **282**, 1245–1252 (2002).

144. B. Carey, B. C. Trapnell, The molecular basis of pulmonary alveolar proteinosis. *Clin. Immunol.* **135**, 223–235 (2010).

145. J. Murphy, R. Summer, A. A. Wilson, D. N. Kotton, A. Fine, The prolonged life-span of alveolar macrophages. *Am. J. Respir. Cell Mol. Biol.* **38**, 380–385 (2008).

146. D. Bedoret, H. Wallemacq, T. Marichal, C. Desmet, F. Q. Calvo, E. Henry, R. Closset, B. Dewals, C. Thielen, P. Gustin, L. De Leval, N. Van Rooijen, A. Le Moine, A. Vanderplasschen, D. Cataldo, P. V. Drion, M. Moser, P. Lekeux, F. Bureau, Lung interstitial macrophages alter dendritic cell functions to prevent airway allergy in mice. *J. Clin. Invest.* **119**, 3723–3738 (2009).

147. A. Isaza-Restrepo, J. S. Martin-Saavedra, J. L. Velez-Leal, F. Vargas-Barato, R. Riveros-Dueñas, The peritoneum: Beyond the tissue - A review. *Front. Physiol.* **9**, 738 (2018).

148. Y. Okabe, R. Medzhitov, Tissue-Specific Signals Control Reversible Program of Localization and Functional Polarization of Macrophages. *Cell*. **157**, 832–844 (2014).

149. E. E. Bou Ghosn, A. A. Cassado, G. R. Govoni, T. Fukuhara, Y. Yang, D. M. Monack, K. R. Bortoluci, S. R. Almeida, L. A. Herzenberg, L. A. Herzenberg, Two physically, functionally, and developmentally distinct peritoneal macrophage subsets. *Proc. Natl. Acad. Sci. U. S. A.* **107**, 2568–2573 (2010).

150. R. C. Paolicelli, G. Bolasco, F. Pagani, L. Maggi, M. Scianni, P. Panzanelli, M. Giustetto, T. A. Ferreira, E. Guiducci, L. Dumas, D. Ragozzino, C. T. Gross, Synaptic pruning by microglia is necessary for normal brain development. *Science (80-.).* **333**, 1456–1458 (2011).

151. S. Epelman, K. J. Lavine, G. J. Randolph, Origin and Functions of Tissue Macrophages. *Immunity*. **41** (2014), pp. 21–35.

152. C. N. Parkhurst, G. Yang, I. Ninan, J. N. Savas, J. R. Yates, J. J. Lafaille, B. L. Hempstead, D. R. Littman, W. B. Gan, Microglia promote learning-dependent synapse formation through brain-derived neurotrophic factor. *Cell*. **155**, 1596–1609 (2013).

153. J. Leid, J. Carrelha, H. Boukarabila, S. Epelman, S. E. W. Jacobsen, K. J. Lavine, Primitive Embryonic Macrophages are Required for Coronary Development and Maturation. *Circ. Res.* **118**, 1498–511 (2016).

154. T. J. Cahill, X. Sun, C. Ravaud, C. Villa Del Campo, K. Klaourakis, I.-E. Lupu, A. M. Lord, C. Browne, S. E. W. Jacobsen, D. R. Greaves, D. G. Jackson, S. A. Cowley, W. James, R. P. Choudhury, J. M. Vieira, P. R. Riley, Tissue-resident macrophages regulate lymphatic vessel growth and patterning in the developing heart. *Development*. **148** (2021), doi:10.1242/dev.194563.

155. A. Shigeta, V. Huang, J. Zuo, R. Besada, Y. Nakashima, Y. Lu, Y. Ding, M. Pellegrini, R. P. Kulkarni, T. Hsiai, A. Deb, B. Zhou, H. Nakano, A. Nakano, Endocardially Derived Macrophages Are Essential for Valvular Remodeling. *Dev. Cell*. **48**, 617-630.e3 (2019).

156. N. R. Wong, J. Mohan, B. J. Kopecky, S. Guo, L. Du, J. Leid, G. Feng, I. Lokshina, O. Dmytrenko, H. Luehmann, G. Bajpai, L. Ewald, L. Bell, N. Patel, A. Bredemeyer, C. J. Weinheimer, J. M. Nigro, A. Kovacs, S. Morimoto, P. O. Bayguinov, M. R. Fisher, W. T. Stump, M. Greenberg, J. A. J. Fitzpatrick, S. Epelman, D. Kreisel, R. Sah, Y. Liu, H. Hu, K. J. Lavine, Resident cardiac macrophages mediate adaptive myocardial remodeling. *Immunity*. **54**, 2072-2088.e7 (2021).

157. M. Hulsmans, S. Clauss, L. Xiao, A. D. Aguirre, K. R. King, A. Hanley, W. J. Hucker, E. M. Wülfers, G.

Seemann, G. Courties, Y. Iwamoto, Y. Sun, A. J. Savol, H. B. Sager, K. J. Lavine, G. A. Fishbein, D. E. Capen, N. Da Silva, L. Miquerol, H. Wakimoto, C. E. Seidman, J. G. Seidman, R. I. Sadreyev, K. Naxerova, R. N. Mitchell, D. Brown, P. Libby, R. Weissleder, F. K. Swirski, P. Kohl, C. Vinegoni, D. J. Milan, P. T. Ellinor, M. Nahrendorf, Macrophages Facilitate Electrical Conduction in the Heart. *Cell*. **169**, 510-522.e20 (2017).

158. S. Wang, Q. Ye, X. Zeng, S. Qiao, Functions of macrophages in the maintenance of intestinal homeostasis. *J. Immunol. Res.* **2019** (2019), doi:10.1155/2019/1512969.

159. L. Franchi, N. Kamada, Y. Nakamura, A. Burberry, P. Kuffa, S. Suzuki, M. H. Shaw, Y. G. Kim, G. Núñez, NLRC4-driven production of IL-1β discriminates between pathogenic and commensal bacteria and promotes host intestinal defense. *Nat. Immunol. 2012 135*. **13**, 449–456 (2012).

160. L. Russo, C. N. Lumeng, Properties and functions of adipose tissue macrophages in obesity. *Immunology*. **155**, 407–417 (2018).

161. J. I. Odegaard, R. R. Ricardo-Gonzalez, M. H. Goforth, C. R. Morel, V. Subramanian, L. Mukundan, A. R. Eagle, D. Vats, F. Brombacher, A. W. Ferrante, A. Chawla, Macrophage-specific PPARγ controls alternative activation and improves insulin resistance. *Nat. 2007 4477148*. **447**, 1116–1120 (2007).

162. K. D. Nguyen, Y. Qiu, X. Cui, Y. P. S. Goh, J. Mwangi, T. David, L. Mukundan, F. Brombacher, R. M. Locksley, A. Chawla, Alternatively activated macrophages produce catecholamines to sustain adaptive thermogenesis. *Nat. 2011 4807375*. **480**, 104–108 (2011).

163. R. M. Pirzgalska, E. Seixas, J. S. Seidman, V. M. Link, N. M. Sánchez, I. Mahú, R. Mendes, V. Gres, N. Kubasova, I. Morris, B. A. Arús, C. M. Larabee, M. Vasques, F. Tortosa, A. L. Sousa, S. Anandan, E. Tranfield, M. K. Hahn, M. Iannacone, N. J. Spann, C. K. Glass, A. I. Domingos, Sympathetic neuron–associated macrophages contribute to obesity by importing and metabolizing norepinephrine. *Nat. Med. 2017 2311*. **23**, 1309–1318 (2017).

164. L. Chorro, F. Geissmann, Development and homeostasis of 'resident' myeloid cells: the case of the Langerhans cell. *Trends Immunol.* **31**, 438–445 (2010).

165. L. De Witte, A. Nabatov, M. Pion, D. Fluitsma, M. A. W. P. De Jong, T. De Gruijl, V. Piguet, Y. Van Kooyk, T. B. H. Geijtenbeek, Langerin is a natural barrier to HIV-1 transmission by Langerhans cells. *Nat. Med. 2007 133*. **13**, 367–371 (2007).

166. J. Valladeau, O. Ravel, C. Dezutter-Dambuyant, K. Moore, M. Kleijmeer, Y. Liu, V. Duvert-Frances, C. Vincent, D. Schmitt, J. Davoust, C. Caux, S. Lebecque, S. Saeland, Langerin, a Novel C-Type Lectin Specific to Langerhans Cells, Is an Endocytic Receptor that Induces the Formation of Birbeck Granules. *Immunity*. **12**, 71–81 (2000).

167. M. Merad, F. Ginhoux, M. Collin, Origin, homeostasis and function of Langerhans cells and other langerin-expressing dendritic cells. *Nat. Rev. Immunol. 2008 812*. **8**, 935–947 (2008).

168. M. B. Madel, L. Ibáñez, A. Wakkach, T. J. De Vries, A. Teti, F. Apparailly, C. Blin-Wakkach, Immune function and diversity of osteoclasts in normal and pathological conditions. *Front. Immunol.* **10**, 1408 (2019).

169. C. E. Jacome-Galarza, G. I. Percin, J. T. Muller, E. Mass, T. Lazarov, J. Eitler, M. Rauner, V. K. Yadav, L. Crozet, M. Bohm, P. L. Loyher, G. Karsenty, C. Waskow, F. Geissmann, Developmental origin, functional maintenance and genetic rescue of osteoclasts. *Nat. 2019 5687753*. **568**, 541–545 (2019).

170. J. W. Ashley, Z. Shi, H. Zhao, X. Li, R. A. Kesterson, X. Feng, Genetic ablation of CD68 results in mice with increased bone and dysfunctional osteoclasts. *PLoS One*. **6** (2011), doi:10.1371/JOURNAL.PONE.0025838.

171. A. Wakkach, M. Rouleau, C. Blin-Wakkach, Osteoimmune interactions in inflammatory bowel disease: Central role of bone marrow Th17 TNFα cells in osteoclastogenesis. *Front. Immunol.* **6**, 640 (2015).

172. L. Ibáñez, G. Abou-Ezzi, T. Ciucci, V. Amiot, N. Belaïd, D. Obino, A. Mansour, M. Rouleau, A. Wakkach, C. Blin-Wakkach, Inflammatory Osteoclasts Prime TNFα-Producing CD4+ T Cells and Express CX3CR1. *J. Bone Miner. Res.* **31**, 1899–1908 (2016).

173. S. Kaur, L. J. Raggatt, L. Batoon, D. A. Hume, J. P. Levesque, A. R. Pettit, Role of bone marrow macrophages in controlling homeostasis and repair in bone and bone marrow niches. *Semin. Cell Dev. Biol.* **61**, 12–21 (2017).

174. R. N. Jacobsen, A. C. Perkins, J. P. Levesque, Macrophages and regulation of erythropoiesis. *Curr. Opin. Hematol.* **22**, 212–219 (2015).

175. R. N. Jacobsen, C. E. Forristal, L. J. Raggatt, B. Nowlan, V. Barbier, S. Kaur, N. van Rooijen, I. G. Winkler, A. R. Pettit, J. P. Levesque, Mobilization with granulocyte colony-stimulating factor blocks medullar erythropoiesis by depleting F4/80+VCAM1+CD169+ER-HR3+Ly6G+ erythroid island macrophages in the mouse. *Exp. Hematol.* **42**, 547-561.e4 (2014).

176. I. G. Winkler, N. A. Sims, A. R. Pettit, V. Barbier, B. Nowlan, F. Helwani, I. J. Poulton, N. Van Rooijen, K. A. Alexander, L. J. Raggatt, J. P. Lévesque, Bone marrow macrophages maintain hematopoietic stem cell (HSC) niches and their depletion mobilizes HSCs. *Blood*. **116**, 4815–4828 (2010).

177. J. E. Cole, I. Park, D. J. Ahern, C. Kassiteridi, D. D. Abeam, M. E. Goddard, P. Green, P. Maffia, C. Monaco, Immune cell census in murine atherosclerosis: cytometry by time of flight illuminates vascular myeloid cell diversity. *Cardiovasc. Res.* **114**, 1360–1371 (2018).

178. L. Farahi, S. K. Sinha, A. J. Lusis, Roles of Macrophages in Atherogenesis. *Front. Pharmacol.* **12**, 3336 (2021).

179. P. Marchio, S. Guerra-Ojeda, J. M. Vila, M. Aldasoro, V. M. Victor, M. D. Mauricio, Targeting early atherosclerosis: A focus on oxidative stress and inflammation. *Oxid. Med. Cell. Longev.* **2019** (2019), doi:10.1155/2019/8563845.

180. J. Mestas, K. Ley, Monocyte-Endothelial Cell Interactions in the Development of Atherosclerosis. *Trends Cardiovasc. Med.* **18**, 228–232 (2008).

181. L. Boring, J. Gosling, M. Cleary, I. F. Charo, Decreased lesion formation in CCR2−/− mice reveals a role for chemokines in the initiation of atherosclerosis. *Nat. 1998 3946696*. **394**, 894–897 (1998).

182. C. S. Robbins, I. Hilgendorf, G. F. Weber, I. Theurl, Y. Iwamoto, J. L. Figueiredo, R. Gorbatov, G. K. Sukhova, L. M. S. Gerhardt, D. Smyth, C. C. J. Zavitz, E. A. Shikatani, M. Parsons, N. Van Rooijen, H. Y. Lin, M. Husain, P. Libby, M. Nahrendorf, R. Weissleder, F. K. Swirski, Local proliferation dominates lesional macrophage accumulation in atherosclerosis. *Nat. Med. 2013 199*. **19**, 1166–1172 (2013).

183. K. J. Moore, F. J. Sheedy, E. A. Fisher, Macrophages in atherosclerosis: a dynamic balance. *Nat. Rev. Immunol. 2013 1310*. **13**, 709–721 (2013).

184. Y. V Bobryshev, E. A. Ivanova, D. A. Chistiakov, N. G. Nikiforov, A. N. Orekhov, Macrophages and Their Role in Atherosclerosis: Pathophysiology and Transcriptome Analysis (2016), doi:10.1155/2016/9582430.

185. J. J. Manning-Tobin, K. J. Moore, T. A. Seimon, S. A. Bell, M. Sharuk, J. I. Alvarez-Leite, M. P. J. De Winther, I. Tabas, M. W. Freeman, Loss of SR-A and CD36 Activity Reduces Atherosclerotic Lesion Complexity Without Abrogating Foam Cell Formation in Hyperlipidemic Mice. *Arterioscler. Thromb. Vasc. Biol.* **29**, 19–26 (2009).

186. A. Zernecke, H. Winkels, C. Cochain, J. W. Williams, D. Wolf, O. Soehnlein, C. S. Robbins, C. Monaco, I. Park, C. A. McNamara, C. J. Binder, M. I. Cybulsky, C. A. Scipione, C. C. Hedrick, E. V. Galkina, T. Kyaw, Y. Ghosheh, H. Q. Dinh, K. Ley, Meta-Analysis of Leukocyte Diversity in Atherosclerotic Mouse Aortas. *Circ. Res.* **127**, 402–426 (2020).

187. G. Chinetti-Gbaguidi, M. Baron, M. A. Bouhlel, J. Vanhoutte, C. Copin, Y. Sebti, B. Derudas, T. Mayi, G. Bories, A. Tailleux, S. Haulon, C. Zawadzki, B. Jude, B. Staels, Human atherosclerotic plaque alternative macrophages display low cholesterol handling but high phagocytosis because of distinct activities of the PPARγ and LXRα pathways. *Circ. Res.* **108**, 985–995 (2011).

188. P. Lin, H. H. Ji, Y. J. Li, S. D. Guo, Macrophage Plasticity and Atherosclerosis Therapy. *Front. Mol. Biosci.* **8**, 324 (2021).

189. K. J. Moore, I. Tabas, Macrophages in the pathogenesis of atherosclerosis. *Cell*. **145**, 341–355 (2011).

190. I. Tabas, Macrophage death and defective inflammation resolution in atherosclerosis. *Nat. Rev. Immunol.* **10**, 36–46 (2010).

191. S. M. Dunlay, S. A. Weston, M. M. Redfield, J. M. Killian, V. L. Roger, Tumor necrosis factor-α and mortality in heart failure: A community study. *Circulation*. **118**, 625–631 (2008).

192. M. Nahrendorf, F. K. Swirski, E. Aikawa, L. Stangenberg, T. Wurdinger, J. L. Figueiredo, P. Libby, R. Weissleder, M. J. Pittet, The healing myocardium sequentially mobilizes two monocyte subsets with divergent and complementary functions. *J. Exp. Med.* **204**, 3037–3047 (2007).

193. A. L. Leblond, K. Klinkert, K. Martin, E. C. Turner, A. H. Kumar, T. Browne, N. M. Caplice, Systemic and Cardiac Depletion of M2 Macrophage through CSF-1R Signaling Inhibition Alters Cardiac Function Post Myocardial Infarction. *PLoS One*. **10**, e0137515 (2015).

194. M. J. Van Amerongen, M. C. Harmsen, N. Van Rooijen, A. H. Petersen, M. J. A. Van Luyn, Macrophage Depletion Impairs Wound Healing and Increases Left Ventricular Remodeling after Myocardial Injury in Mice. *Am. J. Pathol.* **170**, 818–829 (2007).

195. H. B. Sager, M. Hulsmans, K. J. Lavine, M. B. Moreira, T. Heidt, G. Courties, Y. Sun, Y. Iwamoto, B. Tricot, O. F. Khan, J. E. Dahlman, A. Borodovsky, K. Fitzgerald, D. G. Anderson, R. Weissleder, P. Libby, F. K. Swirski, M. Nahrendorf, Proliferation and Recruitment Contribute to Myocardial Macrophage Expansion in Chronic Heart Failure. *Circ. Res.* **119**, 853–864 (2016).

196. C. Q. Chu, M. Field, M. Feldmann, R. N. Maini, Localization of Tumor Necrosis Factor α in Synovial Tissues and at the Cartilage–Pannus Junction in Patients With Rheumatoid Arthritis. *Arthritis Rheum.* **34**, 1125–1132 (1991).

197. I. A. Udalova, A. Mantovani, M. Feldmann, Macrophage heterogeneity in the context of rheumatoid arthritis. *Nat. Rev. Rheumatol. 2016 128*. **12**, 472–485 (2016).

198. A. E. Koch, S. L. Kunkel, J. C. Burrows, H. L. Evanoff, G. K. Haines, R. M. Pope, R. M. Strieter, Synovial tissue macrophage as a source of the chemotactic cytokine IL-8. *J. Immunol.* **147** (1991).

199. A. E. Koch, S. L. Kunkel, L. A. Harlow, B. Johnson, H. L. Evanoff, G. K. Haines, M. D. Burdick, R. M. Pope, R. M. Strieter, Enhanced production of monocyte chemoattractant protein-1 in rheumatoid arthritis. *J. Clin. Invest.* **90**, 772–779 (1992).

200. G. A. Duque, A. Descoteaux, Macrophage cytokines: Involvement in immunity and infectious diseases. *Front. Immunol.* **5**, 491 (2014).

201. C. A. Dinarello, Historical insights into cytokines. *Eur. J. Immunol.* **37**, S34–S45 (2007).

202. J. R. Teijaro, K. B. Walsh, S. Cahalan, D. M. Fremgen, E. Roberts, F. Scott, E. Martinborough, R. Peach, M. B. A. Oldstone, H. Rosen, Endothelial Cells Are Central Orchestrators of Cytokine Amplification during Influenza Virus Infection. *Cell*. **146**, 980 (2011).

203. I. Comerford, S. R. McColl, Mini-review series: focus on chemokines. *Immunol. Cell Biol.* **89**, 183–184 (2011).

204. I. F. Charo, R. M. Ransohoff, The Many Roles of Chemokines and Chemokine Receptors in Inflammation. *N. Engl. J. Med.* **354**, 610–621 (2006).

205. B. A. Premack, T. J. Schall, Chemokine receptors: Gateways to inflammation and infection. *Nat. Med.* **2** (1996), pp. 1174–1178.

206. B. Moser, I. Clark-Lewis, R. Zwahlen, M. Baggiolini, Neutrophil-activating properties of the melanoma growth-stimulatory activity. *J. Exp. Med.* **171**, 1797–1802 (1990).

207. L. M. Pelus, S. Fukuda, Peripheral blood stem cell mobilization: The CXCR2 ligand GROβ rapidly mobilizes hematopoietic stem cells with enhanced engraftment properties. *Exp. Hematol.* **34**, 1010–1020 (2006).

208. A. A. Maghazachi, A. Al-Aoukaty, T. J. Schall, CC chemokines induce the generation of killer cells from CD56+ cells. *Eur. J. Immunol.* **26**, 315–319 (1996).

209. T. A. Donlon, A. M. Krensky, M. R. Wallace, F. S. Collins, M. Lovett, C. Clayberger, Localization of a human T-cell-specific gene, RANTES (D17S136E), to chromosome 17q11.2-q12. *Genomics*. **6**, 548–553 (1990).

210. S. Starckx, P. E. Van Den Steen, A. Wuyts, J. Van Damme, G. Opdenakker, Neutrophil gelatinase B and chemokines in leukocytosis and stem cell mobilization. *Leuk. Lymphoma*. **43** (2002), pp. 233–241.

211. M. Gouwy, S. Struyf, J. Catusse, P. Proost, J. Van Damme, Synergy between proinflammatory ligands of G protein-coupled receptors in neutrophil activation and migration. *J. Leukoc. Biol.* **76**, 185–194 (2004).

212. E. C. Keeley, B. Mehrad, R. M. Strieter, Chemokines as mediators of neovascularization. *Arterioscler. Thromb. Vasc. Biol.* **28**, 1928–1936 (2008).

213. J. H. Dufour, M. Dziejman, M. T. Liu, J. H. Leung, T. E. Lane, A. D. Luster, IFN-γ-Inducible Protein 10 (IP-10; CXCL10)-Deficient Mice Reveal a Role for IP-10 in Effector T Cell Generation and Trafficking. *J. Immunol.* **168**, 3195–3204 (2002).

214. K. E. Cole, C. A. Strick, T. J. Paradis, K. T. Ogborne, M. Loetscher, R. P. Gladue, W. Lin, J. G. Boyd, B. Moser, D. E. Wood, B. G. Sahagan, K. Neote, Interferon–inducible T Cell Alpha Chemoattractant (I-TAC): A Novel Non-ELR CXC Chemokine with Potent Activity on Activated T Cells through Selective High Affinity Binding to CXCR3. *J. Exp. Med.* **187**, 2009–2021 (1998).

215. J. R. Dunkelberger, W. C. Song, Complement and its role in innate and adaptive immune responses. *Cell Res. 2010 201*. **20**, 34–50 (2009).

216. H. Rus, C. Cudrici, F. Niculescu, The role of the complement system in innate immunity. *Immunol. Res. 2005 332*. **33**, 103–112 (2005).

217. X. X. Li, D. M. Gorman, J. D. Lee, R. J. Clark, T. M. Woodruff, Unexpected Off-Target Activities for Recombinant C5a in Human Macrophages. *J. Immunol.* (2021), doi:10.4049/JIMMUNOL.2100444.

218. M. Bosmann, M. D. Haggadone, F. S. Zetoune, J. V. Sarma, P. A. Ward, The interaction between C5a and both C5aR and C5L2 receptors is required for production of G-CSF during acute inflammation. *Eur. J. Immunol.* **43**, 1907–1913 (2013).

219. V. Seow, J. Lim, A. Iyer, J. Y. Suen, J. K. Ariffin, D. M. Hohenhaus, M. J. Sweet, D. P. Fairlie, Inflammatory Responses Induced by Lipopolysaccharide Are Amplified in Primary Human Monocytes but Suppressed in Macrophages by Complement Protein C5a. *J. Immunol.* **191**, 4308–4316 (2013).

220. M. D. Haggadone, J. J. Grailer, F. Fattahi, F. S. Zetoune, P. A. Ward, Bidirectional Crosstalk between C5a Receptors and the NLRP3 Inflammasome in Macrophages and Monocytes. *Mediators Inflamm.* **2016** (2016), doi:10.1155/2016/1340156.

221. X. Zhang, I. Schmudde, Y. Laumonnier, M. K. Pandey, J. R. Clark, P. König, N. P. Gerard, C. Gerard, M. Wills-Karp, J. Köhl, A Critical Role for C5L2 in the Pathogenesis of Experimental Allergic Asthma. *J. Immunol.* **185**, 6741–6752 (2010).

222. F. Ender, A. V. Wiese, I. Schmudde, J. Sun, T. Vollbrandt, P. König, Y. Laumonnier, J. Köhl, Differential regulation of C5a receptor 1 in innate immune cells during the allergic asthma effector phase. *PLoS One*. **12**, e0172446 (2017).

223. D. Rittirsch, M. A. Flierl, B. A. Nadeau, D. E. Day, M. Huber-Lang, C. R. Mackay, F. S. Zetoune, N. P. Gerard, K. Cianflone, J. Köhl, C. Gerard, J. V. Sarma, P. A. Ward, Functional roles for C5a receptors in sepsis. *Nat. Med. 2008 145*. **14**, 551–557 (2008).

224. M. Huber-Lang, J. V. Sarma, D. Rittirsch, H. Schreiber, M. Weiss, M. Flierl, E. Younkin, M. Schneider, H. Suger-Wiedeck, F. Gebhard, S. D. McClintock, T. Neff, F. Zetoune, U. Bruckner, R.-F. Guo, P. N. Monk, P. A. Ward, Changes in the Novel Orphan, C5a Receptor (C5L2), during Experimental Sepsis and Sepsis in Humans. *J. Immunol.* **174**, 1104–1110 (2005).

225. J. Lim, A. Iyer, J. Y. Suen, V. Seow, R. C. Reid, L. Brown, D. P. Fairlie, C5aR and C3aR antagonists each

inhibit diet-induced obesity, metabolic dysfunction, and adipocyte and macrophage signaling. *FASEB J.* **27**, 822–831 (2013).

226. J. Phieler, K.-J. Chung, A. Chatzigeorgiou, A. Klotzsche-von Ameln, R. Garcia-Martin, D. Sprott, M. Moisidou, T. Tzanavari, B. Ludwig, E. Baraban, M. Ehrhart-Bornstein, S. R. Bornstein, H. Mziaut, M. Solimena, K. P. Karalis, M. Economopoulou, J. D. Lambris, T. Chavakis, The Complement Anaphylatoxin C5a Receptor Contributes to Obese Adipose Tissue Inflammation and Insulin Resistance. *J. Immunol.* **191**, 4367–4374 (2013).

227. G. H. Wadhams, J. P. Armitage, Making sense of it all: Bacterial chemotaxis. *Nat. Rev. Mol. Cell Biol.* **5** (2004), pp. 1024–1037.

228. X. Yang, D. Dormann, A. E. Münsterberg, C. J. Weijer, Cell movement patterns during gastrulation in the chick are controlled by positive and negative chemotaxis mediated by FGF4 and FGF8. *Dev. Cell*. **3**, 425–437 (2002).

229. F. J. Martini, M. Valiente, G. L. Bendito, G. Szabó, F. Moya, M. Valdeolmillos, O. Marín, Biased selection of leading process branches mediates chemotaxis during tangential neuronal migration. *Development*. **136**, 41–50 (2009).

230. A. I. Chernyavsky, J. Arrendondo, L. M. Marubio, S. A. Grando, Differential regulation of keratinocyte chemokinesis and chemotaxis through distinct nicotinic receptor subtypes. *J. Cell Sci.* **117** (2004), pp. 5665–5679.

231. M. T. Quinn, S. Parthasarathy, D. Steinberg, Lysophosphatidylcholine: a chemotactic factor for human monocytes and its potential role in atherogenesis. *Proc. Natl. Acad. Sci.* **85**, 2805–2809 (1988).

232. L. Schneider, M. Cammer, J. Lehman, S. K. Nielsen, C. F. Guerra, I. R. Veland, C. Stock, E. K. Hoffmann, B. K. Yoder, A. Schwab, P. Satir, S. T. Christensen, Directional cell migration and chemotaxis in wound healing response to PDGF-AA are coordinated by the primary cilium in fibroblasts. *Cell. Physiol. Biochem.* **25**, 279–292 (2010).

233. P. Vitorino, T. Meyer, Modular control of endothelial sheet migration. *Genes Dev.* **22**, 3268–3281 (2008).

234. A. Bianco, M. Poukkula, A. Cliffe, J. Mathieu, C. M. Luque, T. A. Fulga, P. Rørth, Two distinct modes of guidance signalling during collective migration of border cells. *Nature*. **448**, 362–365 (2007).

235. I. Rink, J. Rink, D. Helmer, D. Sachs, K. Schmitz, A Haptotaxis Assay for Leukocytes Based on Surface-Bound Chemokine Gradients. *J. Immunol.* **194**, 5549–5558 (2015).

236. G. E. Jones, Cellular signaling in macrophage migration and chemotaxis. *J. Leukoc. Biol.* **68**, 593–602 (2000).

237. J. Schwarz, V. Bierbaum, J. Merrin, T. Frank, R. Hauschild, T. Bollenbach, S. Tay, M. Sixt, M. Mehling, A microfluidic device for measuring cell migration towards substrate-bound and soluble chemokine gradients. *Sci. Rep.* **6**, 1–12 (2016).

238. L. Boneschansker, H. Nakayama, M. Eisenga, J. Wedel, M. Klagsbrun, D. Irimia, D. M. Briscoe, Netrin-1 Augments Chemokinesis in CD4 + T Cells In Vitro and Elicits a Proinflammatory Response In Vivo. *J. Immunol.* **197**, 1389–1398 (2016).

239. F. G. Gervais, R. P. G. Cruz, A. Chateauneuf, S. Gale, N. Sawyer, F. Nantel, K. M. Metters, G. P. O'Neill, Selective modulation of chemokinesis, degranulation, and apoptosis in eosinophils through the PGD2 receptors CRTH2 and DP. *J. Allergy Clin. Immunol.* **108**, 982–988 (2001).

240. F. Vianello, I. T. Olszak, M. C. Poznansky, Fugetaxis: Active movement of leukocytes away from a chemokinetic agent. *J. Mol. Med.* **83** (2005), pp. 752–763.

241. B. McDonald, K. Pittman, G. B. Menezes, S. A. Hirota, I. Slaba, C. C. M. Waterhouse, P. L. Beck, D. A. Muruve, P. Kubes, Intravascular danger signals guide neutrophils to sites of sterile inflammation. *Science (80-.).* **330**, 362–366 (2010).

242. C. Debru, A particular form of chemotaxis: Necrotaxis. An historical view. *Blood Cells*. **19**, 5–23 (1993).

243. X. Trepat, Z. Chen, K. Jacobson, Cell migration. *Compr. Physiol.* **2**, 2369–2392 (2012).

244. D. E. Frank, W. G. Carter, Laminin 5 deposition regulates keratinocyte polarization and persistent migration. *J. Cell Sci.* **117**, 1351–1363 (2004).

245. M. Mihlan, K. M. Glaser, M. W. Epple, T. Lämmermann, Neutrophils: Amoeboid Migration and Swarming Dynamics in Tissues. *Front. Cell Dev. Biol.* **10**, 610 (2022).

246. P. Friedl, B. Weigelin, Interstitial leukocyte migration and immune function. *Nat. Immunol.* **9**, 960–969 (2008).

247. K. Wolf, R. Müller, S. Borgmann, E. B. Bröcker, P. Friedl, Amoeboid shape change and contact guidance: T-lymphocyte crawling through fibrillar collagen is independent of matrix remodeling by MMPs and other proteases. *Blood*. **102**, 3262–3269 (2003).

248. G. Germena, E. Hirsch, PI3Ks and small GTPases in neutrophil migration: Two sides of the same coin. *Mol. Immunol.* **55**, 83–86 (2013).

249. L. K. Fritz-Laylin, S. J. Lord, R. D. Mullins, WASP and SCAR are evolutionarily conserved in actin-filled pseudopod-based motility. *J. Cell Biol.* **216**, 1673–1688 (2017).

250. A. J. Ridley, M. A. Schwartz, K. Burridge, R. A. Firtel, M. H. Ginsberg, G. Borisy, J. T. Parsons, A. R. Horwitz, Cell Migration: Integrating Signals from Front to Back. *Science (80-.).* **302** (2003), pp. 1704–1709.

251. S. L. Gupton, K. Eisenmann, A. S. Alberts, C. M. Waterman-Storer, mDia2 regulates actin and focal adhesion dynamics and organization in the lamella for efficient epithelial cell migration. *J. Cell Sci.* **120**, 3475–3487 (2007).

252. G. Constantin, C. Laudanna, Leukocyte chemotaxis: from lysosomes to motility. *Nat. Immunol.* **11**, 463–464 (2010).

253. M. Kelly, J. M. Hwang, P. Kubes, Modulating leukocyte recruitment in inflammation. *J. Allergy Clin. Immunol.* **120**, 3–10 (2007).

254. G. Bouma, T. Nikolic, J. ?C. M. C. Coppens, C. G. van Helden-Meeuwsen, P. ?M. J. M. Leenen, H. A. Drexhage, S. Sozzani, M. A. Versnel, P. ?M. J. M. Leenen, C. G. van Helden-Meeuwsen, J. ?C. M. C. Coppens, G. Bouma, M. A. Versnel, S. Sozzani, T. Nikolic, NOD mice have a severly impaired ability to recruit leukocytes into sites of inflammation. *Eur. J. Immunol.* **35**, 225–235 (2005).

255. F. Barros-Becker, P. Y. Lam, R. Fisher, A. Huttenlocher, Live imaging reveals distinct modes of neutrophil and macrophage migration within interstitial tissues. *J. Cell Sci.* **130**, 3801–3808 (2017).

256. A. N. Rumianek, D. R. Greaves, How Have Leukocyte In Vitro Chemotaxis Assays Shaped Our Ideas about Macrophage Migration? *Biology (Basel).* **9**, 1–13 (2020).

257. F. J. Pixley, Macrophage migration and its regulation by CSF-1. *Int. J. Cell Biol.* **2012** (2012), doi:10.1155/2012/501962.

258. A. D. Ma, A. Metjian, S. Bagrodia, S. Taylor, C. S. Abrams, Cytoskeletal Reorganization by G Protein-Coupled Receptors Is Dependent on Phosphoinositide 3-Kinase γ, a Rac Guanosine Exchange Factor, and Rac. *Mol. Cell. Biol.* **18**, 4744–4751 (1998).

259. M. MacHacek, L. Hodgson, C. Welch, H. Elliott, O. Pertz, P. Nalbant, A. Abell, G. L. Johnson, K. M. Hahn, G. Danuser, Coordination of Rho GTPase activities during cell protrusion. *Nature*. **461**, 99–103 (2009).

260. W. E. Allen, G. E. Jones, J. W. Pollard, A. J. Ridley, Rho, Rac and Cdc42 regulate actin organization and cell adhesion in macrophages. *J. Cell Sci.* **110**, 707–720 (1997).

261. A. P. Wheeler, C. M. Wells, S. D. Smith, F. M. Vega, R. B. Henderson, V. L. Tybulewicz, A. J. Ridley, Rac1 and Rac2 regulate macrophage morphology but are not essential for migration. *J. Cell Sci.* **119**, 2749–2757 (2006).

262. S. Tsuboi, Requirement for a Complex of Wiskott-Aldrich Syndrome Protein (WASP) with WASP

Interacting Protein in Podosome Formation in Macrophages. *J. Immunol.* **178**, 2987–2995 (2007).

263. S. Vemula, J. Shi, P. Hanneman, L. Wei, R. Kapur, ROCK1 functions as a suppressor of inflammatory cell migration by regulating PTEN phosphorylation and stability. *Blood*. **115**, 1785–1796 (2010).

264. M. Okigaki, C. Davis, M. Falascat, S. Harroch, D. P. Felsenfeld, M. P. Sheetz, J. Schlessinger, Pyk2 regulates multiple signaling events crucial for macrophage morphology and migration. *Proc. Natl. Acad. Sci. U. S. A.* **100**, 10740–10745 (2003).

265. K. A. Owen, F. J. Pixley, K. S. Thomas, M. Vicente-Manzanares, B. J. Ray, A. F. Horwitz, J. T. Parsons, H. E. Beggs, E. R. Stanley, A. H. Bouton, Regulation of lamellipodial persistence, adhesion turnover, and motility in macrophages by focal adhesion kinase. *J. Cell Biol.* **179**, 1275–1287 (2007).

266. M. R. Miller, S. D. Blystone, M. R. Miller, S. D. Blystone, Human Macrophages Utilize the Podosome Formin FMNL1 for Adhesion and Migration. *CellBio*. **4**, 1–11 (2015).

267. L. Taylor, M. H. Brodermann, D. McCaffary, A. J. Iqbal, D. R. Greaves, Netrin-1 Reduces Monocyte and Macrophage Chemotaxis towards the Complement Component C5a. *PLoS One*. **11**, e0160685 (2016).

268. M. Penzo, D. M. Habiel, M. Ramadass, R. R. Kew, K. B. Marcu, Cell migration to CXCL12 requires simultaneous IKKα and IKKβ-dependent NF-κB signaling. *Biochim. Biophys. Acta - Mol. Cell Res.* **1843**, 1796–1804 (2014).

269. S. E. Webb, J. W. Pollard, G. E. Jones, Direct observation and quantification of macrophage chemoattraction to the growth factor CSF-1. *J. Cell Sci.* **109**, 793–803 (1996).

270. M. Y. Murray, T. P. Birkland, J. D. Howe, A. D. Rowan, M. Fidock, W. C. Parks, J. Gavrilovic, Macrophage Migration and Invasion Is Regulated by MMP10 Expression. *PLoS One*. **8**, e63555 (2013).

271. M. L. Gruen, M. Hao, D. W. Piston, A. H. Hasty, Leptin requires canonical migratory signaling pathways for induction of monocyte and macrophage chemotaxis. *Am J Physiol Cell Physiol*. **293**, 1481–1488 (2007).

272. A. J. Iqbal, D. Regan-Komito, I. Christou, G. E. White, E. McNeill, A. Kenyon, L. Taylor, T. S. Kapellos, E. A. Fisher, K. M. Channon, D. R. Greaves, A real time chemotaxis assay unveils unique migratory profiles amongst different primary murine macrophages. *PLoS One*. **8**, e58744 (2013).

273. E. Van Goethem, R. Poincloux, F. Gauffre, I. Maridonneau-Parini, V. Le Cabec, Matrix Architecture Dictates Three-Dimensional Migration Modes of Human Macrophages: Differential Involvement of Proteases and Podosome-Like Structures. *J. Immunol.* **184**, 1049–1061 (2010).

274. K. Talkenberger, E. Ada Cavalcanti-Adam, A. Voss-Böhme, A. Deutsch, Amoeboid-mesenchymal migration plasticity promotes invasion only in complex heterogeneous microenvironments. *Sci. Rep.* **7** (2017), doi:10.1038/s41598-017-09300-3.

275. C. Cougoule, E. Van Goethem, V. Le Cabec, F. Lafouresse, L. Dupré, V. Mehraj, J. L. Mège, C. Lastrucci, I. Maridonneau-Parini, Blood leukocytes and macrophages of various phenotypes have distinct abilities to form podosomes and to migrate in 3D environments. *Eur. J. Cell Biol.* **91**, 938–949 (2012).

276. C. Grabher, A. Cliffe, K. Miura, J. Hayflick, R. Pepperkok, P. Rørth, J. Wittbrodt, Birth and life of tissue macrophages and their migration in embryogenesis and inflammation in medaka. *J. Leukoc. Biol.* **81**, 263–271 (2007).

277. D. Y. S. Vogel, P. D. A. M. Heijnen, M. Breur, H. E. de Vries, A. T. J. Tool, S. Amor, C. D. Dijkstra, Macrophages migrate in an activation-dependent manner to chemokines involved in neuroinflammation. *J. Neuroinflammation*. **11**, 23 (2014).

278. J. Renkawitz, A. Kopf, J. Stopp, I. de Vries, M. K. Driscoll, J. Merrin, R. Hauschild, E. S. Welf, G. Danuser, R. Fiolka, M. Sixt, Nuclear positioning facilitates amoeboid migration along the path of least resistance. *Nature*. **568**, 546–550 (2019).

279. A. J. Iqbal, E. McNeill, T. S. Kapellos, D. Regan-Komito, S. Norman, S. Burd, N. Smart, D. E. W. Machemer, E. Stylianou, H. McShane, K. M. Channon, A. Chawla, D. R. Greaves, Human CD68 promoter GFP

transgenic mice allow analysis of monocyte to macrophage differentiation in vivo. *Blood*. **124**, e33–e44 (2014).

280. P. J. Gough, S. Gordon, D. R. Greaves, The use of human CD68 transcriptional regulatory sequences to direct high-level expression of class A scavenger receptor in macrophages in vitro and in vivo. *Immunology*. **103**, 351–361 (2001).

281. C. mun Chen, J. Krohn, S. Bhattacharya, B. Davies, A comparison of exogenous promoter activity at the ROSA26 locus using a ΦiC31 integrase mediated cassette exchange approach in mouse ES cells. *PLoS One*. **6** (2011), doi:10.1371/JOURNAL.PONE.0023376.

282. H. Dolatshad, D. Biggs, R. Diaz, N. Hortin, C. Preece, B. Davies, A versatile transgenic allele for mouse overexpression studies. *Mamm. Genome*. **26**, 598–608 (2015).

283. I. Park, M. E. Goddard, J. E. Cole, N. Zanin, L.-P. P. Lyytikäinen, T. Lehtimäki, E. Andreakos, M. Feldmann, I. Udalova, I. Drozdov, C. Monaco, C-type lectin receptor CLEC4A2 promotes tissue adaptation of macrophages and protects against atherosclerosis. **13** (2022), doi:10.1038/s41467-021-27862-9.

284. N. M. Oliveira, K. R. Foster, W. M. Durham, *Proc. Natl. Acad. Sci.*, in press, doi:10.1073/pnas.1600760113.

285. P. J. Murray, T. A. Wynn, Protective and pathogenic functions of macrophage subsets. *Nat. Rev. Immunol. 2011 1111*. **11**, 723–737 (2011).

286. L. Chávez-Galán, M. L. Olleros, D. Vesin, I. Garcia, Much more than M1 and M2 macrophages, there are also CD169+ and TCR+ macrophages. *Front. Immunol.* **6**, 263 (2015).

287. T. A. Wynn, A. Chawla, J. W. Pollard, Macrophage biology in development, homeostasis and disease. *Nat. 2013 4967446*. **496**, 445–455 (2013).

288. W. L. Breslin, K. Strohacker, K. C. Carpenter, D. L. Haviland, B. K. McFarlin, Mouse blood monocytes: Standardizing their identification and analysis using CD115. *J. Immunol. Methods*. **390**, 1–8 (2013).

289. J. K. Ma, M. Y. Platt, J. Eastham-Anderson, J. S. Shin, I. Mellman, MHC class II distribution in dendritic cells and B cells is determined by ubiquitin chain length. *Proc. Natl. Acad. Sci. U. S. A.* **109**, 8820–8827 (2012).

290. B. E. Clausen, C. Burkhardt, W. Reith, R. Renkawitz, I. Förster, Conditional gene targeting in macrophages and granulocytes using LysMcre mice. *Transgenic Res.* **8**, 265–277 (1999).

291. K. Grabert, A. Sehgal, K. M. Irvine, E. Wollscheid-Lengeling, D. D. Ozdemir, J. Stables, G. A. Luke, M. D. Ryan, A. Adamson, N. E. Humphreys, C. J. Sandrock, R. Rojo, V. A. Verkasalo, W. Mueller, P. Hohenstein, A. R. Pettit, C. Pridans, D. A. Hume, A Transgenic Line That Reports CSF1R Protein Expression Provides a Definitive Marker for the Mouse Mononuclear Phagocyte System. *J. Immunol.* **205**, 3154–3166 (2020).

292. C. L. Holness, R. P. Da Silva, J. Fawcett, S. Gordon, D. L. Simmons, Macrosialin, a mouse macrophage-restricted glycoprotein, is a member of the lamp/lgp family. *J. Biol. Chem.* **268**, 9661–9666 (1993).

293. D. A. Chistiakov, M. C. Killingsworth, V. A. Myasoedova, A. N. Orekhov, Y. V. Bobryshev, CD68/macrosialin: not just a histochemical marker. *Lab. Investig. 2017 971*. **97**, 4–13 (2016).

294. D. O'Reilly, C. M. Quinn, T. El-Shanawany, S. Gordon, D. R. Greaves, Multiple Ets Factors and Interferon Regulatory Factor-4 Modulate CD68 Expression in a Cell Type-specific Manner. *J. Biol. Chem.* **278**, 21909–21919 (2003).

295. D. R. Greaves, S. Gordon, Macrophage-Specific Gene Expression: Current Paradigms and Future Challenges. *Int. J. Hematol. 2002 761*. **76**, 6–15 (2002).

296. A. C. Li, F. R. B. Guidez, J. G. Collier, C. K. Glass, The Macrosialin Promoter Directs High Levels of Transcriptional Activity in Macrophages Dependent on Combinatorial Interactions between PU.1 and c-Jun. *J. Biol. Chem.* **273**, 5389–5399 (1998).

297. C. Langlet, S. Tamoutounour, S. Henri, H. Luche, L. Ardouin, C. Grégoire, B. Malissen, M. Guilliams, CD64 Expression Distinguishes Monocyte-Derived and Conventional Dendritic Cells and Reveals Their Distinct

Role during Intramuscular Immunization. *J. Immunol.* **188**, 1751–1760 (2012).

298. E. Allen, A. C. Bakke, M. Z. Purtzer, A. Deodhar, Neutrophil CD64 expression: distinguishing acute inflammatory autoimmune disease from systemic infections. *Ann. Rheum. Dis.* **61**, 522–525 (2002).

299. W. K. Kim, C. M. McGary, G. E. Holder, A. R. Filipowicz, M. M. Kim, H. A. Beydoun, Y. Cai, X. Liu, C. Sugimoto, M. J. Kuroda, Increased Expression of CD169 on Blood Monocytes and Its Regulation by Virus and CD8 T Cells in Macaque Models of HIV Infection and AIDS. *AIDS Res. Hum. Retroviruses*. **31**, 696 (2015).

300. Y. Uchida, G. Nishitai, K. Kikuchi, T. Shibuya, K. Asano, M. Tanaka, CD204-positive monocytes and macrophages ameliorate septic shock by suppressing proinflammatory cytokine production in mice. *Biochem. Biophys. Reports*. **23**, 100791 (2020).

301. A. dos Anjos Cassado, F4/80 as a major macrophage marker: The case of the peritoneum and spleen. *Results Probl. Cell Differ.* **62**, 161–179 (2017).

302. A. Meghraoui-Kheddar, S. Barthelemy, A. Boissonnas, C. Combadière, Revising CX3CR1 Expression on Murine Classical and Non-classical Monocytes. *Front. Immunol.* **11**, 1117 (2020).

303. R. Dong, M. Zhang, Q. Hu, S. Zheng, A. Soh, Y. Zheng, H. Yuan, Galectin-3 as a novel biomarker for disease diagnosis and a target for therapy (Review). *Int. J. Mol. Med.* **41**, 599–614 (2018).

304. R. P. Da Silva, S. Gordon, Phagocytosis stimulates alternative glycosylation of macrosialin (mouse CD68), a macrophage-specific endosomal protein. *Biochem. J*. **338**, 687–694 (1999).

305. H. Yoshida, O. Quehenberger, N. Kondratenko, S. Green, D. Steinberg, Minimally Oxidized Low-Density Lipoprotein Increases Expression of Scavenger Receptor A, CD36, and Macrosialin in Resident Mouse Peritoneal Macrophages. *Arterioscler. Thromb. Vasc. Biol.* **18**, 794–802 (1998).

306. S. Zeibig, M. Büttcher, S. Goebel, J. Pauli, A. Hunger, M. Ungerer, M. Gawaz, G. Münch, The scavenger receptor CD68 regulates platelet mediated oxidized low-density lipoprotein (oxLDL) deposition in atherosclerotic vessels at an early stage of atherosclerosis in LDLr-/-/ApoBec-/- mice. *Cell. Physiol. Biochem.* **52**, 681–695 (2019).

307. M. C. De Beer, Z. Zhao, N. R. Webb, D. R. Van der Westhuyzen, W. J. S. De Villiers, Lack of a direct role for macrosialin in oxidized LDL metabolism. *J. Lipid Res.* **44**, 674–685 (2003).

308. L. Song, C. Lee, C. Schindler, Deletion of the murine scavenger receptor CD68. *J. Lipid Res.* **52**, 1542–1550 (2011).

309. I. E. Papageorgiou, A. Lewen, L. V. Galow, T. Cesetti, J. Scheffel, T. Regen, U. K. Hanisch, O. Kann, TLR4-activated microglia require IFN-γ to induce severe neuronal dysfunction and death in situ. *Proc. Natl. Acad. Sci. U. S. A.* **113**, 212–217 (2016).

310. X. P. Lin, N. Almqvist, E. Telemo, Human small intestinal epithelial cells constitutively express the key elements for antigen processing and the production of exosomes. *Blood Cells. Mol. Dis.* **35**, 122–128 (2005).

311. S. J. Cha, K. Park, P. Srinivasan, C. W. Schindler, N. Van Rooijen, M. Stins, M. Jacobs-Lorena, CD68 acts as a major gateway for malaria sporozoite liver infection. *J. Exp. Med.* **212**, 1391–1403 (2015).

312. Y. H. Ni, L. Ding, X. F. Huang, Y. chun Dong, Q. G. Hu, Y. Y. Hou, Microlocalization of CD68+ tumor-associated macrophages in tumor stroma correlated with poor clinical outcomes in oral squamous cell carcinoma patients. *Tumor Biol.* **36**, 5291–5298 (2015).

313. A. Nagy, Cre Recombinase: The Universal Reagent for Genome Tailoring (2000), doi:10.1002/(SICI)1526-968X(200002)26:2.

314. H. Kim, M. Kim, S.-K. Im, S. Fang, Mouse Cre-LoxP system: general principles to determine tissue-specific roles of target genes Cre-loxP System. *Lab Anim Res*. **34**, 147–159 (2018).

315. I. Dragatsis, S. Zeitlin, A method for the generation of conditional gene repair mutations in mice. *Nucleic*

Acids Res. **29**, e10 (2001).

316. J. Brocard, X. Warot, O. Wendling, N. Messaddeq, J. L. Vonesch, P. Chambon, D. Metzger, Spatio-temporally controlled site-specific somatic mutagenesis in the mouse. *Proc. Natl. Acad. Sci. U. S. A.* **94**, 14559–14563 (1997).

317. A. K. Indra, X. Warot, J. Brocard, J.-M. Bornert, J.-H. Xiao, P. Chambon, D. Metzger, Temporally-controlled site-specific mutagenesis in the basal layer of the epidermis: comparison of the recombinase activity of the tamoxifen-inducible Cre-ER T and Cre-ER T2 recombinases. *Nucleic Acids Res.* **27**, 4324–4327 (1999).

318. R. S. Donocoff, N. Teteloshvili, H. Chung, R. Shoulson, R. J. Creusot, Optimization of tamoxifen-induced Cre activity and its effect on immune cell populations. *Sci. Reports 2020 101*. **10**, 1–12 (2020).

319. C. J. Bult, J. A. Blake, C. L. Smith, J. A. Kadin, J. E. Richardson, A. Anagnostopoulos, R. Asabor, R. M. Baldarelli, J. S. Beal, S. M. Bello, O. Blodgett, N. E. Butler, K. R. Christie, L. E. Corbani, J. Creelman, M. E. Dolan, H. J. Drabkin, S. L. Giannatto, P. Hale, D. P. Hill, M. Law, A. Mendoza, M. McAndrews, D. Miers, H. Motenko, L. Ni, H. Onda, M. Perry, J. M. Recla, B. Richards-Smith, D. Sitnikov, M. Tomczuk, G. Tonorio, L. Wilming, Y. Zhu, Mouse Genome Database (MGD) 2019. *Nucleic Acids Res.* **47**, D801–D806 (2019).

320. D. R. Greaves, C. M. Quinn, M. F. Seldin, S. Gordon, Functional comparison of the murine macrosialin and human CD68 promoters in macrophage and nonmacrophage cell lines. *Genomics*. **54**, 165–168 (1998).

321. M. M. Pillai, B. Hayes, B. Torok-Storb, Inducible transgenes under the control of the hCD68 promoter identifies mouse macrophages with a distribution that differs from the F4/80 and CSF-1R expressing populations. *Exp. Hematol.* **37**, 1387 (2009).

322. T. Turner-Stokes, A. G. Diaz, D. Pinheiro, M. Prendecki, S. P. McAdoo, C. Roufosse, H. Terence Cook, C. D. Pusey, K. J. Woollard, Live imaging of monocyte subsets in immune complex-mediated glomerulonephritis reveals distinct phenotypes and effector functions. *J. Am. Soc. Nephrol.* **31**, 2523–2542 (2020).

323. R. Lang, R. L. Rutschman, D. R. Greaves, P. J. Murray, Autocrine Deactivation of Macrophages in Transgenic Mice Constitutively Overexpressing IL-10 Under Control of the Human CD68 Promoter. *J. Immunol.* **168**, 3402–3411 (2002).

324. J. M. Vieira, S. Norman, C. V. Del Campo, T. J. Cahill, D. N. Barnette, M. Gunadasa-Rohling, L. A. Johnson, D. R. Greaves, C. A. Carr, D. G. Jackson, P. R. Riley, The cardiac lymphatic system stimulates resolution of inflammation following myocardial infarction. *J. Clin. Invest.* **128**, 3402–3412 (2018).

325. F. C. Simões, T. J. Cahill, A. Kenyon, D. Gavriouchkina, J. M. Vieira, X. Sun, D. Pezzolla, C. Ravaud, E. Masmanian, M. Weinberger, S. Mayes, M. E. Lemieux, D. N. Barnette, M. Gunadasa-Rohling, R. M. Williams, D. R. Greaves, L. A. Trinh, S. E. Fraser, S. L. Dallas, R. P. Choudhury, T. Sauka-Spengler, P. R. Riley, Macrophages directly contribute collagen to scar formation during zebrafish heart regeneration and mouse heart repair. *Nat. Commun.* **11** (2020), doi:10.1038/S41467-019-14263-2.

326. E. McNeill, A. J. Iqbal, D. Jones, J. Patel, P. Coutinho, L. Taylor, D. R. Greaves, K. M. Channon, Tracking Monocyte Recruitment and Macrophage Accumulation in Atherosclerotic Plaque Progression Using a Novel hCD68GFP/ApoE-/- Reporter Mouse-Brief Report. *Arterioscler. Thromb. Vasc. Biol.* **37**, 258–263 (2017).

327. K. Rahman, Y. Vengrenyuk, S. A. Ramsey, N. R. Vila, N. M. Girgis, J. Liu, V. Gusarova, J. Gromada, A. Weinstock, K. J. Moore, P. Loke, E. A. Fisher, Inflammatory Ly6Chi monocytes and their conversion to M2 macrophages drive atherosclerosis regression. *J. Clin. Invest.* **127**, 2904–2915 (2017).

328. K. Franke, J. Kalucka, S. Mamlouk, R. P. Singh, A. Muschter, A. Weidemann, V. Iyengar, S. Jahn, K. Wieczorek, K. Geiger, M. Muders, A. M. Sykes, D. M. Poitz, T. Ripich, T. Otto, S. Bergmann, G. Breier, G. Baretton, G. H. Fong, D. R. Greaves, S. Bornstein, T. Chavakis, M. G. Joachim Fandrey, B. Wielockx, HIF-1α is a protective factor in conditional PHD2-deficient mice suffering from severe HIF-2α–induced excessive erythropoiesis. *Blood*. **121**, 1436–1445 (2013).

329. C. L. Abram, G. L. Roberge, Y. Hu, C. A. Lowell, Comparative analysis of the efficiency and specificity of myeloid-Cre deleting strains using ROSA-EYFP reporter mice. *J. Immunol. Methods*. **408**, 89–100 (2014).

330. J. Shi, L. Hua, D. Harmer, P. Li, G. Ren, in *Methods in Molecular Biology* (Humana Press Inc., 2018; https://link.springer.com/protocol/10.1007/978-1-4939-7837-3_24), vol. 1784, pp. 263–275.

331. N. Faust, F. Varas, L. M. Kelly, S. Heck, T. Graf, Insertion of enhanced green fluorescent protein into the lysozyme gene creates mice with green fluorescent granulocytes and macrophages. *Blood*. **96**, 719–726 (2000).

332. R. T. Sasmono, D. Oceandy, J. W. Pollard, W. Tong, P. Pavli, B. J. Wainwright, M. C. Ostrowski, S. R. Himes, D. A. Hume, A macrophage colony-stimulating factor receptor–green fluorescent protein transgene is expressed throughout the mononuclear phagocyte system of the mouse. *Blood*. **101**, 1155–1163 (2003).

333. L. Deng, J. F. Zhou, R. S. Sellers, J. F. Li, A. V. Nguyen, Y. Wang, A. Orlofsky, Q. Liu, D. A. Hume, J. W. Pollard, L. Augenlicht, E. Y. Lin, A Novel Mouse Model of Inflammatory Bowel Disease Links Mammalian Target of Rapamycin-Dependent Hyperproliferation of Colonic Epithelium to Inflammation-Associated Tumorigenesis. *Am. J. Pathol.* **176**, 952–967 (2010).

334. N. Mossadegh-Keller, S. Sarrazin, P. K. Kandalla, L. Espinosa, E. Richard Stanley, S. L. Nutt, J. Moore, M. H. Sieweke, M-CSF instructs myeloid lineage fate in single haematopoietic stem cells. *Nat. 2013 4977448*. **497**, 239–243 (2013).

335. S. Jung, J. Aliberti, P. Graemmel, M. J. Sunshine, G. W. Kreutzberg, A. Sher, D. R. Littman, Analysis of Fractalkine Receptor CX 3 CR1 Function by Targeted Deletion and Green Fluorescent Protein Reporter Gene Insertion . *Mol. Cell. Biol.* **20**, 4106–4114 (2000).

336. M. Ferron, J. Vacher, Targeted expression of Cre recombinase in macrophages and osteoclasts in transgenic mice. *genesis*. **41**, 138–145 (2005).

337. E. Schaller, A. J. Macfarlane, R. A. Rupec, S. Gordon, A. J. McKnight, K. Pfeffer, Inactivation of the F4/80 Glycoprotein in the Mouse Germ Line. *Mol. Cell. Biol.* **22**, 8035–8043 (2002).

338. F. Jardí, M. R. Laurent, V. Dubois, R. Khalil, L. Deboel, D. Schollaert, L. Van Den Bosch, B. Decallonne, G. Carmeliet, F. Claessens, D. Vanderschueren, A shortened tamoxifen induction scheme to induce CreER recombinase without side effects on the male mouse skeleton. *Mol. Cell. Endocrinol.* **452**, 57–63 (2017).

339. R. Ye, Q. A. Wang, C. Tao, L. Vishvanath, M. Shao, J. G. McDonald, R. K. Gupta, P. E. Scherer, Impact of tamoxifen on adipocyte lineage tracing: Inducer of adipogenesis and prolonged nuclear translocation of Cre recombinase. *Mol. Metab.* **4**, 771–778 (2015).

340. H. M. Jahn, C. V. Kasakow, A. Helfer, J. Michely, A. Verkhratsky, H. H. Maurer, A. Scheller, F. Kirchhoff, Refined protocols of tamoxifen injection for inducible DNA recombination in mouse astroglia. *Sci. Reports 2018 81*. **8**, 1–11 (2018).

341. S. Daemen, M. M. Chan, J. D. Schilling, Comprehensive analysis of liver macrophage composition by flow cytometry and immunofluorescence in murine NASH. *STAR Protoc.* **2** (2021), doi:10.1016/J.XPRO.2021.100511.

342. S. Travaglione, L. Falzano, A. Fabbri, A. Stringaro, S. Fais, C. Fiorentini, Epithelial cells and expression of the phagocytic marker CD68: scavenging of apoptotic bodies following Rho activation. *Toxicol. Vitr.* **16**, 405–411 (2002).

343. M. M. Bjørklund, A. K. Hollensen, M. K. Hagensen, F. Dagnæs-Hansen, C. Christoffersen, J. G. Mikkelsen, J. F. Bentzon, Induction of atherosclerosis in mice and hamsters without germline genetic engineering. *Circ. Res.* **114**, 1684–1689 (2014).

344. C. C. Bain, D. A. Gibson, N. J. Steers, K. Boufea, P. A. Louwe, C. Doherty, V. González-Huici, R. Gentek, M. Magalhaes-Pinto, T. Shaw, M. Bajénoff, C. Bénézech, S. R. Walmsley, D. H. Dockrell, P. T. K Saunders, N. N. Batada, S. J. Jenkins, "Rate of replenishment and microenvironment contribute to the sexually dimorphic phenotype and function of peritoneal macrophages" (2020), (available at http://immunology.sciencemag.org/).

345. S. Gordon, P. R. Taylor, Monocyte and macrophage heterogeneity. *Nat. Rev. Immunol. 2005 512*. **5**, 953–964 (2005).

346. A. Amanzada, I. Ahmed Malik, M. Blaschke, S. Khan, H. Rahman, G. Ramadori, F. Moriconi, Identification of CD68+ neutrophil granulocytes in in vitro model of acute inflammation and inflammatory bowel disease. *Int. J. Clin. Exp. Pathol.* **6**, 561 (2013).

347. D. L. Kline, E. E. Cliffton, Lifespan of leucocytes in man. *J. Appl. Physiol.* **5**, 79–84 (1952).

348. E. McNeill, A. J. Iqbal, D. Jones, J. Patel, P. Coutinho, L. Taylor, D. R. Greaves, K. M. Channon, Tracking monocyte recruitment and macrophage accumulation in atherosclerotic plaque progression using a novel hCD68GFP/ApoE -/- reporter mouse - Brief report. *Arterioscler. Thromb. Vasc. Biol.* **37**, 258–263 (2017).

349. A. L. McCubbrey, K. C. Allison, A. B. Lee-Sherick, C. V. Jakubzick, W. J. Janssen, Promoter Specificity and Efficacy in Conditional and Inducible Transgenic Targeting of Lung Macrophages. *Front. Immunol.* **8**, 24 (2017).

350. H. Bouabe, K. Okkenhaug, Gene Targeting in Mice: a Review. *Methods Mol. Biol.* **1064**, 315 (2013).

351. B. Zheng, M. Sage, E. A. Sheppeard, V. Jurecic, A. Bradley, Engineering Mouse Chromosomes with Cre-loxP: Range, Efficiency, and Somatic Applications. *Mol. Cell. Biol.* **20**, 648 (2000).

352. A. J. Song, R. D. Palmiter, Detecting and Avoiding Problems When Using the Cre/lox System. *Trends Genet.* **34**, 333 (2018).

353. F. Ijaz, K. Ikegami, Knock-in of Labeled Proteins into 5'UTR Enables Highly Efficient Generation of Stable Cell Lines. *Cell Struct. Funct.* **46**, 21–35 (2021).

354. Y. Liu, J. Hermes, J. Li, M. Tudor, Endogenous locus reporter assays. *Methods Mol. Biol.* **1755**, 163–177 (2018).

355. W. Pu, L. He, X. Han, X. Tian, Y. Li, H. Zhang, Q. Liu, X. Huang, L. Zhang, Q. D. Wang, Z. Yu, X. Yang, N. Smart, B. Zhou, Genetic targeting of organ-specifc blood vessels. *Circ. Res.* **123**, 86–99 (2018).

356. H. Jin, K. Liu, J. Tang, X. Huang, H. Wang, Q. Zhang, H. Zhu, Y. Li, W. Pu, H. Zhao, L. He, Y. Li, S. Zhang, Z. Zhang, Y. Zhao, Y. Qin, S. Pflanz, K. E. I. Kasmi, W. Zhang, Z. Liu, F. Ginhoux, Y. Ji, B. He, L. Wang, B. Zhou, Genetic fate-mapping reveals surface accumulation but not deep organ invasion of pleural and peritoneal cavity macrophages following injury. *Nat. Commun. 2021 121*. **12**, 1–15 (2021).

357. X. Han, Z. Zhang, L. He, H. Zhu, Y. Li, W. Pu, M. Han, H. Zhao, K. Liu, Y. Li, X. Huang, M. Zhang, H. Jin, Z. Lv, J. Tang, J. Wang, R. Sun, J. Fei, X. Tian, S. Duan, Q. D. Wang, L. Wang, B. He, B. Zhou, A suite of new Dre recombinase drivers markedly expands the ability to perform intersectional genetic targeting. *Cell Stem Cell*. **28**, 1160-1176.e7 (2021).

358. G. B. Ryan, G. Majno, *Inflammation* (The Upjohn Company, Kalamazoo, 1977).

359. H. Harris, Role of chemotaxis in inflammation. *Physiol. Rev.* **34**, 529–562 (1954).

360. R. Snyderman, S. E. Mergenhagen, in *Immunobiology of the Macrophage*, D. S. Nelson, Ed. (Academic Press, Inc., 1976), pp. 323–350.

361. H. Harris, Chemotaxis of granulocytes. *J. Pathol. Bacteriol.* **LX**, 135–146 (1953).

362. S. Boyden, The chemotactic effect of mixtures of antibody and antigen on polymorphonuclear leucocytes. *J. Exp. Med.* **115**, 453–466 (1962).

363. L. P. Bignold, Measurement of chemotaxis of polymorphonuclear leukocytes in vitro. The problems of the control of gradients of chemotactic factors, of the control of the cells and of the separation of chemotaxis from chemokinesis. *J. Immunol. Methods*. **108**, 1–18 (1988).

364. E. K. Frow, J. Reckless, D. J. Grainger, Tools for anti-inflammatory drug design: in vitro models of leukocyte migration. *Med Res Rev*. **24**, 276–298 (2004).

365. A. R. Dwyer, L. G. Ellies, A. L. Holme, F. J. Pixley, A three-dimensional co-culture system to investigate macrophage-dependent tumor cell invasion. *J. Biol. Methods*. **3**, e49 (2016).

366. G. Zhou, H. Loppnow, T. Groth, A macrophage/fibroblast co-culture system using a cell migration chamber to study inflammatory effects of biomaterials. *Acta Biomater.* **26**, 54–63 (2015).

367. S. Mi, Z. Du, Y. Xu, Z. Wu, X. Qian, M. Zhang, W. Sun, Microfluidic co-culture system for cancer migratory analysis and anti-metastatic drugs screening. *Sci. Reports 2016 61*. **6**, 1–11 (2016).

368. S. Chung, R. Sudo, P. J. MacK, C. R. Wan, V. Vickerman, R. D. Kamm, Cell migration into scaffolds under co-culture conditions in a microfluidic platform. *Lab Chip*. **9**, 269–275 (2009).

369. C. Venter, C. Niesler, A triple co-culture method to investigate the effect of macrophages and fibroblasts on myoblast proliferation and migration. *Biotechniques*. **64**, 52–58 (2018).

370. J. Chakrabarti, M. Dua-Awereh, M. Schumacher, A. Engevik, J. Hawkins, M. A. Helmrath, Y. Zavros, Sonic Hedgehog acts as a macrophage chemoattractant during regeneration of the gastric epithelium. *npj Regen. Med. 2022 71*. **7**, 1–16 (2022).

371. A. P. Gee, Advantages and limitations of methods for measuring cellular chemotaxis and chemokinesis. *Mol. Cell. Biochem.* **62**, 5–11 (1984).

372. W. Falk, R. H. Goodwin, E. J. Leonard, A 48-well micro chemotaxis assembly for rapid and accurate measurement of leukocyte migration. *J. Immunol. Methods*. **33**, 239–247 (1980).

373. S. H. Zigmond, Ability of polymorphonuclear leukocytes to orient in gradients of chemotactic factors. *J. Cell Biol.* **75**, 606–616 (1977).

374. D. Zicha, G. A. Dunn, A. F. Brown, A new direct-viewing chemotaxis chamber. *J. Cell Sci.* **99** (1991).

375. D. Lauffenburger, C. Rothman, S. H. Zigmond, Measurement of leukocyte motility and chemotaxis parameters with a linear under-agarose migration assay. *J. Immunol.* **131**, 940–7 (1983).

376. P. Zengel, A. Nguyen-Hoang, C. Schildhammer, R. Zantl, V. Kahl, E. Horn, µ-Slide Chemotaxis: A new chamber for long-term chemotaxis studies. *BMC Cell Biol.* **12**, 21 (2011).

377. E. Berthier, E. W. K. Young, D. Beebe, Engineers are from PDMS-land, Biologists are from Polystyrenia. *Lab Chip*. **12**, 1224 (2012).

378. L. Tweedy, P. A. Thomason, P. I. Paschke, K. Martin, L. M. Machesky, M. Zagnoni, R. H. Insall, Seeing around corners: Cells solve mazes and respond at a distance using attractant breakdown. *Science*. **369** (2020), doi:10.1126/science.aay9792.

379. E. K. Sackmann, A. L. Fulton, D. J. Beebe, The present and future role of microfluidics in biomedical research. *Nature*. **507**, 181–189 (2014).

380. E. Berthier, A. M. Dostie, U. N. Lee, J. Berthier, A. B. Theberge, Open Microfluidic Capillary Systems. *Anal. Chem.* **91**, 8739 (2019).

381. J. Yu, E. Berthier, A. Craig, T. E. de Groot, S. Sparks, P. N. Ingram, D. F. Jarrard, W. Huang, D. J. Beebe, A. B. Theberge, Reconfigurable open microfluidics for studying the spatiotemporal dynamics of paracrine signalling. *Nat. Biomed. Eng.* **3**, 830 (2019).

382. E. J. Walsh, A. Feuerborn, J. H. R. Wheeler, A. Na Tan, W. M. Durham, K. R. Foster, P. R. Cook, A. N. Tan, W. M. Durham, K. R. Foster, P. R. Cook, Microfluidics with fluid walls. *Nat. Commun.* **8**, 816 (2017).

383. C. Soitu, A. Feuerborn, A. N. Tan, H. Walker, P. A. Walsh, A. A. Castrejón-Pita, P. R. Cook, E. J. Walsh, Microfluidic chambers using fluid walls for cell biology. *Proc. Natl. Acad. Sci. U. S. A.* **115**, E5926–E5933 (2018).

384. C. Deroy, F. Nebuloni, P. R. Cook, E. J. Walsh, C. Deroy, F. Nebuloni, E. J. Walsh, P. R. Cook, Microfluidics on Standard Petri Dishes for Bioscientists. *Small Methods*. **5**, 2100724 (2021).

385. C. Deroy, N. Stovall-Kurtz, F. Nebuloni, C. Soitu, P. R. Cook, E. J. Walsh, Predicting flows through

microfluidic circuits with fluid walls. *Microsystems Nanoeng. 2021 71*. **7**, 1–9 (2021).

386. C.-Y. Liao, M. J. Song, Y. Gao, A. S. Mauer, A. Revzin, H. Malhi, Hepatocyte-Derived Lipotoxic Extracellular Vesicle Sphingosine 1-Phosphate Induces Macrophage Chemotaxis. *Front. Immunol.* **9**, 2980 (2018).

387. P. Pakshir, M. Alizadehgiashi, B. Wong, N. M. Coelho, X. Chen, Z. Gong, V. B. Shenoy, C. McCulloch, B. Hinz, Dynamic fibroblast contractions attract remote macrophages in fibrillar collagen matrix. *Nat. Commun.* **10**, 1–17 (2019).

388. C. Soitu, N. Stovall-Kurtz, C. Deroy, A. A. Castrejón-Pita, P. R. Cook, E. J. Walsh, Jet-Printing Microfluidic Devices on Demand. *Adv. Sci.* (2020), doi:10.1002/advs.202001854.

389. L. E. Hind, J. L. Mackay, D. Cox, D. A. Hammer, Two-dimensional motility of a macrophage cell line on microcontact-printed fibronectin. *Cytoskeleton*. **71**, 542–554 (2014).

390. E. Um, J. M. Oh, J. Park, T. Song, T.-E. Kim, Y. Choi, C. Shin, D. Kolygina, J.-H. Jeon, B. A. Grzybowski, Y.-K. Cho, Immature dendritic cells navigate microscopic mazes to find tumor cells. *Lab Chip*. **19**, 1665–1675 (2019).

391. R. R. Kay, P. Langridge, D. Traynor, O. Hoeller, Changing directions in the study of chemotaxis. *Nat. Rev. Mol. Cell Biol. 2008 96*. **9**, 455–463 (2008).

392. A. Sagar, W. Dai, M. Minot, R. LeCover, J. D. Varner, Reduced order modeling and analysis of the human complement system. *PLoS One*. **12**, e0187373 (2017).

393. H. O. J. Morad, S. C. Belete, T. Read, A. M. Shaw, Time-course analysis of C3a and C5a quantifies the coupling between the upper and terminal Complement pathways in vitro. *J. Immunol. Methods*. **427**, 13–18 (2015).

394. D. A. Guertin, D. M. Sabatini, Cell Size Control. *eLS* (2006), doi:10.1038/NPG.ELS.0003359.

395. L. Tweedy, O. Susanto, R. H. Insall, Self-generated chemotactic gradients-cells steering themselves. *Curr. Opin. Cell Biol.* **42**, 46–51 (2016).

396. K. Kienle, K. M. Glaser, S. Eickhoff, M. Mihlan, K. Knöpper, E. Reátegui, M. W. Epple, M. Gunzer, R. Baumeister, T. K. Tarrant, R. N. Germain, D. Irimia, W. Kastenmüller, T. Lämmermann, Neutrophils self-limit swarming to contain bacterial growth in vivo. *Science (80-.).* **372** (2021), doi:10.1126/SCIENCE.ABE7729.

397. S. Uderhardt, A. J. Martins, J. S. Tsang, T. Lämmermann, R. N. Germain, Resident Macrophages Cloak Tissue Microlesions to Prevent Neutrophil-Driven Inflammatory Damage. *Cell*. **177**, 541–555 (2019).

398. C. A. Parent, P. N. Devreotes, A Cell's Sense of Direction. *Science (80-.).* **284**, 765–769 (1999).

399. C. E. Petrie Aronin, Y. M. Zhao, J. S. Yoon, N. Y. Morgan, T. Prüstel, R. N. Germain, M. Meier-Schellersheim, Migrating Myeloid Cells Sense Temporal Dynamics of Chemoattractant Concentrations. *Immunity*. **47**, 862-874.e3 (2017).

400. M. A. Qasaimeh, M. Pyzik, M. Astolfi, S. M. Vidal, D. Juncker, Neutrophil Chemotaxis in Moving Gradients. *Adv. Biosyst.* **2**, 1700243 (2018).

401. R. J. Petrie, K. M. Yamada, Fibroblasts Lead the Way: A Unified View of 3D Cell Motility. *Trends Cell Biol.* **25** (2015), pp. 666–674.

402. D. Lucy, G. S. D. Purvis, L. Zeboudj, M. Chatzopoulou, C. Recio, C. J. R. Bataille, G. M. Wynne, D. R. Greaves, A. J. Russell, A Biased Agonist at Immunometabolic Receptor GPR84 Causes Distinct Functional Effects in Macrophages. *ACS Chem. Biol.* **14**, 2055–2064 (2019).

403. G. Digiacomo, I. Tusa, M. Bacci, M. G. Cipolleschi, P. Dello Sbarba, E. Rovida, Fibronectin induces macrophage migration through a SFK-FAK/CSF-1R pathway. *Cell Adhes. Migr.* **11**, 327–337 (2017).

404. A. J. Iqbal, E. McNeill, T. S. Kapellos, D. Regan-Komito, S. Norman, S. Burd, N. Smart, D. E. W. Machemer, E. Stylianou, H. McShane, K. M. Channon, A. Chawla, D. R. Greaves, Human CD68 promoter GFP

transgenic mice allow analysis of monocyte to macrophage differentiation in vivo. *Blood*. **124**, e33–e44 (2014).

405. F. Burger, D. Baptista, A. Roth, K. J. Brandt, R. F. da Silva, F. Montecucco, F. Mach, K. Miteva, Single-Cell RNA-Seq Reveals a Crosstalk between Hyaluronan Receptor LYVE-1-Expressing Macrophages and Vascular Smooth Muscle Cells. *Cells 2022, Vol. 11, Page 411*. **11**, 411 (2022).

406. K. W. K. Kim, D. Shim, J. S. Lee, K. Zaitsev, J. W. Williams, K. W. K. Kim, M. Y. Jang, H. S. Jang, T. J. Yun, S. H. P. Lee, W. K. Yoon, A. Prat, N. G. Seidah, J. J. H. Choi, S. H. P. Lee, S. H. Yoon, J. W. Nam, J. K. Seong, G. T. Oh, G. J. Randolph, M. N. Artyomov, C. Cheong, J. J. H. Choi, Transcriptome analysis reveals nonfoamy rather than foamy plaque macrophages are proinflammatory in atherosclerotic murine models. *Circ. Res.* **123**, 1127–1142 (2018).

407. A. Hwee Ying Lim, S. Yng Lim, C. Kun Tan, D. G. Jackson, Hyaluronan Receptor LYVE-1-Expressing Macrophages Maintain Arterial Tone through Hyaluronan-Mediated Regulation of Smooth Muscle Cell Collagen LYVE-1 on macrophage engages HA on smooth muscle for collagen degradation. *Immunity*. **49**, 326–341 (2018).

408. J. Wang, E. Guan, G. Roderiquez, V. Calvert, R. Alvarez, M. A. Norcross, Role of Tyrosine Phosphorylation in Ligand-independent Sequestration of CXCR4 in Human Primary Monocytes-Macrophages. *J. Biol. Chem.* **276**, 49236–49243 (2001).

409. J. J. T. Otten, S. C. A. De Jager, A. Kavelaars, T. Seijkens, I. Bot, E. Wijnands, L. Beckers, M. M. Westra, M. Bot, M. Busch, B. Bermudez, T. J. C. Van Berkel, C. J. Heijnen, E. A. L. Biessen, Hematopoietic G-protein-coupled receptor kinase 2 deficiency decreases atherosclerotic lesion formation in LDL receptor-knockout mice. *FASEB J.* **27**, 265–276 (2013).

Appendix

Appendix 1. List of publications

Rumianek AN, Greaves DR. How Have Leukocyte In Vitro Chemotaxis Assays Shaped Our Ideas about Macrophage Migration? Biology (Basel). 2020 Dec 2;9(12):439. doi: 10.3390/biology9120439.

Rumianek AN, Davies B, Channon KM, Greaves DR, Purvis GSD. A human CD68 promoter-driven inducible Cre recombinase mouse line allows specific targeting of tissue resident macrophages. Front Immunol. 2022 Jul 6;13:918636. doi: 10.3389/fimmu.2022.918636.

Deroy C*, **Rumianek AN***, Wheeler JHR, Nebuloni F, Cook PR, Greaves DR, Walsh EJ. Assaying macrophage chemotaxis using fluid-walled microfluidics. Adv. Mater. Technol. 2022, 2200279. https://doi.org/10.1002/admt.202200279 (*co-first author)

Deroy C, Wheeler JHR, **Rumianek AN**, Cook PR, Durham WM, Foster K, Walsh EJ. Reconfigurable Microfluidic Circuits for Isolating and Retrieving Cells of Interest. ACS Appl Mater Interfaces 2022. doi: 10.1021/acsami.2c07177

Appendix 2. Projects Contributions

hCD68-CreERT2 mice were conceptualised by Prof David R Greaves and created in collaboration with Dr Ben Davies in the Wellcome Trust Centre for Human Genetics. All experiments were designed by Agata Rumianek, Dr Gareth Purvis and Prof Greaves and performed by Agata Rumianek with help from Dr Purvis. Data was analysed and presented by Agata Rumianek with help from Dr Purvis and Prof Greaves.

The robotic printer used in experiments was designed and patented by iotaSciences LTD. Creating a macrophage chemotaxis assay with the robot was conceptualised by Prof David Greaves and Prof Edmond Walsh. All experiments were designed by Agata Rumianek, Dr Cyril Deroy, Prof Greaves, Prof Walsh and Prof Peter Cook. All experiments were performed by Agata Rumianek and Cyril Deroy. Data was analysed and presented by Agata Rumianek and Cyril Deroy with help from Dr Jamie Wheeler (Matlab scripts).